# Acknowledgements

First and foremost, I would like to thank my *super*visor Dr Eva Hevia for three years packed full of wise words and boundless energy. It has been my absolute pleasure to do chemistry in your lab and I am grateful for all the help you have given me and the endless ideas. Thank you for your care and attention helping to make this thesis the best thesis possible! I couldn't have done any of it without you. If you ever run out of ideas (unlikely, I know) don't forget you could always drown some ants in hexane and run them down the GC (ah, good times!)

Special thanks to fellow Hevias/Hevia Alumni, Matt, Zoe, Vicki, Emma, Thomas, Alberto and the extended family of R5-26; it's been hard work, but you've made it exceedingly good fun. A few choice quotes in memory of my time in the lab: "you're not supposed to just read the slides" (you had to be there, eh Ben?), "if two T-Rexs are fighting in George Square, would they be more interested in each other or eating us?" and "I've been fighting with my hobbit"! Shout out to Ben and Matt for inventing the Sharibu. Bless you both! To all the project students that have worked with me over the years (Andy, Lisa, Nick, Kelvin and Angeles) thank you all for your dedication and contributions to the work!

I must also thank Professor Robert Mulvey for the kind encouragement and suggestions after group meetings, Dr Charlie O'Hara for training in, and use of, the GC, Dr Pablo Garcia-Alvarez for teaching me how to use DOSY (it's super cool!), Craig Irving's unending NMR help and Pat Keating's expertise in the GC/MS. Also, my thanks go to Dr Alan Kennedy, Dr Jan Klett, Dr Luca Russo and Professor Bill Clegg for the numerous X-ray structures, which bring a little bit of sunshine to my life.

Like probably every PhD student before me, I can hardly believe it's now at an end. It's been a wonderful experience and I know that is down to the great people I have had the pleasure to get to know over these past few years. Of all my happy memories, top of the list are: the LA trip – outstanding! Eva and Zoe on the Tower

of Terror, just hilarious! The trip to the synchrotron is also high up the list; what geek couldn't love taking a walk around a particle accelerator? Finally, I can't resist it, Brad Pitt filming right outside the university! After our trip to Hollywood, Hollywood came to us.

And now we get to the most important paragraph in the whole thesis: my family. David, my biggest fan, you have never relented in your encouragement or belief in me. I think I've been Mrs Baillie for long enough, what do you say? (Ha ha!) Jonathan and Petra, you kept me sane more than you know and you could always lift my spirit when things weren't going to plan! You have been strong when I needed it and silly when I needed that more. Thank you Baillies! David: DOSY-doh. Jonathan: lunch buddy! Petra: all plastics are polymers, but not all polymers are plastics! Now, how about a cruise?

# Abstract

Building on recent successes in mixed-metal chemistry, this research project aims to enhance the understanding of the complicated correlations existing between structural patterns and reactivities of alkali metal magnesiates and zincates together with exploring their applications in a number of fundamental organic transformation reactions such as metallation, alkyl addition and metal-halogen exchange reactions.

Elucidating the effect that donor solvents can exert on the overall constitution of organometallic reagents, a series of novel solvated [(donor)$MMgR_3$] and [$(donor)_2M_2MgR_4$] (donor = THF, dioxane, TMEDA, PMDETA; M = Li, Na, K; R = $CH_2SiMe_3$) compounds have been prepared and fully characterised both in the solid-state and in solution using multinuclear NMR (including $^1$H-DOSY NMR) studies. A rich variety of structural motifs has been disclosed which range from simple monomers when polydentate ligands such as PMDETA are employed, such as [(PMDETA)$LiMgR_3$] (**6**) and [$(PMDETA)_2MMgR_4$] (M = Na (**9**), K (**11**)), to much more complex polymeric structures using oxygen donor ligands dioxane or THF, such as [$\{(dioxane)_2LiMgR_3\}_\infty$] (**3**), [$\{(dioxane)Li_2Mg_2R_6\}_\infty$] (**4**) and [$\{(THF)LiMgR_3\}_\infty$] (**2**). The first examples of unsolvated trisalkyl magnesiates [$\{NaMgR_3\}_\infty$] (**12**) and [$\{KMgR_3\}_\infty$] (**16**) have been unveiled which exhibit distinct 2D supramolecular structures in the solid-state constructed exclusively of electron deficient M-C bonds. The ability of novel potassium magnesiates to participate in direct magnesium-hydrogen exchange reactions was assessed with several aromatic and heteroaromatic substrates.

In addition, key reaction intermediates have been structurally defined from metallation, alkyl addition and metal-halogen exchange reactions which provide compelling evidence that the outcome of these reactions are reliant on subtle changes in the coordination sphere of the bimetallic reagent employed. Thus, the reactivity of heteroleptic zincate [(THF)LiZn(TMP)(*t*Bu)$_2$] (**22**) towards pyrazine has demonstrated that despite the presence of two nucleophilic *t*Bu groups the selective

two-fold deprotonation of the heterocycle pyrazine is preferred to form the unprecedented 2,5-di-zincated pyrazine molecule. These results are in contrast with those observed when pyrazine is confronted by the homoleptic alkyl zincate [(PMDETA)LiZn($t$Bu)$_3$] (**23**) where the chemoselective addition of a $t$Bu group to the $\alpha$-C of the heterocycle takes place under mild reaction conditions. Focussing on metal-halogen exchange reactions, the addition of Li$O t$Bu has proved to greatly activate $ZnEt_2$ towards zinc-iodine exchange reactions with 2-iodoanisole under mild conditions.

Novel bimetallic approaches which allow the selective C4 functionalisation of unsaturated N-heterocyclic carbene IPr have been developed. Thus, the first direct zincation of an NHC was achieved by reacting sodium zincate [(TMEDA)Na(TMP)($t$Bu)Zn($t$Bu)] with IPr to form [(THF)$_3$Na(IPr*)Zn($t$Bu)$_2$] (**41**). **41** exhibits a unique chemical profile and can react efficiently with [ClAu($PPh_3$)] to form an unprecedented bis-gold [ClAu(IPr*)Au($PPh_3$)] (**47**) species. Extension of these reactivity studies to Na/Mg combinations allows the isolation of the first sodium magnesiate containing a deprotonated carbene molecule [(THF)$_3$Na(IPr*)Mg($CH_2SiMe_3$)$_2$(THF)] (**50**).

# Publications

*"Synthesis, structural elucidation and diffusion-ordered NMR studies of homoleptic alkyllithium magnesiates: donor-controlled structural variations in mixed-metal chemistry"* **Sharon E. Baillie**, William Clegg, Pablo Garcıa-Alvarez, Eva Hevia, Alan R. Kennedy, Jan Klett and Luca Russo, *Organometallics,* **2012**, *31*, 5131.

*"New lithium-zincate approaches for the selective functionalisation of pyrazine: direct dideprotozincation vs. nucleophilic alkylation"* **Sharon E. Baillie**, Victoria L. Blair, David C. Blakemore, Duncan Hay, Alan R. Kennedy, David C. Pryde and Eva Hevia*, Chem. Commun*., **2012**, *48*, 1985.

*"A new polymeric alkyl/alkoxide magnesium–sodium inverse crown complex"* **Sharon E. Baillie**, Victoria L. Blair, Eva Hevia and Alan R. Kennedy*, Acta Cryst*., **2011**, *C67*, 249.

*"Synthesis and characterization of an infinite sheet of metal–alkyl bonds: unfolding the elusive structure of an unsolvated alkali-metal trisalkylmagnesiate"* **Sharon E. Baillie**, William Clegg, Pablo Garcıa-Alvarez, Eva Hevia, Alan R. Kennedy, Jan Klett and Luca Russo, *Chem. Commun.,* **2011**, *47*, 388.

Other publications not related to this work

*"Synthesis of mixed alkali-metal-zinc enolate complexes derived from 2,4,6-trimethylacetophenone: new inverse crown structures"* **Sharon E. Baillie**, Eva Hevia, Alan R. Kennedy, and Robert E. Mulvey, *Organometallics* **2007,** *26,* 204.

# Conference Presentations

1. "*New structural and reactivity insights in magnesiate and zincate chemistry*"; Hamilton-Barrett Postgraduate Prize Award lecture, University of Strathclyde, Oct

2011.

2. "*New structural insights in mixed-metal magnesiate and zincate chemistry*"; 6th WestCHEM Research Day, Glasgow University, June 2011.

3. "*New structural insights in mixed-metal magnesiate and zincate chemistry*"; American Chemical Society, 241st National Meeting, California, March 2011.

## Conference Poster Presentations

1. "*New lithium-zincate approaches for the selective functionalization of pyrazine: direct dideprotonation vs. nucleophilic alkylation*"; North West Organic Chemistry Symposium, Liverpool University, July 2012.

2. "*Probing the structures of a series of lithium magnesiates*"; Universities of Scotland Inorganic Conference, Glasgow University, July 2011.

3. "*Unveiling the Structure of Unsolvated Alkali-Metal Magnesiates*"; Royal Society of Chemistry Young Members' Symposium, Manchester University, October 2010.

4. "*Unveiling the Structure of Unsolvated Alkali-Metal Magnesiates*"; Universities of Scotland Inorganic Conference, Durham University, July 2010.

# Table of Common Abbreviations

| | |
|---|---|
| acac | Acetylacetonate |
| AMM*M* | Alkali-metal-mediated metallation |
| AMM*Mg* | Alkali-metal-mediated magnesiation |
| AMM*Mn* | Alkali-metal-mediated manganation |
| AMM*Zn* | Alkali metal mediated zincation |
| *a*NHC | *Abnormal* N-Heterocyclic carbene |
| Ar | Aryl |
| *n*Bu | $(CH_2)_3CH_3$ |
| *t*Bu | $C(CH_3)_3$ |
| CCDB | Cambridge crystallographic database |
| CIP | Contacted ion-pair |
| COSY | $^1H$-$^1H$ correlated spectroscopy |
| Cp | Cyclopentadiene anion $(C_5H_5)^-$ |
| DA | Diisopropylamide |
| DCM | Dichloromethane |
| DFT | Density functional theory |
| Dipp | Diisopropylphenyl |
| DOSY | Diffusion ordered NMR spectroscopy |
| Dppf | 1,1'-bis(diphenylphosphino)ferrocene |
| Ee | Enantiomeric excess (%) |
| Et | Ethyl |
| $Et_2O$ | Diethyl ether |
| FW | Formula weight |
| G | Grams |
| H | Hours |
| HMDS | Hexamethyldisilazide |
| HOESY | Heteronuclear Overhauser effect spectroscopy |
| HSQC | Heteronuclear single quantum correlation spectroscopy |
| IBu | 1,3-di-*tert*-butylmidazol-2-ylidene |
| ICE | Inverse crown ether |

| | |
|---|---|
| IMes | 1,3-dimesityimidazol-2-ylidene |
| IPr | 1,3-bis-(2,6-diisopropylphenyl)imidazol-2-ylidene |
| IPr* | :C{[N(2,6-*i*Pr$_2$C$_6$H$_3$)]$_2$CHC} |
| LDA | Lithium diisopropylamide |
| M | Molar |
| Me | Methyl |
| MHz | Megahertz |
| mL | Millilitres |
| mmol | Millimoles |
| NHC | N-Heterocyclic carbene |
| NHDC | N-Heterocyclic dicarbene |
| NMP | *N*-methylpyrrolidinone |
| NMR | Nuclear magnetic resonance |
| | s – singlet |
| | d – doublet |
| | t – triplet |
| | q – quartet |
| | m – multiplet |
| | b – broad |
| NOESY | Nuclear Overhauser effect spectroscopy |
| Nu | Nucleophile |
| PGSE | Pulsed gradient spin echo |
| Ph | Phenyl |
| PhN | Phenylnaphthalene |
| PMDETA | *N*,*N*,*N*',*N*'',*N*''-pentamethyldiethylenetriamine |
| Ppm | Parts per million |
| Pr | Propyl |
| SSIP | Solvent separated ion-pair |
| THF | Tetrahydrofuran |
| TMEDA | *N*,*N*,*N*',*N*'-tetramethylethylenediamine |
| TMP | 2,2,6,6-tetramethylpiperidide |
| TMP(H) | 2,2,6,6-tetramethylpiperidine |

| | |
|---|---|
| TMS | Trimethylsilyl or tetramethylsilane |
| TPhN | 1,2,3,4-tetraphenylnaphthalene |

# Table of Contents

# Table of Compounds

| Number | Compound | Number | Compound |
|---|---|---|---|
| 1 | $[LiMgR_3]$ | 2 | 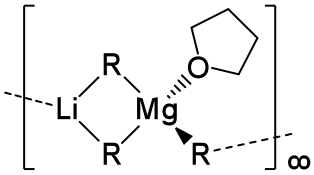 $[\{(THF)LiMgR_3\}_\infty]$ |
| 3 | 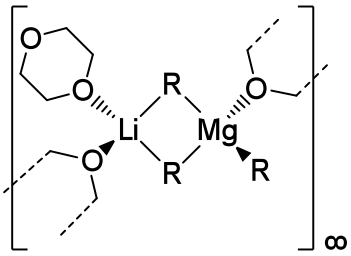 $[\{(dioxane)_2LiMgR_3\}_\infty]$ | 4 | 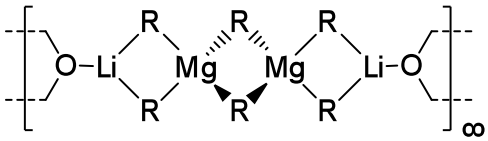 $[\{(dioxane)Li_2Mg_2R_6\}_\infty]$ |
| 5 | 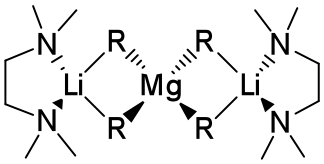 $[(TMEDA)_2Li_2MgR_4]$ | 6 | 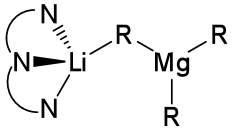 $[(PMDETA)LiMgR_3]$ |
| 7 | 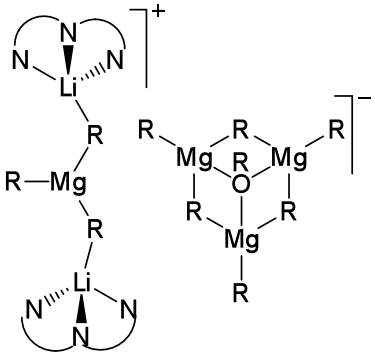 $[\{(PMDETA)_2Li_2MgR_3\}^+\{Mg_3R_6(OR)\}^-]$ | 8 | 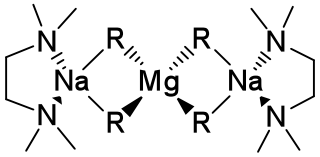 $[(TMEDA)_2Na_2MgR_4]$ |
| 9 | 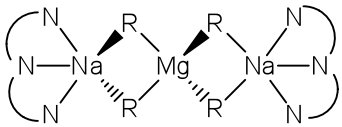 $[(PMDETA)_2Na_2MgR_4]$ | 10 | 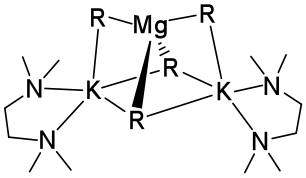 $[(TMEDA)_2K_2MgR_4]$ |

| Number | Compound | Number | Compound |
|---|---|---|---|
| **11** | 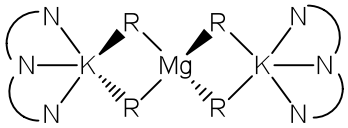 [(PMDETA)$_2$K$_2$MgR$_4$] | **12** | **[{NaMgR$_3$}$_\infty$]** |
| **13** | **[{(NaR)$_4$}$_\infty$]** | **14** | [Na$_2$MgR$_4$] |
| **15** | 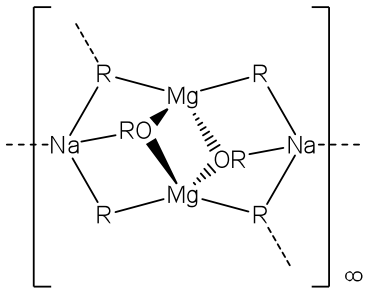 [{NaMgR$_2$OR}$_\infty$] | **16** | **[{KMgR$_3$}$_\infty$]** |
| **17** | **[{(C$_6$H$_6$)KMgR$_3$}$_\infty$]** | **18** | **[{(Cp$_2$Fe)KMgR$_3$}$_\infty$]** |
| **19** | 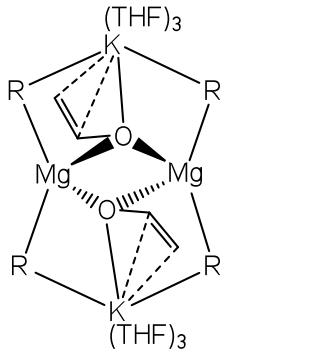 [{(THF)$_3$K(R)(OCH=CH$_2$)MgR}$_2$] | **20** | 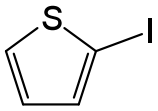 |
| **21** | 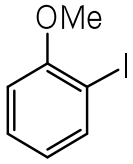 | **22** | **[(THF)LiZn(TMP)(*t*Bu)$_2$]** |

| Number | Compound | Number | Compound |
|---|---|---|---|
| 23 | [(PMDETA)LiZn(*t*Bu)$_3$] | 24 | 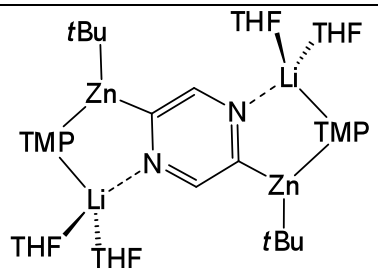 [2,5-{(THF)$_2$LiZn(TMP)(*t*Bu)}$_2$($C_4N_2H_2$)] |
| 25 | 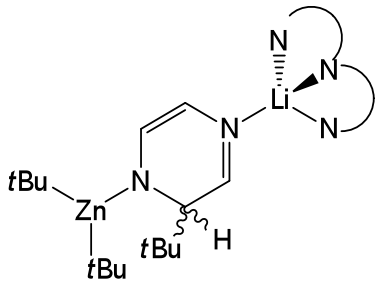 [(PMDETA)Li{$C_4N_2H_4$(*t*Bu)}Zn(*t*Bu)$_2$] | 26 | 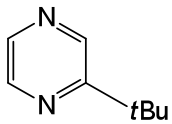 |
| 27 | 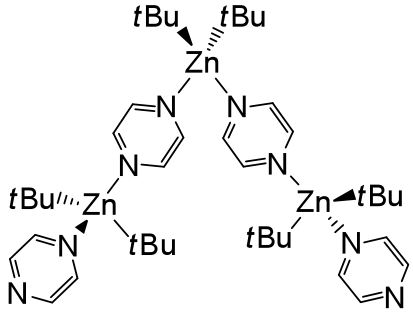 [{Zn(*t*Bu)$_2$}$_3${$C_4N_2H_4$}$_4$] | 28 | 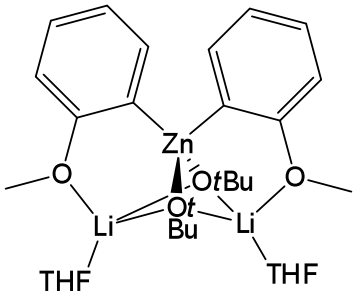 [(THF)$_2$Li$_2$(O*t*Bu)$_2$Zn(*o*-$C_6H_4$-OMe)$_2$] |
| 29 | 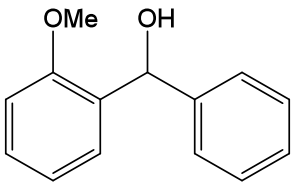 | 30 | 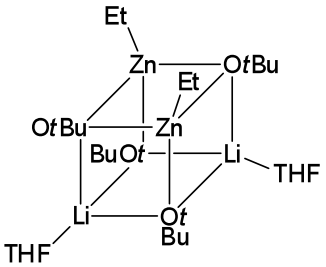 [{(THF)Li(O*t*Bu)$_2$ZnEt}$_2$] |
| 31 | 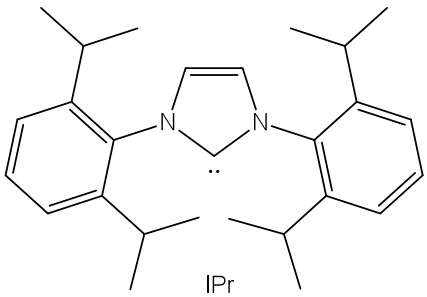 IPr | 32 | 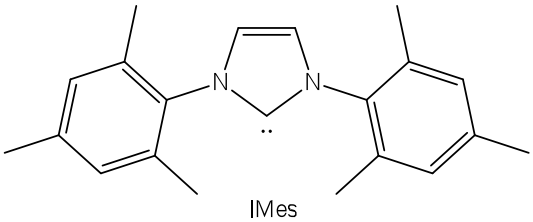 IMes |

| Number | Compound | Number | Compound |
|---|---|---|---|
| **33** | 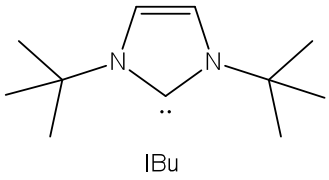 IBu | **34-39** | 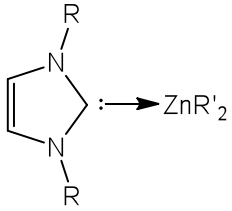 **34**, R = Dipp, R' = Me<br>**35**, R = Dipp, R' = *t*Bu<br>**36**, R = Mes, R' = Me<br>**37**, R = Mes, R' = *t*Bu<br>**38**, R = *t*Bu, R' = Me<br>**39**, R = *t*Bu, R' = *t*Bu |
| **40** | 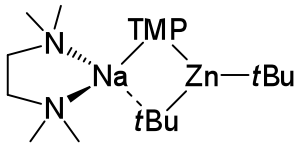 [(TMEDA)Na(TMP)(*t*Bu)Zn(*t*Bu)] | **41** | 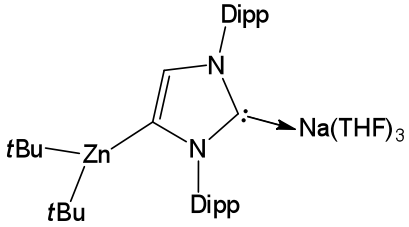 [(THF)$_3$Na(IPr*)Zn(*t*Bu)$_2$] |
| **42** | 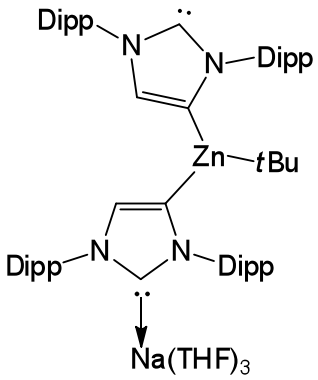 [(THF)$_3$Na(IPr*)Zn(IPr*)(*t*Bu)] | **43** | 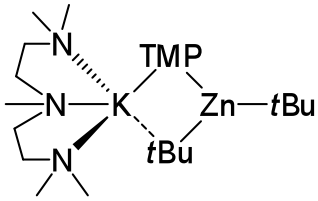 [(PMDETA)K(TMP)(*t*Bu)Zn(*t*Bu)] |
| **44** | 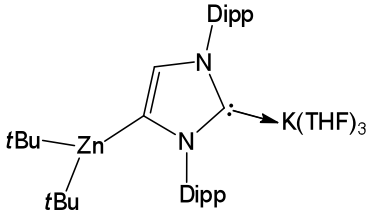 [(THF)$_3$K(IPr*)Zn(*t*Bu)$_2$] | **45** | 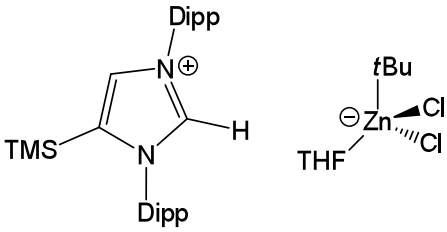 [{TMS-IPr(H)}$^+${(THF)Zn(*t*Bu)Cl$_2$}$^-$] |
| **46** | 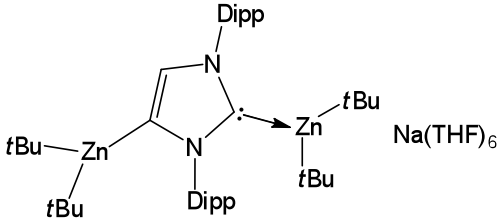 [{Na(THF)$_6$}$^+${(tBu)$_2$Zn(IPr*)Zn(tBu)$_2$}$^-$] | **47** | 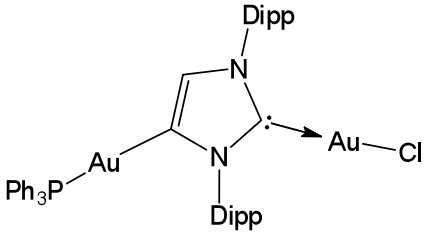 [ClAu(IPr*)Au(PPh$_3$)] |

| Number | Compound | Number | Compound |
|---|---|---|---|
| **48** | 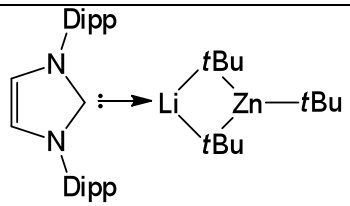 [IPr·LiZntBu$_3$] | **49** | 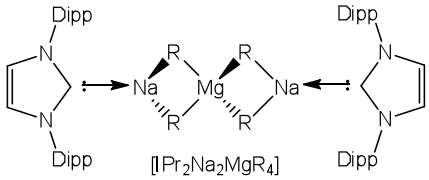 [IPr$_2$Na$_2$MgR$_4$] |
| **50** | 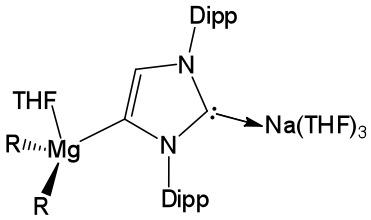 [(THF)$_3$Na(IPr*)Mg(R)$_2$(THF)] | | |

# Chapter 1: General introduction to mixed-metal chemistry

## 1.1 Historic background of mixed-metal chemistry

This introduction to the area of mixed-metal chemistry aims to provide an overview of the major developments in organometallic chemistry, within the context of main group metals, from its origins over 150 years ago through to current applications. It will discuss the synergy observed when an alkali metal is coupled in the same organometallic reagent with a second, less polar metal, in particular magnesium or zinc. For the purposes of this work zinc will not be considered a transition metal: IUPAC defines a transition metal as "*an element whose atom has an incomplete d sub-shell, or which can give rise to cations with an incomplete d sub-shell*",[1] and zinc has a full (stable) $d^{10}$ shell when in its most common oxidation state of +2. The chemistry of zinc is often considered similar to that of the main group metals, especially of magnesium which also primarily forms a +2 oxidation state. In addition, Mg and Zn are of comparable size (6-coordinate radii of $Mg^{2+}$ = 0.86 Å, $Zn^{2+}$ = 0.88 Å);[2] however, when magnesium loses two electrons it is left with the electronic configuration of neon [Ne] whereas zinc has the configuration $[Ar]3d^{10}$, meaning that although the charge and size of the $M^{2+}$ ions are essentially the same, as $Zn^{2+}$ has ten (polarisable) d-shell electrons it can be considered much "softer" than $Mg^{2+}$. Further, zinc is markedly more electronegative than magnesium and therefore prefers to form more covalent M-C interactions, leading to divergent chemistry related to these two metals.

Of particular importance to chemists in general, be they inorganic, organic or physical chemists, is the two-pronged consideration of structure and reactivity, whereby knowledge of the former can lead to insights on the latter. This concept will be explored in detail in the following chapters.

In the mid nineteenth century Wanklyn synthesised the first known heterobimetallic compound, $NaZnEt_3$, by reacting sodium metal with diethyl zinc.[3] This discovery in 1858 makes it amongst the oldest known class of mixed-metal compound. Despite

going on to carry out a number of reactivity studies on the intriguing compound,[4] this multimetallic complex received little attention until well into the twentieth century. Almost a hundred years after Wanklyn's discovery, Wittig's pioneering work with mixed-metal systems led to the term 'ate' being coined to describe the compound $LiZnPh_3$ and, by extension, describe the nature of this class of complexes.[5] In general terms these organometallic 'ate' compounds contain an alkali metal (usually Li, Na or K) combined with a second metal of lower polarity M-C bonds (for example magnesium or zinc) with an array of anionic ligands (such as alkyl and amine groups). 'Ate' complexes will commonly be classed as either tri- or tetraorganometallates with the general formulae $M^IM^{II}R_3$ and $M^I_2M^{II}R_4$ respectively, where $M^I$ is the alkali metal, $M^{II}$ is the divalent metal and R is the anionic ligand. The anionic ligands will coordinate, as far as sterically possible, around the stronger Lewis acid (*i.e.* the low polarity metal) and the complexes may be considered $[\{M^I\}^+\{M^{II}R_3\}^-]$ for triorganometallates or $[\{M^I_2\}^{2+}\{M^{II}R_4\}^{2-}]$ for tetraorganometallates.

Heading towards and into the twenty first century, inorganic chemists continued to investigate the structure of 'ate' complexes by means of X-ray crystallographic studies, including the seminal work by Weiss.[6] Thus, his example in 1981 confirmed the bimetallic constitution of the tetramethylmagnesiate complex $[(TMEDA)_2Li_2MgMe_4]$ where TMEDA = *N,N,N',N'*-tetramethylethylenediamine (**Figure 1.1**).[7] The structure shows tetrahedral coordination around magnesium with the methyl groups forming unsymmetrical μ bridges between the magnesium and the TMEDA-solvated lithium.

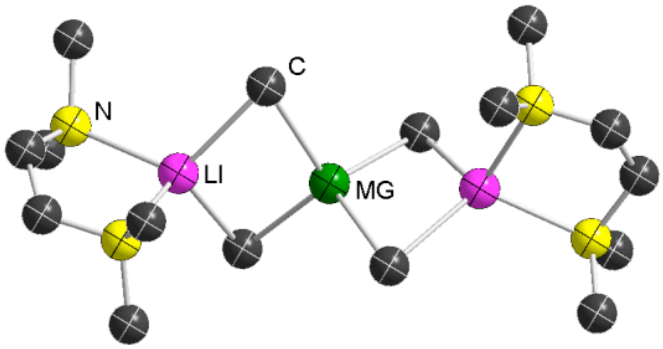


**Figure 1.1**: Molecular structure of $[(TMEDA)_2Li_2MgMe_4]$. Hydrogen atoms omitted for clarity.[7]

During the last decade these bimetallic compounds have attracted widespread interest from the community of synthetic organic chemists and they have emerged as highly versatile organometallic reagents that can participate in a number of fundamental organic transformations such as metallation reactions (metal-H exchange), metal-halogen exchange reactions, nucleophilic addition and transition metal-catalysed cross-coupling reactions (*vide infra*). Major landmarks that demonstrate the synthetic utility of this class of compounds are Knochel's "turbo-Grignard" reagents, "RMgCl·LiCl",[8] and the development by Uchiyama of lithium zincates,[9] as well as structural and reactivity studies carried out by Mulvey *et al* that has contributed towards understanding the synergic effects taking place in alkali-metal–mediated metallation (AMM*M*) reactions.[10]

## 1.2 Preparation of mixed-metal reagents

There are two main synthetic methodologies to prepare bimetallic reagents:

(i) Cocomplexation Method: where both homometallic reagents are combined, usually in the presence of a Lewis donor such as THF or TMEDA, which favours deaggregation of the starting materials (**Scheme 1.1**), or,

(ii) Metathesis Method: where a polar organometallic reagent (such as LiR, where R = alkyl or amide) is reacted with an inorganic salt of a less polar metal (such as $ZnCl_2$ or $MgCl_2$) (**Scheme 1.2**).

The cocomplexation method is a reliable method which can form triorganometallates or tetraorganometallates depending on the stoichiometry applied, *i.e.* for a triorganometallate a 1:1 ratio of $M^IR$ to $M^{II}R_2$ is used whereas a 2:1 stoichiometry is employed in the synthesis of a tetraorganometallate (**Scheme 1.1a** and **b**). Providing extra versatility, this approach can also be used in the synthesis of heteroleptic reagents by the choice of different R groups on the group 1 reagent with those present on the diorganozinc/magnesium reagent (**Scheme 1.1c**), for example, the cocomplexation of a lithium amide with a dialkyl zinc reagent (**Scheme 1.1d**).

Cocomplexation reactions of this type have been previously reported in the literature as an efficient method to prepare bimetallic compounds as for example $NaMgBu_3$ by reacting BuNa and $Bu_2Mg$.[11] Furthermore, theoretical studies have revealed that in this case the formation of this mixed Na-Mg compound is energetically favoured, even in the absence of a Lewis base, despite the polymeric structures of both monometallic components.[11]

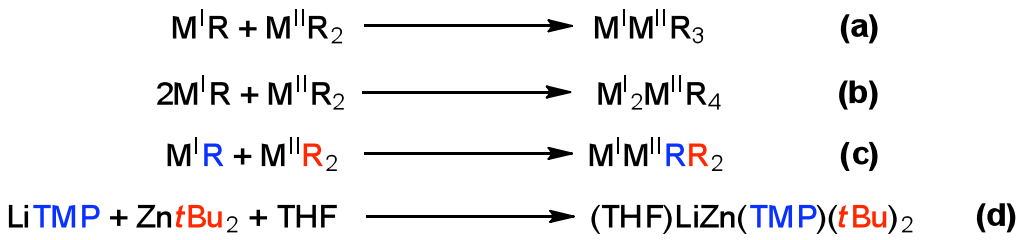


**Scheme 1.1**: Synthesis of mixed-metal reagents from the cocomplexation method: (a) a triorganometallate, (b) a tetraorganometallate, (c) a heteroleptic triorganometallate and (d) a specific example.

The metathesis method, used commonly in organic synthesis to prepare 'ate compounds *in situ*, relies on the formation of the ionic inorganic salts MX (M = Li, Na, K and X = halide) as the driving force due to the large lattice energy. As with the cocomplexation approach, the synthesis of triorgano- or tetraorganometallates is possible depending on the stoichiometry involved: a 1:3 ratio of the Zn or Mg salt with the group 1 organometallic compound will result in a triorganometallate, whereas the ratio of 1:4 is employed if the tetraorganometallate is required (**Scheme 1.2a** and **b**). Heteroleptic reagents can be accessed by reacting a Grignard reagent with an organo-alkali metal with differing R groups (**Scheme 1.2c**) or by the stepwise addition of $M^IR$ then $M^IR'$ to $M^{II}X_2$. In every case, concomitant $M^IX$ will form when this metathesis approach is used as an *in situ* methodology and the presence of this salt can have a profound effect on the reactivity of the newly generated organometallic reagents, if used without purification[12] as will be discussed in **Chapter 6**. Additionally, the use of ethereal solvents (THF or diethyl ether) tends to be mandatory to favour for the dissolution of the inorganic salt $M^{II}X_2$, and this can limit the number of polar organometallic reagents that can be used since they can give side reactions with the solvents (as for example α-deprotonation or

ether cleavage), as well as affect the overall constitution of these reagents (see **Chapters 2** and **3** for the discussion of the effects of donor molecules to mixed-metal reagents).

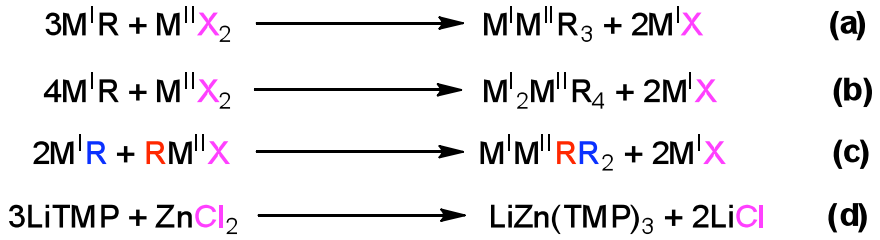


**Scheme 1.2**: Synthesis of mixed-metal reagents from the metathesis method: (a) a triorganometallate, (b) a tetraorganometallate, (c) a heteroleptic triorganometallate from a Grignard reagent and (d) a specific example.

## 1.3 Synergic reactivity: the "complex metallators"

The use of traditional monometallic methodologies is still ubiquitous in synthesis, for example organolithium reagents such as *n*-butyllithium (*n*BuLi) or lithium amides such as lithium diisopropylamide (LDA) are often the reagent of choice when performing deprotonative metallation reactions.[13] However, these workhorses of chemistry are not without their limitations. Notably, these reagents exhibit low functional group tolerance, generate low-stability intermediates, and they can suffer from alternative competing side reaction pathways. In order to overcome some of these important drawbacks they often require the use of subambient temperatures which can be problematic and costly on an industrial scale. As such, the search for reagents that can perform efficient and selective metallation reactions is vigorous in the research community and draws chemists worldwide, from both inorganic and organic disciplines. The "Grand Challenge" facing this area is to develop reagents that have high functional group tolerance and high selectivity, whilst maintaining the high reactivity typically associated with conventional organolithium reagents, ideally at ambient temperature. A number of reagents have come to the fore in recent years, which can collectively be classed as "complex metallators", and which are more elaborate than their simple organolithium reagent precursors with the common

feature that they all display bimetallic constitutions. A selection of complex metallators is shown in **Figure 1.2**.

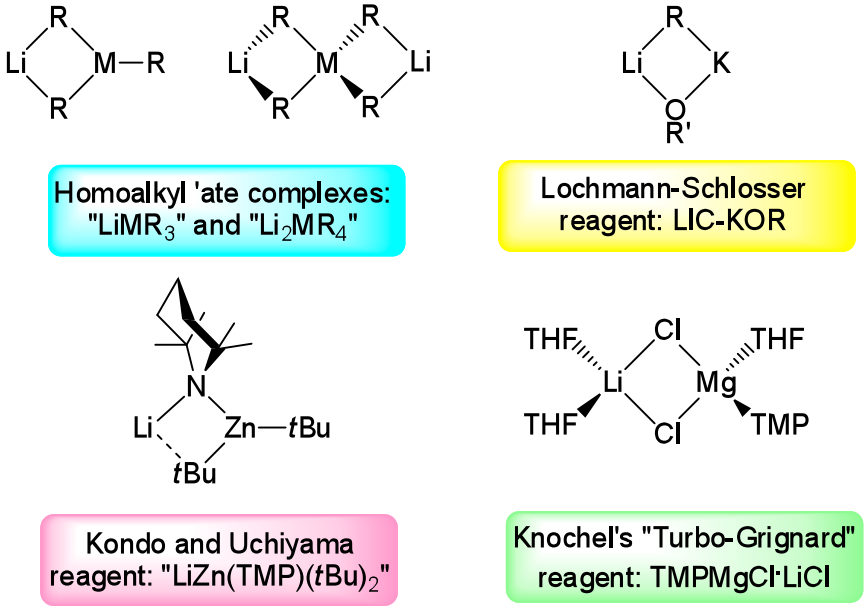


**Figure 1.2:** Chem Draw representation of a selection of complex metallators

Significant recent advances in the development of these complex metallators means the synthetic chemist now has a range of choices available when carrying out fundamental organic transformation, including but not limited to metallation and metal-halogen exchange reactions, where the judicious selection of mixed-metal reagent can bring high levels of selectivity, coupled with excellent functional group tolerance and superior reactivity. The application of complex metallators in synthesis will now be examined.

## 1.4 Applications of mixed-metal reagents in synthesis

### 1.4.1 Deprotonative metallation

Deprotonative metallation, where a non-polar C-H bond is transformed into a much more polar M-C bond, constitutes one of the most important and fundamental synthetic methodologies and is carried out on a daily basis in many laboratories across the world. Amongst the many investigations into efficient proton abstraction,

recently Mongin has successfully employed homoalkyl 'ate complexes $LiMgBu_3$ and $Li_2MgBu_4$ for the deprotonation of a wide range of heterocycles including fluoroaromatics,[14] thiophenes,[15] furans,[16] benzoxazole and oxazole,[17] with the resulting magnesiate being trapped by an electrophile or involved in a palladium-catalysed cross-coupling reaction. In the magnesiation of furan, Mongin observed an increase in yield of the final quenched product when moving from lithium tributylmagnesiate to the stoichiometric variant dilithium tetrabutylmagnesiate, a representative example of which is shown in **Scheme 1.3**.

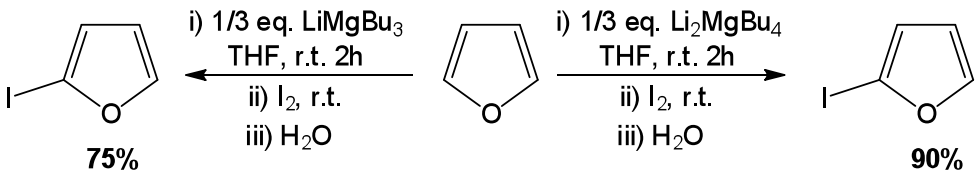


**Scheme 1.3:** Comparison of the deprotonation of furan with a trialkylmagnesiate and a tetraalkylmagnesiate, followed by quenching with iodine.[16]

While studying the performance of these lithium magnesiates in the deprotonation of thiophene, Mongin noted the positive influence on the reaction yields in the presence of TMEDA, however no structural evidence was offered to account for this increase in reactivity.[15] The contribution of Mongin and co-workers extends beyond homoalkyl alkali metal magnesiates, with the development and application of the amido alkali metal zincate "$LiZn(TMP)_3$" and cadmate "$LiCd(TMP)_3$".[18] The homoleptic zincate base is able to deprotonate a number of sensitive diazine species such as pyrazine, quinoxaline, pyridazine and pyrimidine.[19] In addition, a wide range of heterocyclic species including benzoxazole, benzothiazole, benzothiophene, benzofuran, *N*-Boc indole, *N*-Boc pyrrole and *N*-phenylpyrazole,[20] have been subjected to the protocol, with yields ranging from 25-73% after electrophilic quench with iodine.

Using a combination of empirical observations and DFT calculations, Mongin *et al* investigated the use of different homoleptic and heteroleptic lithium zincates towards anisole (and forward functionalization with iodine or cross-coupling) to ascertain the most efficient mode of synergic metallation.[21] These studies indicated that replacing

homoleptic TMP with diisopropylamide (DA) or piperidide (P), or employing a heteroleptic trisamide mixture of 2:1 TMP/DA, TMP/P, DA/TMP and P/TMP, resulted in a lowering of efficacy of the metallation. Replacing one TMP equivalent with a butyl group gave slightly reduced yields compared to the homoleptic TMP base.

In all these reaction, the putative zincate "$LiZn(TMP)_3$" is prepared by the metathesis method, *i.e.* three equivalents of LiTMP are reacted with [$ZnCl_2$·TMEDA] and the resulting mixed-metal species is used without further purification from the LiCl generated *in situ*. Spectroscopic analysis of the reaction mixture has detected free LiTMP and $Zn(TMP)_2$[22] which is in agreement with calculations that show the homometallic species to be more favoured separately than the cocomplex.[23] This could be a result of the great steric hindrance imposed by three molecules of the bulky TMP ligand. The authors therefore propose that metallation is carried out by LiTMP and the resultant aryl lithium intermediate undergoes a transmetallation with $Zn(TMP)_2$, generating a more stable zincated species. Somewhat surprisingly, the presence and potential interaction of LiCl is overlooked despite the pioneering work of Knochel's turbo-Grignard reagents which demonstrate the superior reactivity of Grignard reagents (RMgX) by the addition of LiCl to the reaction mixture (*vide infra*). Furthermore, Collum has reported that the presence of even 0.5 mol% of LiCl can greatly accelerate the metallation of certain arenes by LDA.[24] Mulvey and co-workers have conducted a comprehensive solution study of "$LiZn(TMP)_3$" which has the empirical formulation "(TMEDA)·LiTMP·$Zn(TMP)_2$·2LiCl" when all its components in solution are accounted for. Using DOSY NMR studies (*vide infra*) it was concluded that $Zn(TMP)_2$ is not interacting with the LiTMP in solution, supporting the previous findings that homometallic lithiation takes place, followed by transmetallation. The active species carrying out the metallation appears to be a cocomplex between LiTMP and two equivalents of LiCl with a degree of interaction from TMEDA which is undergoing a dynamic coordination/decoordination equilibrium: LiTMP·2LiCl TMEDA (**Figure 1.3**).[25]

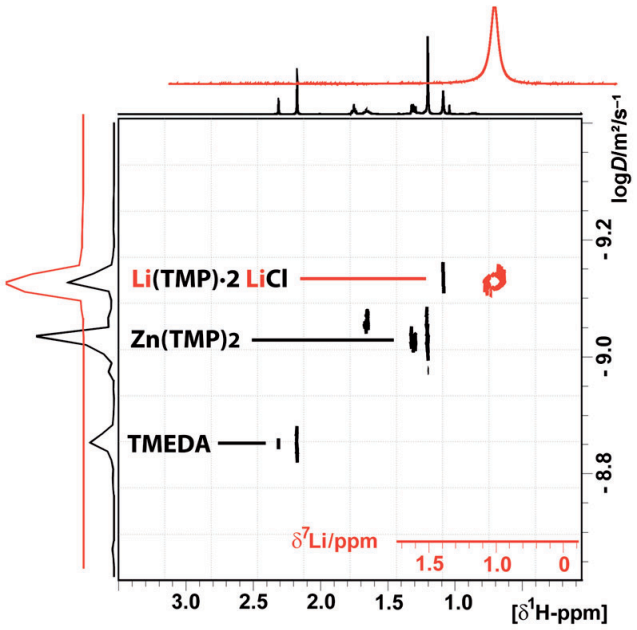


**Figure 1.3:** $^{1}$H (black) and $^{7}$Li (red) DOSY spectra for the *in situ* mixture of "(TMEDA)·LiTMP·Zn(TMP)$_2$·2LiCl" in d$_8$-THF.[25]

As well as supporting Mongin's reactivity studies, which proposed that putative base "LiZn(TMP)$_3$" initially reacts *via* lithiation of the aromatic substrate followed by transmetallation with Zn(TMP)$_2$, these DOSY NMR studies also predict that the active species in solution is a cocomplex of LiTMP and LiCl. The important role of inorganic salts in the reactivity of organometallic bases will be discussed further in **Chapter 6**.

A significant advance in the area of 'ate complexes carrying out metallation reactions came from Kondo and co-workers in 1999 with the development of a heteroleptic lithium dialkyl monoamido zincate, [LiZn(TMP)(*t*Bu)$_2$].[26] Prepared by the cocomplexation of Zn*t*Bu$_2$ with LiTMP in THF, this mixed-metal reagent was found to be highly efficient and regioselective, able to perform proton abstraction on a variety of functionalised aromatics at room temperature, with the resulting arylzincates being intercepted by electrophilic quench with iodine to afford the corresponding *ortho*-iodinated species in yields of 73-99% (**Scheme 1.4**).

The complexity of these "complex metallators" has been highlighted by Kondo *et al* by revealing that in the metallation of bromopyridines the regioselectivity can be tuned by judicious choice of the amide group incorporated into the zincate reagent.

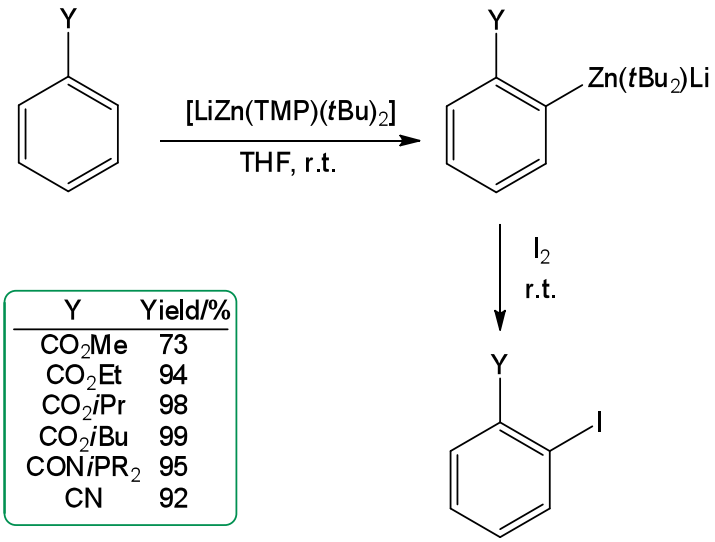


| Y | Yield/% |
|---|---|
| $CO_2Me$ | 73 |
| $CO_2Et$ | 94 |
| $CO_2iPr$ | 98 |
| $CO_2iBu$ | 99 |
| $CONiPR_2$ | 95 |
| CN | 92 |

**Scheme 1.4:** Metallation using a heteroleptic mixed Li-Zn reagent followed by electrophilic quench with $I_2$.

The authors have reported that when employing a di-*t*-butyl monoamido lithium zincate, the position of the metallation (and ultimate location of iodine post quench) depends on whether the amide employed is TMP or DA. When 2-bromopyridine is subjected to [LiZn(TMP)($t$Bu)$_2$] followed by reaction with iodine in diethyl ether ($Et_2O$) the major product formed is 2-bromo-6-iodopyridine in 86% yield. Alternatively, switching the base for [LiZn(DA)($t$Bu)$_2$] in THF, metallation followed by electrophilic quench by iodine gave the 2-bromo-3-iodopyridine isomer in 72% yield (**Scheme 1.5**).

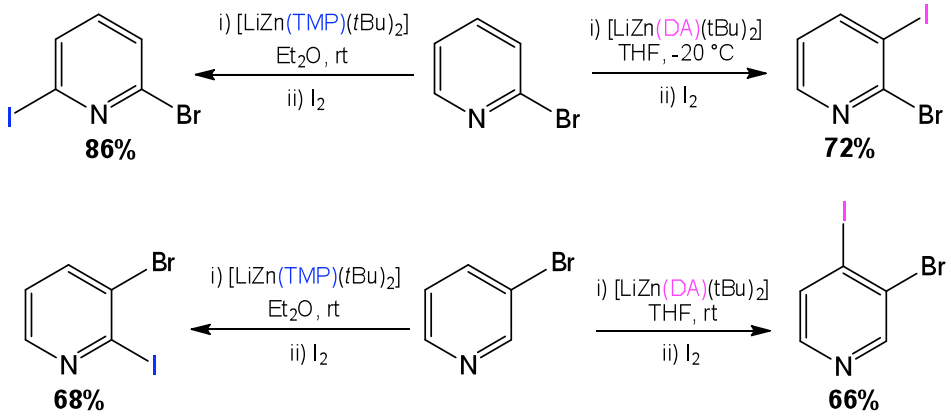


**Scheme 1.5:** Metallation of 2- or 3-bromopyridine using TMP-zincate or DA-zincate followed by electrophilic quench with iodine.

A similar distinction in selectivity was observed using 3-bromopyridine as a substrate where the TMP base preferentially metallated the 2-position and the DA base favoured the 4-position in 68% and 66% yields respectively (**Scheme 1.5**).[27]

An added advantage to the use of bimetallic bases is that, in certain cases, they can display unprecedented regioselectivities, which are not available through conventional monometallic reagents. Thus, Mulvey has reported the synergic *meta*-magnesiation of toluene using the monoalkyl-bisamido complex [(TMEDA)Na(TMP)(*n*Bu)Mg(TMP)] (**Scheme 1.6**).[28] This regioselectivity is unique on two main counts. Firstly, this selectivity is contrary to that observed by conventional bases such as BuLi/TMEDA which deprotonate toluene exclusively at the methyl position, thus generating a benzyl anion that is stabilised by resonance. Secondly, this reaction is formally a magnesiation as the departing proton in the toluene molecule has been replaced by a magnesium atom (**Figure 1.4**), which is in sharp contrast with the complete lack of reactivity observed with organomagnesium reagents such as Grignard reagents or dialkylmagnesium reagents.

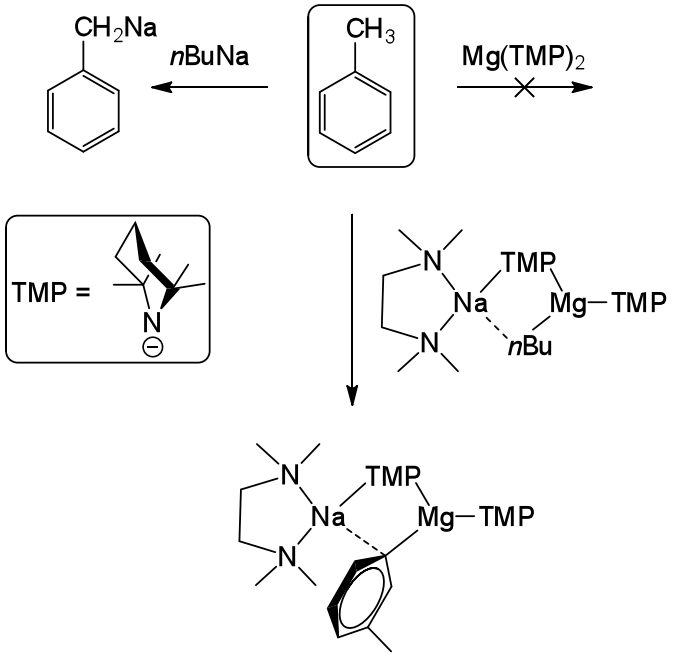


**Scheme 1.6:** Meta-metallation of toluene using monoalkyl bisamido sodium magneisate.

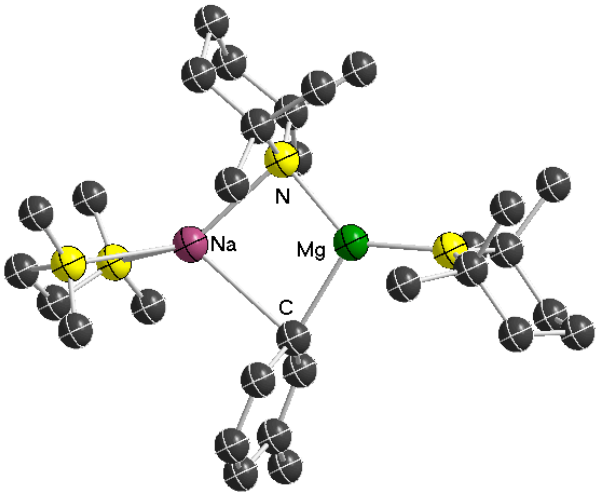


**Figure 1.4:** Molecular structure of the *meta*-magnesiation of toluene facilitated by alkali-metal–mediated magnesiation. Hydrogen atoms omitted for clarity.

This type of deprotonation has been described as an alkali-metal–mediated magnesiation (AMM*Mg*) where magnesium is the active metal in charge of performing the deprotonation but sodium is required for the reaction to take place. This special regioselectivity can, in part, be rationalised by the different bonding modes of sodium and magnesium that help to stabilise the metallated arene. The π-interactions of the Na with the arene initially fixes the position that deprotonation is going to occur. Further stabilisation of metallated toluene is achieved by the combination of Na-π bonding with the formation of strong sigma Mg-C bonds.

The mixed sodium-magnesium base is prepared in a straightforward cocomplexation reaction combining equimolar amounts of BuNa, $MgBu_2$, and TMEDA with 2 molar equivalents of TMP(H). In the absence of TMEDA an unprecedented two-fold deprotonation at the 2 and 5 positions of toluene is observed, which illustrates the key role that the donor solvents can play in tuning the regioselectivity of these reactions.[29] Additionally, this magnesiate base is able to remove protons from benzene ($pK_a$ = 43) , highlighting the synergic partnership of both metals within the 'ate, as neither of the homometallic components (NaTMP and BuMgTMP) are able to metallate the low acidity hydrogens from the aromatic benzene ring to any significant extent.[30]

Furthermore, Mulvey has shown that alkali-metal–mediated metallation is applicable to other low polarity metals, such as zinc (alkali-metal–mediated zincations, AMM*Zn*) or manganese (II) (alkali-metal–mediated manganation, AMM*Mn*). With regards AMM*Zn*, of particular note is a recent report in *Science* for the unprecedented metallation of THF at room temperature by the bimetallic reagent [(TMEDA)Na(TMP)(R)Zn(R)] (R = $CH_2SiMe_3$) (**Scheme 1.7**).[31] Ethers are notoriously difficult to metallate in a controlled fashion with conventional polar organolithium reagents due to the high instability of the metallated product and subsequent ether cleavage. In the case of THF this often leads to spontaneous ring opening *via* a [3+2] cycloreversion pathway giving a mixture of ethene and the enolate of acetaldehyde as unwanted by-products (**Scheme 1.7**).[13] Applying the sodium zincate mixed-metal base to THF led to the synergic entrapment of the α-zincated THF product in a satisfactory 53% crystalline yield.

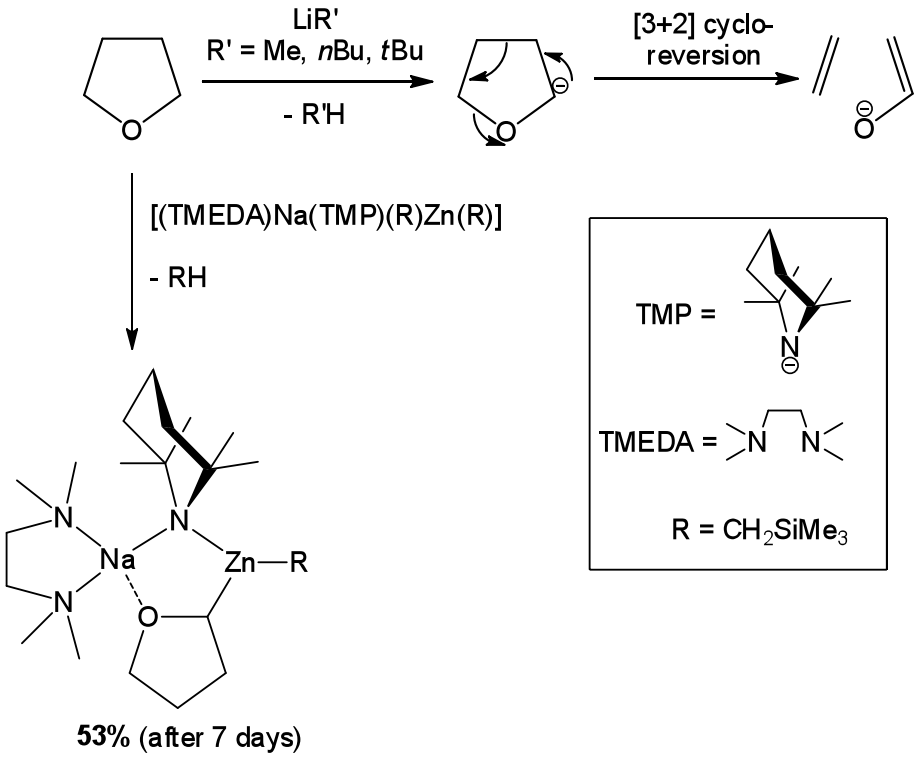


**Scheme 1.7:** Comparison of the synergic metallation of THF using a sodium zincate with the common decomposition pathway observed with conventional organolithium reagents.

An example of a deft application of alkali-metal–mediated manganation is the selective two-fold deprotonation of ferrocene (**Scheme 1.8**).[32] Individually neither LiTMP nor $MnR_2$ can abstract a proton from ferrocene; however, when combined in the mixed-metal lithium-manganese base the synergic reactivity leads to dimanganation of the substrate.

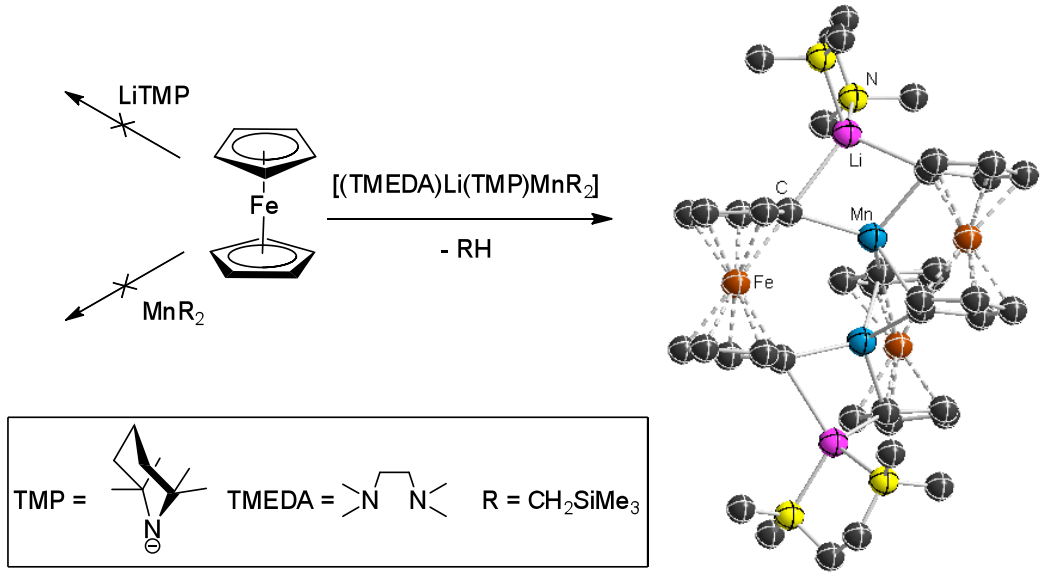


**Scheme 1.8:** Dimanganation of ferrocene by the mixed lithium-manganese base.

Another important category to be discussed whilst considering the synergic effect of mixed-metal systems is "turbo-Grignard" chemistry. In 1912 the contribution of Victor Grignard to the progress of organic chemistry was recognised when he was awarded the Nobel Prize for Chemistry for the discovery of the Grignard reagent, "RMgX", which had a less polar M-C bond than a corresponding LiR reagent and therefore could display a greater functional group tolerance and a higher level of selectivity. Having stated that, the Grignard reagent could be quite sluggish to react and long reaction times or even elevated temperatures were required. Almost a century later, innovations from the Knochel group have led to greatly enhanced reactivities of this monometallic reagent by the seemingly simple addition of LiCl to solutions of RMgX.[8, 33] Turbo-Grignard reagents of the type "$R_2NMgCl{\cdot}LiCl$" (where $NR_2$ = $i Pr_2N$ or TMP) have captured widespread interest amongst the community of synthetic chemists due to their enhanced kinetic basicity leading to the magnesiation of substrates previously untouched by conventional Grignard reagents.

The methodology is further enhanced by high functional group tolerance and excellent regioselectivities observed with a number of aromatic and heteroaromatic molecules as well as by the fact that they are relatively easy to prepare by combining Grignard reagents with LiCl. By way of example, **Scheme 1.9** shows the regioselective metallation and further reaction with an electrophile of a pyrimidine derivative. Following inverse addition of the pyrimidine to a solution of "(TMP)MgCl·LiCl" and trapping with iodine, the product was isolated in 67% yield.

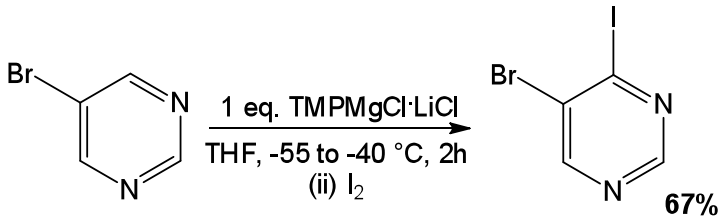


**Scheme 1.9:** Regioselective magnesiation of a pyrimidine derivative and quench with iodine.

Significantly, Knochel has recently shown that the turbo-Grignard reagent can be applied on a multigram scale (80 – 100 mmol) with yields comparable with small scale reactions (1 – 2 mmol).[34] The importance of this bimetallic reagent is further underlined by the fact that it is now commercially available as a solution in THF. Whilst the extent of applicability of the turbo-Grignard reagent was extensively probed, the structural make-up of the reagent itself remained in the dark until 2008, when its structure was revealed.[35] Preparation of the reagent, either by Knochel's pathway of mixing *i*PrMgCl·LiCl with TMP(H) in THF or by mixing $MgCl_2$ with LiTMP in THF, led to the isolation and characterisation of the lithium magnesiate $[(THF)_2Li(Cl)_2Mg(THF)(TMP)]$ (**Scheme 1.10**).[35]

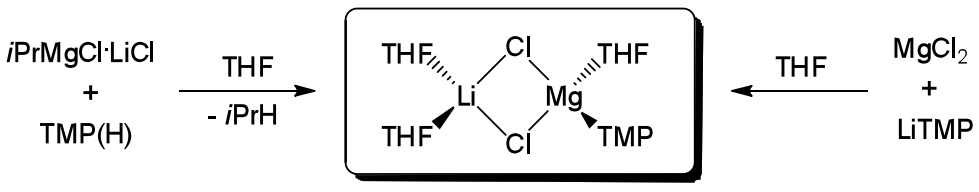


**Scheme 1.10**: Synthesis of the structurally defined turbo-Grignard reagent $[(THF)_2Li(Cl)_2Mg(THF)(TMP)]$.

Elucidation of the structure of the turbo-Grignard reagent allows some insights into the magnesiating ability of the base. For example, the reagent is a molecular species and is not a salt. Also, the active TMP ligand binds to Mg and not Li showing that when it reacts with a substrate the deprotonation is a true magnesiation. As the Mg-TMP bond is terminal, only one bond needs to be broken to release the active base. Inspection of the Mg atom shows it to be coordinatively saturated; however, the solvating THF molecule is potentially labile which could facilitate the coordination of an aromatic substrate prior to magnesiation. Finally, the 'ate character of magnesium ($LiMgR_3$ can be considered "$Li^+MgR_3^-$"), increased by the presence of strongly electronegative ligands, could be key rationale for the augmented reactivities of these bases.

Recently, a study analysing the composition of this product in THF solutions using diffusion-ordered NMR spectroscopy (DOSY) (*vide infra*) shed new light on the true constitution of these reagents in solution.[36] This methodology is comparable with chromatography in NMR terms, whereby individual components present in solution can be identified and their sizes estimated, which are inversely proportional to their diffusion coefficients, (*D*).[37] Although the exact solution structure of this mixed-metal reagent cannot be unequivocally established, these studies conclude that the solid-state structure is not retained in solution and that the lithium- and magnesium-containing species do not form strongly contacted ion-pairs, and a solvent separated ion-pair structure where Li is solvated by THF molecules is probably more accurate.[36]

A discussion of deprotonative metallation with respect to complex metallators could not be concluded without mentioning the "superbase". The addition of an alkali metal alkoxide MOR (M = Na, K) to an organolithium reagent LiR' leads to the class of metallators known as Lochmann-Schlosser reagents (LiR'-MOR), so named because of the independent simultaneous reporting by Lubomir Lochmann and Manfred Schlosser in the mid-1960s.[38] The increased basicity found by the presence of an alkoxide had been reported twenty years previously by Morton *et al*, who applied the "alkoxide effect" to polymerisation reactions. Morton observed an

increase in reaction rate and higher yields of metallated product with the addition of sodium isopropoxide, or potassium isopropoxide, to a suspension of the already highly basic *n*-pentylsodium.[39] Notably, it was also found that this combination of *n*-pentylsodium with sodium isopropoxide could metallate ethene directly to vinyl sodium.[40] Despite the work of Morton, the "alkoxide effect" lay dormant for 20 years until rediscovered and refreshed by Lochmann and Schlosser. The Lochmann-Schlosser reagent, commonly known as LIC-KOR, which pairs *n*-butyllithium with potassium *t*-butoxide, can be described as a "superbase" due to the dramatic enhancement of reactivity when compared to a mixture of an alkyllithium with a lithium butoxide. Indeed, the reactivity can be increased by a factor of more than $10^6$.[41] The reactivity of LIC-KOR can be considered intermediate between *n*-butyllithium and *n*-butylpotassium, but, unlike *n*-butylpotassium, LIC-KOR is stable in THF at -75 ºC.[42] **Table 1.1** shows some examples of the greater metallating power of the superbase compared to pentylsodium.

**Table 1.1:** Metallation of hydrocarbons by pentylsodium or a superbasic mixture[42]

| Metallation reaction | Metallator | Conditions | Quench | Yield/% |
|---|---|---|---|---|
| 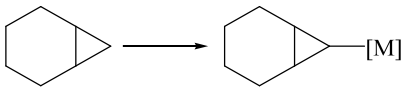  | $NaC_5H_{11}$ | Petroleum ether, 100 h, 25 ºC | $CO_2$ | 3 |
| | $NaC_5H_{11}$/ KO*t*Bu | Petroleum ether, 50 h, 25 ºC | $CO_2$ | 30 |
| 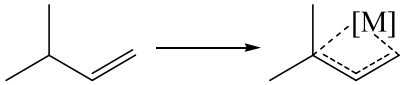  | $NaC_5H_{11}$ | Petroleum ether, 24 h, 25 ºC | $CO_2$ | 0 |
| | $LiC_4H_9$/ KO*t*Bu | THF, 1 h, -55 ºC | $CO_2$ | 74 |

In the metallation of low acidity C-H bonds, as shown above, the superbase is an excellent reagent; however, in the search for a metallator with high functional group tolerance the superbase is often too aggressive and its synthetic utility is therefore limited. Despite the importance of these mixtures, the constitution of these reagents in solution still remains hidden.

### 1.4.2 Metal-halogen exchange reactions

Along with deprotonative metallation reactions, halogen-metal exchange processes constitute a cornerstone methodology in organic synthesis and amongst the most

powerful methods for the functionalisation of aromatic molecules. These reactions involve the activation of a C-X bond (where X is usually I or Br), which is transformed to a more reactive C-M bond, in a single step (**Scheme 1.11**). This methodology can offer a greater regiospecific control in comparison with deprotonative metallation, as the resultant location of the metal is governed by the halogen position, in contrast to the multitude of carbon-hydrogen bonds often available in organic molecules for deprotonation reactions.

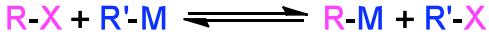


**Scheme 1.11:** General equation showing halogen-metal exchange.

As shown in **Scheme 1.11**, halogen-metal exchange reactions are an equilibrium process, whereby the formation of the more stable, less basic, organometallic species will be favoured.[43] If the equilibrium towards the exchange product is only moderately favourable, the newly formed organometallic species can react with the unconsumed precursor organo-halide species, resulting in the Wurtz coupled product and the high lattice energy metal-halide product (**Scheme 1.12**).

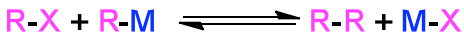


**Scheme 1.12:** General equation showing the Wurtz product, a possible side reaction from halogen-metal exchange.

Unwanted side reactions can be suppressed by the addition of two equivalents of organometallic reagent. Thus, the addition of a second equivalent of *t*-butyllithium reacts with the concomitant *t*-butyl iodide generated during the exchange reaction to yield lithium iodide and isobutylene. Subsequent quench with benzophenone gives the desired product in *ca.* 90% yield (**Scheme 1.13**).[44]

Exchange of a C-X bond for a M-C bond is a kinetic process, as such these reactions are usually carried out at low temperatures to favour this fast exchange over competitive side reactions such as deprotonative metallation and addition reactions. A number of factors can control the rate of the halogen-metal exchange reaction.

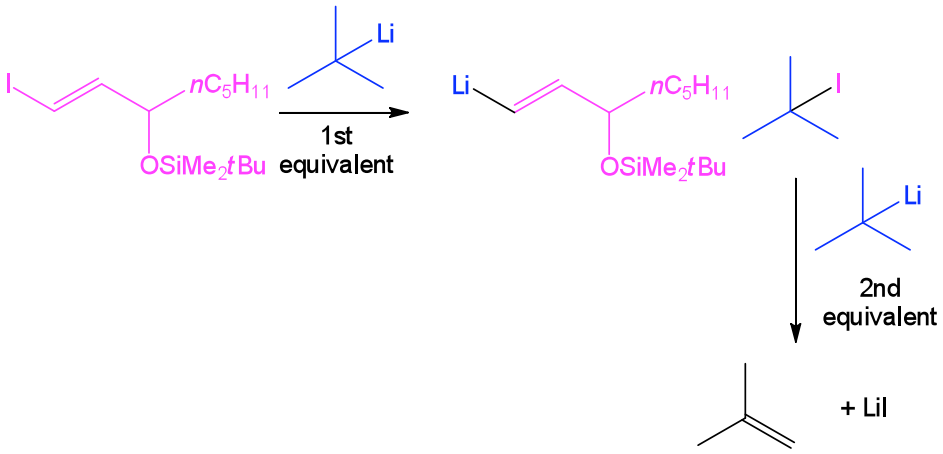


**Scheme 1.13:** Use of two equivalents of *t*BuLi in a halogen-metal exchange reaction.

Firstly, the identity of the halogen influences the reaction rate, with reactivity of the order I > Br > Cl > F observed. Bromine- and iodine-lithium exchange will occur widely and as such ArBr and ArI substrates are generally applicable in exchange reactions. Chlorine-lithium exchange would be advantageous due to the wide availability and low cost of Ar-Cl compounds; however, Cl-Li exchange has limited synthetic utility due to the strength of the Cl-C bond, with competing metallation (hydrogen-lithium exchange) reactions usually being more favourable.[45] Activation of a C-F bond is, at present, best accomplished by an organometallic reagent in the presence of a transition metal catalyst.[46] In addition, the choice of solvent influences the rate of reaction, with ethereal solvents (which favour the deaggregation of the organometallic species) accelerating the exchange, even at the extremely low temperatures employed to favour the kinetic halogen-metal exchange product over other competing processes, for example deprotonation reactions.[47]

Application of the halogen-metal exchange reaction as an intermediate in regiospecific functionalisation of organic molecules dates from the late 1930s when Wittig described the bromine-lithium exchange of dibromo-dimethoxybenzene with PhLi, and contemporaneously Gilman reported the lithiation of 2-bromoanisole by *n*-BuLi followed by carbonation in 47% yield.[48] The regiospecificity, coupled with the functional group tolerance observed due to the speed of reaction, makes this methodology a valuable addition to the synthetic chemist's toolkit; however, the conditions that are necessitated by the reaction, namely low temperatures (usually

-78 ºC) and use of ethereal solvents, limits its wider use in scaled-up industrial syntheses due to the restrictive expense of large-scale cryogenics and the process safety concerns over the hazardous properties of ethers. Recent research has therefore focussed on carrying out this pivotal reaction under more environmentally friendly, mild conditions and the use of alternative solvents, whilst maintaining the appeal of the regiospecific control that these reactions offer.

Moving away from monometallic halogen-lithium exchange reactions, the past decade has witnessed significant advances towards the goal of increased functional group tolerance under mild conditions in halogen-metal exchange reactions by the application of selected complex metallators (*vide supra*). Specifically, the 'ate complexes $LiMR_3$ and $Li_2MR_4$, where M is typically Mg or Zn, and a derivation of Knochel's turbo-Grignard reagent, *i*PrMgCl·LiCl, have come to the fore as key bimetallic reagents for this purpose (**Figure 1.5**).

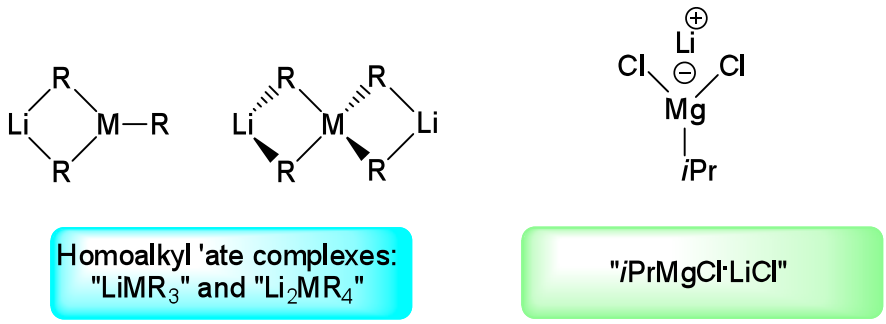


**Figure 1.5:** Selection of complex metallators successfully employed in halogen-metal exchange reactions.

Although neutral diorganozinc compounds were first synthesised by Frankland in 1848, constituting the oldest "main-group" organometallic reagent known,[49] their relative low reactivity caused them to be generally dismissed in favour of well established, more polar, organolithium reagents when performing halogen-metal exchange reactions. As recently as 2004, neutral organozinc compounds of the type $R_2Zn$ were considered very poor reagents towards aromatic iodides until Knochel demonstrated that employing a solvent mixture of $Et_2O$/NMP 1:10 (NMP = *N*-methylpyrrolidinone) resulted in the formation of the aryl(alkyl)zinc product in yields greater than 90%.[50] Moreover, the remaining alkyl group can be activated towards exchange with a further molecule of ArI by adding catalytic amounts of an

inorganic salt, such as Li(acac) (10 mol%) which is proposed to form a mixed-metal reagent *in situ* by cocomplexation with $ZnR_2$ (**Scheme 1.14**). The mild reaction conditions allow for a range of sensitive organic functional groups to be tolerated, for example ketones, isothiocyanates and aldehydes.[50] The proposed nucleophilic catalysis of the iodine-zinc exchange reaction is shown in **Scheme 1.14**.[50]

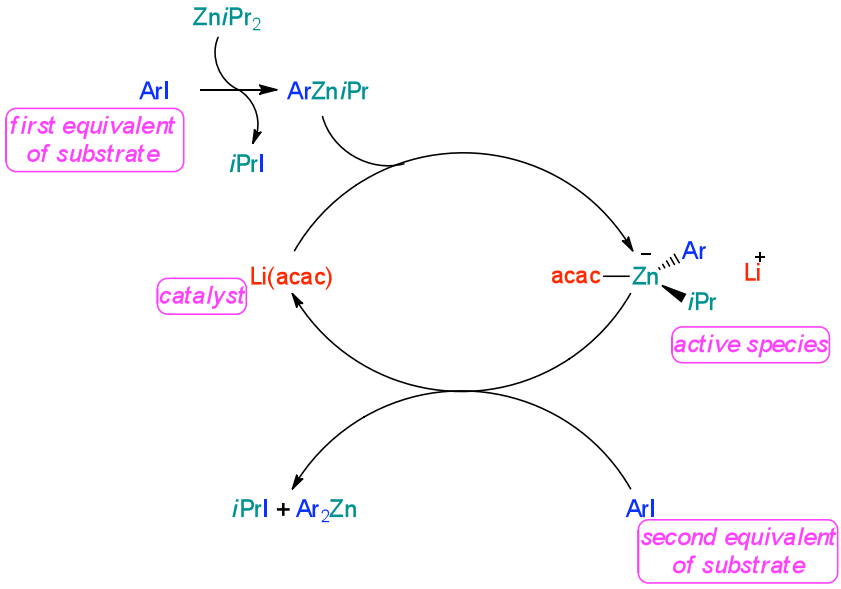


**Scheme 1.14**: Catalytic cycle of the iodine-zinc exchange reaction.

Following transfer of the first *i*Pr group and concomitant formation of *i*PrI and the aryl(alkyl) zinc product, Li(acac) complexes with the diorganozinc generating the active species. The key step in the activation of the second *i*Pr group is the formation of the active zincate species which allows for the preparation of a highly functionalised diaryl zinc derivative. The preparation of arylzinc compounds is particularly important due to the ability of these species to take part directly in Negishi cross-coupling reactions.[51] At this stage it is noteworthy to mention that the formation of a bimetallic reactive species was postulated, but no tangible structural or spectroscopic evidence was provided.

In 1994 Kondo demonstrated the high functional group tolerance of the triorganozincate $LiZnMe_3$ by subjecting functionalised aromatic iodides to halogen-zinc exchange.[52] As shown in **Scheme 1.15**, the bimetallic system efficiently

zincates a number of substrates in good yields, even in the presence of sensitive organic functionalities, such as unprotected ester and nitro groups, although low temperatures are required (-78 °C).

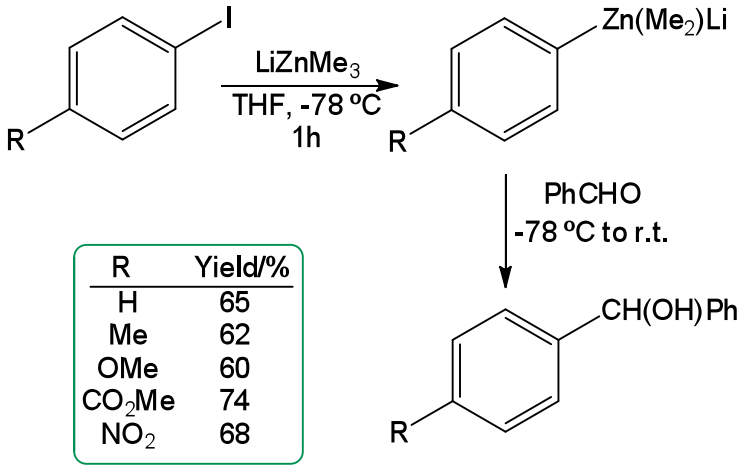


| R | Yield/% |
|---|---|
| H | 65 |
| Me | 62 |
| OMe | 60 |
| $CO_2Me$ | 74 |
| $NO_2$ | 68 |

**Scheme 1.15**: Iodine-zinc exchange using a mixed Li-Zn reagent followed by reaction with benzaldehyde.

This protocol appears to exhibit poor atom economy, whereby only one carbanionic methyl group is utilised, and potentially "wastes" the two remaining methyl groups of the zincate. Shortly after, the same group then reported that moving from lithium trimethylzincate to the stoichiometric variant dilithium tetramethylzincate, enabled the activation of stronger (and therefore less reactive) C-Br bonds, although the yields were moderate (**Scheme 1.16**).[53]

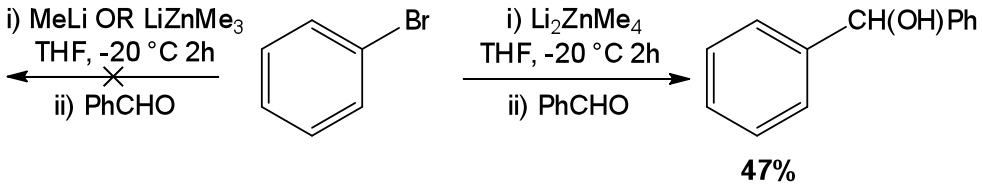


**Scheme 1.16:** Comparison of the bromine-zinc exchange ability of lithium trimethylzincate and dilithium tetramethylzincate, followed by trapping with benzaldehyde.

This synthetic procedure could be upgraded by using the more reactive $Li_2Zn$*t*$Bu_4$.[9] Thus, the relevant halogen-metal exchange product could now be isolated in

excellent yields (74%) after 2 hours. In addition, the dilithium tetra-*t*-butylzincate was also shown to be compatible with esters, amides and acidic functional groups (*i.e.* N-H or O-H), achieving up to quantitative yields following trapping with various electrophiles (**Scheme 1.17**).

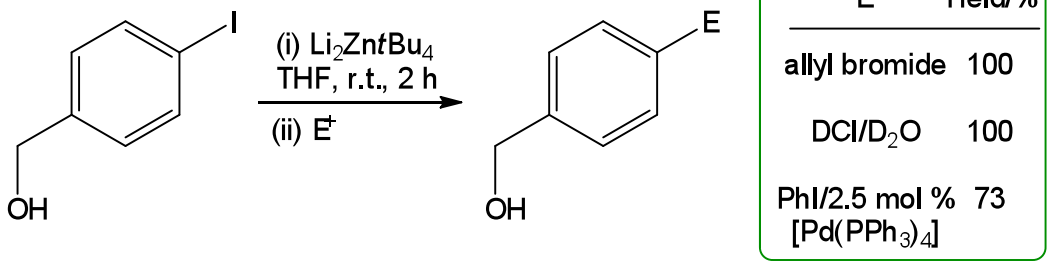


**Scheme 1.17**: Iodine-zinc exchange using $Li_2Znt Bu_4$ followed by reaction with various electrophiles.

Interest in organomagnesium reagents to effect halogen-metal exchange reactions has witnessed a resurgence in the past few decades. Being less polar than their organolithium analogues, organomagnesium reagents react considerably more slowly, thus leading to higher temperatures required to carry out the reaction and under these conditions the functional group tolerance of these reagents can be greatly decreased. In 2000, Oshima reported the first application of lithium magnesiates to promote direct Mg-X exchange. These bimetallic species were able to smoothly exchange with both aryl iodides and aryl bromides at low temperatures, including examples of "non activated" aryl groups, that is to say, with substrates not bearing an electron-withdrawing group. For example, the reaction of $LiMgiPrBu_2$ with bromobenzene proceeded quantitatively to the corresponding arylmagnesiate. A selection of bromine-magnesium exchange reactions and subsequent trapping with electrophiles is shown in **Scheme 1.18**.[54]

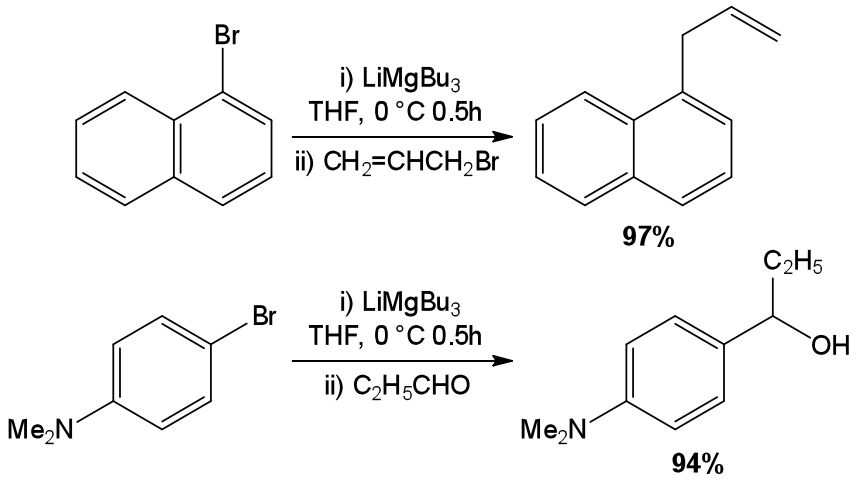


**Scheme 1.18:** Representative examples of the application of a lithium trialkylmagnesiate in bromine-magnesium exchange reactions followed by trapping with an electrophile.

Mongin extended the methodology to include bromoquinolines by reacting with $LiMgBu_3$ in toluene at -10 °C, thereby generating a convenient access to functionalised quinolines after quenching the resulting organomagnesium derivatives with several electrophiles in good yields (**Scheme 1.19**).[55]

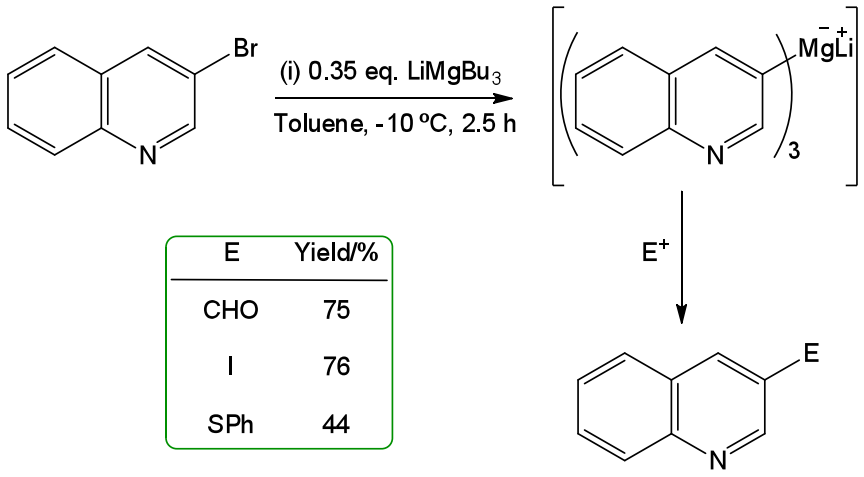


| E | Yield/% |
|---|---|
| CHO | 75 |
| I | 76 |
| SPh | 44 |

**Scheme 1.19:** Functionalisation of quinolines *via* bromine-magnesium exchange followed by an electrophilic quench.

The polybasicity of the complex metallator is also demonstrated as only 0.35 equivalents of base are employed with yields of up to 75% attained. Due to the relative stability of these organometallic species, these reactions can be performed at

-10 ºC while still suppressing problematic side reactions, unlike lithium-bromine exchange which requires temperatures of -78 ºC. In this report the authors proposed the formation of the tris(aryl) magnesiate shown in brackets in **Scheme 1.19**; however, no characterisation (either spectroscopic or structural) was provided.[55]

Another major landmark in this area came from Knochel with his breakthrough publication in 2004 on the effect of adding LiCl to *i*PrMgCl. The stoichiometric addition of lithium chloride to isopropylmagnesium chloride led to increased conversions and rate enhancements of halogen-metal exchange when compared with carrying out the same reaction in the absence of the salt. The resulting reagent, *i*PrMgCl·LiCl, is activated towards halogen-metal exchange reactions in an analogous fashion with the closely related amido reagent (TMP)MgCl·LiCl being activated towards deprotonative metallation reactions (*vide supra*). For example, 4-bromoanisole undergoes a poor 18% conversion after 68 hours at room temperature in the presence of *i*PrMgCl alone; however, when one molar equivalent of LiCl was added a 70% conversion was achieved.[8a] Knochel has shown this methodology to be applicable to a wide selection of bromobenzenes[8a] and heterocycles,[56] including unprotected uracil derivatives.[57]

This key breakthrough has propelled the applications of Grignard reagents in synthesis, and has opened a new efficient route to prepare highly functionalised organometallic reagents. Significantly, this relevant mixed-metal reagent is now commercially available as a solution in THF.

### 1.4.3 Nucleophilic addition

'Ate compounds have also shown an enhanced nucleophilic power, which finds widespread applications in addition reactions, as for example, nucleophilic alkylations of ketones and aldehydes. When performing 1,2-addition protocol on ketones, organolithium and Grignard reagents can lead to the formation of the reduction product (through β-hydride elimination) or aldol dimerisation product (if

α-hydrogens are present) in competition with the desired 1,2-addition, giving an overall reduction in yield and potential purification problems.

Studies by Ishihara examined the treatment of acetophenone with homometallic BuLi, BuMgCl and $MgBu_2$ and compared these results with the application of mixed-metal lithium magnesiate $LiMgBu_3$ to the same substrate.[58] The results, summarised in **Table 1.2**, demonstrate the high selectivity and nucleophilicity of the magnesiate reagent, which completely suppresses the competing side reactions and gives the product in an excellent 82% yield. In contrast, the homometallic reagents display poorer selectivity, with a mixture of products formed in each case, and overall reduced nucleophilicity, with a maximum yield of the desired product a modest 62% for BuLi, 50% for BuMgCl and 48% for $MgBu_2$.

**Table 1.2**: Addition to acetophenone by various reagents.

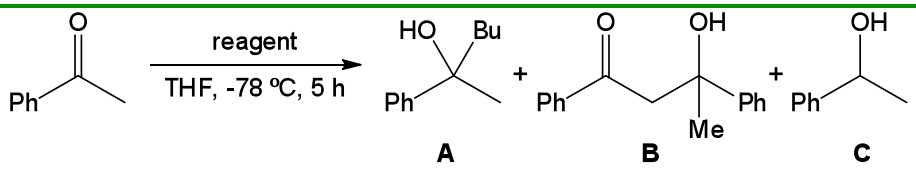


| Reagent | A/% | B/% | C/% |
|---|---|---|---|
| BuLi | 62 | 7 | 0 |
| BuMgCl | 50 | 9 | 8 |
| $MgBu_2$ | 48 | 27 | 20 |
| $LiMgBu_3$ | 82 | 0 | 0 |

This methodology proved to be effective for a number of alkyl or aryl lithium magnesiates $LiMgR_3$, R = Bu, Ph, Me, Et in yields of 64-99% when added to benzophenone.[58]

Changing the secondary metal in the 'ate system from magnesium to zinc gives a "softer" nucleophile in the form of $LiZnR_3$ and complexes of this type have emerged as selective reagents for the conjugate 1,4-addition to α,β-unsaturated compounds. In 1977 Isobe reported the use of a variety of triorganozincates in the conjugate addition

to a cyclopentadien-1-one derivative as shown in **Table 1.3**. The triorganozincate systems, prepared by the metathesis method of adding a ratio of 1:3 RLi to $ZnCl_2$ in THF, showed the protocol could be applied to primary, secondary and tertiary alkyl groups; although yield did suffer with increasing bulk, the selectivity of the reaction remained as the 1,4-addition product. Problems were encountered with the phenyl and acetylenic zincates, which the authors attribute to the "stabilised covalent carbon-zinc bonds". Following on from this pioneering work, the use of lithium triorganozincates for performing conjugate addition reactions has grown steadily.[59]

**Table 1.3:** Scope of triorganozincate reagents for 1,4-addition.

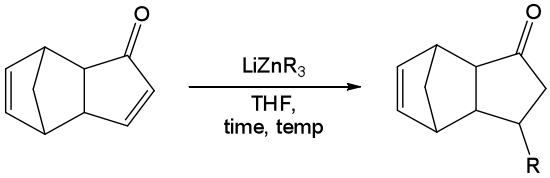


| R | Time/mins | Temp/°C | Yield/% |
|---|---|---|---|
| Me | 30 | 0 | 92 |
| *n*Bu | 30 | -78 – 0 | 92 |
| *s*Bu | 60 | -78 | 66 |
| *t*Bu | 60 | -78 | 58 |
| Ph | 180 | -78 | 15 |
| 1-butynyl | 180 | -78 | 0 |

### 1.4.4 Transition metal catalysed cross-coupling reactions

Metal-catalysed cross-coupling reactions play a pivotal role in the creation of C-C or C-N bonds.[60] The importance of this class of reaction was recognised in 2010 by the award of the Nobel Prize in Chemistry to Heck, Suzuki and Negishi for their role in utilising Pd-catalysed cross-coupling reactions in organic synthesis.[61] A general mechanism of the reaction is shown in **Scheme 1.20**: following oxidative addition of the substrate (usually an aromatic halide) to the Pd catalyst transmetallation occurs

with the coupling partner and finally reductive elimination regenerates the catalyst to generate the relevant cross-coupled product.

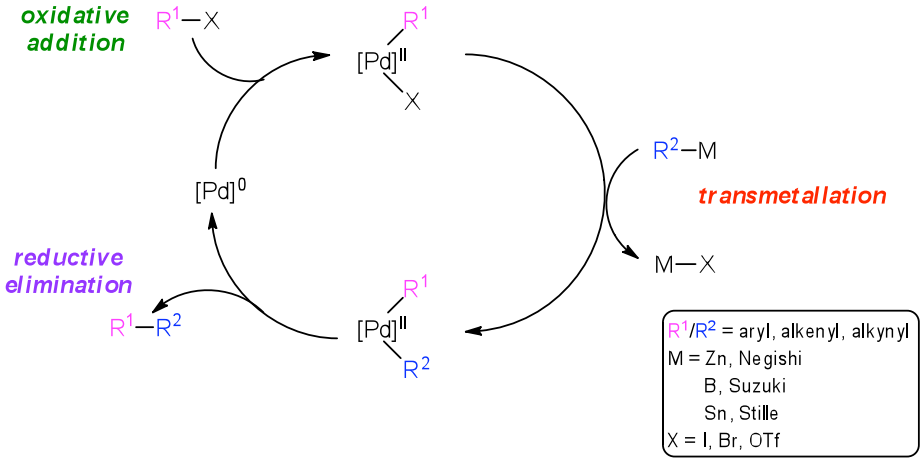


**Scheme 1.20:** General scheme for the Pd-catalysed cross-coupling reaction.

As can be seen in the above scheme, the Negishi cross-coupling reaction uses zinc in the transmetallation step and as such an organometallic fragment already bearing zinc is predisposed to undergo a cross-coupling reaction.[62]

A systematic study by Hevia and co-workers combined the application of mixed-metal systems to metal-halogen exchange in the first instance using a magnesium zincate and then further functionalization of the intermediate by Pd-catalysed Negishi coupling. Reaction of the structurally elucidated solvent-separated ion pair (SSIP) dimagnesium trisalkyl zincate with 4-iodotoluene revealed all three *t*-butyl groups were activated towards the exchange process, and the resulting trisaryl zincate was subjected to Pd-catalysed Negishi cross-coupling methodology giving the final product in excellent yields of up to 93% (when isolated crystals of the trisaryl zincate were used in the cross-coupling reaction), as shown in **Scheme 1.21**.[63]

This reaction displays excellent atom economy as all three alkyl arms are initially activated towards iodine-zinc exchange resulting in the trisaryl zincate intermediate, which has proved to be an efficient transmetallating reagent for the subsequent cross-coupling step.

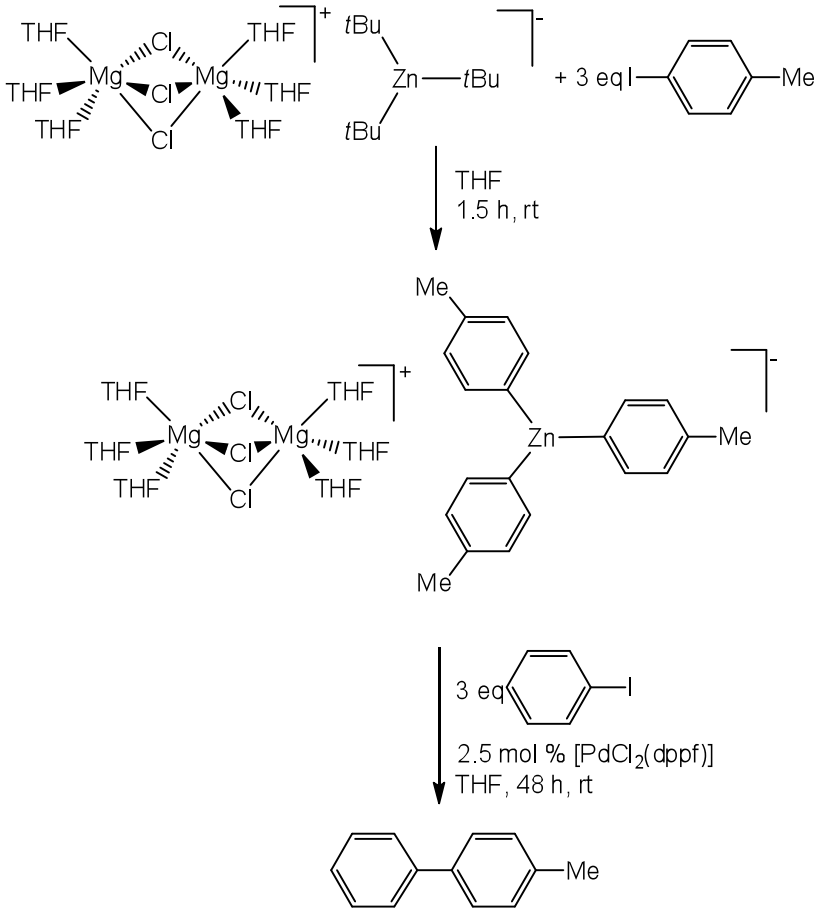


**Scheme 1.21:** Formation of trisaryl zincate followed by Pd-catalysed cross-coupling reaction.

## 1.5 Elucidation of crystal structures and introduction to Diffusion-ordered Spectroscopy (DOSY) NMR

### 1.5.1 Solid-state determination: single crystal X-ray diffractometry

When considering organometallic compounds, arguably the most important method of investigating the interactions of the metal and its surrounding ligands in the solid-state is through X-ray crystallographic analysis. Beginning in 1963 with the publication of the single crystal X-ray determination of ethyllithium[64] and closely followed by Weiss's X-ray powder diffraction studies of methyllithium,[65] this technique immediately paid dividends to the scientific community by revealing both compounds to be aggregates of tetramers. Methyllithium forms a distorted $Li_4C_4$

cube with the corners occupied by lithium atoms alternating with carbon atoms (**Figure 1.6**). Each carbon rests above a face of the $Li_4$ tetrahedron and interacts *via* three short contacts to three of the lithium atoms in its tetramer, and also forms a longer contact with a neighbouring tetramer, giving carbon a coordination number of 7. This arrangement leads to a body-centred cubic lattice and each tetramer interacts with its the eight neighbours. The low volatility and nonmelting character of $(LiMe)_4$ is a result of this extended three-dimensional arrangement of molecules.

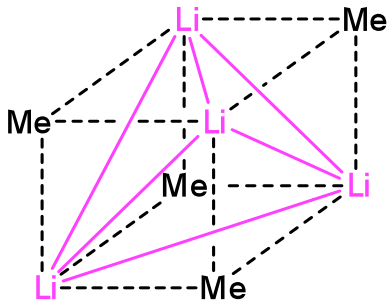


**Figure 1.6:** Chem Draw representation of a tetrameric unit of $(LiMe)_4$. Pink lines indicate the $Li_4$ distorted tetrahedron and do not represent bonds

Weiss, a true pioneer in this area of main group chemistry, has also published the structures of methyllithium-containing methylsodium,[66], pure methylsodium,[67] and methylpotassium,[68] as well as the heavier alkali metal analogues with rubidium and cesium.[69]

In general, the number of solvent-free polar organometallic compounds structurally characterised is relatively scarce, the main reason being their tendencies to form polymeric arrangements which are very insoluble in non-polar solvents such as hexane or benzene resulting in difficulty in their crystallisation. Addition of an ether or tertiary amines to an organometallic species changes the structure and therefore the reactivity of the compound. For example, *n*BuLi exists as a hexamer in hydrocarbon solvents[70] and is inert towards benzene; however, addition of the didentate amine donor TMEDA leads to quantitative deprotonation of the arene molecule to form PhLi·TMEDA.[71] The solid-state structure of TMEDA-solvated *n*BuLi was elucidated simultaneously in 1993 by Mulvey[72] and Williard.[73] Addition of substoichiometric amounts of TMEDA to a solution of *n*BuLi in hexane

resulted in partial cleavage of the hexameric structure of *n*BuLi to yield the formation of TMEDA-bridged $(n\text{BuLi})_4$ tetramers, adopting a zig-zag polymeric structure.[72] Williard also reported the crystal structure elucidation of the dimer $(n\text{BuLi}\cdot\text{TMEDA})_2$ when a slight excess of the amine is added, with TMEDA acting in its more familiar role as a chelating ligand coordinating to the alkali metal.[73] **Table 1.4** summarises these findings.

**Table 1.4:** Aggregation state of *n*BuLi with varying degrees of solvation with TMEDA

| Organometallic compound | Equivalents of TMEDA | Solvent | Species |
|---|---|---|---|
| *n*BuLi[70] | - | Hexane | Hexamer |
| $[(n\text{BuLi})_4(\text{TMEDA})]_\infty$ [72] | 0.25 | Hexane | Polymer of tetramers |
| $(n\text{BuLi}\cdot\text{TMEDA})_2$[73] | 1.5 | Hexane | Dimer |

Turning to mixed-metal compounds, Weiss has also made many valuable contributions reporting the structures of several 'ate complexes, including the tetramethylmagnesiate $[(\text{TMEDA})_2\text{Li}_2\text{MgMe}_4]$[7] and the tetraphenylmagnesiate $[(\text{PMDETA})_2\text{Na}_2\text{MgPh}_4]$[74] which both display a M···Mg···M (M = Li or Na) linear arrangement with the metals connected by the alkyl ligands and each alkali metal coordinated to a Lewis donor (TMEDA or PMDETA) (**Figure 1.7**).

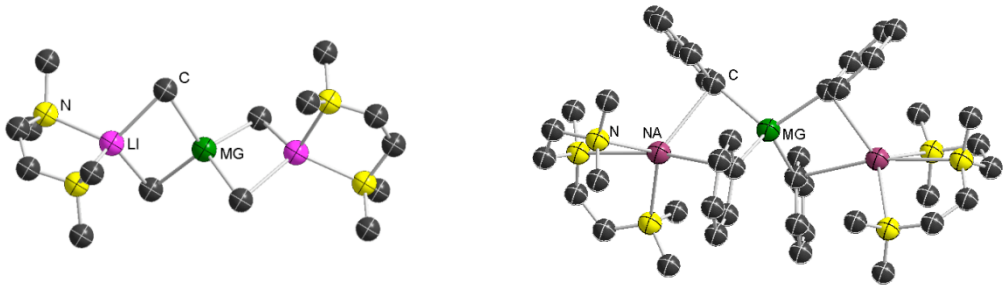


**$[(\text{TMEDA})_2\text{Li}_2\text{MgMe}_4]$** **$[(\text{PMDETA})_2\text{Na}_2\text{MgPh}_4]$**

**Figure 1.7:** Molecular structures of $[(\text{TMEDA})_2\text{Li}_2\text{MgMe}_4]$[7] and $[(\text{PMDETA})_2\text{Na}_2\text{MgPh}_4]$.[74] Hydrogen atoms have been omitted for clarity.

Of particular note at this juncture is that despite the number of structures reported by Weiss and others in the past three decades,[6] to date the structures of unsolvated alkyl alkali-metal magnesiates have remained elusive.

### 1.5.2 Structures in solution: diffusion-ordered spectroscopy (DOSY)

When considering the structure of an organometallic species in solution, the structure determined by X-ray crystallography may not necessarily be present exclusively, it may be one of a number of components or, indeed, it may not be present at all as the crystallised product is "commonly believed to represent the least soluble derivative in the pot".[75] As such, determination of the degree of aggregation of the organometallic species in solution is complementary to the solid-state structure. The tool most commonly employed when probing the structure of a species in solution is nuclear magnetic resonance (NMR). This powerful technique is ubiquitous in chemistry, with information readily available about the chemical environment of a molecule from chemical shift and multiplicity data acquired from even the simplest 1D NMR spectra. A detailed picture of the molecule can be built up using a combination of 1D and 2D NMR experiments, for example correlation spectroscopy (COSY) which allows for the determination of atoms that are spin-spin coupled to each other, Heteronuclear Multiple Quantum Coherence (HMQC) which indicates connectivity between two different nuclear species, and nuclear Overhauser effect spectroscopy (NOESY) which establishes "through space" interactions.[76]

Another important NMR method for the characterisation of molecules in solution, although not as extensively explored as the methods mentioned above, is diffusion ordered spectroscopy (DOSY). Expanding on pulsed gradient spin-echo (PGSE) diffusion spectroscopy developed in the 1960s,[77] Johnson developed a 2D NMR experiment in 1992 where one dimension shows the familiar chemical shift information and the second dimension separates the species in solution by their diffusion properties.[78] This technique, known as DOSY, has been colloquially described as "chromatography by NMR" and can be used to identify different aggregates present in solution. For example, complex mixtures of natural products

geraniol, camphene and quinine can be resolved,[79] in addition, recent reports have shown that the binding of a drug candidate in a mixture of test compounds to a target molecule can be assessed.[80]

Pioneering work by Williard at the turn of the century saw the first example of DOSY NMR spectroscopy being used to assess the differing aggregates of an organolithium reagent in solution by employing the technique with *n*BuLi.[81] Since then Williard has remained at the forefront of this research and seminal work by his group has shown that there is a linear correlation between the measured diffusion coefficients and the formula weights of the aggregates in solution.[37, 82] As such, using simple organic hydrocarbons with known formula weight as references, a calibration curve can be plotted and the formula weight of unknown aggregates in solution can be estimated in terms of their formula weight or volume. The internal standards must follow certain criteria, namely they must be inert to the other molecules in solution, their chemical shifts should not overlap, they should not coordinate to complexes within solution, they should be soluble in the NMR solvent and they should cover a large molecular weight distribution.[37] This technique was used to calculate the formula weights of the mixed aggregates species formed during the asymmetric addition of *n*BuLi to aldehydes.[83]

Recent applications of DOSY NMR towards organometallic reagents in solution have succeeded in shedding some light on the constitution of these species on addition of donor substrates, for example the deaggregation of trimethylsilylmethyl lithium $[LiCH_2SiMe_3]_6$ to ether solvated tetramers with $Et_2O$ and dimers with chelating dimethoxyethane[84] or $Me_2N(CH_2)_2OMe$.[85]. Although $^1H$ DOSY is most commonly used, other nuclei can be used. $^{13}C$ DOSY was used in the study of THF-solvated LDA compounds,[86] and $^{31}P$ NMR was used to investigate the formula weights in solution of a number of manganese complexes.[87]

The technique can be applied to bimetallic systems and Mulvey *et al* have investigated the active species carrying out metallation reactions in the presence of putative reagent "$LiZn(TMP)_3$", which appears to be a cocomplex between LiTMP

and two equivalents of LiCl with a degree of interaction from TMEDA (*vide supra*).[25] Further, they have examined turbo-Grignard reagents "$R_2NMgCl{\cdot}LiCl$" ($R_2N$ = $i$Pr$_2$N, TMP) by the same means, revealing a solvent-separated ion pair (SSIP) is most likely present with these complexes,[36] in contrast to the contacted ion pair (CIP) solid-state TMP structure [$(THF)_2Li(Cl)_2Mg(THF)(TMP)$] (*vide supra*).[35] The subtle changes between addition of tridentate donors PMDETA and diglyme to mixed-metal "$LiZnMe_3$" produces CIP and SSIP structures respectively in the solid-state, which have been shown to be retained in solution by $^1$H DOSY NMR experiments.[88]

### 1.6 Aims and structure of this report

A general overview of some of the most significant developments in mixed-metal chemistry has been presented here within the context of some fundamental organic transformation reactions, for example deprotonative metallation and halogen-metal exchange reactions; however, this introduction is not intended to be considered an exhaustive study of this important and flourishing area of modern chemistry. Despite some prominent organic studies, the identity of many of the key organometallic reagents involved in most of these reactions remains elusive.

Building on these important precedents, the first part of this thesis will focus on advancing the understanding of the effect of donor solvents on the structure and composition of homoleptic alkali metal magnesiates containing alkyl ligands by assessing the cocomplexation reactions of alkali metal alkyls MR (where M = Li, Na, K) with $MgR_2$ (R = $CH_2SiMe_3$, the monosyl group). Thus, **Chapters 2** and **3** will examine in detail the synthesis and structural authentication of a series of alkyl alkali metal magnesiates, including a variety of novel solvated lithium magnesiates, as well as the first examples of a solvent-free alkali metal magnesiates. These new species will be characterised using a combination of X-ray crystallography and multinuclear NMR spectroscopy, including DOSY NMR, which provides new insights into the real constitution of these organometallic compounds in solution. **Chapter 4** then relates the structure of these bimetallic reagents with their ability to act as deprotonating reagents using the potassium magnesiate species as a case study. The

main focus of the second part of this thesis are alkali metal zincates, thus, **Chapter 5** will continue to explore the application of mixed-metal reagents in synthesis but will concentrate on the cooperative effects of lithium and zinc, unveiling new bimetallic approaches for the functionalization of pyrazine as well as delineating a novel mild protocol for zinc-iodine exchange, with key reaction intermediates being structurally defined. **Chapter 6** will broaden the scope of substrates investigated by applying mixed-metal chemistry to the emerging area of N-heterocyclic carbenes and examine the ability of bimetallic reagents to functionalise N-heterocyclic carbene molecules through direct zincation. **Chapter 7** will conclude the findings from this body of work and look towards the future. Finally **Chapter 8** will describe the experimental techniques employed and the synthesis of all new compounds reported.

# Chapter 2: Synthesis, structural elucidation and DOSY NMR studies of homoleptic alkyllithium magnesiates: donor-controlled structural variations in mixed-metal chemistry

## 2.1 Introduction to alkali-metal magnesiate chemistry

The importance of organolithium reagents in the modern age would be difficult to underestimate; indeed, in excess of 95% of all natural product syntheses are subjected to a lithium-induced transformation along their synthetic sequence.[89] Li, the lightest metal, is an imperfect partner for its large (by comparison) organic fragment, and the extremely polar lithium-carbon bond gives rise to the high reactive qualities for which lithium is well known. The voracity with which lithium can react can be disadvantageous and low temperatures are often required for their use and this can be problematic on an industrial scale. From a synthetic standpoint, a severe drawback to these polar reagents is the poor selectivity in the presence of sensitive functional groups.

Looking to lithium's diagonal neighbour in the periodic table, magnesium in its own right offers several advantages to the synthetic chemist. Magnesium reagents can display simpler aggregation patterns in solution[90] when compared with their lithium counterparts.[91] Importantly, the less polar magnesium-carbon bond allows for greater selectivity and higher functional group tolerance under moderate conditions.[56b, 92]

As mentioned in **Chapter 1**, a significant advance in s-block metal-induced organic transformations has recently come from the marriage of lithium and magnesium together in the same molecular reagent. These bimetallic reagents have emerged as a selective and versatile family of compounds exhibiting unique chemical properties which cannot be replicated by either organolithium or organomagnesium reagents on their own.[10, 93]. These bimetallic reagents have witnessed a recent rise in popularity with applications in a myriad of fundamental organic transformations such as nucleophilic addition,[58, 94] halogen-metal exchange reactions[54-55, 95] or deprotonative metallation reactions to name a few.[14-18, 96]

Recent breakthroughs in this chemistry include Knochel's turbo Grignard reagents RMgCl·LiCl which allow direct magnesiation of highly functionalised aromatic molecules *via* magnesium-halogen exchange reactions without the need for cryogenic conditions.[8a],[56],[57] Mixed alkyl-amido magnesiates are also highly efficient, versatile bases in deprotonative metallation reactions exhibiting unique regioselectivities that cannot be reproduced by classical metallating reagents such as lithium amides as illustrated most remarkably in the unprecedented fourfold deprotonation of ferrocene, ruthenocene and osmocene by solvent-free sodium magnesiate [NaMg(N*i*Pr$_2$)$_3$].[97] Homoleptic alkyl magnesiates (which, depending on their stoichiometry, can be grouped as triorganomagnesiates MMgR$_3$ or tetraorganomagnesiates M$_2$MgR$_4$, where M = alkali metal, R = alkyl group) are also useful reagents, finding extensive application not only in magnesium-halogen exchange and deprotonation reactions but also in alkylation reactions of ketones due to their exceptional carbonucleophilicity.[58] Thus for example, LiMgBu$_3$ and Li$_2$MgBu$_4$ promote the selective deprotonation of sensitive heterocycles such as fluoropyridines, oxazoles or thiophenes, generating lithium arylmagnesiates which can then be trapped with electrophiles or used as organometallic precursors in Pd-catalysed cross-coupling reactions.[14-17] Related to these findings, several reports have shown the advantages of using these homoleptic mixed-metal reagents in magnesium-bromine exchange reactions of aromatic molecules,[4] allowing the use of milder reaction conditions to those required when organolithium reagents are employed, due primarily to the greater stability of the mixed-metal intermediates involved in the reactions. Some of these studies highlight the importance of the presence of Lewis donors such as TMEDA (*N,N,N',N'*-tetramethylethylenediamine) or THF in the reaction media for these reactions to take place. However, despite the important synthetic applications of these mixed-metal reagents, there is still a considerable lack of knowledge on their constitution (either in solution or in the solid-state), as well as in the role that different solvents or donor molecules can play in tuning their structure and/or reactivity. Thus, although the last few years have seen an increasing interest in the constitution of alkali-metal magnesiates, and despite their numerous synthetic applications, there very few examples of homoleptic alkyl lithium-magnesiates to have been structurally defined.[7, 98]

The two-pronged consideration of structure and reactivity is, as always, difficult to separate. Stalke recently described the *structure-reactivity* relationship as '*the "Holy Grail" of lithiumorganic chemistry*'[99] emphasising the difficulty of the quest involved but also hinting at the potential rewards of enlightenment associated with its discovery. Similarly, Schlosser states *'... no difference in organometallic reactivity patterns can be rationalised unless the metal and its specific interactions with the accompanying backbone, the surrounding solvent, and the substrate of the reaction, are explicitly taken into account. In other words, in order to understand* reactivity *we need a detailed knowledge of the* structures *involved.'*[42] again revealing the intrinsic relationship between structure and reactivity. In the quest for "better reactions" (for example, enhanced regioselectivity or greater functional group tolerance), too often the wider consideration of structure is overlooked and reagents are applied in an almost "hit and miss" way in a bid to blindly find one that works in what can be a wasteful trial-and-error fashion. In conjunction with the impressive reactivity and selectivity demonstrated by eminent synthetic chemistry research groups around the world, structural chemists have not been lax in the area of lithium magnesiates. In fact, seminal work by Weiss into the structure of 'ate complexes by means of X-ray crystallographic studies predates the current infusion of interest in the area.[6] Previous work by Mulvey *et al* on the molecular structure of these bimetallic reagents, including the recent elucidation of the turbo-Hauser base (TMPMgCl·LiCl) has greatly increased the understanding of these reagents.[35]

## 2.2 Novel research in alkali-metal magnesiate chemistry

Building on these pioneering contributions,[10] presented in this chapter is the synthesis and characterisation of new homoleptic lithium magnesiate reagents incorporating the monosyl ligand $CH_2SiMe_3$ in the presence of a variety of Lewis basic donors; tetrahydrofuran (THF), 1,4-dioxane, *N,N,N',N'*-tetramethylethylenediamine (TMEDA) and *N,N,N',N'',N''*-pentamethyldiethylene-triamine (PMDETA), which widens the knowledge of heterobimetallic chemistry by investigating the structural effects imposed by a variety of donors. The constitution of these bimetallic compounds has been assessed in both the solid-state and solution

using a combination of X-ray crystallographic studies and multinuclear NMR spectroscopy, including $^{1}$H diffusion-ordered ($^{1}$H-DOSY) NMR experiments which provide new insights into the real constitution of these organometallic compounds in solution and count towards the greater understanding of the unique reactivity displayed by 'ate reagents.

**Chapters 3** and **4** will extend the investigations to include the heavier s-block metals Na and K and will elucidate, for the first time, the novel structures of donor-free homoleptic alkali-metal magnesiates $[\{NaMg(CH_2SiMe_3)_3\}_\infty]$ and $[\{KMg(CH_2SiMe_3)_3\}_\infty]$ which display distinct extended 2D polymeric networks constructed exclusively of electron-deficient M-C bonds.

## 2.3 Donor controlled structural variations in homoleptic alkyl lithium magnesiate complexes

### 2.3.1 Preparation of starting materials

Synthetic endeavours towards the preparation of novel alkyl alkali-metal magnesiates began with the synthesis of the homometallic precursors $MgR_2$, NaR and KR (R = $CH_2SiMe_3$). $MgR_2$ was prepared by forming the Grignard reagent $(CH_2SiMe_3)MgCl$ from Mg turnings and $ClCH_2SiMe_3$, followed by manipulation of the Schlenk equilibrium *via* the addition of dioxane (**Scheme 2.1**). In 1929 Schlenk and son reported that, in ethereal solvents, Grignard reagents undergo a redistribution and an equilibrium exists between the Grignard reagent and the diorganomagnesium ($MgR_2$) and magnesium dihalide ($MX_2$) species. Addition of 1,4-dioxane forms an insoluble polymeric adduct with magnesium dihalide, precipitating it from the mixture.[100] Following filtration of the by-product and removal of solvent, the desired $MgR_2$ was purified *via* sublimation with typical yields of between 63-70%, and used in further reactions.

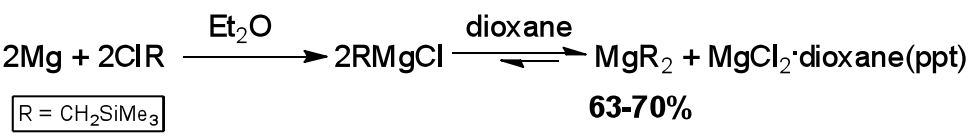


**Scheme 2.1:** Preparation of $MgR_2$

NaR and KR were prepared by the metathesis reaction of LiR and MO*t*Bu (M = Na, K) in hexane, with typical yields of between 75-80% (**Scheme 2.2**).

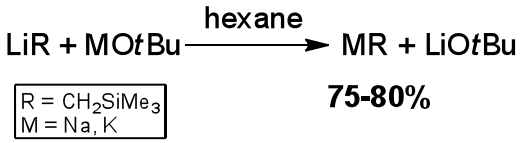


**Scheme 2.2:** Preparation of NaR and KR

All the starting materials described here are extremely pyrophoric and were handled with strict Schlenk line techniques and stored under argon in a glove box.

### 2.3.2 Synthesis of homoleptic alkyllithium magnesiates

Firstly the reaction of equimolar amounts of LiR with $MgR_2$ ($R = CH_2SiMe_3$) was examined, using non-coordinating hexane as a solvent. Gentle heating of the suspension gave a colourless solution. This enhanced solubility suggested the formation of a mixed-metal complex since $MgR_2$ on its own is totally insoluble in this solvent. This increased solubility for magnesiate reagents when compared with their homometallic components has several precedents in the literature[101] and DFT studies have revealed that their formation *via* co-complexation reagents is energetically preferred.[11] Slow cooling of the solution resulted in the deposition of colourless needle crystals of lithium magnesiate [$LiMg(CH_2SiMe_3)_3$] (**1**) in a 96% yield. Being soluble in deuterated benzene, these crystals were analysed by multinuclear ($^1H$, $^{13}C$ and $^7Li$) NMR spectroscopy. The most diagnostic resonance in the $^1H$ NMR spectrum was a singlet at -1.36 ppm for the trimethylsilylmethyl C$H_2$ group which appears significantly downfield to that found in monometallic $LiCH_2SiMe_3$ (-1.92 ppm) and cannot relate to $Mg(CH_2SiMe_3)_2$ which is insoluble in benzene and as such no comparison can be made. Unfortunately, despite the reproducibility of the synthesis of **1**, single crystal diffraction could not be carried out due to the degradation of the product.

Lewis basic donors monodentate tetrahydrofuran (THF), didentate 1,4-dioxane and *N,N,N',N'*-tetramethylethylenediamine (TMEDA) and tridentate *N,N,N',N'',N''*-pentamethyldiethylenetriamine (PMDETA) were added to **1** to study their coordination (**Scheme 2.3**). Adducts [{(THF)$LiMgR_3$}$_\infty$] (**2**), [{(dioxane)$_2$$LiMgR_3$}$_\infty$] (**3**), [(TMEDA)$_2$$Li_2MgR_4$] (**5**) and [(PMEDTA)$LiMgR_3$] (**6**) were formed from the addition of one molar equivalent of the relevant donor to the homoleptic trisalkyl magnesiate [$LiMgR_3$] (**1**) and compound [{(dioxane)$Li_2Mg_2R_6$}$_\infty$] (**4**) with the addition of substoichiometric 0.25 equivalents of 1,4-dioxane (**Scheme 2.3**).

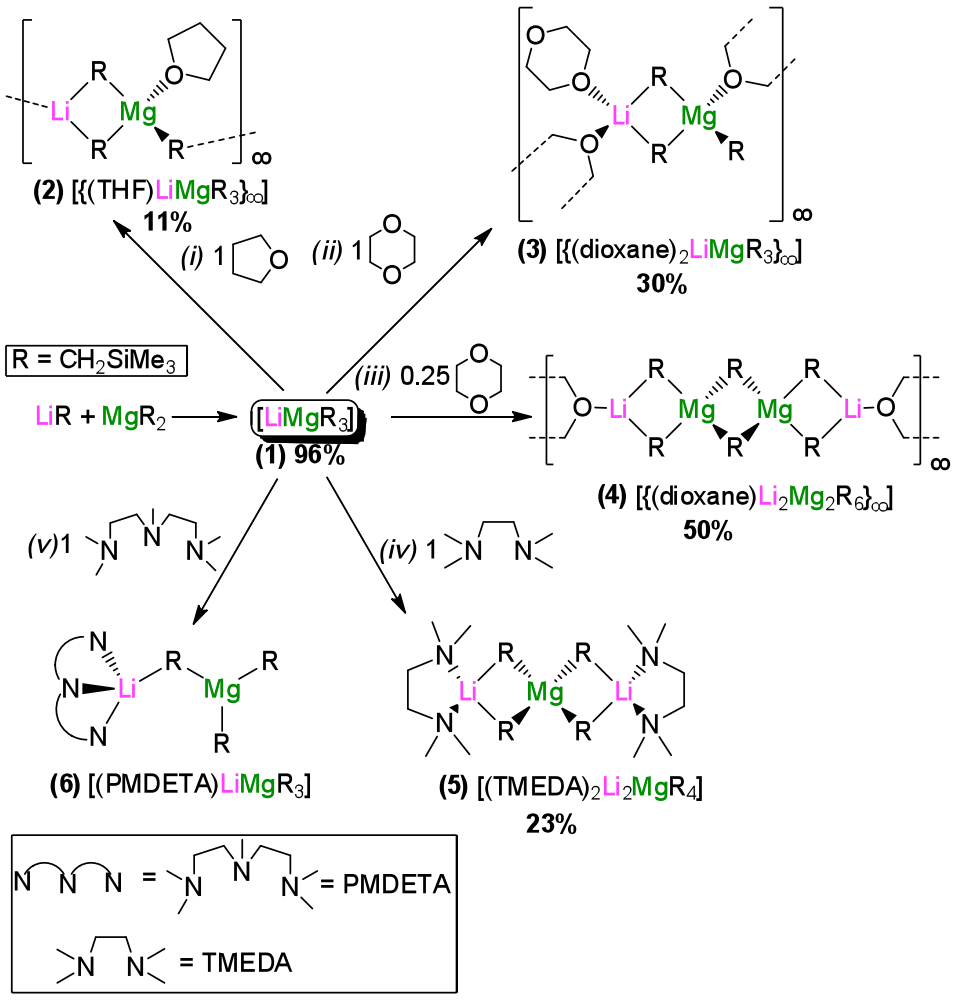


**Scheme 2.3**: Reactivity of **1** with selected Lewis bases (i) THF; (ii) dioxane (1 eq); (iii) dioxane (0.25 eq); (iv) TMEDA; (v) PMDETA

All donor-solvated compounds were characterised by multinuclear NMR spectroscopy and their structures were elucidated by X-ray crystallography which

confirmed their bimetallic constitution and revealed the changes imposed on the structure and constitution of the magnesiates depending on the donor molecule present in the bimetallic species.

Compound **2** was isolated as colourless crystals in a modest 11% yield due to a great extent by its excellent solubility in hexane at room temperature (this yield could be improved upon by concentration of the filtrate and storage at -30 °C giving a microcrystalline solid and an overall yield of 93%). Dioxane adducts **3** and **4** were obtained in 30% and 50% yield respectively. Taking into account their constitution (**3** contains two molecules of dioxane whereas **4** contains 0.5 eq of dioxane per $\{LiMgR_3\}$ fragment) and the stoichiometries employed for their preparation (1 equiv and 0.25 equiv of dioxane for **3** and **4** respectively), a maximum yield of 50% (with respect to Li) could be expected for both species.

Contrasting with the triorganomagnesiate formulation $\{LiMgR_3\}$ exhibited by **2**, **3**, **4** and **6** (*vide infra*), the addition of TMEDA to **1** seems to induce a change in its formulation affording the lithium-rich species (or "higher order" magnesiate) $[(TMEDA)_2Li_2MgR_4]$ (**5**) along with the formation of $MgR_2$. The formation of **5** (which could only be isolated in a 23% yield, again with a maximum yield possible of 50% with respect to Li) could be considered a possible redistribution process of a putative triorganomagnesiate $[(TMEDA)LiMgR_3]$ as shown in **Equation 2.1**. Processes of this type are known in mixed-metal chemistry[102] and can be favoured by the crystallisation process. Compound **5** can be rationally prepared by reacting a 2:1:2 TMEDA:$MgR_2$:LiR mixture in hexane, which allowed its isolation in a 56% yield.

$$2[(TMEDA)LiMgR_3] \rightleftharpoons [(TMEDA)_2Li_2MgR_4] + MgR_2$$

**Equation 2.1**: Redistribution to form the tetraalkyl magnesiate

Compound **6** is an oil at room temperature which negates an accurate determination of its isolated yield. Notwithstanding, NMR analysis of the crude product of the co-complexation reaction suggests that its formation is quantitative (no other organometallic species were detected in solution).

### 2.3.2.1 Monodentate oxygen donor: THF

THF-solvated triorganomagnesiate **2** exhibits a polymeric structure (**Figure 2.1**) made up by {(THF)LiMgR$_3$} units, where two of the alkyl groups act as bridges between Li and Mg featuring a four-membered [LiCMgC] ring whereas the remaining alkyl group on Mg bonds to a Li centre of a neighbouring unit through a methylene group, giving rise to a 1D chain structure which allows each Li atom to attain further stabilisation by increasing its coordination number. Surprisingly, in contrast with other lithium magnesiates which also contain THF as part of their molecular structure, in **2** THF coordinates to Mg, reflecting the strong Lewis acidity of Mg in comparison to Li. In the extended structure of **2** (**Figure 2.1**) the THF molecules and the SiMe$_3$ groups (from the alkyl groups which connect the monomeric units) adopt an alternate disposition across the Li···Mg···C vector.

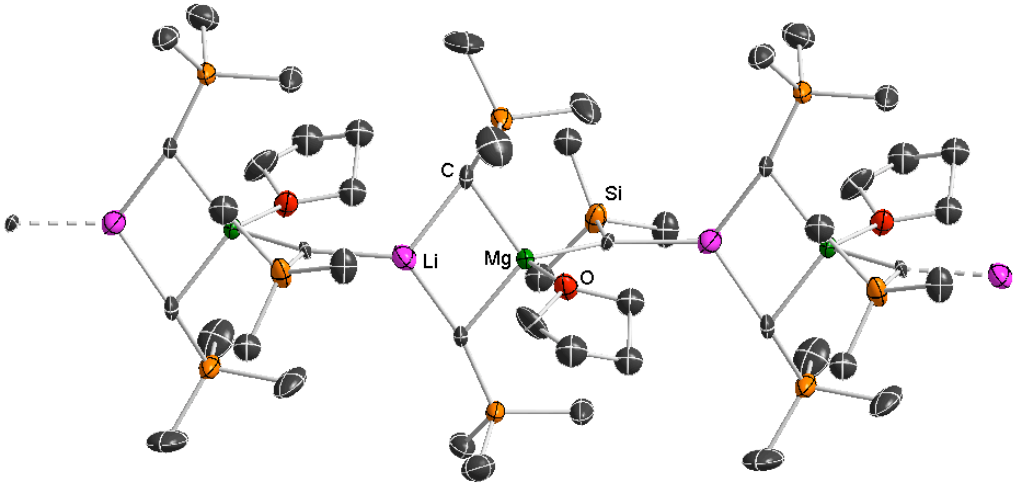


**Figure 2.1**: Polymeric section of **2** demonstrating propagation and showing selected atom labelling. Displacement ellipsoids are drawn at the 50% probability level. Hydrogen atoms, disorder in THF and disorder in one TMS group have been omitted for clarity. The unit cell of **2** contains three crystallographically independent molecules with identical connectivity.

Unfortunately, a large amount of motion in the THF molecules in **2** adversely affects the precision of this structure and therefore prevents discussion of any geometrical parameters, although its connectivity is definite. To the best of our knowledge **2**

constitutes the first example of a homoleptic lithium magnesiate which exhibits a polymeric structure to be structurally defined; furthermore the propagation of this structure which occurs exclusively through the formation Li-C electron deficient bonds with a neighbouring unit is extremely rare in mixed-metal chemistry.[103]

### 2.3.2.2 Didentate oxygen donor: dioxane

Attention was then turned to related oxygen-donor dioxane, which, possessing two oxygen atoms at the positions 1 and 4, precludes this didentate donor operating in a chelating fashion but it is well known to favour the formation of polymeric structures acting as a bridging ligand in main group chemistry.[104] Thus, the reaction of **1** with equimolar amounts of dioxane led to the isolation of $[\{(dioxane)_2LiMgR_3\}_\infty]$ (**3**) as colourless crystals, structure of which was determined by X-ray crystallography (**Figure 2.2**).

Displaying a polymeric arrangement (**Figure 2.2** and **Table 2.1**), **3** contains the same basic $\{LiMgR_3\}$ organometallic core of **2** forming four-membered [LiCMgC] rings, however now the polymeric chain is constructed *via* Li-O and Mg-O dative bonding with dioxane molecules alternately bridging the Li of one $\{LiMgR_3\}$ monomer to the Li of the next unit ($R_3MgLi\text{-}O(CH_2\text{-}CH_2)_2O\text{-}LiMgR_3$), then bridging Mg to Mg in a similar fashion, resulting in a 'head-to-head', 'tail-to-tail' repeating pattern. Thus, contrasting with **2**, the remaining alkyl group of the $\{LiMgR_3\}$ units is not involved in the formation of the polymer and coordinates exclusively to the Mg atom. The structure is completed by an additional molecule of dioxane bonded terminally to lithium. Taking into consideration the coordination modes of dioxane to the mixed-metal fragments in **3**, three distinct types of donor molecules are observed within the asymmetric unit (two molecules acting as bridges propagating the polymeric structure with one of them connecting Li atoms and the other one the Mg centres and a third type terminally bonded to Li). Within the asymmetric unit both Mg and Li exhibit distorted tetrahedral geometries (bond angles covering the range 99.66(6)º to 122.45(8)º and 101.96(12)º to 116.90(14)º for Mg and Li respectively). As expected, the Mg-C bonds of the bridging alkyl groups are elongated (mean Mg-C bond length

2.231 Å) in comparison with that found for the terminal $CH_2SiMe_3$ group (2.1494(16) Å).

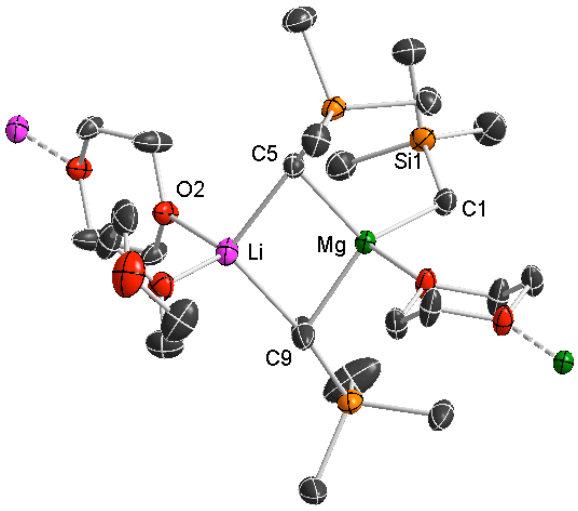


**Figure 2.2a**: Monomeric section of **3**. Displacement ellipsoids are drawn at the 50% probability level. Hydrogen atoms and disorder in one dioxane and one TMS group have been omitted for clarity.

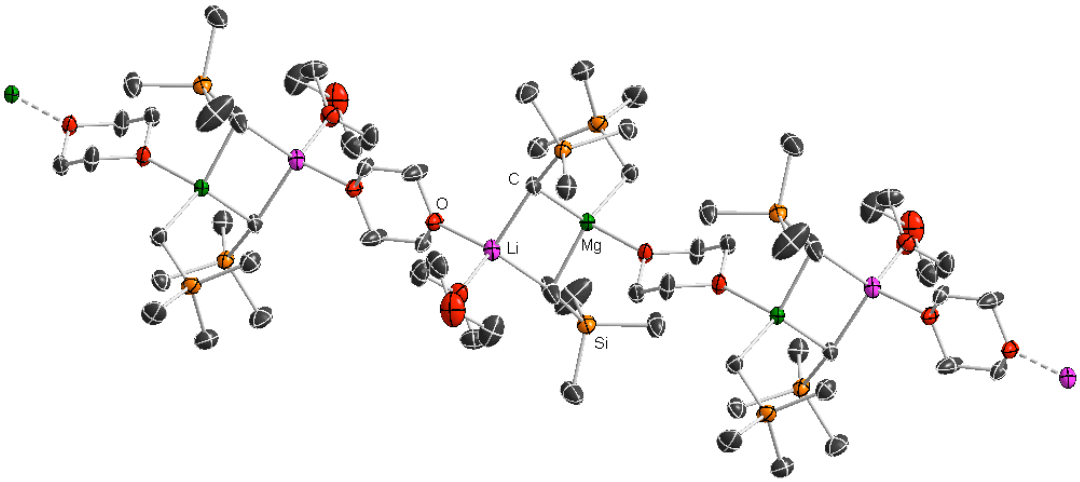


**Figure 2.2b**: Polymeric section of **3** showing propagation and selected atom labelling. Displacement ellipsoids are drawn at the 50% probability level. Hydrogen atoms have been omitted for clarity. Selected bond angles and distances: C1-Mg-C5 116.36(7)°, C1-Mg-C9 122.45(8)°, C9-Mg-C5 107.03(6)°, C1-Mg-O1 99.66(6)°, O2-Li-O3 101.96(12)°, C9-Li-O2 116.90(14)°: Li-C9 2.268(3) Å, Li-C5 2.281(3) Å, Mg-C9 2.229(2) Å, Mg-C5 2.2322(16) Å, Mg-C1 2.1494(16) Å, Li-O3 1.977(3) Å, Li-O2 2.011(3) Å, Mg-O1 2.1289(12) Å.

The Mg-C bond distances found in **3** are within the range of those reported for other structurally defined compounds containing the $CH_2SiMe_3$ ligand, as for example [(TMEDA)NaMg(TMP)$_2$($CH_2SiMe_3$)] (2.179 Å)[105] and [(PMDETA)KMg(TMP)$_2$($CH_2SiMe_3$)] (2.202 Å).[106] A search in the CCDB revealed that the polymeric structure of **3** is unknown in magnesiate chemistry, constituting the first example of an alkali-metal magnesiate solvated by dioxane although a close precedent can be found in the mixed lithium-gallium complex [(dioxane)$_3$Li$_2$Ga$_2$R$_8$] (R = $CH_2SiMe_3$), containing a Li···Ga···Ga···Li tetranuclear arrangement, where each lithium coordinates to two molecules of dioxane, one of them acting as 1-4 oxygen donor, propagating a polymeric chain arrangement whereas the other one coordinates terminally to Li.[107]

Addition of a sub-stoichiometric amount of dioxane (0.25 equiv) allowed the isolation of a different polymeric structure [{(dioxane)Li$_2$Mg$_2$R$_6$}$_\infty$] (**4**), comprised of a dimeric trisalkyl magnesiate unit [{LiMgR$_3$}$_2$] linked through bridging dioxane molecules solvating the lithium atoms (**Figure 2.3**). The magnesium atoms in **4** adopt a distorted tetrahedral geometry surrounded by four carbon atoms that form a {MgCMgC} planar four-membered ring (sum of angles 359.7°) which is orthogonal to two adjacent [LiCMgC] rings (sum of angles 358.6°). Whilst this core motif of three fused four-membered rings, comprising tetranuclear alkali-metal···Mg···Mg···alkali-metal, has previously been reported,[36, 108] examples are still somewhat rare. The Mg-C distances in **4** (mean length 2.236 Å) are comparable with the bridging Mg-C bond lengths in **3** (mean length 2.231 Å). Unlike **3**, each Li atom in **4** is now only tricoordinate, bonding to two bridging alkyl groups and one oxygen atom of a dioxane ligand, consequently the Li-C bond lengths in **4** are slightly shorter than in **3** (average of 2.171 Å in **4** versus 2.275 Å in **3**). In addition, the Li atoms in **4** attain higher coordination by interacting with the Me groups of neighbouring $SiMe_3$ group through stabilising secondary electrostatic interactions, for example Li1···C10 2.613(5) Å. Interactions of this type have been recently reported in other main group compounds containing $CH_2SiMe_3$ ligands.[84, 109]

In contrast to THF-solvated polymer **2**, which propagates uniquely through the alkyl group, structures **3** and **4** polymerise through the didentate bridging nature of dioxane which links the [$LiMgR_3$] and [$\{LiMgR_3\}_2$] units together respectively. By employing less donor molecules a longer chain organometallic oligomer is trapped, allowing a greater insight into the constitution of unsolvated species **1**, the structure of which is still elusive. A similar strategy was employed by Mulvey by adding a weak solvating ligand (1,4-dimethylpiperazine) to lithium anilide which gave a pentanuclear structure.[110]

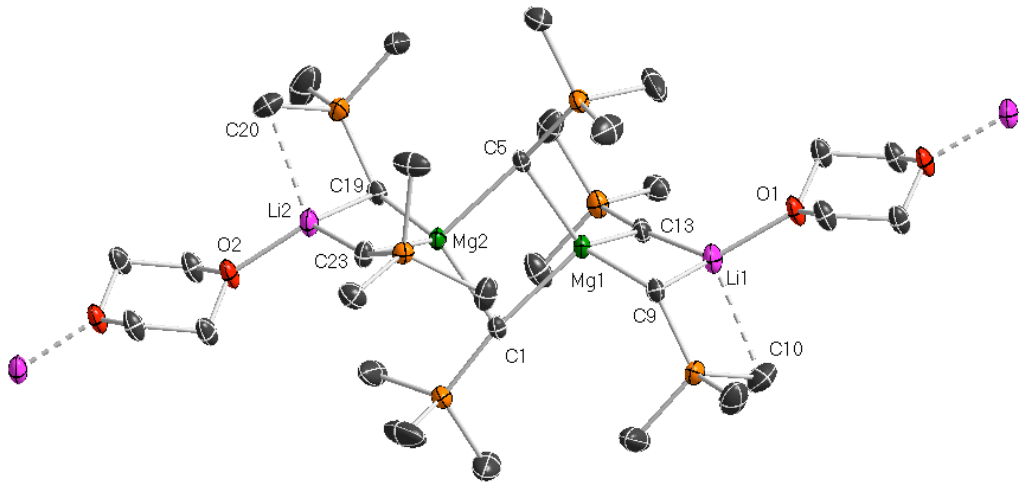


**Figure 2.3**: Portion of polymeric **4** showing selected atom labelling. Displacement ellipsoids are drawn at the 50% probability level. Hydrogen atoms have been omitted for clarity. Selected bond angles and distances, Li1-C13-Mg1 73.574(3)°, Li1-C9-Mg1 74.575(3)°, O1-Li1-C13 124.717(3)°, O1-Li1-C9 115.973(4)°: Li1-O1 1.978(3) Å, Li2-O2 1.936(3) Å, Mg1-C5 2.242(2) Å, Mg1-C13 2.229(2) Å, Mg1-C9 2.240(2) Å, Mg2-C1 2.231(2) Å.

### 2.3.2.3 Didentate nitrogen donor: TMEDA

Switching to nitrogen as a donor atom, the chelating didentate ligand TMEDA not only disfavours polymerisation, giving rise to a monomer, but even more significantly it alters the stoichiometry of the mixed-metal species resulting in tetraalkyl magnesiate [$(TMEDA)_2Li_2MgR_4$] (**5**) (**Figure 2.4**). This monomeric structure exhibits a classical "Weiss motif" found in [$(TMEDA)_2Li_2MgMe_4$][7] with tetrahedral coordination around magnesium with the R groups forming bridges

between the magnesium and the outer TMEDA-solvated lithium atoms. The rarity of **5** is evidenced by Weiss's methyl analogue being the single entry in the Cambridge Crystallographic Database of a tetraalkyl magnesiate displaying a contact ion pair trinuclear structure (Li···Mg···Li), whereas the remaining three TMEDA-solvated alkyllithium magnesiate structures known exhibit solvent-separated ion pair structural motifs.[98, 111] Unfortunately all samples were weakly diffracting and the resulting dataset thus gives only a low resolution model that is used merely to confirm connectivity, hence the discussion of geometric parameters in **5** will be waived.

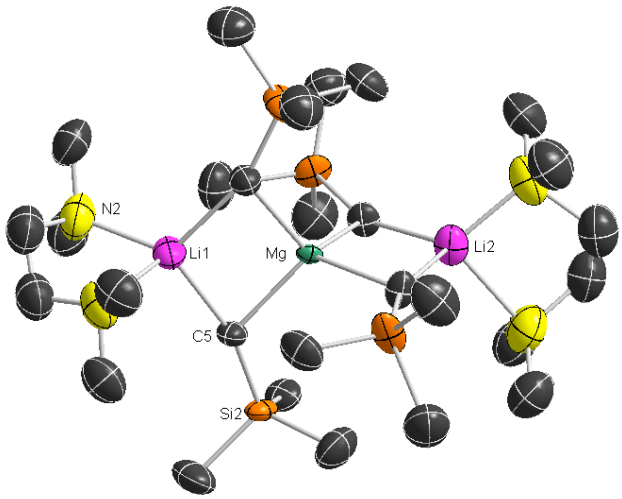


**Figure 2.4:** Asymmetric unit of **5** showing selected atom labelling. Displacement ellipsoids are drawn at the 50% probability level. Hydrogen atoms omitted for clarity.

### 2.3.2.4 Tridentate nitrogen donor: PMDETA

Employing the tridentate nitrogen donor PMDETA in a 1:1 ratio with the trisalkyl magnesiate precursor an oil formed, which, on cooling to -30 °C for 4 days deposited crystals of [(PMDETA)LiMgR$_3$] (**6**) suitable for X-ray crystallography (**Figure 2.5** and **Table 2.1**). The three chelating nitrogen atoms from the donor molecule dominate the electron deficient lithium and the result is a monomeric structure comprising one Li and one Mg centre which are connected by a single alkyl group with the two remaining R groups binding terminally on the Mg. As expected, trigonal planar Mg (the sum of angles around Mg = 359º) forms shorter bonds with the

terminal alkyl groups (mean length 2.1544 Å) than the bridging alkyl group (Mg-C2 bond length 2.1930(16) Å) due to the higher coordination of the latter. Li resides in a distorted tetrahedral environment (average angle = 106.7º), bonding to a single alkyl group and capped by the tridentate PMDETA molecule. Unlike the [$LiMgR_3$] variants **2**, **3** and **4**, where a [LiCMgC] four-membered rings are observed, **6** adopts a much more open structural motif which can be envisaged as an intermediate between a contacted and solvent separated ion pair structure. Thus **6** displays a remarkably obtuse Li-C-Mg bond angle (149.419(2)°) which contrast with the values found in related **3** and **4** (average Li-C-Mg bond angles of 74.102° and 74.058° in **3** and **4** respectively), as well as exhibiting a significantly elongated (and therefore weaker) Li-C bond (2.326(3) Å *vs* 2.275 and 2.171 Å for **3** and **4** respectively). On the other hand the Li-N bonds found in **6** are almost identical to those reported in the closely related homometallic structure [(PMDETA)$LiCH_2SiMe_3$].[112]

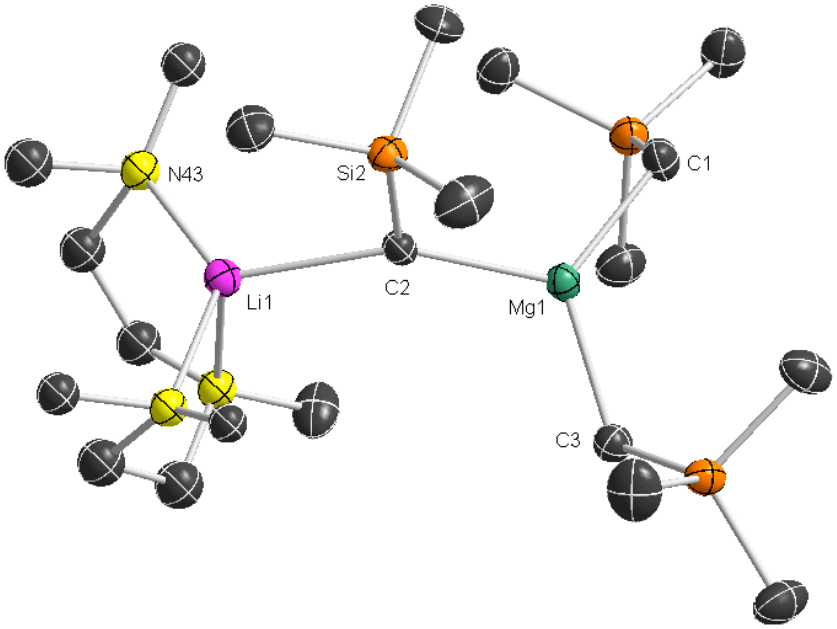


**Figure 2.5**: Asymmetric unit of **6** showing selected atom labelling. Displacement ellipsoids are drawn at the 50% probability level. Hydrogen atoms and minor disorder in PMDETA omitted for clarity. Selected bond angles and distances, Li1-C2-Mg1 149.419(2)°, C2-Mg1-C1 119.298(2)°, C2-Mg1-C3 117.897(1)°, C1-Mg1-C3 122.121(2)°. Li1-C2 2.326(3) Å, Mg1-C3 2.1531(16) Å, Mg1-C1 2.1556(16) Å, Mg1-C2 2.1930(16) Å.

### 2.3.2.5 Formation of a cationic lithium magnesiate

In a duplicate reaction, large crystals formed readily in the freezer that, unlike **6**, did not rapidly redissolve at room temperature. Analysis of these crystals by X-ray crystallography revealed a fortuitous inclusion of traces of oxygen, resulting in the heterometallic mixed alkyl-alkoxo compound $[\{(PMDETA)_2Li_2MgR_3\}^+\{Mg_3R_6(OR)\}^-]$ (**7**) (**Scheme 2.4** and **Figure 2.6**). Exhibiting a distinctive structural motif, this mixed Li-Mg alkyl-alkoxo compound displays a solvent-separated ion pair structure. In the trinuclear anion, the magnesium centres are connected through three $\mu_2$-alkyl ligands and one $\mu_3$-alkoxide $OCH_2SiMe_3$ group, resulting from oxygen insertion into a Mg−C bond. The anionic cluster is completed by three terminal alkyl groups, each bonded to one Mg, giving rise to a pseudocubane structure with a missing vertex. Alternatively this anion can be envisaged as an anionic inverse crown ether complex (*vide infra*) comprising a six-membered $\{Mg_3C_3\}$ ring hosting an alkoxide group in its core. Although several alkyl-alkoxo magnesium compounds have been structurally characterized,[113] the structure of this anionic fragment is unprecedented. A related example of a neutral homoleptic magnesium alkoxide with a missing-corner cubane structure has been reported.[114] Even more unusual is the constitution of the cationic component of **7** $\{(PMDETA)_2Li_2MgR_3\}^+$ which is completely unique in mixed-metal chemistry, and represents, to the best of our knowledge, the first example of a cationic lithium magnesiate. **7** consists of a trinuclear Li···Mg···Li arrangement held together by two alkyl groups which act as bridges between the metals and two molecules of donor PMDETA which coordinate to the lithium atoms. Magnesium completes its trigonal coordination by bonding to one terminal R group. Similarly to **6**, the Li-C bonds are significantly longer (Li1-C35 2.341(4) Å, Li2-C39 2.366(4) Å) than those found in the related lithium magnesiates **3** and **4**. The synthesis of **7** could be reproduced by deliberately by exposing **6** to $O_2$ for 30 minutes (using a drying tube), with crystals isolated in a 34% yield which were confirmed by $^1$H NMR spectroscopy to be **7** (**Scheme 2.4**).

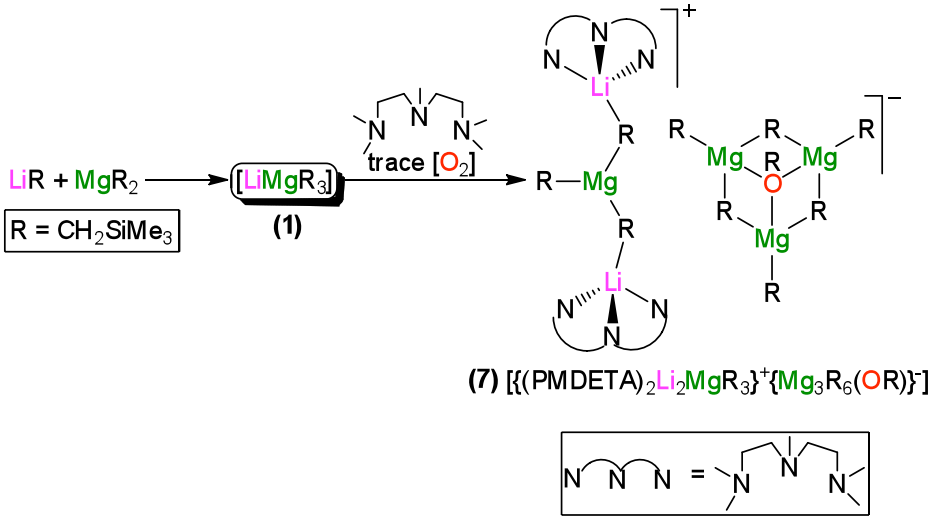


**Scheme 2.4**: Formation of **7** *via* oxygen insertion

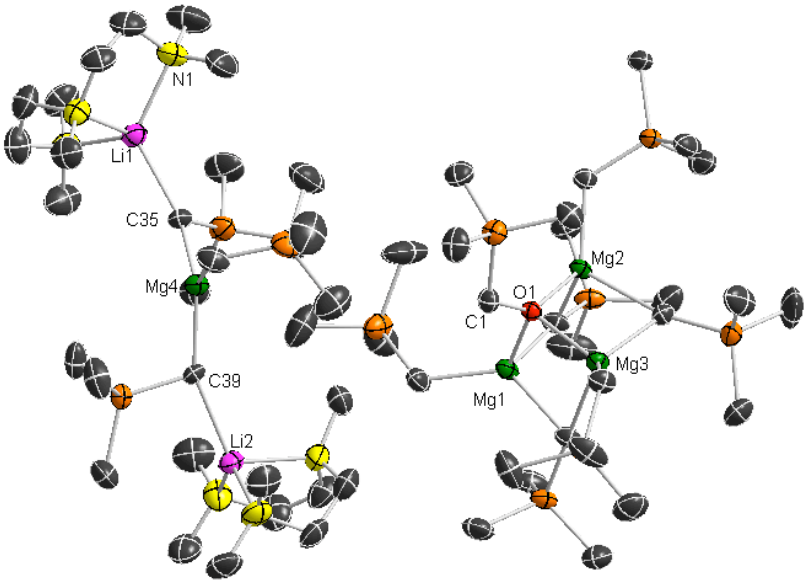


**Figure 2.6**: Asymmetric unit of **7** showing selected atom labelling. Displacement ellipsoids are drawn at the 50% probability level. Hydrogen atoms and disorder in one PMDETA molecule omitted for clarity. Selected bond angles and distances, Mg3-O1-C1 116.71(11)°, Mg2-O1-Mg3 91.83(3)°, Mg2-O1-Mg1 92.33(5)°; Li1-C35 2.341(4) Å, Li2-C39 2.366(4), Mg4-C31 2.131(2) Å, Mg4-C39 2.1818(19) Å, Mg4-C35 2.183(2), Mg2-O1 2.0478(12) Å, Mg3-O1 2.0586(14) Å, Mg1-O1 2.0447(13) Å.

The formation of **7** is in contrast with recent precedents on controlled exposure of oxygen to alkali metal magnesiates which have led to the isolation of inverse crown ether complexes;[93b, 115] macrocyclic cationic structures hosting oxygen or alkoxide anions in their core. A plausible explanation for this difference could be the presence of tridentate donor PMDETA which, by solvating the lithium atoms, limits their coordination requirement to a single alkyl group, precluding the closure of a cycle structure and favouring instead a linear arrangement such as that in **7**. The synthesis of cationic mixed-metal fragments such as that present in **7** could be of potential importance for the design of new catalytic systems, bearing in mind the high activity that cationic alkyl magnesium compounds exhibit in, for example, ring-opening polymerisation reactions[116] as well as recent reports[10, 93] which have advanced the understanding of how bimetallic systems can operate synergically.

**Table 2.1:** Key bond lengths of compounds **3**, **4**, **6** and **7** in Å. Where no ESDs are shown a mean bond length is reported.

| | **3** | **4** | **6** | **7**[a] |
|---|---|---|---|---|
| Li-C | 2.275 | 2.171 | 2.326(3) | 2.354 |
| Mg-$C_T$ | 2.1494(16) | - | 2.1544 | 2.131(2) |
| Mg-$C_{Br}$ | 2.231 | 2.236 | 2.1930(16) | 2.1824 |
| Li-O | 1.994 | 1.957 | - | - |
| Li-N | - | - | 2.110 | 2.121 |
| Mg-O | 2.1289(12) | - | - | - |

[a] Cation only

### 2.3.3 Constitution in solution

In conjunction with their solid-state characterisation, all compounds have also been examined in solution using multinuclear ($^1$H, $^{13}$C, $^7$Li) NMR spectroscopy in $C_6D_6$ solutions (see **Table 2.2** for key chemical shifts). For compounds **1**-**6** a single set of resonances for the alkyl ligand $CH_2SiMe_3$ was observed. Taking into account the different structures observed by X-ray crystallography, where in many occasions different types of alkyl groups are present, this strongly suggests that for some of

these compounds the solid-state structures are not retained in deuterated benzene solution.

**Table 2.2:** Selected NMR shifts of LiR and compounds **1**-**7** in deuterated benzene solutions

| | $\delta^{1H}C\boldsymbol{H}_2$/ ppm | $\delta^{13C}\boldsymbol{C}H_2$/ ppm | $\delta^{7Li}$/ ppm |
|---|---|---|---|
| LiR | -1.92 | - | - |
| $[LiMgR_3]$ **1** | -1.36 | -2.21 | 0.38 |
| $[\{(THF)LiMgR_3\}_\infty]$ **2** | -1.31 | -3.33 | 1.24 |
| $[\{(dioxane)_2LiMgR_3\}_\infty]$ **3** | -1.51 | - | 1.25 |
| $[\{(dioxane)Li_2Mg_2R_6\}_\infty]$ **4** | -1.47 | - | 0.32 |
| $[(TMEDA)_2Li_2MgR_4]$ **5** | -1.99 | -3.19 | 0.88 |
| $[(PMDETA)LiMgR_3]$ **6** | -1.31 | -3.28 | 0.76 |
| $[\{(PMDETA)_2Li_2MgR_3\}^+\{Mg_3(R)_6(OR)\}^-]$ **7** | -1.11(br) | - | 0.20 |

Regarding the chemical shifts observed for the monosyl group, TMEDA adduct **5**, which displays a tetraalkyl core $[Li_2MgR_4]$, shows a resonance for the M-C$\boldsymbol{H}_2$ considerably upfield (at -1.99 ppm) from those observed in the species displaying a trisalkyl core $[LiMgR_3]$ (**1**-**4**, **6**) (ranging from -1.31 to -1.51 ppm). Indeed, at -1.99 ppm these protons are even more shielded than in the homometallic LiR species (-1.92 ppm) (no comparison can be made with $MgR_2$ which, due to its polymeric structure, is insoluble in deuterated benzene). In contrast, the relevant carbon signal in the $^{13}C\{^1H\}$ spectra does not show a significant difference between the tetraalkyl and trisalkyl species, with **5** resonating at -3.19 ppm, a chemical shift between those observed for unsolvated species **1** (-2.21 ppm) and THF adduct **2** (-3.33 ppm). Having stated that, it should be noted that due to the reduced solubility of dioxane-solvated **3** and **4**, and the decomposition of **7**, less data is available overall for comparison of the $^{13}C\{^1H\}$ chemical shifts.

$^1H$ NMR analysis of **2** in $C_6D_6$ showed a singlet at -1.31 ppm corresponding to the M-C$\boldsymbol{H}_2$ group, a singlet at 0.35 ppm for the methyl groups of the alkyl ligand and

two multiplets at 1.15 and 3.40 ppm for the C$H_2$ and OC$H_2$ of the THF ligand respectively. The resonances for the THF ligand in **2** appear at a different chemical shift to those observed for free THF (1.40 and 3.57 ppm for the C$H_2$ and OC$H_2$ groups respectively), suggesting that THF remains coordinated to **2** in $C_6D_6$ solution, which was confirmed by a $^1$H-DOSY experiment (*vide infra*). Similarly, the dioxane molecules in **3** and **4** display a different resonance to that of the free dioxane (moving upfield when coordinated to a metal, with a OC$H_2$ resonance at 3.30 and 3.21 ppm for **3** and **4** respectively compared to 3.36 ppm in free dioxane) but despite the presence of three distinct dioxane molecules in the solid-state structure of **3**, only one singlet is observed, suggesting that either the polymeric structure is not retained and/or that a dynamic equilibrium is taking place which rapidly interconverts the dioxane molecules.

Furthermore, inspection of the crystal structure of **3** shows two bridging and one terminal R group; however, the presence of only one set of signals at room temperature suggests a dynamic interconversion is occurring between the R groups. Thus, a variable temperature $^1$H NMR experiment was undertaken in $d_8$-toluene which showed that when the temperature is gradually reduced to 215 K, the corresponding singlet observed for the C$H_2$ group splits into two resonances, with an approximate 2:1 integration at -1.52 and -1.64 ppm respectively (**Figure 2.7**), which supports the presence of a fast dynamic process taking place at room temperature which exchange the bridging and terminal alkyl groups.

As mentioned earlier, tetraalkyl species **5** shows the most upfield resonance of the C$H_2$ group due to the relative increase in charge on the anionic R groups, that is to say **5** can be considered $MgR_4^{2-}$ compared to $MgR_3^-$ in compounds **1**-**4** and **6**. All R groups are equivalent and display sharp signals. The TMEDA signals are indicative of the molecule remaining coordinated in the solvent, as the protons of the ethylene bridge are found to be more upfield (at 1.65 ppm) than the methyl protons (at 2.02 ppm) of the ligand and when free this pattern is reversed (at 2.36 and 2.12 ppm for the C$H_2$ and C$H_3$ protons respectively).

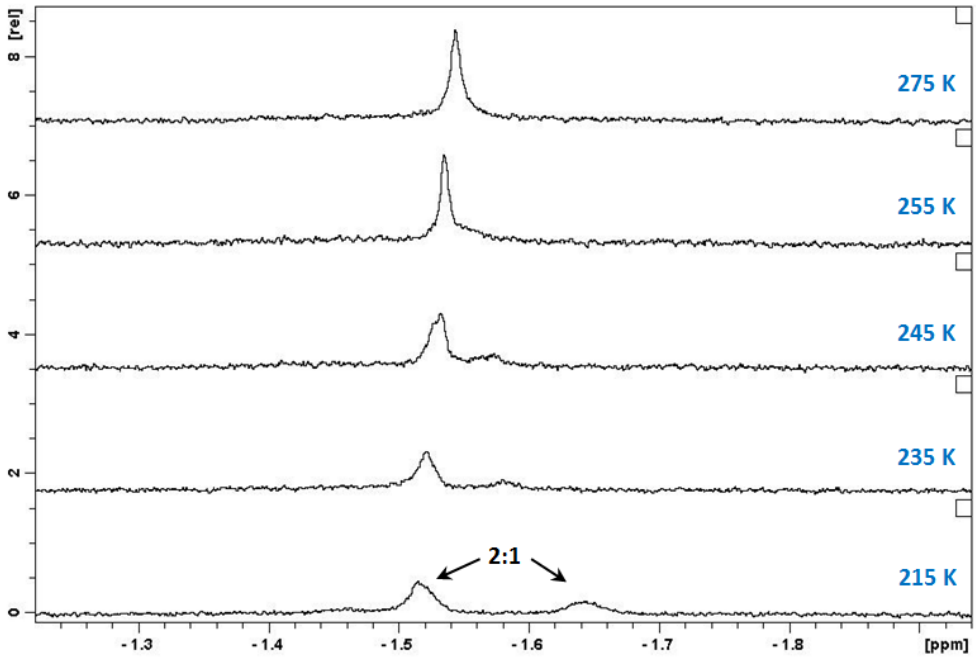


**Figure 2.7**: Variable temperature experiment of **3** in deuterated toluene showing splitting of the M-C$H_2$ signal at 215 K from the two bridging and one terminal R group.

Comparing the NMR data obtained for **6** with **7** shows a downfield shift in the C$H_2$ group of the alkyl ligand (from -1.31 ppm in **6** to -1.11 ppm in **7**) as may be expected due to the Mg-rich nature of **7** where a large contribution is made from the anion. The most notable feature in the NMR of **7** is the presence of a singlet at 3.93 ppm integrating to 2 hydrogens and corresponding to the methylene group of the single alkoxy ligand $MgOCH_2SiMe_3$. Inspection of the stoichiometry of **7** shows a 2:1 Mg:Li ratio. Additionally, in **7**, a broad multiplet is observed at room temperature for the alkyl C$H_2$ and C$H_3$ groups as a result of the overlapping of the resonances corresponding to the different alkyl ligands present: in both the anion and the cation there are bridging and terminal alkyl ligands, accounting for four distinct types of R ligand in total.

### 2.3.3.1 DOSY NMR studies of polymeric structures

Considering the defining role that aggregation plays in modulating the reactivity of organometallic compounds as well as the fact crystal structures of many of these

species do not correlate with their constitution in solution, it was decided to perform $^{1}$H NMR diffusion-ordered spectroscopy experiments ($^{1}$H-DOSY) of polymeric structures **2-4**, in order to assess their aggregation in $C_6D_6$ solutions. It has been shown that, using hydrocarbons as references, accurate estimations of formula weights of aggregates in solution can be ascertained.[36-37, 81, 117] 1,2,3,4-tetraphenylnaphthalene (TPhN), 1-phenylnaphthalene (PhN) and tetramethylsilane (TMS) were chosen as internal standards for this study as they have good solubility in benzene with minimal overlapping signals and are inert to **2** (**Figure 2.8**).

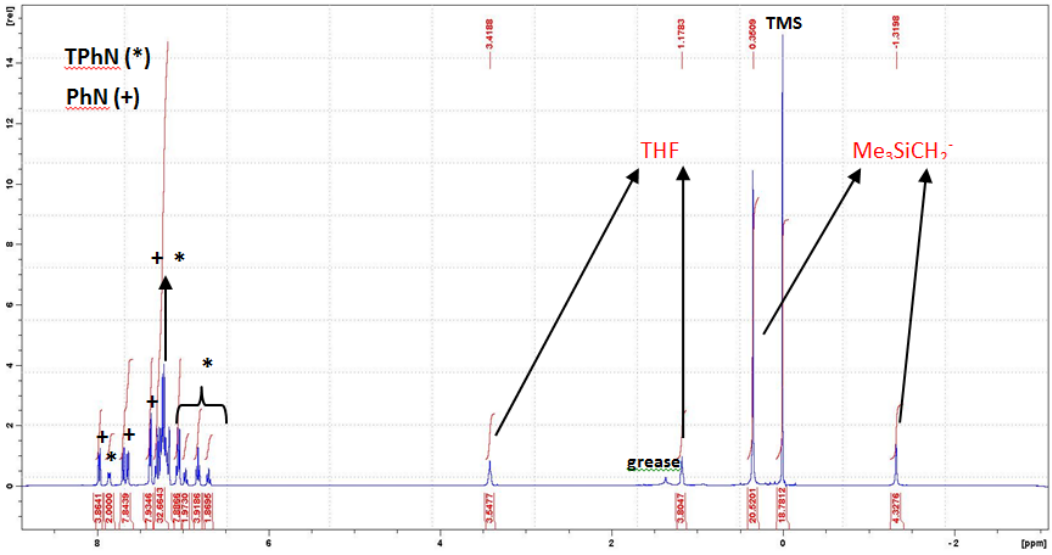


**Figure 2.8**: $^{1}$H NMR spectrum of [LiMg(CH$_2$SiMe$_3$)$_3$(THF)] (**2**), TPhN, PhN and TMS at 27 °C in $C_6D_6$ (traces of grease are also observed).

From this experiment it can be deduced that the $Me_3SiCH_2^-$ and THF ligands belong to the same sized molecule (both have the same diffusion coefficients lying on the same line in the second dimension), which indicates that THF remains attached to **2** in solution, as in the solid-state, and is not replaced by $C_6D_6$ (**Figure 2.9a**). As all the different components of the mixture separate clearly in the diffusion dimension with a relative size sequence TPhN > $Me_3SiCH_2^-$ = THF >> PhN >> TMS according to their decreasing diffusion coefficient values $D$ [$D$(TPhN) = 7.1(1) x $10^{-10}$ m$^2$ s$^{-1}$ < $D$($Me_3SiCH_2^-$ and THF) = 7.6(1) x $10^{-10}$ m$^2$ s$^{-1}$ << $D$(PhN) = 1.22(2) x $10^{-09}$ m$^2$ s$^{-1}$ << $D$(TMS) = 1.92 x $10^{-09}$ m$^2$ s$^{-1}$], a correlation between log $D$ and log FW (FW=

molecular weight) of the linear least-squares fit to the internal standards can be established (log *D* = -0.6636·log FW – 7.3888; r = 0.9976, **Figure 2.9b**).

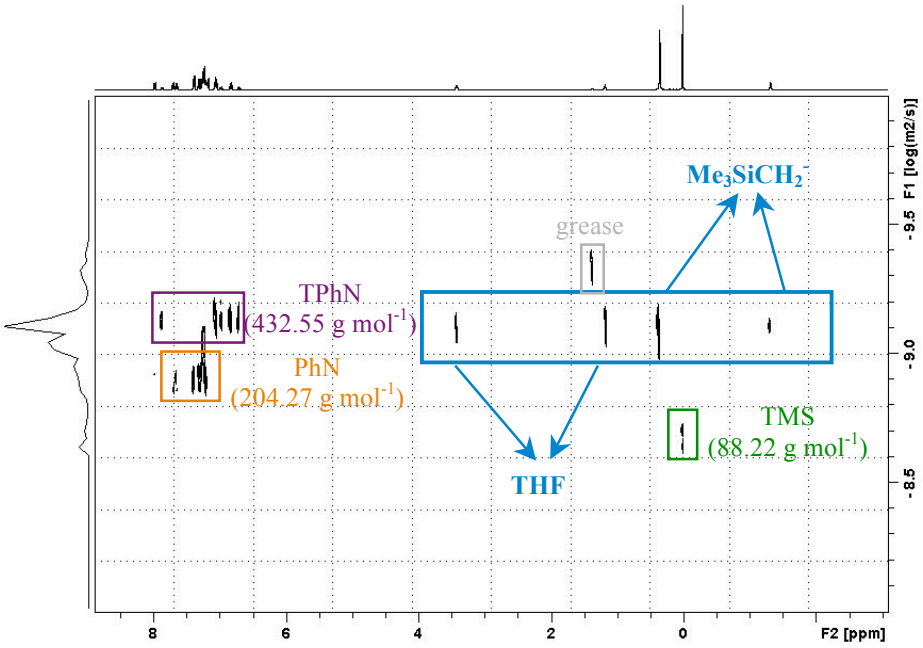


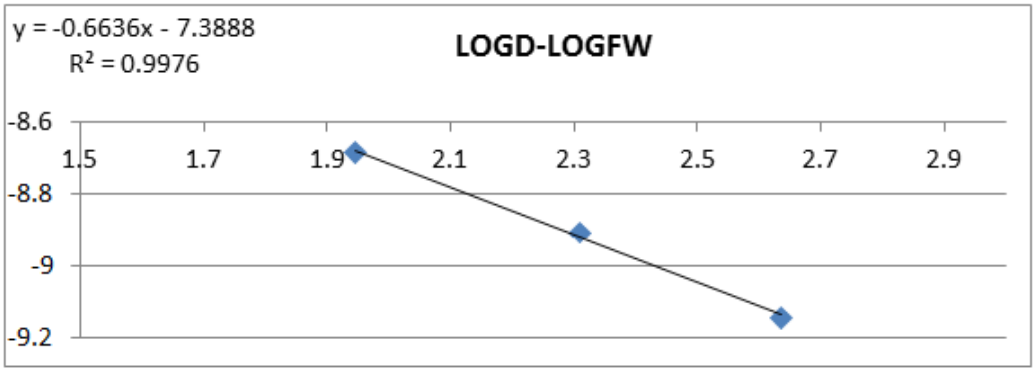


**Figure 2.9**: (a) $^{1}$H-DOSY NMR spectrum of **2**, TPhN, PhN and TMS in $C_6D_6$ at 298 K (some traces of grease also observed) (b) log *D* – log FW representation from the $^{1}$H-DOSY data obtained for the mixture of TPhN, PhN and TMS in $C_6D_6$ (data for the components of **2** is not included).

By interpolating the value of log *D* for **2** in this calibration curve, an approximate value of its molecular weight in solution can be estimated, which turned out to be 410 g mol$^{-1}$. Analysis of these data suggests that the polymeric constitution of **2** in

the solid-state is not retained in solution, as the error associated with much smaller aggregates such as a dimer [{LiMgR$_3$(THF)}$_2$] or a trimer [{LiMgR$_3$(THF)}$_3$] is quite high (44 and 63% respectively). Thus it appears that a substantial deaggregation of the 1D polymer occurs in solution and a good correlation is observed for a monomeric [LiMgR$_3$.THF] unit (-13%); however, when consideration is given to a structure in which lithium is further solvated by a molecule of deuterated solvent and even closer correlation is found (9% error from the predicted formula weight) (**Figure 2.10**). Such electrostatic interactions are well known between alkali-metals and neutral arene molecules in organometallic chemistry.[118]

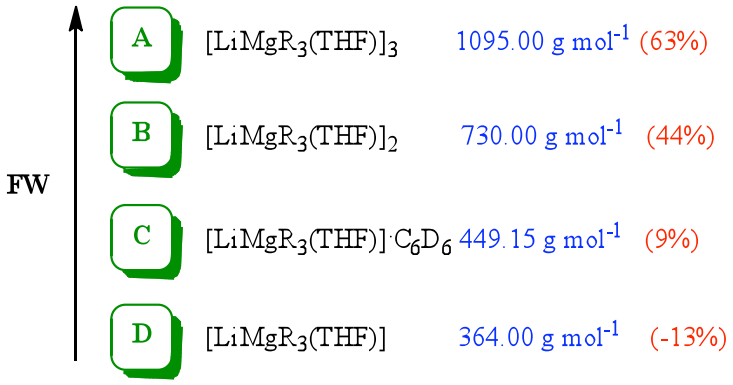


**Figure 2.10** Possible species of LiMg(CH$_2$SiMe$_3$)$_3$(THF)] (**2**) in C$_6$D$_6$ with errors (in brackets) respect to the FW value predicted through the DOSY study.

In order to ascertain if the THF ligand remains attached to Mg (as in the solid-state) or fluctuates to Li in solution, a heteronuclear Overhauser effect spectroscopy (HOESY)[119] NMR experiment was performed to detect "through space" connectivities between nonbonded nuclei. In C$_6$D$_6$ solution the Li atoms in **2** show a strong interaction with the protons of the methylene bridge and weaker interactions with the methyl groups attached to silicon (**Figure 2.11**); however, no interactions are observed between the THF protons and Li strongly suggesting that the THF molecule remains coordinated to Mg. Thus, collectively these NMR studies indicate that although the polymeric structure of **2** is not retained in benzene solution, where a monomeric arrangement is more likely to be formed, the Lewis base THF remains

attached to the more electronegative Mg, with Li probably forming electrostatic interactions with Li···$MeSiMe_2$ as well as with $C_6D_6$ (**Figure 2.12**).

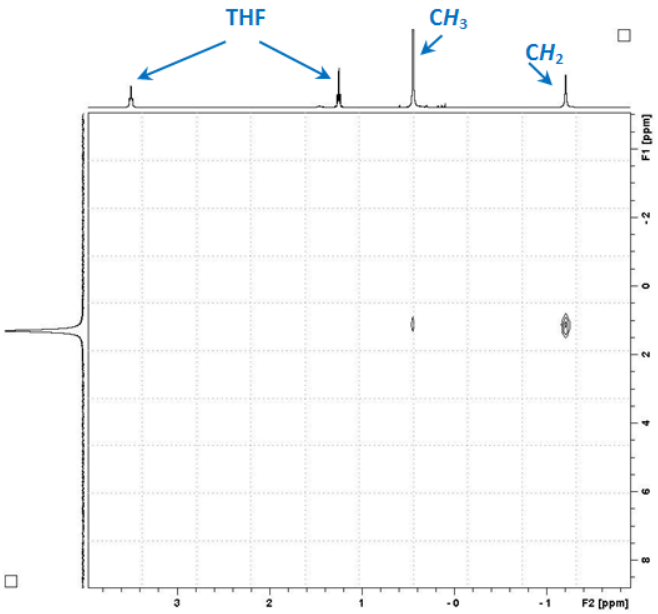


**Figure 2.11:** HOESY experiment showing cross-peaks between $^{1}H$ (x-axis) and $^{7}Li$ (y-axis) in **2**.

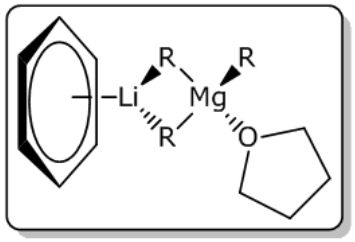


**Figure 2.12:** Proposed $C_6D_6$ solution structure of in **2**.

Turning to dioxane-solvated polymers **3** and **4**, $^{1}H$-DOSY experiments were carried out using the same internal reference standards as described above. For the "dioxane-rich" polymer **3**, which sees a 2:1 stoichiometry of dioxane to trisalkyl magnesiate unit [$LiMgR_3$], DOSY NMR experiments showed that dioxane and R ligands are not aligned as they display different *D* values, indicating they do not belong to similar sized species (**Figure 2.13**). As all the different components of the mixture separate clearly in the diffusion dimension with a relative size sequence TPhN > $Me_3SiCH_2^-$ >> PhN > dioxane >> TMS according to their decreasing *D* values [*D*(TPhN) = 7.36 x $10^{-10}$ $m^2$ $s^{-1}$ < *D*($Me_3SiCH_2^-$) = 7.86 x $10^{-10}$ $m^2$ $s^{-1}$ << *D*(PhN) = 1.22 x $10^{-09}$ $m^2$ $s^{-1}$ < *D*(dioxane) = 1.23 x $10^{-09}$ $m^2$ $s^{-1}$ << *D*(TMS) = 2.13 x $10^{-09}$ $m^2$ $s^{-1}$] an approximate

molecular weight for the R and dioxane ligands from **3** in solution can be interpolated, which turn out to be 393 and 201 g $mol^{-1}$ respectively. The FW inferred for the R species in solution (393 g $mol^{-1}$) is in good agreement with the FW of [(dioxane)$LiMgR_3$] (381 g $mol^{-1}$, error with respect to DOSY size = -3%).

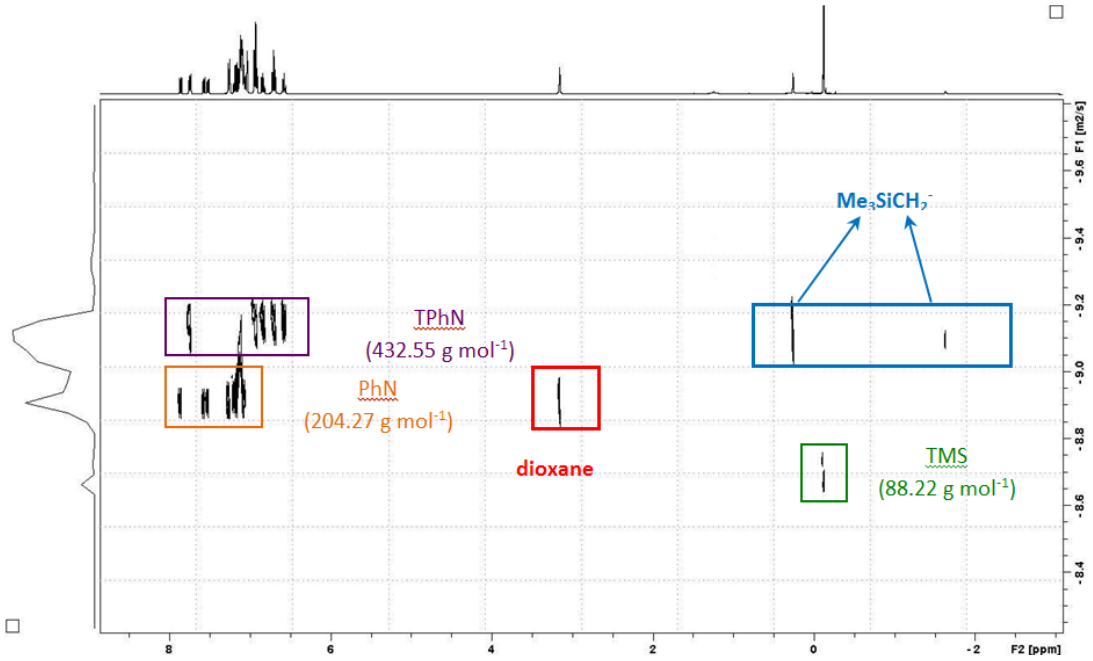


**Figure 2.13**: $^1$H-DOSY NMR spectrum of [(dioxane)$_2$LiMg($CH_2SiMe_3$)$_3$] (**3**), TPhN, PhN and TMS at 27 °C in $C_6D_6$ (signal intensity of the MC*H*$_2$ cross point was increased for presentational purposes).

The inferred size for the dioxane in solution differs substantially from the FW of [(dioxane)$LiMgR_3$] (381 g $mol^{-1}$, error with respect to DOSY size = 47%) and from the FW of free dioxane (88 g $mol^{-1}$, error with respect to DOSY size = -148%). Furthermore, when free dioxane is subjected to a $^1$H-DOSY experiment following the standard procedure described above with the same internal standards, a FW of 89 g $mol^{-1}$ is interpolated (error with respect to DOSY size of 1%). These results, coupled with the different chemical shifts observed for the dioxane protons in the $^1$H NMR spectra in **3** in comparison with that found for free dioxane, indicate that in solution the dioxane molecules partially dissociate from the {$LiMgR_3$} unit. A plausible situation could be the dissociation of the bridging dioxane molecules which propagate the polymeric structure of **3**, which would give rise to the formation of

monomeric {(dioxane)LiMgR$_3$} aggregates, as similarly described for **2**. A comparison of the estimated FW of the {LiMgR$_3$} unit (393 g mol$^{-1}$) and the $^1$H-DOSY experiment shows a good agreement with this solution scenario ({(dioxane)LiMgR$_3$}, 381 g mol$^{-1}$, -3% from the predicted FW value); however, it must be noted that this dynamic equilibrium can give an artificial estimate of the molecular weight of the R-containing molecules, as the value obtained for the diffusion coefficient *D* will be the average of the diffusion coefficients of the individual species in which R is reasonably involved (as for example [(dioxane)LiMgR$_3$], [(dioxane)$_2$LiMgR$_3$] or LiMgR$_3$).[120]

With respect to dioxane-solvated polymer **4**, $^1$H-DOSY experiments revealed deaggregation to two sizes of distinct dioxane-containing lithium magnesiate species in solution (species A and B, **Figure 2.14**). However, due to the overlap of the signals between these species the FW for the individual components in solution cannot be ascertained due to interference. Furthermore, some caution would have to be applied as the signals corresponding to species A lie slightly out of the range of the diffusion coefficients delimited by the trend-line.

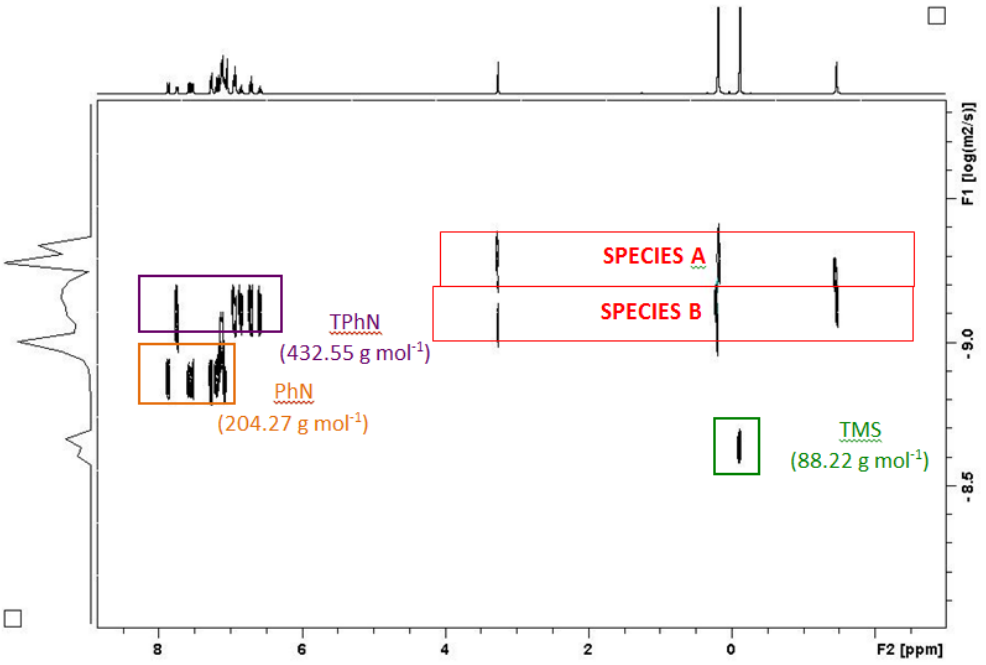


**Figure 2.14**: $^1$H-DOSY NMR spectrum of [(dioxane)Li$_2$Mg$_2$(CH$_2$SiMe$_3$)$_6$] (**4**), TPhN, PhN and TMS at 27 °C in C$_6$D$_6$.

Switching to deuterated toluene as a solvent, crystals of **4** were dissolved to allow for low temperature $^{1}$H NMR analysis of the solution. At 298 K an expected 1:3 ratio of dioxane: R group is observed. However, on cooling to 270 K the proportion of dioxane falls to 0.25:3, and the solution becomes cloudy, suggesting that a less soluble dioxane-containing species is precipitating. Unfortunately a low temperature DOSY experiment could not be carried out due to the lower solubility of the product, suggesting aggregation is taking place at low temperature.

## 2.4 Conclusions

Highlighting the structural diversity of alkali-metal magnesiates, this systematic study of the co-complexation reactions of homometallic alkyls LiR and $MgR_2$ in the presence of several Lewis bases, including TMEDA and THF, two of the most commonly used donor molecules in organic synthesis for the activation of organometallic reagents such as BuLi or RMgX, has revealed that the final outcome of these reactions is controlled by the donor ligand employed. Thus, for oxygen donors such as THF and dioxane, the formation of polymeric chains **2**, **3** and **4** is observed, although two distinct types of supramolecular arrangements are seen for each donor. For THF adduct **2**, an unusual structure is obtained, comprising an infinite chain held together by intermolecular Mg-C-Li electron deficient bonds. Contrastingly, for the dioxane-containing polymers, **3** and **4** are formed as a consequence of the ability of this donor to act as a 1,4-bridge through its two oxygen atoms, linking $\{LiMgR_3\}$ or $\{LiMgR_3\}_2$ units to afford **3** and **4** respectively. The use of didentate and tridentate N-donor ligands TMEDA and PMDETA allows the formation of discrete molecular structures, although they have markedly different effects on the constitution/structure of the lithium magnesiate. TMEDA induces a redistribution process of the mixed-metal precursor $[LiMgR_3]$ (**1**) to form the higher order tetraorganomagnesiate $[(TMEDA)_2Li_2MgR_4]$ (**5**) along with $MgR_2$. On the other hand, PMDETA is found to form monomeric complex $[(PMDETA)LiMgR_3]$ (**6**) which, exhibiting an unusual open structural motif can be envisaged as an intermediate between a solvent-separated ion pair and a contacted ion pair magnesiate structure. This compound can react with $O_2$ to yield the novel

$[\{(PMDETA)_2Li_2Mg(CH_2SiMe_3)_3\}^+\{Mg_3(CH_2SiMe_3)_6(OCH_2SiMe_3)\}^-]$ (**7**) which represents to the best of our knowledge the first example of a cationic lithium magnesiate moiety. Shedding new light on the constitution of these new mixed-metal species in solution, compounds **2**-**7** were characterized by $^1H$, $^{13}C$ and $^7Li$ NMR, with the aid of $^1H$-DOSY NMR which revealed that the supramolecular structures of compounds **2**, **3** and **4** are not retained in solution, breaking into smaller monomeric aggregates, where the interaction with the Lewis donor is maintained.

Collectively these results highlight the complexity chemistry that lithium magnesiates can display in solution and shed new light in the effect that donor solvents play in the structure/constitution of these intriguing bimetallic reagents.

# Chapter 3: Homoleptic alkyl magnesiate complexes of heavier alkali-metals

## 3.1 Nitrogen donor Lewis bases with sodium and potassium

Descending the s-block sees an increase in the size of the metals and concomitant change in physical properties, such as decreasing melting point (from 180.5 °C for Li to 28.59 °C for Cs) and ionisation enthalpies, ranging between 520.1 kJ $mol^{-1}$ observed with lithium to 375.6 kJ $mol^{-1}$ with cesium (for first ionisation enthalpies).[2] Notably, the electropositivity increases with increasing size and the resulting compounds are more reactive and less soluble which makes their preparation and characterisation synthetically challenging, as side reactions can occur such as metallation of the solvent, β-elimination or self-metallation.

### 3.1.1 Complexes of sodium

Building on the findings with lithium magnesiates described in **Chapter 2**, attention then turned to the synthesis of related alkyl sodium magnesiates. To this end, TMEDA was firstly added to an equimolar mixture of NaR and $MgR_2$. As with the corresponding lithium example, the tetraalkylmagnesiate formed with concomitant formation of $MgR_2$ suggesting that if the expected [(TMEDA)$NaMgR_3$] product is formed it must undergo a redistribution to yield [$(TMEDA)_2Na_2MgR_4$] along with $MgR_2$ (**Scheme 3.1**, **Figure 3.1**). Amendment of the stoichiometry to a 2:1:2 ratio of NaR:$MgR_2$:TMEDA resulted in the formation of **8** in 54% isolated yield.

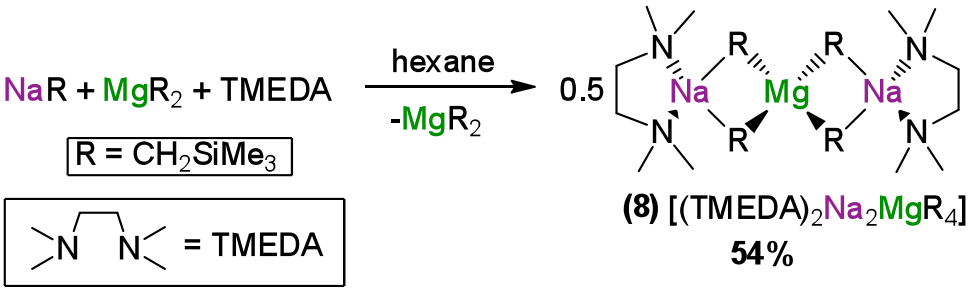


**Scheme 3.1:** Synthesis of **8**

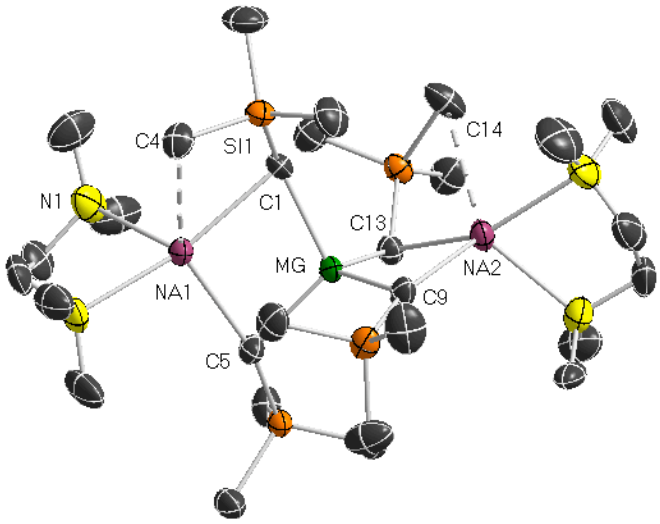


**Figure 3.1:** Molecular structure of **8**. Displacement ellipsoids are drawn at the 50% probability level. Hydrogen atoms and minor disorder in TMEDA omitted for clarity. Selected bond angles and distances, Mg-C1 2.291(2) Å, Mg-C5 2.237(2) Å, Mg-C9 2.251(2) Å, Mg-C13 2.280(2) Å, Na1-C1 2.556(2) Å, Na1-C5 2.659(2) Å, Na1-C4 2.953(3) Å, Na2-C9 2.623(2) Å, Na2-C13 2.568(2) Å; C1-Mg-C13 105.36(9)°, C5-Mg-C9 116.02(9)°, C9-Mg-C13 110.99(8)°, N1-Na1-N2 74.87(8)°, N1-Na1-C5 111.83(9)°, N2-Na1-C1 166.59(8)°, N3-Na2-N4 75.57(8)°, N3-Na2-C9 117.78(8)°, N3-Na2-C13 147.19(8)°, Na1···Mg···Na2 156.72(4)°.

The structure of **8** was confirmed by X-ray crystallography. In line with the related Li structure **5**, **8** also adopts a linear "Weiss motif", and the alkyl groups form unsymmetric μ bridges between the central magnesium atom and the sodium atoms, with a bent arrangement found between the Na1···Mg···Na2 of 156.72(4)º. Mg adopts a slightly distorted tetrahedral geometry with a modest range of angles found, from 105.36(9)º to 116.02(9)º with an average value of 109.4º. Na coordinates to a TMEDA molecule, which fills two of its coordination sites, and also binds to two bridging alkyl groups. Na is found to have more distortion in its tetrahedral environment, due to the acute angles enforced by the chelation of the donor molecule (N1-Na1-N2 74.87(8)º and N3-Na2-N4 75.57(8)º), with average angles around Na1 and Na2 both equalling 108.3º. To quantify further, Houser *et al* reported a convenient geometric index ($\tau_4$) for four-coordinate complexes to define the molecular shape of a structure, and its alignment to a perfect tetrahedron (**Equation 3.1**).[121]

$$\tau_4 = \frac{360° - (\alpha + \beta)}{141°}$$

**Equation 3.1**: Houser geometry index for four-coordinate complexes, $\tau_4$, where $\alpha$ and $\beta$ are the two largest angles around the atom

The value of $\tau_4$ will range from unity for a perfect tetrahedron as $\alpha$ and $\beta$, the largest angles around the atom of interest, will both equal 109.5, thus $\tau_4$ = (360 – (109.5 + 109.5))/141 = 1. In the case of a square planar geometry $\tau_4$ will be zero: $\alpha = \beta = 180$, giving 0/141 = 0. All intermediate structures will have a value 0-1. In **8**, the largest angles around Mg, hence $\alpha$ and $\beta$ values, are 116.02° and 110.99°. Applying **Equation 3.1** $\tau_4$ = (360 – (116.02 + 110.19))/141 = 0.95, confirming a geometry only slightly distorted from tetrahedral. Looking at Na1, the $\alpha$ and $\beta$ values are 166.59° and 111.83°, giving a $\tau_4$ value of 0.58, which shows a distinct distortion from tetrahedral enforced by the chelating TMEDA molecule. Inspection of Na2 ($\alpha$ = 147.19°, $\beta$ = 117.78°) reveals $\tau_4$ to be 0.67, demonstrating a significant degree of distortion.

The Na-C bond distances (mean length 2.6015 Å) fall within the range found in the literature for similar compounds.[105, 122] Comparing the structure of **8** with the lithium analogue **5** shows little deviation in the Mg-C bond distances (mean distance of 2.268 Å in **5** and 2.265 Å in **8**) but a notable difference is observed in the alkali metal-C bond distance (from a mean distance of 2.228 Å in **5** to 2.602 Å in **8**) as would be expected due to the increased radii of the cation. The more covalent Mg-C interactions may be considered the anchoring bonds, giving a $[MgR_4]^{2-}$ framework and the more ionic alkali metal-carbon are ancillary, giving a CIP structure.[93b] In addition, the sodium atoms attain a higher coordination by forming a long distance interaction with the Me groups of neighbouring $SiMe_3$ groups (Na1···Me(C4) 2.953(3) Å). Analysis by NMR was straight forward, with the proton spectra showing singlets at -1.78 ppm for the methylene group attached to the metal, 0.47 ppm for the methyl of the alkyl group and signals at 1.67 and 1.92 ppm for the C$H_2$ and C$H_3$ groups of TMEDA respectively.

Moving to the tridentate nitrogen donor PMDETA, tetraalkylmagnesiate **9** was prepared by the addition of equimolar equivalents of NaR and $MgR_2$ in hexane, followed by one equivalent of PMDETA. After gentle heating to afford a solution, storage in the freezer for 16 hours resulted in the formation of good-sized crystals, which were isolated in the drybox in 26% isolated yield (with respect to NaR). As with the closely related TMEDA adduct, the PMDETA molecule was also shown to form the tetraalkylmagnesiate (from a redistribution of [(PMDETA)$NaMgR_3$] to **9** and $MgR_2$), as confirmed by X-ray crystallography (**Scheme 3.2**, **Figure 3.2**). A microcrystalline yield of 57% was attained when the synthesis was carried out using the correct stoichiometry with respect to the product. The formation of the tetraalkylmagnesiate **9** is in contrast to the Li variant, where the trialkylmagnesiate [(PMDETA)$LiMgR_3$] **6** could be isolated (*vide supra*).

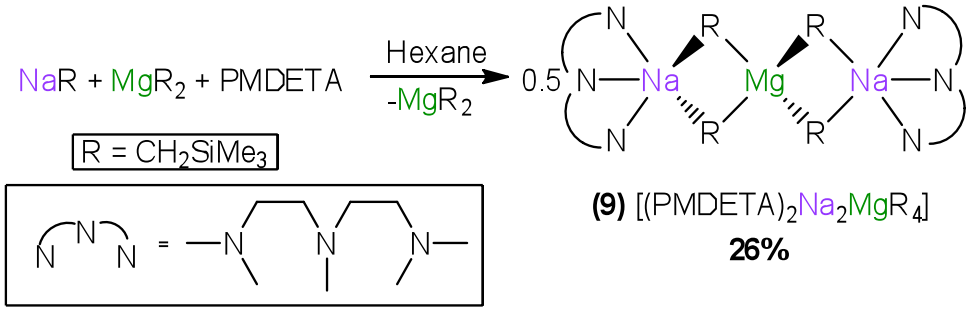


**Scheme 3.2:** Synthetic route to **9**

The solid-state structure of **9** is akin to the structure of [$(PMDETA)_2Na_2MgPh_4$] reported by Weiss in 1989.[74] Na is pentacoordinated in a distorted trigonal bipyramidal environment, bonded to two bridging R groups and three chelating N atoms from a molecule of PMDETA. The Na-C bond distances are slightly shorter in **9** than the related Weiss structure (mean length of 2.711 Å in **9** versus 2.789 Å). Comparing the Na-C bond distances with the TMEDA adduct **8** (mean length 2.6015 Å) reveals a lengthening (weakening of the Na-C bond), due to the increased coordination number of the Na atom which is now coordinated to three N donor atoms of the PMDETA ligand instead of two in TMEDA. Mg is surrounded by four carbanionic ligands and adopts a very slightly distorted tetrahedral geometry ($\tau_4$ value of 0.94) with an average angle of 109.5º observed, with a range covering

102.78(19)º to 114.80(2)º. The Mg-C bond distances (average length 2.289 Å) are comparable with those found in the related TMEDA structure **8** (mean length 2.26475 Å). The sodium atoms and magnesium in **9** adopt an almost linear arrangement, with an angle of 174.69(7)º observed. In contrast, the TMEDA adduct **8** displays a Na···Mg···Na angle of 156.72(4)º, which may be forced by the presence of secondary interactions obtained from neighbouring methyl groups in the tetracoordinated Na in **8** which is not observed in the pentacoordinated Na in **9**.

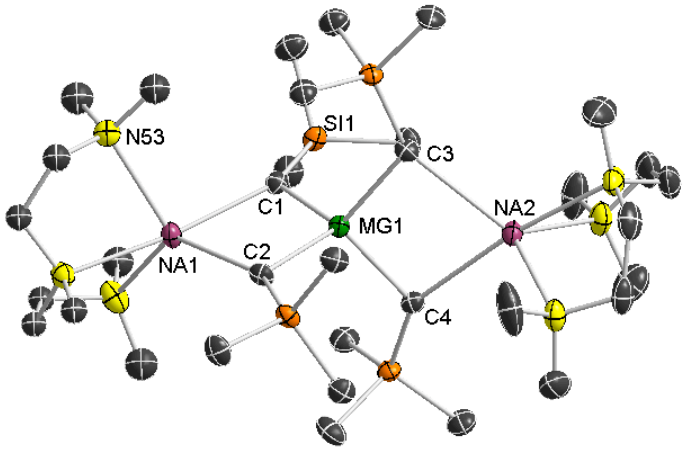


**Figure 3.2:** Molecular structure of **9**. Displacement ellipsoids are drawn at the 50% probability level. Hydrogen atoms and minor disorder in one PMDETA molecule omitted for clarity. Selected bond distances and angles; Mg-C1 2.293(5) Å, Mg-C4 2.2689(5) Å, Mg-C3 2.296(5) Å, Mg-C2 2.298(5) Å, Na1-C1 2.650(5) Å, Na1-C2 2.714(5) Å, Na2-C4 2.739(5) Å, Na2-C3 2.741(5) Å; C4-Mg-C1 110.70(19)°, C4-Mg-C3 102.78(19)°, C1-Mg-C3 114.8(2)°, C4-Mg-C2 111.81(19)°, C1-Mg-C2 104.05(18)°, C3-Mg-C2 112.96(18)°, Na1···Mg···Na2 174.69(7)°.

These investigations into solvated alkyl sodium magnesiates suggest that in the presence of N-chelating donors for Na/Mg combinations the stoichiometric variant $Na_2MgR_4$ seems to be more favoured than $NaMgR_3$. Furthermore, it shows that by changing the hapticity of the donor from didentate ligand TMEDA to tridentate ligand PMDETA has very little difference in the structure of the bimetallic compound, which is in contrast with the Li structure which showed a marked difference in the structures obtained by adding TMEDA *cf* PMDETA.

### 3.1.2 Complexes of potassium

Potassium was next examined in order to evaluate the role played by the alkali metal in this family of magnesiate structures as the electron count increases from [He]2s (Li), [Ne]2s (Na) to [Ar]2s (K). Organopotassium reagents exhibit low solubility and are unstable and as such very few compounds have been elucidated;[123] however, addition of $MgR_2$ and *N*-donor ligands can stabilise potassium and lead to the successful isolation and characterisation of these heavier alkali metal complexes.[124] As before, *N*-donor chelating ligands TMEDA and PMDETA were examined. As shown in **Scheme 3.3**, addition of an equimolar amount of TMEDA to a stirred suspension of KR and $MgR_2$ in hexane gave the same discreet formula obtained with the lithium and sodium analogues $[(TMEDA)_2M_2MgR_4]$ (M = Li **5**, Na **8**, K **10**) in a 60% yield (with respect to KR). This result was somewhat unexpected as the larger K ion would not be anticipated to remain four-coordinate. Furthermore, achieving the same molecular formula for Li, Na and K derivatives is exceptionally rare.[125] Thus, for example, recent work by O'Hara has shown that for the TMEDA-solvated potassium diphenylamide, each K atom binds to *two* molecules of TMEDA with one acting as a chelating ligand and one acting as a monodentate bridge which coordinates through one of the N atoms (mimicking a PMDETA ligand) allowing K to achieve pentacoordination and resulting in a polymeric chain (**Figure 3.3**).[126]

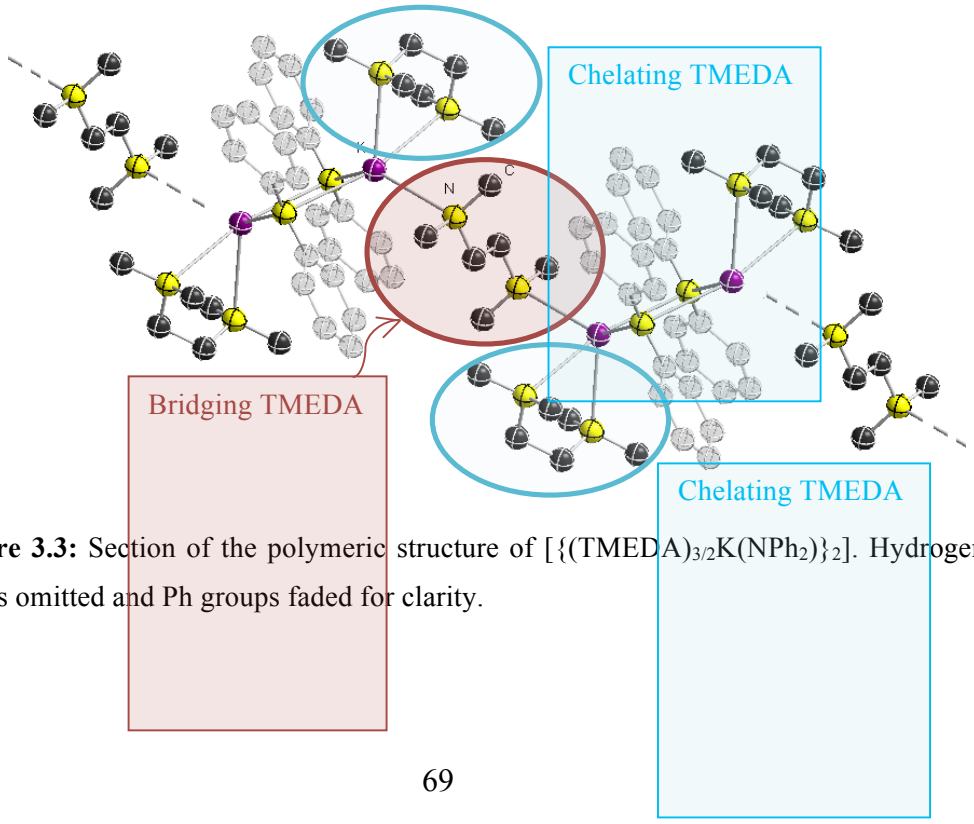


**Figure 3.3:** Section of the polymeric structure of $[\{(TMEDA)_{3/2}K(NPh_2)\}_2]$. Hydrogen atoms omitted and Ph groups faded for clarity.

With respect to complex **10**, X-ray crystallographic analysis of the light orange crystals revealed a structure that deviates from the pseudo-linear alkali metal···Mg···alkali metal exhibited by Li and Na analogues **5** and **8** respectively (**Figure 3.4**).

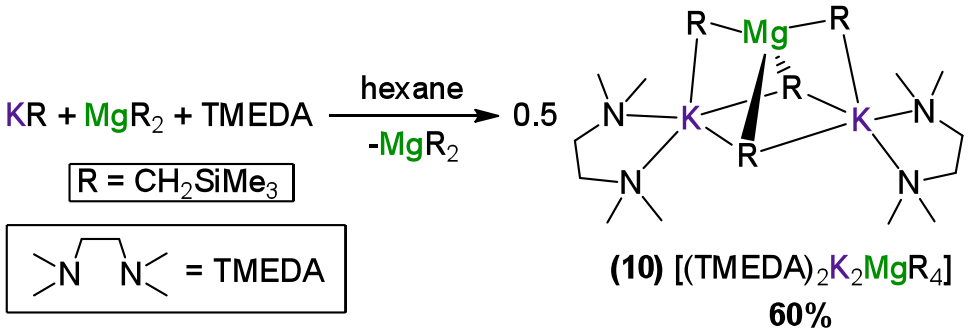


**Scheme 3.3:** Preparation of **10**

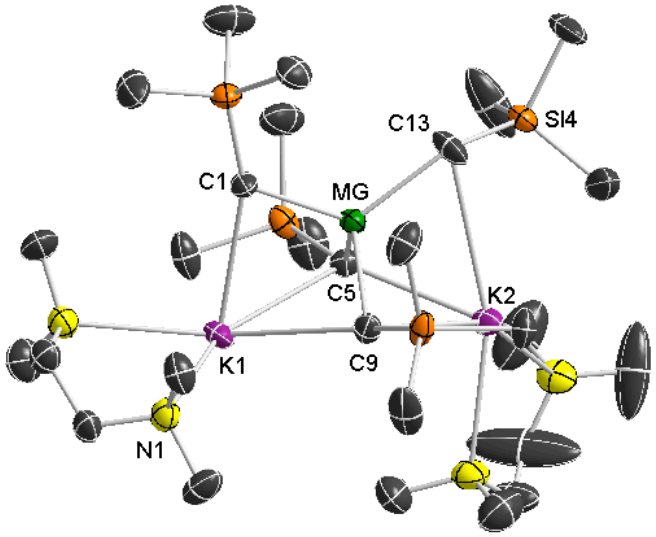


**Figure 3.4:** Molecular structure of **10**. Displacement ellipsoids are drawn at the 50% probability level. Hydrogen atoms have been omitted for clarity. Selected bond angles and distances, Mg-C1 2.232(2) Å, Mg-C5 2.2951(18) Å, Mg-C9 2.314(2) Å, Mg-C13 2.3202(2) Å, K1-N1 2.9036(17) Å, K1-N2 2.8599(18) Å, K1-C1 3.418(2) Å, K1-C5 3.116(2) Å, K1-C9 3.006(2) Å, K2-N3 2.9016(19) Å, K2-N4 2.8466(18) Å, K2-C5 3.159(2) Å, K2-C9 3.199(2) Å, K2-C13 3.0428(18) Å; C1-Mg-C5 109.33(8)°, C1-Mg-C9 111.39(9)°, C1-Mg-C13 120.09(8)°, C5-Mg-C9 102.41(7)°, C5-Mg-C13 110.94(7)°, C9-Mg-C13 101.04(8)°, K1···Mg···K2 100.145(19)°.

As can be seen from **Figure 3.4**, each K atom attains pentacoordination in **10**, resting in a distorted trigonal bipyramid geometry, by binding to three alkyl ligands and a chelating molecule of TMEDA. In order to achieve this pentacoordination the K1···Mg···K2 angle is approaching right-angled at 100.145(19)º, and the common "Weiss motif" observed in the Li and Na analogues is bent and distorted, allowing K to interact with three of the four R groups. Mg is tetracoordinated, bonding to four alkyl groups in a distorted tetrahedral fashion, with an average angle of 109.2º and a $\tau_4$ value of 0.91, showing this structure to be furthest from a perfect tetrahedron out of the Li, Na and K analogues, which could be due to the different types of alkyl groups present in **10**. To elaborate, in structures **5** and **8**, each alkyl group bridges between one alkali metal and Mg; however, in **10** C5 and C9 interact with each K and Mg, achieving a coordination number of 6 (each carbon interacts with two K atoms, one Mg atom, one Si atom and two H atoms) whereas C1 and C13 coordinate to one K and Mg and attain a coordination number of 5. Despite these differences in the coordination number of the R groups, the Mg-C bonds are all similar in length (mean length 2.290 Å). In addition, in spite of the much larger alkali metal present, the Mg-C bond distances are comparable with the TMEDA-solvated structures **5** (Li compound, 2.268 Å) and **8** (Na compound, 2.26475 Å). Comparing the average $M^I$-C bond lengths in **10** with **5** (2.228 Å) and **8** (2.6015 Å) reveals the distances in **10** to be much longer, due to the increase in radii moving down group 1. The K-C distances range from 3.006(2) Å (K1-C9) to 3.418(2) Å (K1-C1) which may be anticipated as a result of the different R groups present (C9 coordinates to both K and Mg whereas C1 coordinates to only one K and the Mg); however the bond length of K2-C13 (C13 coordinates to one K and Mg, as per C1) is short at 3.0428(18) Å and more similar to the bond length of C9, as such there is no distinct pattern in K-C bond distances depending on the different coordination numbers of the alkyl groups present. Having stated that, the K-C bond distances in **10** fall within the range of other K-C bond lengths reported in the literature.[106, 123, 127]

Inspection of the $^1$H NMR of **10** does distinguish between the different electronic environments of the carbanions, with a splitting of the C$H_2$ and even the C$H_3$ groups observed at room temperature, showing two different R group environments are

present, suggesting the solid-state structure is retained in $C_6D_6$ solution. The resonances for the TMEDA protons are atypical, giving an overlapping signal at 1.93-1.94 ppm for the methylene and methyl protons, which are normally well defined (*vide infra*), suggesting a dynamic exchange may be taking place in solution between potassium solvated by the Lewis donor and potassium interacting with the arene solvent. This structure represents, as far as we can ascertain, the first homoleptic alkyl K-Mg compound to be structurally defined.

To complete these investigations, PMDETA was added to an equimolar mixture of KR and $MgR_2$ in hexane resulting in an oil forming. Storing the Schlenk in the freezer overnight resulted in the crop of crystals depositing in 50% yield (with respect to KR). Confirmation of the bimetallic constitution of **11** was established by X-ray crystallographic studies (**Scheme 3.4**, **Figure 3.5**).

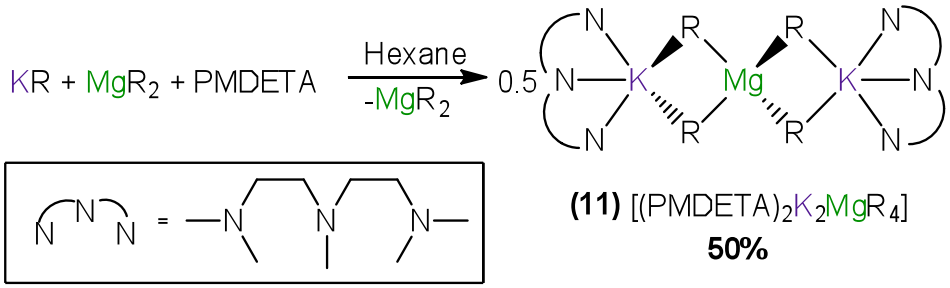


**Scheme 3.4:** Preparation of **11**

Structure **11** is a return to the "Weiss motif", showing a linear K···Mg···K arrangement (angle 174.18(3)º) previously described for **5**, **8** and **9**. K is pentacoordinated and bonds to the three nitrogen atoms from a solvating PMDETA ligand and two bridging alkyl groups, adopting a distorted trigonal bipyramidal geometry. The K-C bond lengths in **11** (average 3.0195 Å) are shorter than those found in **10** (mean 3.1568 Å). As found in the other structures described that adopt this linear motif (**5**, **8**, and **9**) and even structure **10** that deviates from it but displays a tetracoordinate Mg, the Mg-C bond lengths are all comparable (mean length in **11** = 2.265 Å). As it appears that the Mg-C bond distances change very little this suggests that the $[MgR_4]^{2-}$ unit is anchoring the structure (with Mg-C σ-bonds), whereas the $M^I$-C interactions are ancillary bonds (electrostatic interactions).[93b]

The Mg atom resides in a slightly distorted tetrahedral environment, with a small deviation of angles around Mg from 106.55(9)º to 114.79(9)º and with an average angle of 109.5º and a $\tau_4$ value of 0.93 indicating the Mg is "more tetrahedral" in **11** than in **10**. $^1$H NMR spectroscopy showed the expected resonances, with singlet signals at -1.56 and 0.47 ppm for the methylene and methyl groups of the alkyl ligand, and signals in the region 1.72-1.94 ppm for the PMDETA molecule.

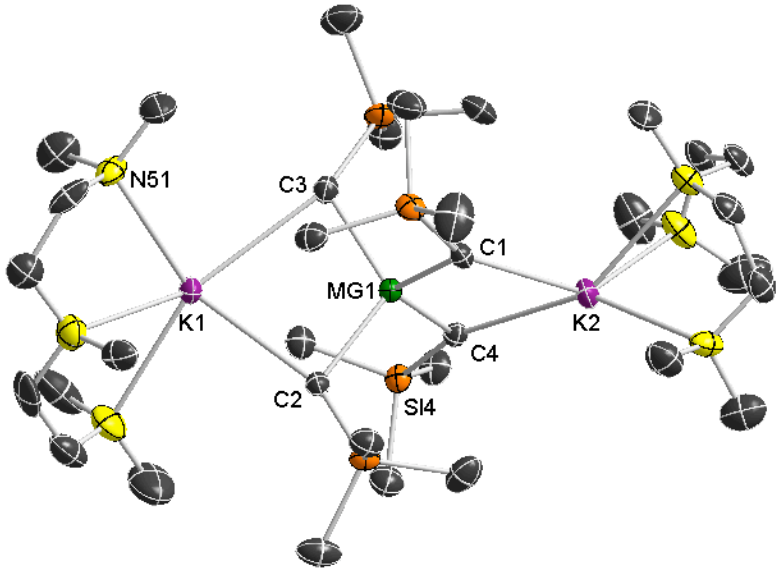


**Figure 3.5:** Molecular structure of **11**. Displacement ellipsoids are drawn at the 50% probability level. Hydrogen atoms and minor disorder in PMDETA omitted for clarity. Selected bond distances and angles, K1-C2 3.002(2) Å, K1-C3 3.062(2) Å, K2-N61 2.870(4) Å, K2-N62 2.871(4) Å, K2-N63 2.877(5) Å, K2-C4 2.999(2) Å, K2-C1 3.015(2) Å, Mg-C2 2.251(2) Å, Mg-C3 2.261(2) Å, Mg-C4 2.273(2) Å, Mg-C1 2.274(2) Å; N51-K1-C3 90.72(11), N52-K1-C3 146.4(2), N53-K1-C3 149.81(7), C2-K1-C3 76.94(6), C2-Mg-C3 113.44(9)°, C2-Mg-C4 106.59(9)°, C3-Mg-C4 107.82(9)°, C2-Mg-C1 106.55(9)°, C3-Mg-C1 107.83(9)°, C4-Mg-C1 114.79(9)°, K2···Mg···K1 174.18(3)°.

### 3.1.3 Structural comparisons in a homologous series: TMEDA

As mentioned previously, the existence of a homologous series of structures with Li, Na and K attaining the same empirical formula is relatively rare,[125, 128] as moving down the s-block the cations show a greater propensity for polarisation and have a

larger coordination sphere and therefore strive to attain a higher coordination number than the smaller Li.[42] Potassium also displays a higher affinity for π-bonding, for example, in the homologous series reported for $PhCH_2M{\cdot}Me_6TREN$ (M = Li, Na, K, $Me_6TREN$ = tris(*N*,*N*-dimethyl-2-aminoethyl)amine) the position of the cation moves from a Li-C σ-interaction to an exclusive K-C π-interaction, with the potassium resting above the aromatic ring.[125] In this instance the homologous series is achieved by the capacity of K to fold the structure in such a way as to allow each K to bond to three of the four alkyl groups present and become five-coordinate. Thus, the series can be described by the general formula $[(TMEDA)_2M_2MgR_4]$ (where M = Li, Na or K), which is in contrast to the different formulae observed mixing the tridentate PMDETA ligand to an equimolar mixture of $M^IR$ and $MgR_2$, where the Li structure (**6**) is a trisalkylmagnesiate $[(PMDETA)LiMgR_3]$ while the Na (**9**) and K (**11**) structures are both tetraalkylmagnesiates $[(PMDETA)_2M_2MgR_4]$ (where M = Na or K). **Figure 3.6** demonstrates the difference in the structural make up of TMEDA solvates $[(TMEDA)_2M_2MgR_4]$ M = Li (**5**) and Na (**8**) analogues, which adopt a linear $M^I{\cdots}Mg{\cdots}M^I$, in comparison with the K structure (**10**).

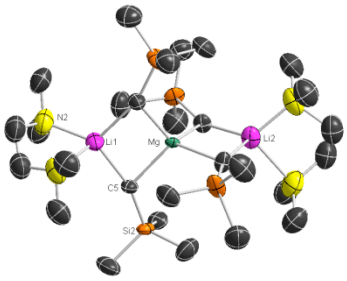


(**5**)

**$[(TMEDA)_2Li_2MgR_4]$**

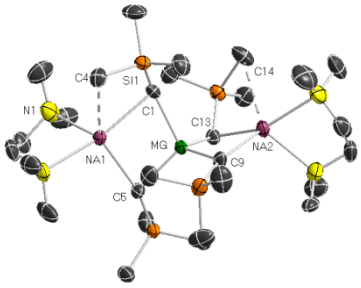


(**8**)

**$[(TMEDA)_2Na_2MgR_4]$**

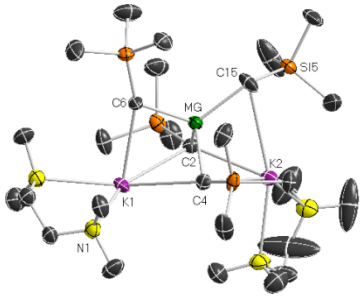


(**10**)

**$[(TMEDA)_2K_2MgR_4]$**

**Figure 3.6:** Molecular structures of **5**, **8** and **10**

The M1···Mg···M2 bond angle decreases from almost linear in the Li structure (175.2(11)º) through bent 156.71(4)º in Na and approaches right-angled 100.145(19)º in the K structure (see **Table 3.1** for selected bond distances and angles of **5**, **8** and **10**). As the radii of the alkali metal increases the alkali metal-carbon bond length also increases in line with what would be expected; the average length for Li-C =

2.228 Å, average length Na-C = 2.6015 Å, average length of K-C = 3.1568 Å. However, the Mg-C bonds are essentially the same in all molecules, displaying very little disparity in bond distance in spite of two different alkyl groups present in **10**. As mentioned previously, the similarity in the Mg-C bond lengths arises from strong, anchoring bonds where the carbanions align around the stronger Lewis acid, and onto which the alkali metals form ancillary M-C bonds.[93b] Sodium derivative **8** can be envisaged as an intermediate between **5** with a four-coordinate Li and a near linear arrangement of the three metals, and **10** with a pentacoordiante K structure and a severe distortion from linearity across the K···Mg···K vector, as although Na is four-coordinate it attains extra stability by interacting electrostatically with the methyl group of the TMS.

**Table 3.1**: Selected bond distances (Å) and angles (°) of **5**, **8** and **10**.

| | **5** | **8** | **10** |
|---|---|---|---|
| $M^I1\cdots Mg\cdots M^I2$ | 175.2(11) | 156.71(4) | 100.145(19) |
| $M^I$-C (average) | 2.228 | 2.6015 | 3.1568 |
| Mg-C (average) | 2.268 | 2.26475 | 2.290 |

**Figure 3.7** shows the $^1$H NMR data for **5**, **8** and **10** in $C_6D_6$ at room temperature. In **5** and **8** all the R groups are equivalent as they all bridge M-Mg (M = Li, Na) and only one set of signals is observed for the methylene and methyl protons. Conversely, two distinct R groups are found in **10**, with two of the alkyl groups having a coordination number of 6 and two of the alkyl groups with a coordination number of 5 (*vide supra*). The singlets of the alkyl C$H_2$ and C$H_3$ protons show splitting, although they are not completely resolved, suggesting that a relatively slow exchange process can be taking place in solution. Surprisingly, moving from Li to Na to K the C$H_2$ group of the alkyl bridges becomes more deshielded and moves downfield, contrary to what would be anticipated with the increasingly electropositive nature of the metal.[42]

TMEDA displays the pattern expected from a coordinated molecule, that is to say, when coordinated, the protons of the ethylene bridge are found more upfield than the methyl protons. This is contrary to what is observed in a non-coordinated molecule

of TMEDA (*i.e.* when a standard $^1$H NMR spectrum is carried out with free TMEDA in $C_6D_6$) where the N-C*H*$_2$C*H*$_2$-N proton signal is found downfield of the larger N(C*H*$_3$)$_3$ signal. Although the peak position of the methyl protons of the TMEDA molecule varies only slightly (a change in 0.10 ppm in total, ranging from 2.02 – 1.92 ppm) in moving from lithium to potassium there is a marked change in the chemical shift of the ethylene protons, with a difference of almost 0.30 ppm observed (range = 1.65 – 1.93 ppm), which suggests that at room temperature some of the TMEDA molecules in **10** may be exchanging with deuterated benzene in line with the affinity of K for π-interactions.[125]

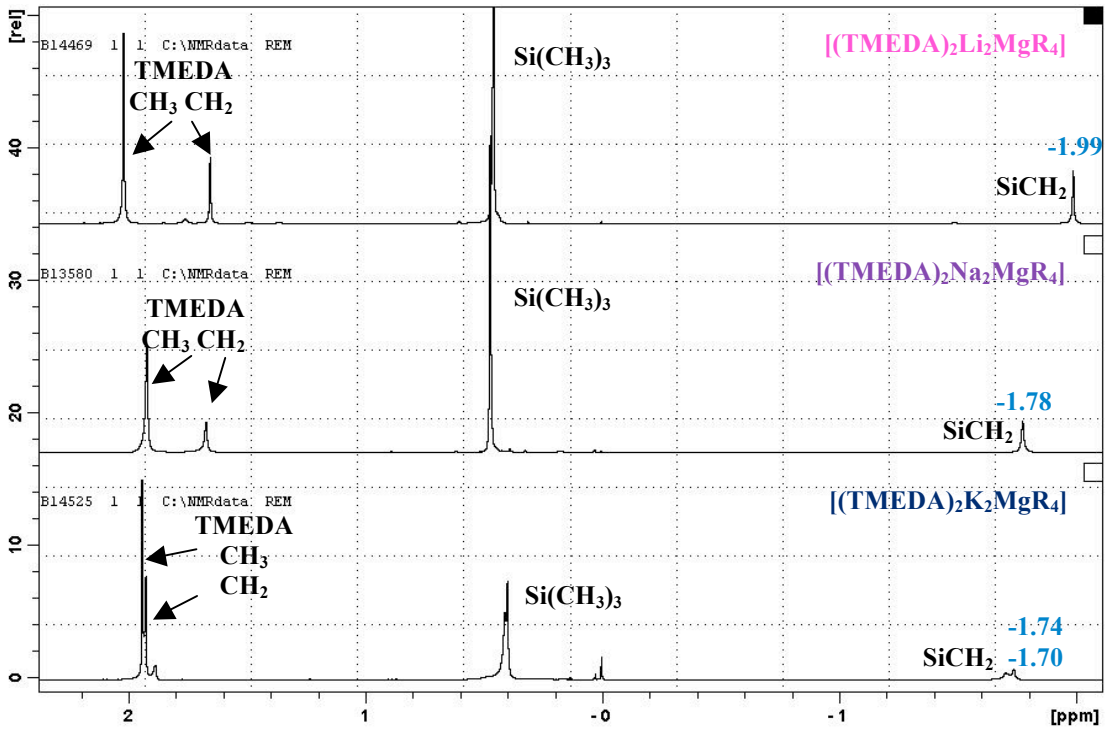


**Figure 3.7**: Comparison of the $^1$H NMR data of a series of [(TMEDA)$_2$M$_2$MgR$_4$] (M = Li, Na, K)

## 3.2 Unveiling the structure of an unsolvated homoleptic alkyl alkali-metal magnesiate

With a number of novel solvated alkali-metal magnesiates incorporating the $CH_2SiMe_3$ alkyl group synthesised to date, attention again turned to the preparation of an elusive solvent-free variant. Despite limited success in the cocomplexation

reaction of LiR with $MgR_2$ (that is to say it is limited due to the fact that although NMR data strongly supports the presence of the mixed-metal complex having been synthesised, no structural evidence could be obtained due to the decomposition of the crystals, *vide supra*), it was deemed logical that investigations continue with the heavier alkali metals Na and K. Research endeavours into the preparation of pure, solvent-free alkyl alkali-metal magnesiates are now presented.

### 3.2.1 Unsolvated sodium magnesiate [$NaMgR_3$]

In the first instance, the reaction of equimolar amounts of NaR and $MgR_2$ in bulk hexane afforded a white precipitate (**Scheme 3.5**). Addition of toluene and gentle heating gave a clear solution. The enhanced solubility together with the lack of colour in the solution were indicative of the formation of a mixed-metal compound as the precursors are both insoluble in the solvent mixture, and even more revealingly, NaR readily deprotonates toluene at room temperature resulting in an orange precipitate forming ($NaCH_2Ph$). On cooling, the colourless solution deposited crystals of **12** as determined by NMR spectroscopy and X-ray crystallography (**Figures 3.8** and **3.9**) in a 49% isolated yield (although NMR analysis of the filtrate demonstrated that the formation of **12** occurs quantitatively).

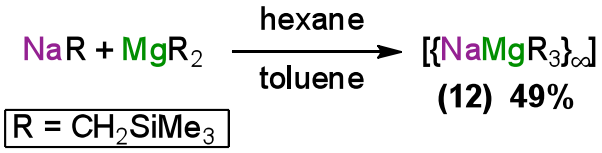


**Scheme 3.5:** Synthesis of **12**

The mixed-metal composition of **12** was confirmed by X-ray crystallography to be a solvent free alkali-metal magnesiate, which is believed to be the first example of its kind to be structurally defined and reported in the scientific literature.[117b] The basic repeat unit of **12**, shown in **Figure 3.8a**, comprises a trigonal planar Mg (sum of angles = 359.2º) bonded to three alkyl groups. One alkyl ligand bridges Mg and Na in the asymmetric unit (Na-C5 = 2.6708(19) Å, Mg-C5 = 2.1617(19) Å) whereas the remaining two alkyl groups bond to Na atoms of neighbouring units, giving rise to an

intricate two-dimensional honeycomb sheet structure which contains 12-atom $\{(NaCMgC)_3\}$ fused rings (**Figure 3.8b**) with the sterically hindered $SiMe_3$ alternately binding to each face of the sheet. Each of these rings accommodates 6 metals (3 Na, 3 Mg) and 6 alkyl ligands and is interconnected with another six rings within the polymeric structure (**Figure 3.9a**).

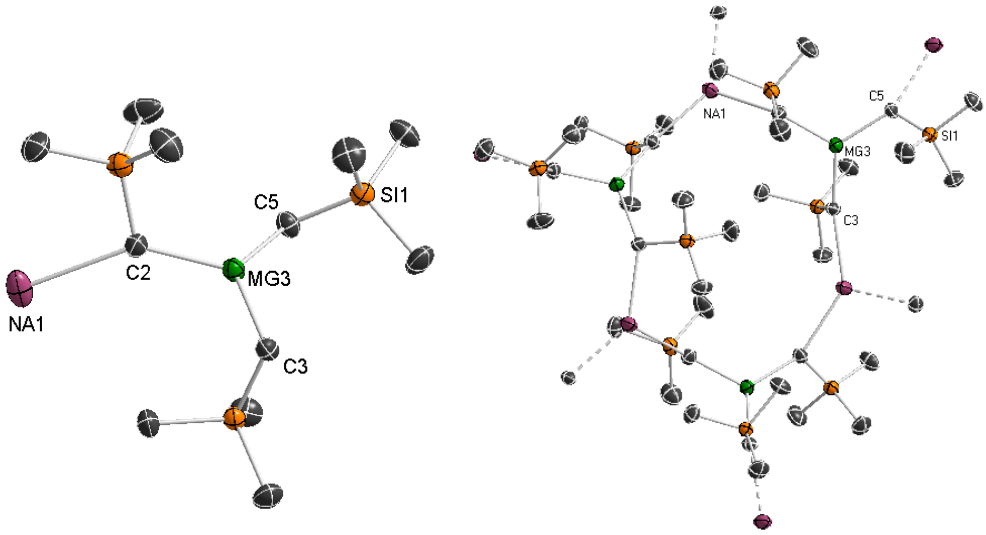


**(a)** **(b)**

**Figure 3.8:** (a) Asymmetric unit of **12**. Displacement ellipsoids are drawn at the 50% probability level. Hydrogen atoms have been omitted for clarity. Selected bond distances and angles, Mg-C1 2.154(2) Å, Mg-C5 2.1617(19) Å, Mg-C2 2.1667(18) Å, Na-C5 2.6708(19) Å; C1-Mg-C5 118.20(7)°, C1-Mg-C9 118.18(7)°, C5-Mg-C9 122.84(8)°. (b) Trimeric 12-membered ring of **12**.

This intriguing fused ring assembly is probably directed by Na, which, in order to attain a higher coordination number under solvent-free conditions needs to connect to three alkyl groups. Additionally, each Na gains further stabilisation by forming a secondary interaction with the methyl group of one $CH_2SiMe_3$ ligand ($Na\cdots MeSiMe_2$ = 3.053(2) Å), which induces a slight pyramidalisation in its geometry (sum of bond angles around Na = 354.6º).

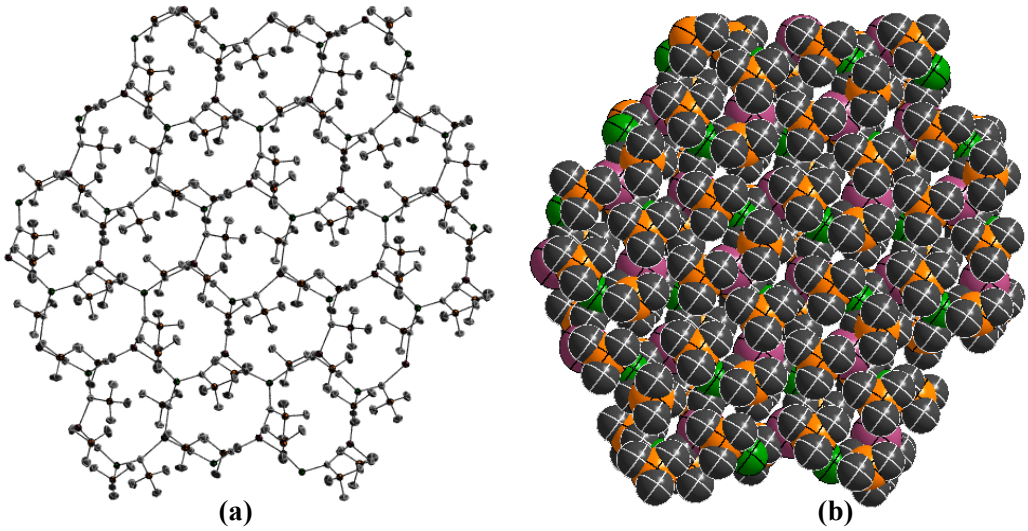


**Figure 3.9:** (a) Polymeric sheet network of **12**. (b) Space-filling model for polymeric structure of **12**. Hydrogen atoms have been omitted for clarity in both models.

In terms of supramolecular chemistry, **12** can be envisaged as a combination of trigonal nodes (Na and Mg centres) connected by alkyl ligands (spacers),[129] giving rise to a 2D infinite network in which all alkyl groups are equivalent, acting as Mg and Na linkers. Analysis of the different metal-carbon bond distances in **12** revealed no significant difference that would define a molecular unit (intramolecular Na-C bond distances = 2.6566(19) Å and 2.700(2) Å *cf* 2.6708(19) Å in the asymmetric unit), indicating that this extended sheet structure is the result of a regular arrangement of Na and Mg cations that are held together by a combination of relatively strong (short) electron-deficient Na-C and Mg-C bonds, with lengths similar to those found in discrete ate molecules.[105]

The unique 2D organometallic honeycomb structure of **12** constitutes, as far as we can ascertain, the first example of a solvent-free alkali-metal trialkylmagnesiate to be structurally defined. This ring-fused assembly is rare in general s-block chemistry, being previously found for lithiated (organosulfonyl)acetonitriles and cyanophosphonates.[130] However, the association between the distinct asymmetric units in these compounds takes pace *via* dative bonds between lithium centres and heteroatomic substituents of the anionic ligands, whereas in **12** the metallic ions are connected by highly polar electron deficient Na-C and Mg-C bonds. The infinitely

aggregated structure of **12** contrasts with solvated structures **8** and **9** which display the bimetallic trinuclear alkali metal···Mg···alkali metal motif. **12** is also markedly different from the structure exhibited by the related solvent-free tris(amido) lithium magnesiate [LiZn(HMDS)$_3$] which is a monomer where lithium is stabilised by forming intramolecular secondary agostic interactions with trimethylsilyl groups.[37] A space-filling model of **12** (**Figure 3.9b**) shows that the trimethylsilyl groups of the R group provide a protective steric shelter of the (reactive) M-C bonds.

As has been previously established, the aggregation of a molecule can play a crucial role in modulating the reactivity of s-block organometallic compounds, and this coupled with the fact that crystal structures of many of these species do not correlate with their constitution in solution[75] led to $^1$H NMR DOSY studies of **12** to be performed to assess its aggregation in $C_6D_6$ solutions. As with previous studies on polymeric structures **1-4** and **6**, 1,2,3,4-tetraphenylnaphthalene (TPhN), 1-phenylnaphthalene (PhN) and tetramethylsilane (TMS) were chosen as internal standards as they have good solubility in benzene with minimal overlapping signals and are inert to **12**. **Figure 3.10** shows the $^1$H-DOSY NMR of **12** in the presence of the internal standards in deuterated benzene at room temperature.

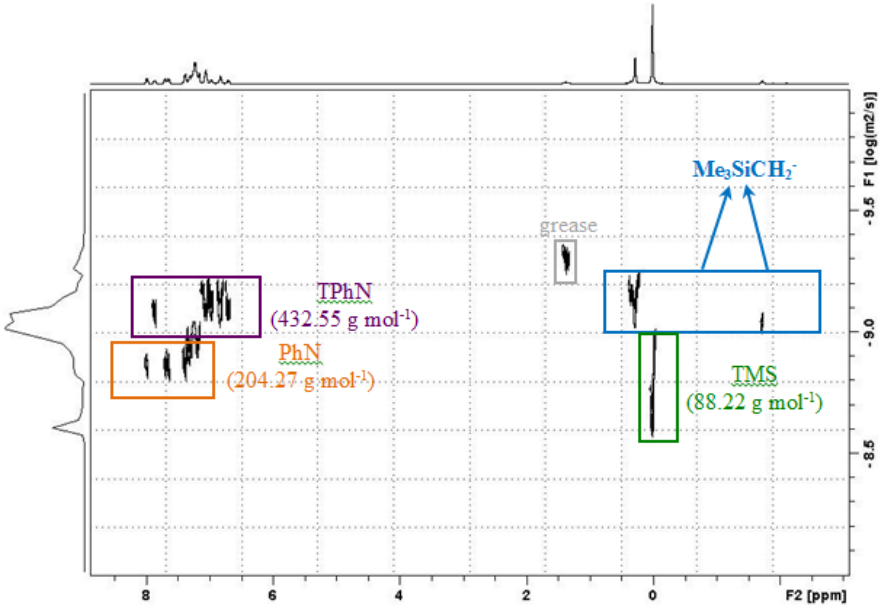


**Figure 3.10:** $^1$H-DOSY NMR spectrum of **12**, TPhN, PhN and TMS in $C_6D_6$ at 298 K. Traces of grease are also observed.

As can be seen in **Figure 3.10** all the different components of the mixture separate clearly in the diffusion dimension with a relative size sequence TPhN > $Me_3SiCH_2^-$ >> PhN >> TMS according to their decreasing *D* values [*D*(TPhN) = 7.2(1) x $10^{-10}$ $m^2$ $s^{-1}$ < *D*($Me_3SiCH_2^-$) = 7.7(2) x $10^{-10}$ $m^2$ $s^{-1}$ << *D*(PhN) = 1.25(1) x $10^{-09}$ $m^2$ $s^{-1}$ << *D*(TMS) = 1.98 x $10^{-09}$ $m^2$ $s^{-1}$]. The relation between log *D* and log FW for the internal standards proved to be approximately linear ($r^2$ = 0.99). As the signals corresponding to the $Me_3SiCH_2^-$ lie within the range of diffusion coefficients delimited by the internal references, the approximate molecular weight can be interpolated from the log *D* vs. log FW trend-line, which turns out to be 409 g $mol^{-1}$. Based on this, **Figure 3.11** depicts some possible species of **12** in solution with their respective FW values and the error for every considered structure with respect to the size predicted for **12** through the $^1$H-DOSY study.

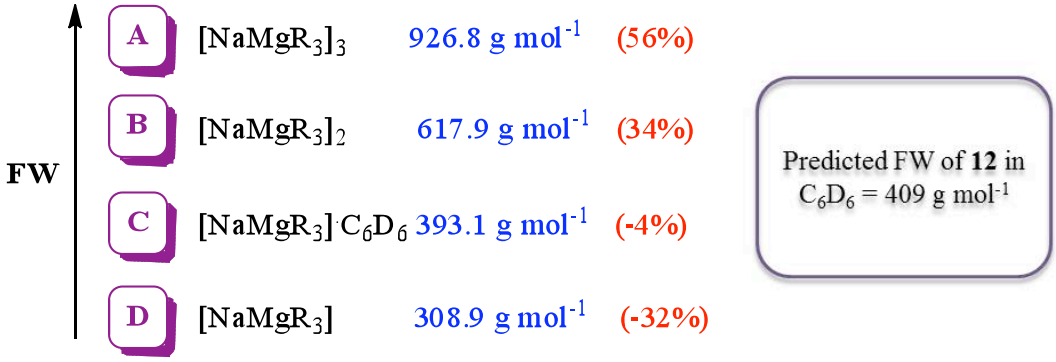


**Figure 3.11:** Possible species of **12** in $C_6D_6$ with errors (in parenthesis) with respect to the estimated FW value predicted through $^1$H-DOSY

Analysis of these data suggests that the highly oligomeric constitution of **12** in the solid-state, which is a 2D-network of monomeric unit [$NaMgR_3$], is not retained in $C_6D_6$ solution as the error associated with much smaller aggregates such as a dimer (**B**) or a trimer (**A**) is quite high (34 and 56% respectively). In addition, when considering **12** as a simple monomer (**D**) there is significant disparity with its calculated molecular weight and the estimated value obtained in the DOSY studies (-32%). These data can be interpreted as the presence of a monomer/dimer equilibrium in solution, and therefore the constitution of **12** could be represented by $[NaMgR_3]_n$ (where n = 1-2). However, a better correlation is observed for a

monomer in which sodium is solvated by a single molecule of deuterated benzene **C** (-4% error). This type of electrostatic interaction between a neutral arene molecule and an alkali-metal is well known in organometallic chemistry,[118] with several examples structurally defined by X-ray crystallography which show that the alkali-metal adopts a perpendicular disposition π engaging with the electron-rich aromatic ring. Moreover, supporting the solution scenario **C** provided by the DOSY studies, compound **12** exhibits excellent solubility in arene solvents (toluene or benzene), in contrast to its complete insolubility in non-polar solvents such as hexane or cyclohexane where these type of π interactions are not possible.

#### 3.2.1.1 Attempts to prepare unsolvated $Na_2MgR_4$ derivative

In order to prepare the stoichiometric variant [$Na_2MgR_4$], the cocomplexation reaction of two molar equivalents of NaR with $MgR_2$ was then explored. A white precipitate was again obtained in bulk hexane that dissolved on addition of toluene followed by gentle heat. The colourless solution deposited colourless crystals on cooling which were used for X-ray crystallographic studies. These studies revealed the constitution of some of the crystals to be the solvent-free sodium alkyl [$\{(NaR)_4\}_\infty$] (**13**) (**Figure 3.12**) while other crystals were found to be sodium magnesiate **12**. These results suggest that if the tetraorganomagnesiate [$Na_2MgR_4$] **14** is formed in solution, under the conditions of crystallisation it must undergo a redistribution to a mixture of **12** and **13** (**Scheme 3.6**). Note that this reorganisation is in stark contrast to that observed in the presence of Lewis basic solvents TMEDA and PMDETA, where the tetraorganomagnesiate is preferentially formed from a triorganomagnesiate reaction mixture forming **8** and **9**, respectively (*vide supra*). Previous reports have already shown that triorganomagnesiates and tetraorganomagnesiates can exist in solution as a complicated mixture of organometallic species in equilibrium with each other.[105] The position of this equilibrium can be modified by changing the temperature, the solvent mixture or by adding a substrate that will react preferentially with one of the mixed-metal compounds.

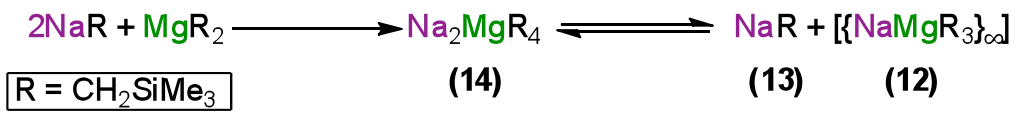


**Scheme 3.6:** Possible disproportionation of tetraalkylmagnesiate $Na_2MgR_4$ to NaR and $NaMgR_3$

In order to gain a better insight into the composition of the white precipitate obtained when two equivalents of NaR are combined with one molar equivalent of $MgR_2$ in neat hexane, the white solid was isolated and analysed by $^1H$ and $^{13}C$ NMR, that is to say, toluene was not added to solubilise the product. These data suggest that in solution tetraalkyl species $[Na_2MgR_4]$ **14** is formed. To elaborate, as shown in **Table 3.2** that compares the chemical shift data observed in the $^1H$ and $^{13}C$ NMR spectra for the monosyl group, the resonance for the C$H_2$ protons in the proposed tetraalkylmagnesiate compound (-1.88 ppm) appears at a chemical shift that lies between those found for the sodium component NaR (-2.44 ppm) and the trialkylmagnesiate **12** (-1.71 ppm). This would support the formation of a tetraorganomagnesiate with a greater carbanionic character than **12**, since the Mg atom would be bonded to four alkyl groups, but also inferior to that exhibited by the alkali-metal species NaR. Further evidence for the formation of **14** in solution is the fact that the tetraalkylmagnesiate fails to deprotonate toluene when added to solubilise the product in the attempted crystallisation of **14** (in contrast with NaR which reacts instantaneously to form benzyl sodium as a bright orange solid), which supports its mixed-metal constitution.

**Table 3.2**: Chemical shifts in the $^1H$ and $^{13}C$ NMR spectra of **12**, **13** and **14** in $C_6D_6$ solution

| Compound | $\delta^{1H}$ C$H_2$ | $\delta^{1H}$ (C$H_3$)$_3$ | $\delta^{13C}$ C$H_2$ | $\delta^{13C}$ (C$H_3$)$_3$ |
|---|---|---|---|---|
| NaR (**13**) | -2.44 | 0.15 | -6.30 | 4.91 |
| $[\{NaMgR_3\}_\infty]$ (**12**) | -1.71 | 0.28 | -2.44 | 4.54 |
| $Na_2MgR_4$ (**14**) | -1.88 | 0.22 | 0.01 | 7.10 |

In order to shed more light on the plausible equilibrium depicted in **Scheme 3.6** a variable temperature $^1H$ NMR study of the proposed tetraalkylmagnesiate species was attempted in deuterated toluene solutions. Unfortunately, the solubility of these

species is extremely dependent on temperature and below 5-10 ºC these solutions turn extremely cloudy, precluding the acquisition of meaningful NMR spectra.

At this juncture it is noteworthy to highlight that previous attempts within our group to crystallise the solvent-free sodium alkyl **13** (using the more conventional metathesis route of reacting LiR with NaO*t*Bu) proved unsuccessful due to its lack of solubility in non-polar solvents. Indeed, very few unsolvated alkyl sodium compounds have been characterised in the solid-state, namely $[\{(NaMe)_4\}_\infty]$,[66] $[\{2(NaEt)_2\}_\infty]$[131] and $[\{NaCH(SiMe_3)_2\}_\infty]$.[132] The crystallisation of **13** is probably aided by the fact that this compound is formed extremely slowly as a consequence of the disproportionation reaction of tetraalkylmagnesiate **14** (**Scheme 3.6**). Thus, it appears that although $Na_2MgR_4$ is formed in a hexane/toluene solution, when the temperature is decreased in order to obtain suitable crystals for X-ray studies, the equilibrium shown in **Scheme 3.6** must lie towards the formation of $NaMgR_3$ and NaR (probably driven by the low solubility of NaR in this solvent system). Inspection of the crystal structure of **13** reveals a polymeric chain structure built up by $(NaR)_4$ tetramers, representing a new addition to the exclusive family of unsolvated sodium organometallics to be structurally defined (**Figure 3.12**).[6, 132-133]

The repeating unit comprises a distorted $Na_4$ tetrahedral core with four alkyl groups, each of them capping a face of the tetrahedron. Two of these alkyl groups also interact with the Na atoms of two neighbouring units (Na2-C2 2.7872(17) Å), giving rise to a chain arrangement. This interaction induces an asymmetry in the structure of the repeating tetrahedron unit with Na2 raising its coordination number to four whereas Na1 is only bonded to three alkyl groups, reflected not only in a variation in the Na-C bond lengths (from 2.5952(19) to 2.8189(18) Å) but also in the non-bonding Na···Na distances (varying from 2.9125(14) to 3.3594(10) Å).

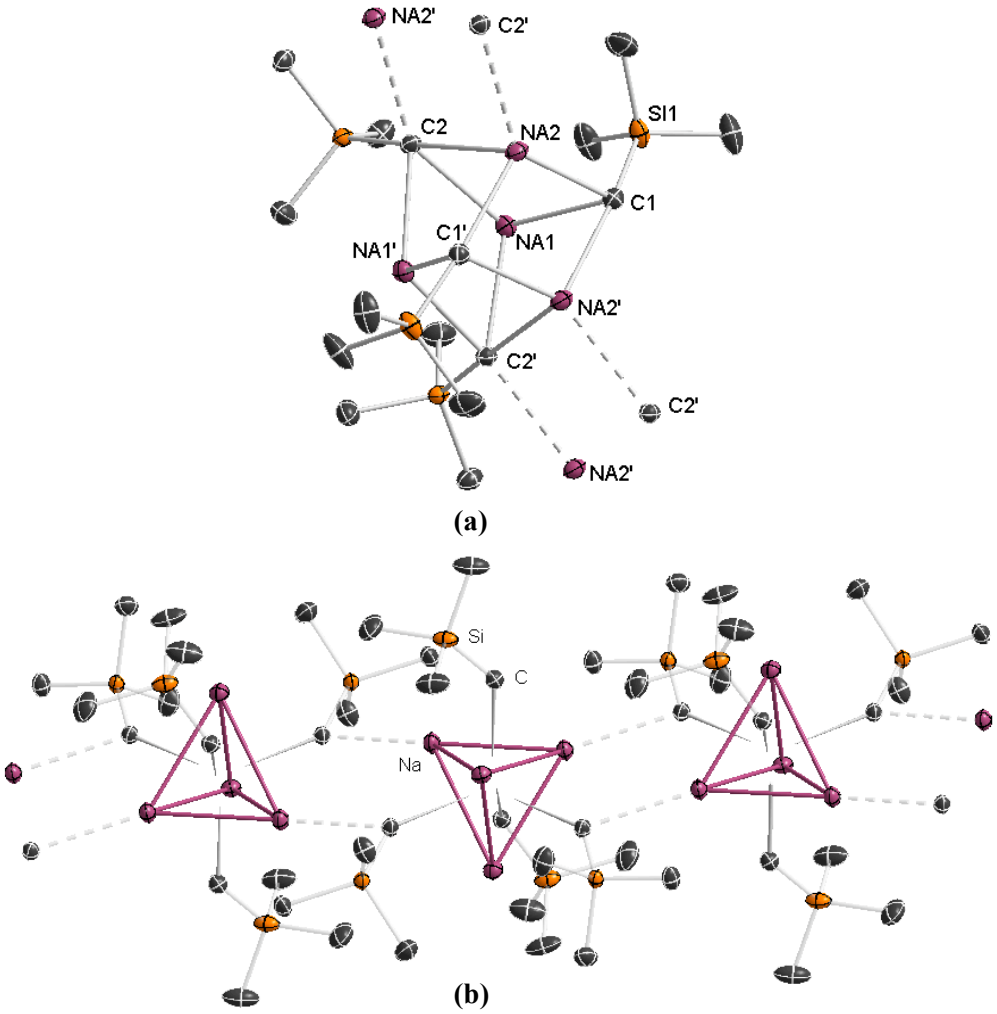


**Figure 3.12:** (a) Tetrahedral unit of **13**. Displacement ellipsoids are drawn at the 50% probability level. Hydrogen atoms have been omitted for clarity. Selected bond angles and distances, Na1-C1 2.5953(19) Å, Na2-C2 2.7872(17) Å, Na2-C2' 2.8189(18) Å, Na2-Na1' 3.3594(10) Å, Na1-Na1' 2.9125(14) Å. (b) Section of the polymeric chain of **13**; purple lines indicate the $Na_4$ distorted tetrahedron and do not represent bonds.

This tetrahedron-based motif is also exhibited by classical organolithium reagents[6] such as MeLi, which is also a polymer of tetramers, and *t*BuLi,[134] and contrasts with the alternating chain structure of $Na^+$ cations and anions of related solvent-free $[\{NaCH(SiMe_3)_2\}_\infty]$ (**Figure 3.13a**).[132] The structure of the lithium congener of **13** was elucidated by Tecle and consists of a discrete hexamer $[(LiCH_2SiMe_3)_6]$ (**Figure 3.13b**).[135]

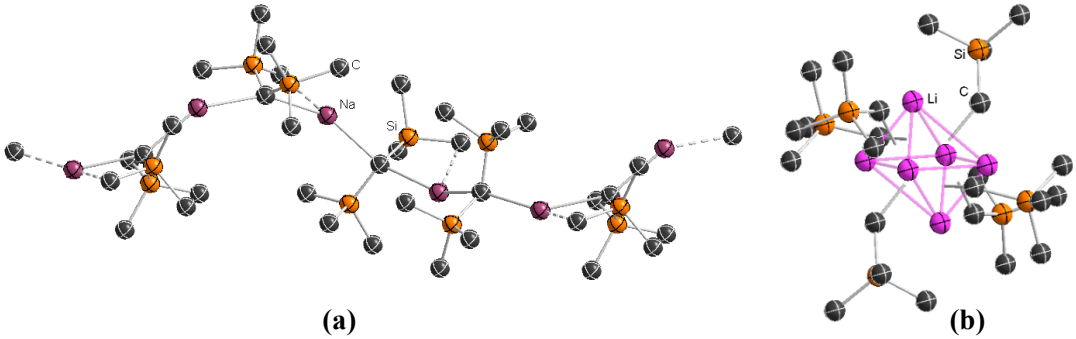


**(a)** **(b)**

**Figure 3.13**: (a) Related bulky alkyl polymeric sodium structure $[\{NaCH(SiMe_3)_2\}_\infty]$[132] and (b) related hexameric lithium structure $[(LiCH_2SiMe_3)_6]$; pink lines indicate the $Li_6$ distorted octahedron and do not represent bonds.[135] Hydrogen atoms have been omitted for clarity.

### 3.2.1.2 Polymeric alkyl/alkoxide inverse crown complex

Alkali metal organometallic compounds can react violently with moisture and oxygen; hence the exclusion of air during the preparation and employment of these complexes is mandatory, with manipulations carried out under a dry inert atmosphere.[136] Having stated that, regulated exposure of metal alkyls to dry oxygen can lead to an interesting array of structures, with oxygen inserting into the metal-carbon bond.[93b, 115b-d, 137] This methodology has been used to synthesise inverse crown complexes, the nomenclature referring to the switched placement of the Lewis base from its conventional hosting positioning in the "crown" to its role as a guest held within the scaffold of Lewis acid metals (**Figure 3.14a**).[115d, 138] The anionic/metal scaffold of an inverse crown complex typically consists of $M^I$ as an alkali metal, $M^{II}$ is usually a divalent metal such as Mg or Zn, and the anionic ligand, L, is an amide, alkoxide or alkyl group. By way of example, Mulvey has encapsulated $O_2^{2-}$ within a $(N_4K_2Mg_2)^{2+}$ core (**Figure 3.14b**).[138b] Also, Lewinski has explored the synthesis of zinc alkyl-peroxides/alkoxides by the direct interaction of $O_2$ with diorganozinc species.[139]

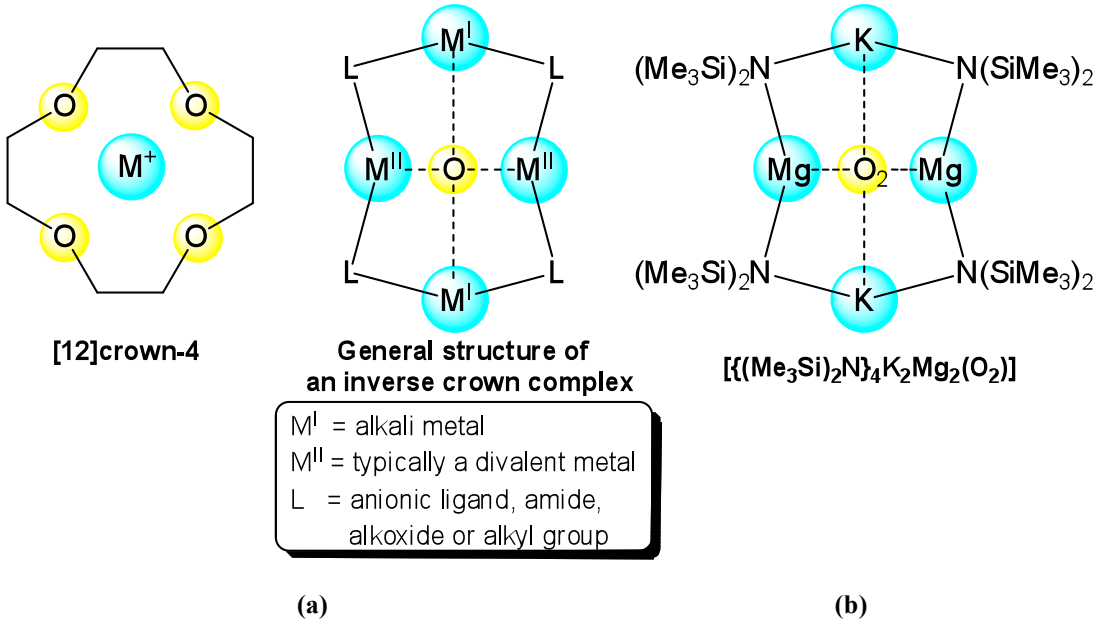


**Figure 3.14**: (a) Conventional crown ether and generalised formula of an inverse crown complex and (b) Amide supported potassium magnesium inverse crown complex.[138b]

Homoleptic trisalkyl sodium magnesiate [{$NaMgR_3$}$_\infty$] **12** was exposed to oxygen in a controlled way to explore the effect oxygen may have on its 2D supramolecular structure. A drying tube (containing $CaCl_2$) was fitted to a Schlenk tube containing the unsolvated magnesiate complex to allow oxygen but disallow moisture from entering the system. Slow cooling of the resulting colourless solution led to the deposition of colourless crystals of [{$NaMgR_2(OR)$}$_\infty$] **15** in 15% yield (**Scheme 3.8**).

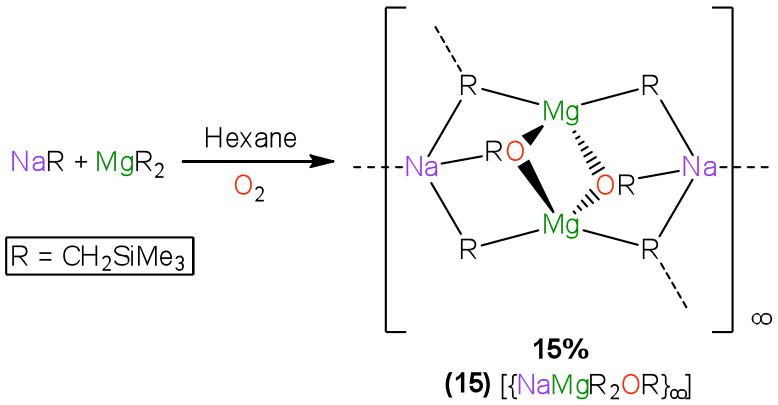


**Scheme 3.8:** Synthetic preparation of **15**.

Looking at its empirical formulation, **15** can be envisaged as the co-complexation product of the bis-alkyl $Mg(CH_2SiMe_3)_2$ and the alkoxide $NaOCH_2SiMe_3$ and as such may be considered an alkaline earth metal relation of the Lochmann-Schlosser reagent, LIC-KOR, which pairs *n*-butyllithium with the heavier alkali metal potassium *tert*-butoxide. LIC-KOR can be described as a "superbase" due to the dramatic enhancement of reactivity in deprotonation reactions when compared to a mixture of an alkyllithium with lithium butoxide.[42] Despite the wide applications of the superbase in synthesis, definitive structural information on the Lochmann-Schlosser reagent has not been forthcoming; however, elucidation of **15** may provide indirect insight into the structural make up of the alkali metal-rich superbase.

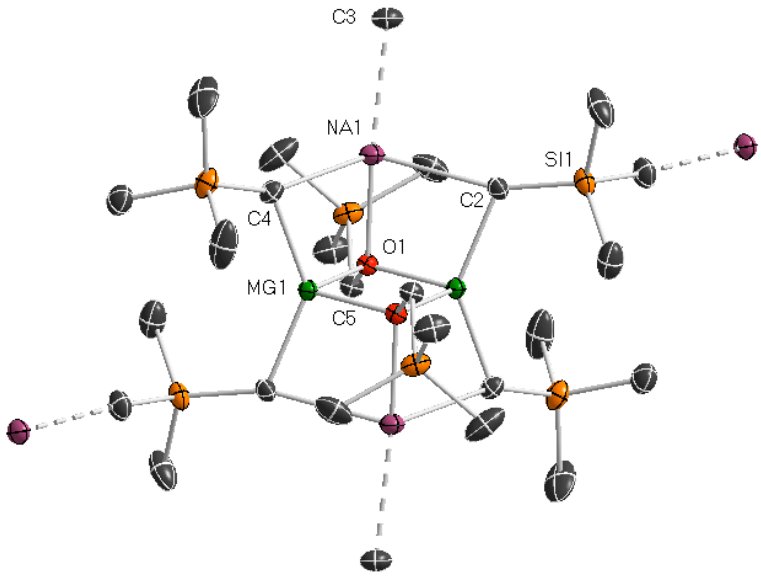


**Figure 3.15:** Repeating dimeric unit of polymeric **15**. Displacement ellipsoids are drawn at the 50% probability level. Hydrogen atoms have been omitted for clarity. Selected bond angles and distances, Na1-C4 2.672(2) Å, Na1-C2 2.684(2) Å, Na1-O1 2.2699(13) Å, Na1-C3#2 2.743(2) Å, Mg1-C2 2.1894(19) Å, Mg1-C4#1 2.1881(19) Å, Mg1-O1 2.0279(14) Å, Mg1-O1#1 2.0332(13) Å; O1-Mg1-O1#1 84.70 (6)°, C4#1-Mg1-C2 138.17 (8)°, O1-Na1-C2 82.75 (6)°, O1-Na1-C3#2 171.83 (7)°.

Contacted ion pair structure **15** features a dimeric arrangement comprising two $\{NaMgR_2(OR)\}$ units where the alkoxide ligand OR is formed as a result of the oxygen insertion into the metal-carbon polar bond of an alkyl group of the bimetallic

precursor [{$NaMgR_3$}$_\infty$], giving rise to a face-fused double heterocubane structure with two missing corners. The OR groups face cap the "top" and "bottom" of the structure, acting as a bridge between two Mg atoms and a Na centre (**Figure 3.15**). Alternatively, this compound can be described as an inverse crown complex consisting of a cationic 8-atom {$NaCMgC$}$_2$ heterobimetallic ring hosting two alkoxide ligands in its core.[93b] This cationic ring adopts a pseudo chair structure with the sodium atoms constituting the "head" and "footrest" of the chair (see the alternative view in **Figure 3.16**).

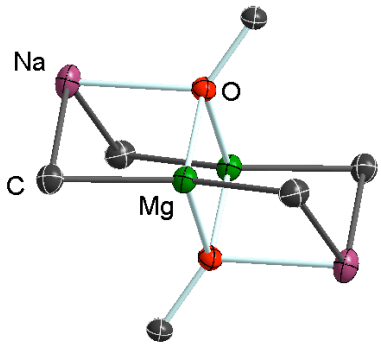


**Figure 3.16:** Alternative view of **15** showing the pseudo chair motif. Displacement ellipsoids are drawn at the 50% probability level. Hydrogen atoms and $SiMe_3$ groups have been omitted for clarity.

Unlike related inverse crown structures where Lewis basic donors such as TMEDA[138a] or an arene molecule[140] coordinate to the alkali metal, in **15** this lack of externally added solvating molecules around sodium is compensated for by additional secondary electrostatic interactions with the methyl group of a $SiMe_3$ fragment from a neighbouring molecule, leading to polymerisation of the eight-membered ring, which, due to the orthogonal arrangement of rings, results in propagation taking place in two dimensions (**Figure 3.17**). Each sodium bonds to two bridging alkyl groups within the repeating molecular unit (Na1-C4 2.672 (2) Å, Na1-C2 2.684 (2) Å) and one alkoxide $OCH_2SiMe_3$ ligand (Na1-O1 2.2699 (13) Å). In addition, sodium also forms a secondary intermolecular interaction with a neighbouring $CH_3$ group (Na1···C3#2 2.743 (2) Å) (**Figure 3.17**); however, of the four alkyl groups present in the ring scaffold of **15** only two alkyl units, diagonally

opposite each other, interact with the neighbouring units. Na is tetracoordinate with a range of angles observed from O1-Na1-C2 82.75 (6)º to O1-Na1-C3#2 171.83 (7)º. Mg resides in a distorted tetrahedral environment bonding to two alkyl groups and two alkoxide ligands (range O1-Na1-O1#1 84.7 (6)º to C4#1-Na1-C2 138.17 (8)º, average 107.3º). Applying **Equation 3.1** (*vide supra*) to quantify the geometric environments of the metals Mg has a $\tau_4$ value of 0.79, indicating clear distortion; however, Na is found to have a $\tau_4$ value of 0.51 indicating large distortion from a perfect tetrahedron, imposed by the formation of a cyclic structure.

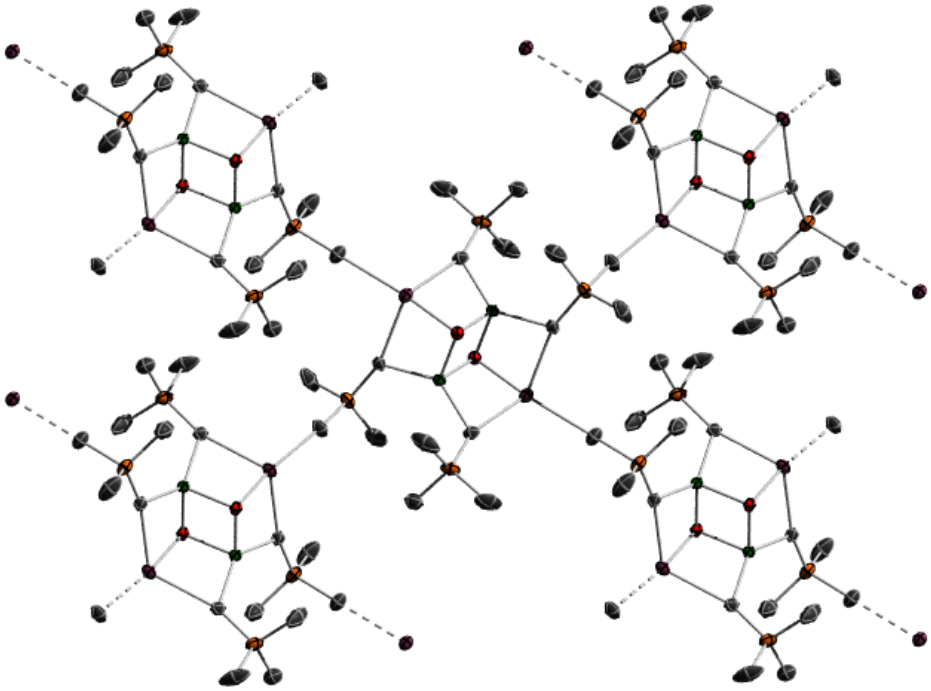

**Figure 3.17:** Polymeric structure of **15**. $SiMe_3$ groups from the alkoxide ($OCH_2SiMe_3$) groups and hydrogen atoms omitted for clarity.

In the oxygen-free parent compound **12**, a very different two-dimensional structure is observed made up of 12-atom $\{(NaCMgC)_3\}$ fused rings; however, as in **15** each alkyl group acts as a bridge between a Na and Mg centre, and similar distances are found in the Na-C bond lengths (2.6708(19) Å in **12**, 2.678 Å average distance in **15**). In addition, the Mg-O distances in **15** (2.0279(13) Å Mg-O1 and 2.0332(13) Å Mg-O1#1) are almost identical to those reported in the closely related inverse crown ether $[\{NaMg(Bu)_2(O\textit{t}Bu)(TMEDA)_2\}]$ (2.028(4) Å Mg-O1#1 and 2.033(4) Å Mg-O1)[138a] and only slightly longer than in the peroxo complex

[{$(Me_3Si)_2N$}$_4K_2Mg_2(O_2)$] (2.010(1) Å Mg-O1#1 and 2.015(1) Å Mg-O1).[138b] In contrast to **15**, [{$NaMg(Bu)_2(OtBu)(TMEDA)_2$}] was formed using a different synthetic approach by the co-complexation of monometallic components NaO*t*Bu and $MgBu_2$ in the presence of TMEDA.

### 3.2.1 Unsolvated potassium magnesiate [$KMgR_3$]

Due to the low solubility of organopotassium complexes in hydrocarbon media very few have been structurally elucidated. Methyl potassium was determined by powder diffraction to display the NiAs structure type.[68] Employing a larger alkyl group containing a stabilising Si in the beta position has seen the confirmation of tris(trimethylsilyl)potassium as a chain, with bridging K-C-K bonds.[141] The donor-free α, α-bis(trimethylsilyl)benzylpotassium also forms a chain through coordination of the K to a neighbouring phenyl unit (K-C range 3.093(2) – 3.522(2) Å).[142] Further stabilisation by Lewis bases allows for the characterisation of the solvated monomer [(PMDETA)$KCPh_3$][124a], solvated dimer [(THF){$KCHPh_2$}$_2$] and solvated chains [{(THF)$KCH(SiMe_3)_2$}$_\infty$][143], [{(TMEDA)$KC(SiMe_3)_3$}$_\infty$][124b] and, [{(PMDETA)$KCH_2SiMe_3$}$_\infty$].[123] Having stated that and encouraged by the preparation and characterisation of solvent-free $NaMgR_3$ (**12**), the same protocol was applied to KR in an attempt to synthesis the potassium analogue (**Scheme 3.7**).

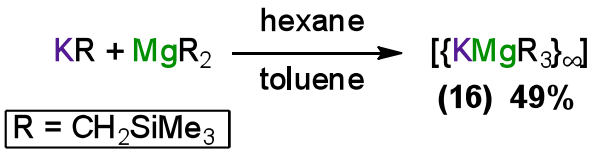


**Scheme 3.7:** Synthesis of **16**.

Equimolar amounts of monometallic alkyls KR and $MgR_2$ were stirred in hexane for one hour after which addition of toluene plus heating gave a clear solution and slow cooling to room temperature deposited a crop of colourless crystals in 49% yield. Analysis by X-ray crystallography showed the crystals to be the unsolvated potassium magnesiate [{$KMgR_3$}$_\infty$] **16** (**Figure 3.18**). Unfortunately, despite repeated preparation and analysis by X-ray, the crystals of **16** were twinned which

precludes meaningful discussion of bond distances and bond angles; however, the connectivity is definite.

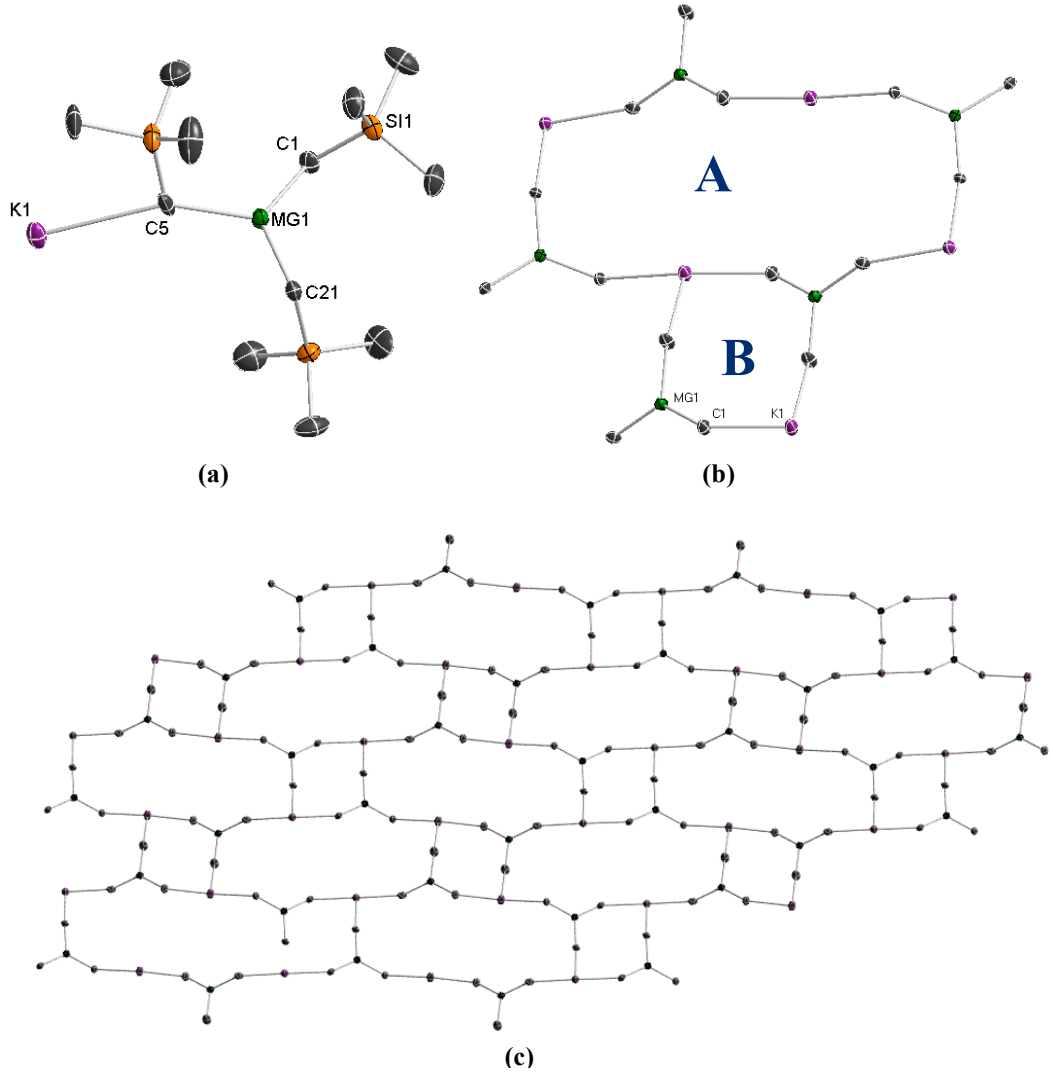


**Figure 3.18:** (a) T-shaped monomeric structure of **16**. (b) Sub-rings A and B made up of T-shaped $KMgR_3$ unites. (c) Sheet network of **16**. Displacement ellipsoids are drawn at the 50% probability level. Hydrogen atoms in all figures and TMS groups in (b) and (c) have been omitted for clarity.

The basic repeat unit of **16** comprises the empirical formula $KMgR_3$ which can be considered a T-shaped building block, identical to that of **12**, but with a bigger cation. The structure polymerises through the formation of new K-C bonds by interacting with neighbouring alkyl groups; however, unlike in **12** where a two-dimensional honeycomb structure is formed as the result of the formation of fused 12-membered rings, a different supramolecular motif is observed. Structure **16**

contains two different types of rings (represented as A and B in **Figure 3.18b**) which are 16-membered $\{KCMgC\}_4$ and 8-membered $\{KCMgC\}_2$ rings respectively. The two-dimensional network is constructed by the fusing of A + B: each B ring is fused to four A rings, and every A ring is fused to four A and four B rings (**Figure 3.18c**). The basket-weave 2D sheet network of **16** is exceptionally rare, having been postulated as a possible arrangement of T-shaped nodes in 2001[129] but not realised until 2005 with the publication of a Sm-Ni bimetallic complex incorporating a picolinic acid ligand.[144]

Analysis of **16** by $^1$H NMR in deuterated benzene revealed a singlet at -1.68 and 0.35 ppm for the methylene and methyl protons respectively, confirming the formation of a mixed-metal species, as the resonances for the monometallic KR are significantly upfield at -2.60 and -0.18 ppm and the monometallic $MgR_2$ is insoluble in the medium. As with the related sheet network **12**, a $^1$H-DOSY experiment was performed to ascertain the extent of aggregation in solution. The same internal standards of 1,2,3,4-tetraphenylnaphthalene (TPhN), 1-phenylnaphthalene (PhN) and tetramethylsilane (TMS) were chosen as they have good solubility in benzene with minimal overlapping signals and are inert to **16**. **Figure 3.19** shows the $^1$H-DOSY NMR of **16** in the presence of the internal standards in deuterated benzene at room temperature, and some possible species of **16** in solution with their respective FW values and the error for every considered structure with respect to the size predicted for **16** through the $^1$H-DOSY study. As can be seen in **Figure 3.19** all the different components of the mixture separate clearly in the diffusion dimension and an approximate molecular weight can be interpolated from the log *D* vs. log FW trend-line, which turns out to be 431 g mol$^{-1}$.

Interpretation of these analyses mirrors that of its Na congener **12**, whereby it is postulated that the solid-state structure of **16**, which is a 2D-network of monomeric unit $[KMgR_3]$, is not retained in $C_6D_6$ solution as the error associated a dimer (**B**) or a trimer (**A**) is quite high (34 and 56% respectively). Neither should **16** be considered as a simple monomer as the error with its calculated molecular weight and the estimated value obtained in the DOSY studies (-32%) is a hindrance. As was

suggested in the case of **12**, these data can be interpreted as the presence of a monomer/dimer equilibrium in solution, and therefore the constitution of **16** could be represented by $[KMgR_3]_n$ (where n = 1-2).

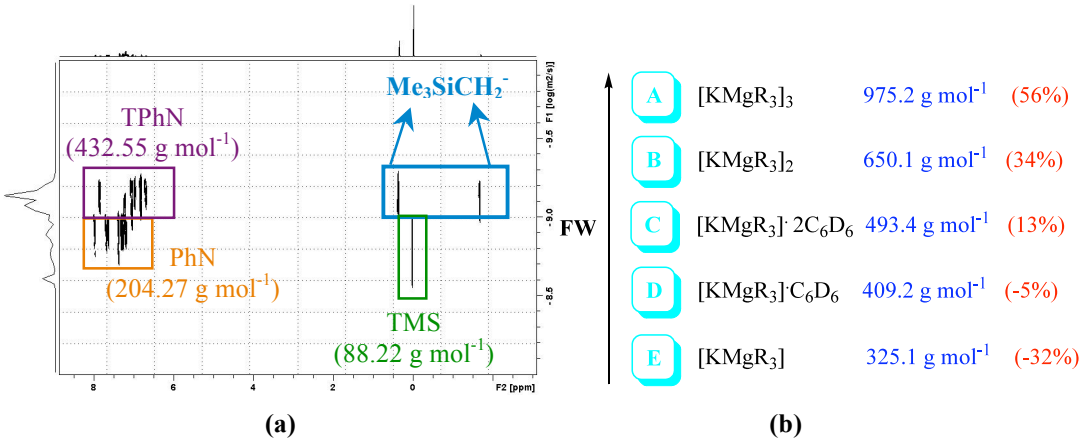


**(a)** **(b)**

**Figure 3.19**: (a) $^1$H-DOSY NMR spectrum of **16**, TPhN, PhN and TMS in $C_6D_6$ at 298 K. (b) Possible species of **16** in $C_6D_6$ with errors (in parenthesis) with respect to the estimated FW value predicted through $^1$H-DOSY

The presence of the deuterated solvent must not be ruled out or indeed underestimated, as the $K^+\cdots$benzene interaction energy is 19 kcal mol$^{-1}$ which is substantial (for comparison, the $K^+\cdots$water interaction is 18 kcal mol$^{-1}$).[145] As such, a monomer in which potassium is solvated by a single molecule of deuterated benzene **D** (-5% error) or, allowing for the increase in size of the cation, by two molecules of deuterated benzene **C** (13% error) (or an equilibrium between both) would be a plausible solution structure of **16**. This type of electrostatic interaction is known in organometallic chemistry, with several examples in the literature of structurally defined molecules displaying a K atom adopting a perpendicular disposition and π-engaging with the electron rich aromatic ring of benzene molecules.[145-146]

### 3.2.2.1 Arene solvation of alkyl potassium magnesiate [$KMgR_3$]

In an attempt to form crystals of high enough quality for X-ray diffraction studies, the method of synthesis of unsolvated potassium magnesiate **16** was probed. As such, after stirring for 1 hour in hexane, benzene was this time added to the slurry, with heat, giving a clear solution, which on cooling deposited colourless crystals in a 45% isolated yield (**Scheme 3.8**). Analysis of the crystals by X-ray crystallography showed them to be the benzene-solvated polymer $[\{(C_6H_6)MgR_3\}_\infty]$**17** (**Figure 3.20**).

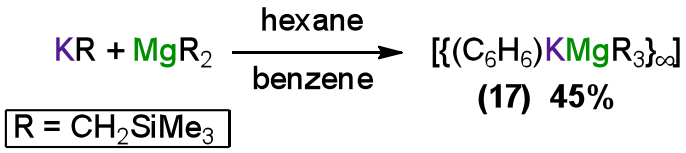


**Scheme 3.8**: Synthetic route to **17**

The crystal structure of **17** reveals an interesting 2D network (**Figure 3.20**). The monomeric unit is similar to that found in the unsolvated structure **16**, but incorporates a molecule of benzene which π-interacts with K *via* electrostatic interactions. In addition K forms an agostic interaction with a methyl group of a TMS (K1-C22 3.294(2) Å) in the monomeric unit. The monomer initially forms a dimer through one of the alkyl groups (C3) resulting in an 8-membered $\{KCMgC\}_2$ ring (**Figure 3.20b**) with the K-C bond distance longer for the linking K-C bond distance (K1-C3 3.374(4) Å) than in the monomeric unit (K1-C2 3.1482(17) Å). In the dimeric unit potassium forms another agostic interaction with a methyl group of a TMS with a short contact observed for K1-C32#1 of 3.1352(18) Å. Overall, K forms σ-bonds with two carbanions in the dimeric ring, forms secondary interactions with two methyl group of adjacent TMS moieties and is further solvated by interacting with the π system of a benzene ring. In **17** benzene caps one K atom with no further interactions with neighbouring K atoms (*i.e.* it does not act in a ditopic manner), however due to disorder in the benzene molecule geometric discussion about K-π interaction will be waived. The dimer then propagates through the alkyl group not incorporated into the ring (C1) and the Mg of a neighbouring unit leading to 4-

membered {MgCMgC} linking rings and giving rise to a chain structure constructed of 4- and 8-membered rings fused at their Mg vertexes (**Figure 3.20c**).

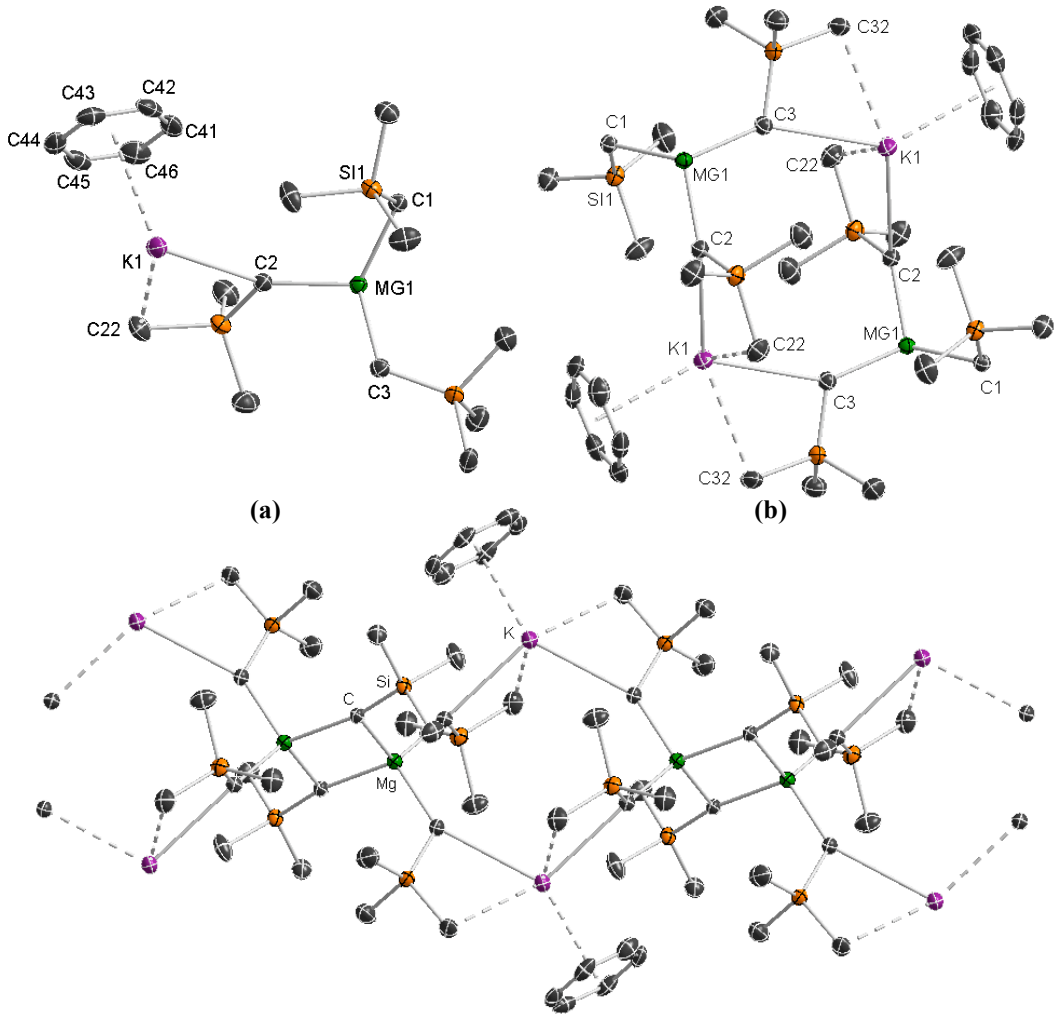


**Figure 3.20**: (a) Monomeric unit of **17.** (b) Dimeric unit of **17**. Selected bond angles and distances, K1-C2 3.1482(17) Å, K1-C3 3.374(4) Å, K1-C22 3.294(2) Å, K1-C32#1 3.1352(18) Å, Mg1-C2 2.2076(18) Å, Mg1-C3 2.2152(18) Å, Mg1-C1 2.2513(18) Å, Mg1-C1#3 2.4296(18) Å; C2-Mg1-C3 105.88(7)°, C2-Mg1-C1 114.38(7)°, C3-Mg1-C1 117.28(8)°, C2-Mg1-C1#3 110.74(7)°, C3-Mg1-C1#3 109.28(7)°, C1-Mg-C1#3 99.12(6)°, Mg1-C2-K1 137.70(8)°, Mg1-C3-K1#1 148.12(8)°. (c) Polymeric chain structure of **17**. In all figures displacement ellipsoids are drawn at the 50% probability level. Hydrogen atoms and disorder in benzene omitted for clarity.

Mg is surrounded by four carbanionic ligands with a slight disparity observed in the Mg-C bond distances in the monomeric unit (average bond distance of Mg-C1, Mg-C2 and Mg-C3 = 2.2247 Å) with the slightly longer one observed when forming the {MgCMgC} ring, Mg1-C1#3 2.4296(18) Å, and adopts a tetrahedral coordination (average angle = 109.4º). Due to the restrictions on discussing the bond parameters of related unsolvated potassium magnesiate **16**, inspection of its sodium congener **12** shows that the average Mg-C bond distance in the unsolvated sodium magnesiate (2.1608 Å) to be shorter than in **17** (average = 2.276 Å from all four ligands) but of the same order as PMDETA-solvated potassium magnesiate **11** (average = 2.265 Å).

As coordinated benzene is present in the molecule, analyses by NMR spectroscopy were carried out in deuterated toluene solutions. Three singlets were observed in the $^{1}$H NMR spectrum, as expected, with one singlet at -1.72 ppm accounting for the methylene bridge, a singlet at 0.28 ppm for the methyl groups and a final singlet at 7.13 ppm for benzene. A $^{1}$H-DOSY experiment was conducted to ascertain the degree of aggregation of polymer **17** in solution for comparison with the related solvent-free potassium magnesiates **16**. As analyses by deuterated toluene NMR had confirmed the presence of benzene in the isolated crystals, the $^{1}$H-DOSY experiment was performed in deuterated benzene. As with **16**, internal standards of 1,2,3,4-tetraphenylnaphthalene (TPhN), 1-phenylnaphthalene (PhN) and tetramethylsilane (TMS) were chosen. Analyses of the $^{1}$H-DOSY data estimated the size of **17** in solution in terms of its FW to be 433 g mol$^{-1}$, making it almost identical, within experimental error, to the estimated FW of **16** (431 g mol$^{-1}$), suggesting that unsolvated polymer **16** and benzene-solvated polymer **17** both deaggregate to the same species in a benzene solution: a monomer of [$KMgR_3$] interacting with one or two molecules of the arene solvent (*vide supra*).

#### 3.2.2.2 Metallocene solvation: a heterotrimetallic system

Having shown the propensity of potassium to π-engage with arene molecules in benzene-solvated trisalkyl magnesiate **17**, investigations turned to the addition of the iron metallocene ferrocene {$Fe(C_5H_5)_2$} to potassium magnesiate **16**. Ferrocene can

act as a π-donor to a cation through its Cp rings $(C_5H_5)^-$[147] or alternatively it can experience metallation of the relatively acidic hydrogens when confronted with a magnesiate,[97, 148] for example, in its unprecedented tetrametallation by trisamido sodium magnesiate "NaMg(N*i*Pr)$_3$" (**Scheme 3.9**).[97]

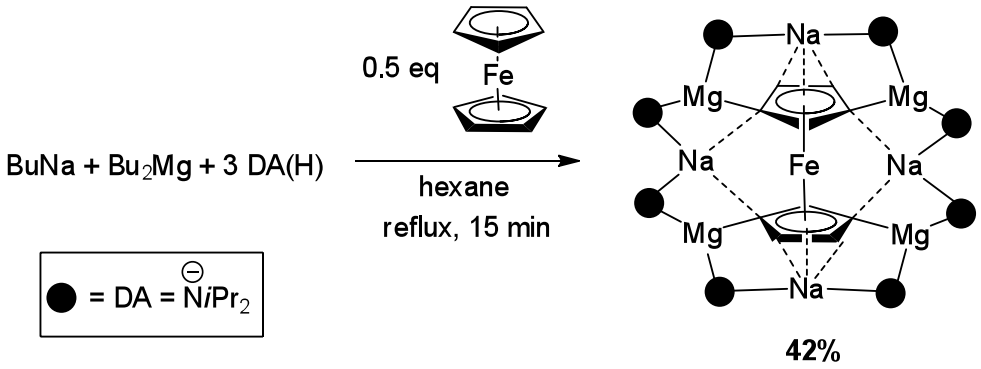


**Scheme 3.9:** Tetrametallation of ferrocene by trisamido sodium magnesiate.

Surprisingly, examples of potassium-ferrocene complexes are exceedingly rare. Indeed, the first example of any kind of interaction between potassium and a metallocene was reported in 2004, with the elucidation of SSIP potassium-magnesium complex $[\{K(Cp_2Fe)_2(CH_2Ph)_2\}^+\{Mg(HMDS)_3\}^-]$ in which the cation $K^+$ is coordinated by two $\eta^5$-ferrocene and two $\eta^3$-toluene molecules (**Figure 3.21**).[147a]

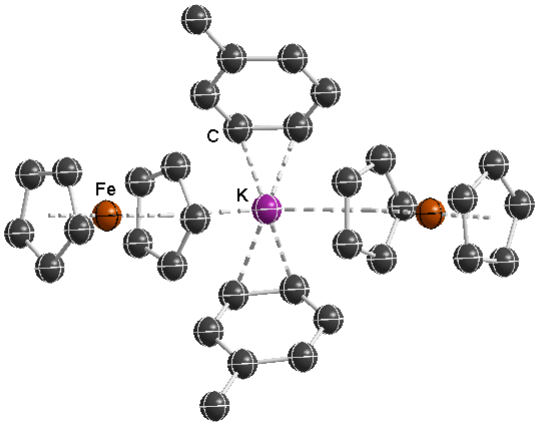


**Figure 3.21**: Molecular structure of the cationic moiety of $[\{K(Cp_2Fe)_2(CH_2Ph)_2\}^+\{Mg(HMDS)_3\}^-]$. Thermal ellipsoids drawn at the 50% probability level. Hydrogens omitted for clarity.

Since then the area has been largely dormant with respect to s-block chemistry, with only one further report of a systematic study of the addition of ferrocene to a homologous series of alkali metals M(HMDS) (where M = Na, K, Rb, Cs).[147b] Extending the scope to include ferrocene-based ligands and incorporating the main group (as opposed to just the s-block) demonstrates further the novelty of this area, as very few examples are found.[149]

Thus, synthetic endeavours to add to this exclusive family of compounds began with the addition of 1 equivalent of ferrocene to an equimolar mixture of KR with $MgR_2$ in hexane giving an orange suspension. Following a 16 h stir the introduction of toluene gave a clear solution that deposited yellow crystals of $[\{(Cp_2Fe)KMgR_3\}_\infty]$ **18** upon storage in the freezer overnight in 26 % isolated yield (**Scheme 3.10**, **Figure 3.22**).

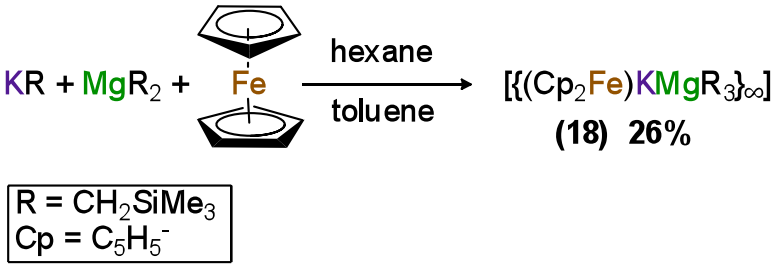


**Scheme 3.12:** Synthesis of **18**

The structural make up of **18** mimics that of **17** in the first instance, where the monomeric unit of $KMgR_3$ is solvated by π-interactions to potassium; in **17** this is provided by benzene whereas in **18** by the Cp ring of a molecule of ferrocene. In addition potassium is further stabilised by an agostic interaction with a neighbouring methyl group K···$MeSiMe_2$ (K1-C6 3.398(2) Å) (**Figure 3.22a**). Initial propagation of the polymer is also similar between **17** and **18** whereby a dimer is formed giving an 8-membered $\{KCMgC\}_2$ ring (**Figure 3.22b** which also denotes a new electrostatic K···$MeSiMe_2$ K1-C10 3.436(2) Å bond which arises when the dimer is formed) which is then fused at Mg to a 4-membered {MgCMgC} ring (**Figure 3.22c**).

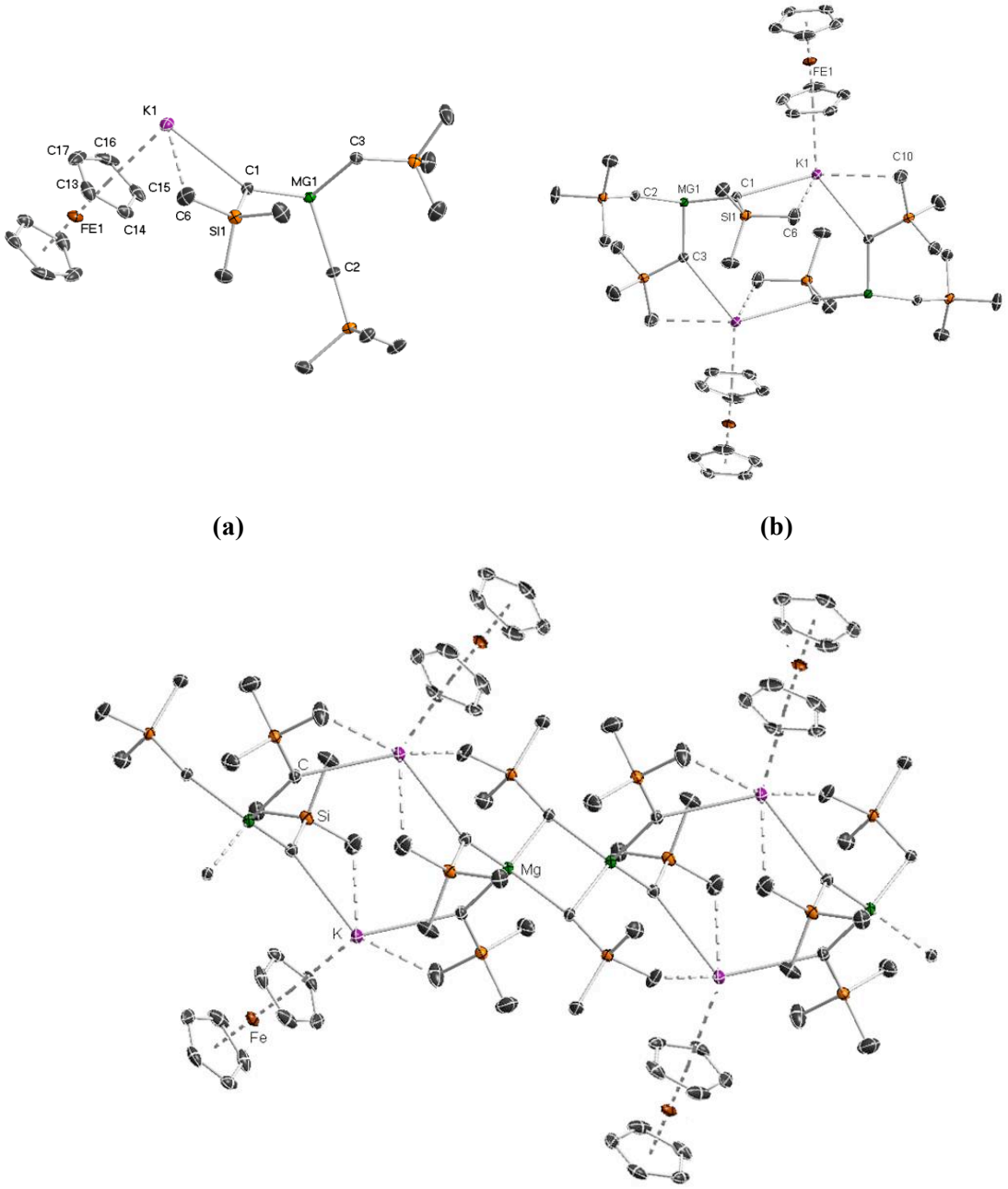


**(a)** **(b)**

**(c)**

**Figure 3.22**: (a) Monomeric unit of **18**. Displacement ellipsoids are drawn at the 50% probability level. Hydrogen atoms and minor disorder in Cp rings omitted for clarity. Selected bond angles and distances, K1-C1 3.1983(12) Å, K1-C3 3.1231(12) Å, K1-C6 3.398(2) Å, K1-C10 3.436(2) Å, K1-C8 3.516(2) Å, K1-C9#1 3.3621(12) Å, Mg1-C1 2.2165(12) Å, Mg1-C2 2.2475(12) Å, Mg1-C3#2 2.2040(12) Å, Mg1-C2#3 2.4268(12) Å; C3#2-Mg1-C1 104.97(5)°, C3#2-Mg1-C2 118.91(5)°, C1-Mg1-C2 113.23(4)°, C3#2-Mg1-C2#3 108.46(4)°, C1-Mg1-C2#3 111.77(4)°, C2-Mg1-C2#3 99.49(4)°. (b) Dimeric unit of **18**. (c) Part of the polymeric structure of **18**.

Whereas in **17** propagation ends with a chain structure, the final constitution of **18** displays an intricate 3D structure where ferrocene acts as a ditopic ligand, propagating the molecule in the second dimension and finally extends in the third dimension due to K forming electrostatic interactions with a neighbouring unit (K1-C9#1 3.3621(12) Å). In **18**, K forms σ-bonds with two carbanions in the dimeric ring together with four secondary interactions with methyl group of adjacent TMS moieties and is further solvated by interacting with the π system of a Cp ring in ferrocene. Unfortunately due to disorder in the Cp rings of the ferrocene molecule no geometric discussion about K-π interaction will take place. The interaction of K and carbanions C1 and C3 (the latter of which forms the dimer) are shorter and stronger (3.1983(12) Å and 3.1321(12) Å respectively) than the agostic interactions observed (average bond distance = 3.428 Å) as would be expected due to the charged nature of the bond. Surrounded by four anionic ligands, Mg is slightly distorted from a perfect tetrahedral geometry, with an average angle of 109.5° and a $\tau_4$ value of 0.91. Analysis of crystals of **18** by NMR suggests that in deuterated benzene solution the ferrocene dissociates, as the singlets in the proton spectrum at -1.67 and 0.36 ppm corresponding to the methylene and methyl protons of the monosyl group respectively matches that of unsolvated potassium magnesiate **16** and cycopentadienyl protons at 4.01 ppm is the same as free ferrocene. The $^{13}C$ resonances for **18** and **16** are also identical with respect to the R group as is the ferrocene signal in **18** with that of free ferrocene.

### 3.3 Conclusions

By studying the cocomplexation reactions of monometallic alkyls MR (were M = Na or K) with $MgR_2$ in the presence of N-donor molecules TMEDA and PMDETA magnesiates **8-11** were synthesised and characterised. The chelating Lewis bases induced a reorganisation to a higher order magnesiate species $[(donor)_2M_2MgR_4]$ (donor = TMEDA or PMDETA, M = Na or K) from the trisalkyl magnesiate mixture. Furthermore, a homologous series of TMEDA-solvated compounds $[(TMEDA)_2M_2MgR_4]$ (M = Li **5**, Na **8** or K **10**) has been described where although the same empirical formula is observed, the structural make up of the series changes

as the cation size increases. The compound of Li, the smallest cation, **5**, has a coordination number of 4 and an almost linear arrangement of Li···Mg···Li. Na compound **8** attains a coordination number of 5 through electrostatic interactions and potassium structure **10** induces a "bending" of the usual linear structure (as observed in **5**, **8**, **9** and **11**) to allow the larger cation to each form three σ-bonds with the bridging carbanionic ligands. In addition, the novel structures of the solvent-free trialkylmagnesiate species **12** and **16** have been uncovered. These unique polymeric structures display unprecedented 2D networks in the solid-state, held together exclusively through electron deficient M-C bonds. Solution studies carried out using $^{1}$H-DOSY have revealed that these polymeric structures undergo significant deaggregation and do not retain their solid-state structures in solution. Attempted synthesis of the unsolvated higher order sodium magnesiate **14** led to the fortuitous characterisation of homometallic species NaR **13** which was revealed to be a polymer of tetramers. Exposure of **12** to dry oxygen resulted in its partial oxidation with oxygen inserting into one of the three alkyl groups of the monomeric unit and producing a polymer constructed of inverse crown ethers **15**. The affinity of K to form π-interactions was demonstrated by introducing benzene to **16** giving chain structure **17**. Also, the exclusive club of metallocene-K structures was added to by the addition of ferrocene to [$KMgR_3$] resulting in an elaborate three-dimensional structure exhibited by **18**.

## Chapter 4: Exploring the reactivity of alkyl potassium magnesiate reagents

### 4.1 Limitations of potassium magnesiate reagents

Potassium lies on the cusp of the group 1 elements between the ubiquitously used Li and Na metals and, by comparison, the seldom explored Rb and Cs. In contrast to the heavier organorubidium and organocesium compounds, organopotassium compounds are often much more manageable in a practical sense, however they are less stable (more reactive) than their organolithium or organosodium analogues[150] and tend to be used synthetically only when an aggressive force is required, for example, in the removal of low acidity hydrogens.

The Lochmann-Schlosser reagent, LIC-KOR, which pairs *n*-butyllithium with potassium *t*-butoxide is, perhaps, the most familiar guise of organometallic potassium to the synthetic chemist. As discussed in **Chapter 1**, the reactivity of LIC-KOR can be considered intermediate between *n*-butyllithium and *n*-butylpotassium, and cryogenic conditions must be strictly adhered to when using the reagent.[42] The demand for very low temperatures coupled with the poor functional group tolerance of LIC-KOR limits its synthetic utility. A notable use of a bimetallic potassium base has been in the sedation of the ethene anion carried out by potassium zincate [(PMDETA)K(TMP)(R)Zn(R)] (R = $CH_2SiMe_3$) reported recently in *Science*.[31] Bubbling ethene through a solution of the zincate base in hexane at 50 °C gave the metallated product after 2 hours in a 51% isolated yield (**Scheme 4.1**).

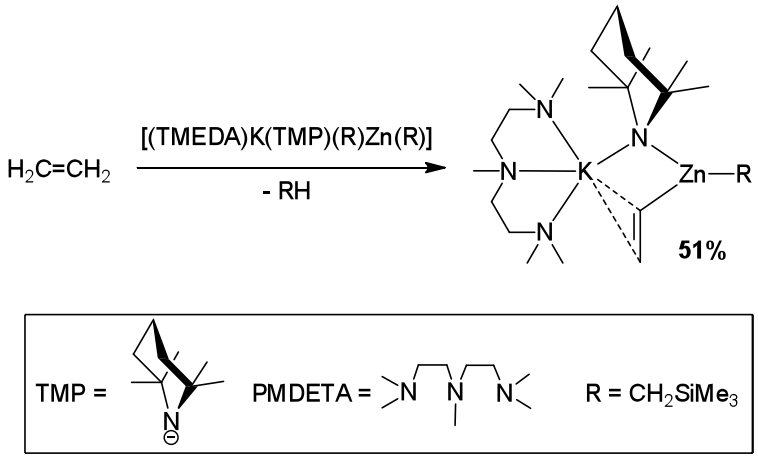

**Scheme 4.1:** Synergic metallation of ethene using a potassium zincate.

Of particular note is the lack of reactivity from the related sodium zincate [(TMEDA)Na(TMP)(R)Zn(R)] (R = $CH_2SiMe_3$) which was only able to synthesise the metallated product in trace amounts, demonstrating the major activating role played by potassium in this reaction.

Previous examples in the literature of potassium-mediated magnesiation taking place are limited to reagents incorporating an amido group. Heteroleptic magnesiate "$KMg(TMP)_2Bu$" is able to monodeprotonate benzene or toluene producing an impressive 24-atom inverse crown structure.[151] Applying the bisamido/monoalkyl [(PMDETA)K(TMP)($CH_2SiMe_3$)Mg(TMP)] reagent in the metallation of anisole, and close monitoring by $^1$H NMR, revealed that this heteroleptic base reacts *via* the amide component in the first instance, generating the kinetic product, which can then react with the alkyl group in the intermediate, giving the thermodynamic *ortho*-magnesiated anisole product[106] (see discussion in **Chapter 5.1.1** about amido *vs* alkyl basicity). In each of these examples, structural characterisation of the product revealed a true magnesiation has taken place, as the removed hydrogen position is filled by a Mg atom. Thus, building on the results delineated in **Chapter 3**, where several alkyl potassium magnesiates have been prepared and fully characterised in solution and in the solid-state, it was then decided to probe the basicity of these monoalkyl reagents by their ability to promote M-H exchange reactions.

Preparation of the potassium magnesiate *in situ* precluded the use of ethereal THF as a solvent, commonly used in organic transformation reactions, due to the reactivity of the homometallic precursor KR. We found KR degraded the ether molecule, which then cocomplexed with $MgR_2$ generating mixed-metal enolate structure **19**, **Figure 4.1**. Synthesis of **19** was carried out by adding THF to KR, giving an instant bright yellow solution. Addition of $MgR_2$ paled the solution which was stirred for 30 minutes. Crystallisation from hexane/THF gave crystals of **19** in an isolated 20% yield (**Scheme 4.2**).

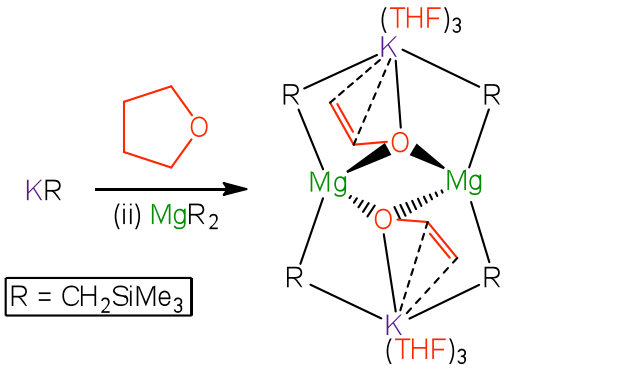


**(19) 20%**

$[\{(THF)_3K(R)(OCH{=}CH_2)MgR\}_2]$

**Scheme 4.2**: Trapping of cleaved THF with a potassium magnesiate.

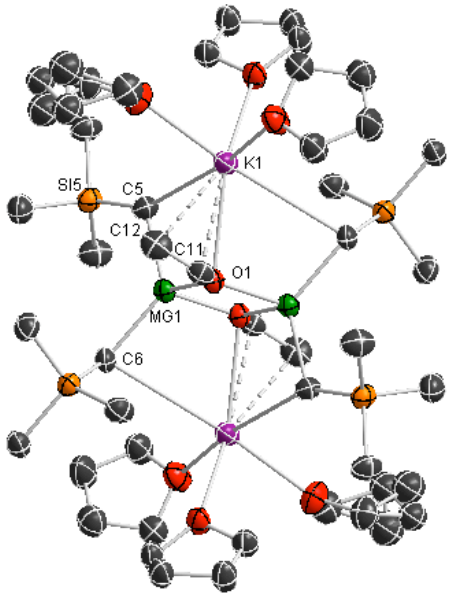


**Figure 4.1**: Molecular structure of **19**. Displacement ellipsoids are drawn at the 50% probability level. Hydrogen atoms and minor disorder in one THF molecule omitted for clarity. Selected bond angles and distances, K1-C5 3.143(6) Å, K1-C6#1 3.440(7) Å, K1-C11 3.094(6) Å, K1-C12 3.234(6) Å, K1-O1 2.856(4) Å, Mg1-C5 2.182(6) Å, Mg1-C6 2.177(6) Å, Mg1-O1 2.047(4) Å, Mg1-O1#1 2.029(4) Å; O#1-Mg-O1 79.59(16)°, C6-Mg-C5 122.3(3)°.

Exhibiting an inverse crown structural motif, **19** can be described as an eight-membered $\{KCMgC\}_2$ ring which has encapsulated in its core two $OCH_2{=}CH_2$ anionic groups. These enolate ligands are generated as the result of the α-metallation of THF to generate a 2-furyl anion which rapidly undergoes [3+2] reverse

cycloaddition to yield ethene and a potassium enolate derived from acetaldehyde. Degradation of this type can be observed using conventional organolithium reagents in THF (**Scheme 4.3**).[13]

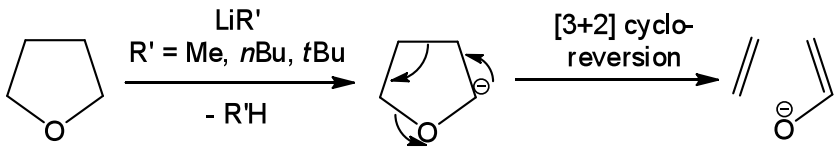


**Scheme 4.3**: Decomposition pathway of THF observed with conventional organolithium reagents.[13]

The scaffold of **19** is reminiscent of **15** which is also an inverse crown complex, and the coordination around Mg is the same in each case, with Mg forming four anionic bonds two of which are with carbon and two with oxygen atoms, and display very similar bond distances in each structure: the average Mg-C distance in **15** is 2.189 Å *vs* 2.179 Å in **19** and the average Mg-O in **15** is 2.030 Å *vs* 2.038 Å in **19**. Potassium forms bonds with the oxygen atom of the enolate, two bridging anionic alkyl groups and π-engages with the unsaturated carbons of the enolate in a $\eta^2$ fashion. It is further solvated by three molecules of THF. Inspection of the K-C bond distances shows the closest contact to be with C11 (K-C11 3.094(6) Å), probably due to the flexibility of the enolate, which is not constrained by the $\{KCMgC\}_2$ ring (K-C5 = 3.143(6) Å, K-C6#1 = 3.440(7) Å). The K-$C_{anion}$ bonds are of the same order in **19** (average = 3.2915 Å) as **17** (average = 3.2611 Å). Inverse crown ether complexes constructed of alkyl ligands are rare in the literature but a related potassium magnesiate was reported by Mulvey from the cocomplexation of KO*t*Bu with $MgBu_2$ which also forms a cationic eight-membered $[\{KCMgC\}_2]$ but now it has encapsulated at its core two butoxide ligands. K attains coordinative saturation by bonding to a molecule of TMEDA.[138a]

## 4.2 Metallation studies and electrophilic interception reactions

Investigations into the efficacy of a monoalkyl potassium magnesiate to carry out metallation reactions began by the addition of three equivalents of thiophene to **17**

(prepared *in situ* by mixing an equimolar amount of KR and $MgR_2$ in hexane/benzene at room temperature, **Scheme 4.4**). Thiophene was chosen as a test substrate as it has a p$K_a$ of 33 in THF, which can be deprotonated by conventional bases such as LiTMP,[152] and three equivalents were used due to the presence of three potential basic arms in **17**. Following a 1 hour stir, iodine (solution in THF) was added in a bid to synthesise 2-iodothiophene (**20**) and the resultant dark brown solution was stirred overnight, whence it was worked-up using standard protocol. Analysis of the crude product attained by $^1$H NMR showed no starting material or product, indeed the only species identifiable by NMR were THF and grease. Thiophene and, to a lesser extent **20**, are volatile and if any remained in the reaction mixture they would be lost during concentration of the crude product on the rotary evaporator.

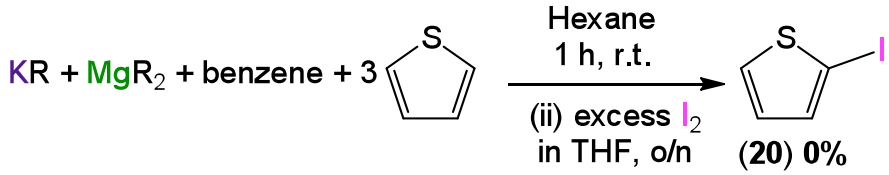


**Scheme 4.4**: Attempted metallation of thiophene with *in situ* preparation of **17**.

Due to the volatile nature of the starting material and **20**, the reaction was repeated and analysis carried out by GC, which confirmed no conversion had taken place and only unreacted thiophene was present. This result showed that polymeric base **17**, which displays infinite aggregation in the solid-state, seems to be unable to promote Mg-H exchange on the relatively acidic substrate thiophene. Anisole was then investigated due to the presence of the methoxy group which can act as a docking site for directed *ortho* metallation[13, 153] and also acidify the *ortho* hydrogen. **Scheme 4.5** shows the attempted metallation of anisole and electrophilic quench with iodine to produce 2-iodoanisole (**21**), however, mirroring the study with thiophene, no reaction was observed and only starting material was present as determined by GC analysis.

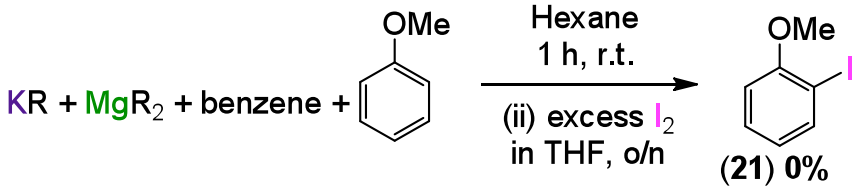


**Scheme 4.5**: Attempted metallation of anisole with *in situ* preparation of **17**.

Modification of an organometallic reagent by the addition of a Lewis base can increase its reactivity as evidenced by the addition of TMEDA to *n*BuLi. *n*BuLi (a hexamer in hydrocarbon solvents)[70] is inert towards benzene; however, addition of TMEDA gives a dimer (*n*BuLi·TMEDA)$_2$[73] which can quantitatively deprotonate the arene molecule to form PhLi·TMEDA.[71] A similar deaggregation is observed between **17** which is a polymer and PMDETA-solvated [(PMDETA)$_2$K$_2$MgR$_4$] **11** which is a discrete molecule, and, significantly, has undergone a redistribution to the higher order magnesiate under the conditions employed for crystallisation. As **17** has been shown to be retarded towards deprotonative metallation with respect to thiophene and anisole, it was hoped that the smaller aggregate **11** would exhibit an enhanced metallating power to promote the Mg-H exchange. Thus, **11** was prepared *in situ* under the same conditions used to prepare the solid-state structure, *i.e.* a 1:1:1 mixture of KR, MgR$_2$ and PMDETA which was then treated with x equivalents of anisole (x = 1, 2, 3. **Scheme 4.6**, **Table 4.1**). In the process of crystallisation a redistribution takes place to the higher order magnesiate and if this occurs in solution then a maximum yield of 50% would be obtained for **11**. Having stated that, as *four* anionic arms are present in **11** then the metallation reaction when x = 1 or 2 could still be obtained in up to 100% (entries 1 and 2 respectively) and up to 66% when x = 3 (entry 3) under the reaction conditions employed.

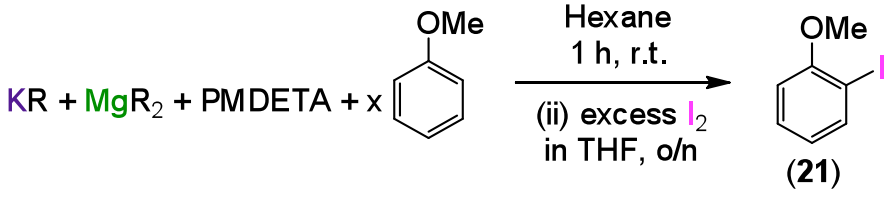


**Scheme 4.6**: Attempted metallation of anisole with *in situ* preparation of **11** using a 1:1:1 ratio of KR:MgR$_2$:PMDETA.

**Table 4.1**: Attempted metallation of anisole followed by trapping with iodine by *in situ* preparation of **11** using a 1:1:1 ratio of KR:$MgR_2$:PMDETA.

| Entry | x | Conversion SM:product |
|---|---|---|
| 1 | 1 | 100:0 |
| 2 | 2 | 100:0 |
| 3 | 3 | 100:0 |

Surprisingly, iodinated product **21** was not observed in any case. To ensure complete dryness and purity of PMDETA, the trisamide was freshly distilled over $CaH_2$ and the reactions repeated, however once again only starting material was observed by GC. Thus, in solution a 1:1:1 mixture of KR:$MgR_2$:PMDETA was showing no reactivity, indicating in that solution a "(PMDETA)$KMgR_3$" species is formed which is not sufficiently reactive to promote Mg-H exchange of anisole. As such, the reaction with anisole was repeated using the rational stoichiometry of **11** (2:1:2 KR:$MgR_2$:PMDETA) which pleasingly gave an 81% yield of **21** from the addition of four equivalents of anisole (**Scheme 4.7**).

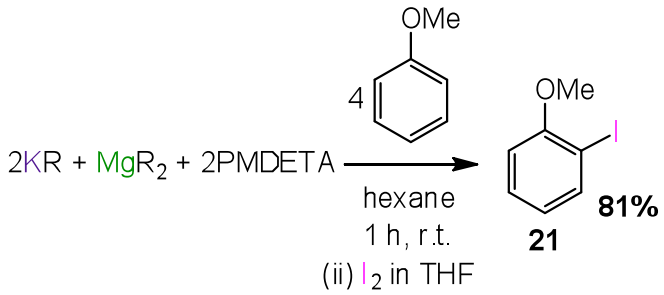


**Scheme 4.7**: Optimised conditions for the preparation of **21**.

In control reactions it was found that $MgR_2$ alone is unable to metallate anisole, with 0% conversion to **21** observed after iodine quench whereas the more aggressive KR was able to carry out the reaction with 75% conversion to **21** on a 1:1 ratio of reagent to substrate (**Scheme 4.8**). The reaction conditions shown in **Scheme 4.7** therefore display good atom economy as all four R groups of magnesiate reagent **11** seem to be activated towards exchange, including the alkyl groups on Mg that were previously

unable to carry out Mg-H exchange. Although attempts to obtain crystals suitable for X-ray diffraction of the organometallic intermediates from the reaction were unsuccessful, previous precedents in the literature would indicate that a magnesiation is taking place.[106, 151]

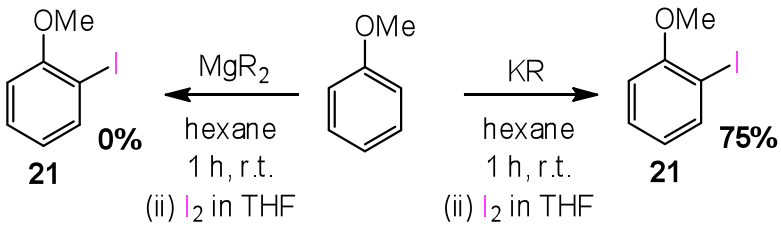


**Scheme 4.8**: Reactions of $MgR_2$ and KR with anisole.

Using the optimised conditions shown in **Scheme 4.7**, the scope of the reaction towards a number of substrates was next probed (**Table 4.2**). The tetraalkyl dipotassium magnesiate mixture proved to be an effective metallating agent for a range of aromatic substrates, giving a quantitative conversion to the corresponding iodinated product after quench in the case of 4-methoxypyridine (entry 1). Trifluorotoluene was also converted quantitatively, although the selectivity of the reaction varied depending on the temperature employed: at 0 °C an *ortho*:*meta* ratio of 22:78 was observed, whereas at room temperature the *ortho* product was preferentially formed in a 68:32 ratio (entry 2). These data suggest that metallation at the *meta* position is the kinetic product where less steric hindrance is present (the $CF_3$ group is intermediate in size between *i*Pr and *t*Bu groups)[154] and metallation at the *ortho* position is the thermodynamic product aided by the activating $CF_3$ which enhances the acidity of the *ortho* hydrogen. In this regard, theoretical calculations modelled on the homometallic reagent *t*BuLi/TMEDA showed that the *ortho*-lithiated product is favoured over the meta-metallated isomer by 7.48 kcal $mol^{-1}$.[155] Entries 3 and 4 showed an excellent conversion to iodinated product at 0 °C (98 and 90 respectively); however, performing the reaction at room temperature saw a drop in yield of desired product and an increase in side-products, although no starting material was observed, indicating that although cryogenic conditions are not

necessary, a degree of temperature control is required to hinder unwanted side-reactions for these sensitive substrates.

**Table 4.2**: Scope of substrates metallated by an *in situ* mixture of **11**.

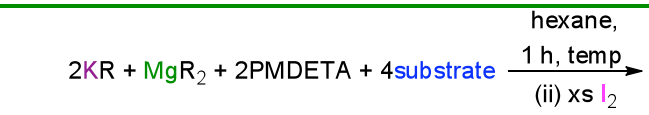


| Entry | Starting material | Product | Temp/°C | Yield/% |
|---|---|---|---|---|
| 1 | 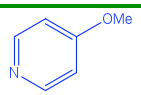 | 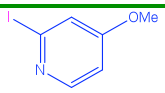 | 0 | >99 |
| 2 | 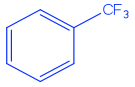 | 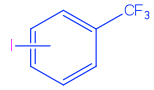 | 0<br>r.t. | >99 22:78 *ortho*:*meta*<br>>99 68:32 *ortho*:*meta* |
| 3 |  | 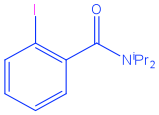 | 0<br>r.t. | 98<br>56 |
| 4 | 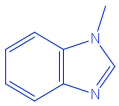 | 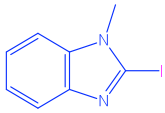 | 0<br>r.t. | 90<br>64 |
| 5 | 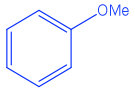 | 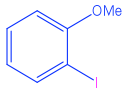 | 0<br>r.t. | 42<br>81 |
| 6 |  | 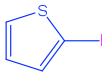 | 0<br>r.t. | 65<br>87 |
| 7 | 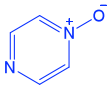 | - | 0 | -[a] |
| 8 |  | - | 0 | -[a] |
| 9 |  | - | 0 | -[a] |
| 10 | 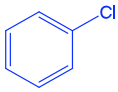 | - | 0 or r.t. | -[b] |
| 11 | 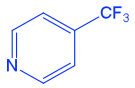 | - | 0 or r.t. | -[b] |

[a]Complex mixture of products by GC. [b]100% starting material.

Conversely, for anisole the reaction was retarded at 0 °C (42%) and ambient temperature was needed to achieve a good conversion (81%, entry 5). Five-membered heterocycle thiophene showed a similar pattern with a modest 65% conversion to 2-iodothiophene at 0 °C which increased to 87% at room temperature (entry 6) which an equimolar solution of KR, $MgR_2$ and PMDETA was unable to deprotonate. Contrasting with the reactivity of "$LiZn(TMP)_3$", which is able to deprotonate diazines at room temperature,[22] **11** was not able to promote the selective deprotonation of electron-deficient N-heterocycles (detailed in entries 7-9) even at 0 °C (no temperatures lower than 0 °C were studied). A complex mixture of products was obtained, although no starting material could be detected. On the other hand, it was insufficiently reactive for chlorobenzene and 4-trifluoromethyl pyridine at either 0 °C or room temperature, with only starting material observed in each case.

## 4.3 Conclusions

The widely discussed concept of structure controlling reactivity (the "Holy Grail" of organometallic chemistry) has been probed by studying the reactivity of the trialkylmagnesiate mixture prepared from KR, $MgR_2$ and benzene (**17**) compared with mixtures containing Lewis donor PMDETA. Studies have shown the trialkylmagnesiate mixtures to be retarded towards deprotonative metallation at ambient temperature with respect to thiophene and anisole. The stoichiometry of the reaction mixture containing PMDETA has been shown to be paramount, with a 1:1:1 ratio of KR, $MgR_2$ and PMDETA displaying no reactivity towards anisole yet a 2:1:2 mixture reacted readily with the same substrate giving the product after quench in an excellent 81% yield. Applying the higher order magnesiate mixture to a range of organic substrates gave good results, with many examples undergoing smooth metallation and electrophilic quench at room temperature, whereas some sensitive substrates required the use of cooler reaction conditions (0 °C).

These results open up new possibilities for using alkyl potassium magnesiates in synthesis, an area that is largely unexplored. The use of potassium in synthesis is usually limited to the LIC-KOR superbase, which pairs two alkali metals (lithium

and potassium), and has limited synthetic applicability due to the need to employ very low temperatures and its poor functional group tolerance. In contrast, **11** can be used to promote M-H exchange at ambient temperature or 0 °C for a range of substrates, and displays good atom economy, with all four arms activated towards exchange.

# Chapter 5: Investigating the cooperative effect of lithium and zinc

## 5.1 Introduction to the action of alkali metal zincates and salt effects

As delineated in **Chapter 1**, alkali metal zincates constitute the oldest class of mixed-metal reagent known with the report by Wanklyn of the synthesis of sodium triethyl zincate, $NaZnEt_3$ in 1858.[3] Revived by Wittig almost one hundred years later with the synthesis and application of lithium triphenyl zincate $LiZnPh_3$,[5] these bimetallic reagents have been an area of interest to many prominent research groups, both organic and inorganic, in the last few decades. Thus, alkali metal zincates have been successfully used in the functionalization of organic molecules by their part in metallation reactions,[22, 156] metal-halogen exchange reactions[52] and nucleophilic addition reactions.[59] The mode of action of alkali metal zincates has been the subject of much study both theoretical and experimental, in particular when a heteroleptic amido/alkyl base is employed in a metallation reaction as the reaction can proceed *via* alkyl or amido basicity.

### 5.1.1 An amido or an alkyl base?

Trapping of the reaction intermediate formed from the metallation of benzene with heteroleptic bimetallic base [(TMEDA)Na(TMP)(*t*Bu)Zn(*t*Bu)] showed an overall alkyl basicity, with the product shown in **Scheme 5.1** isolated and structurally elucidated by X-ray crystallography by Mulvey and co-workers.[157]

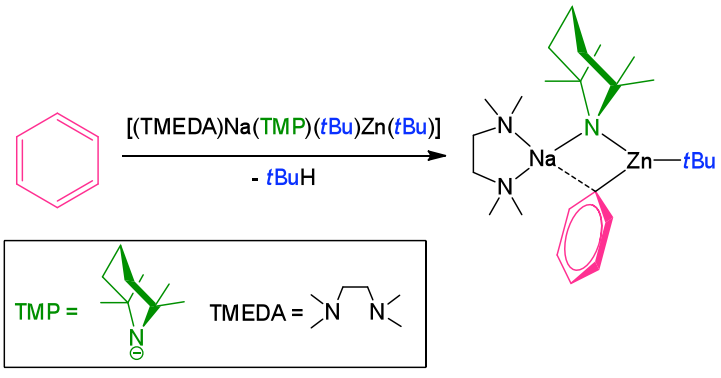


**Scheme 5.1:** Metallation of benzene by sodium zincate base.

Theoretical studies using DFT calculations carried out by Mulvey supported the alkyl basicity of the zincate by demonstrating a gain in energy on the loss of *t*BuH of -21.9 kcal mol$^{-1}$ compared to only -1.5 kcal mol$^{-1}$ if amido basicity were preferred and TMP(H) was lost (**Figure 5.1**).[157]

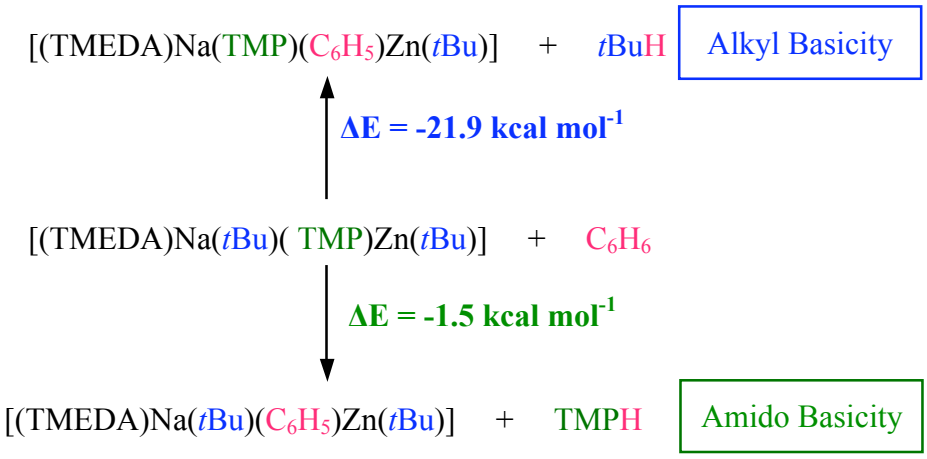


**Figure 5.1**: Summary of DFT calculations for the reaction of [(TMEDA)Na(TMP)(*t*Bu)Zn(*t*Bu)] with benzene.

Further theoretical studies by Uchiyama, which used a simplified version of the base, replacing the *t*Bu groups with Me groups and TMP with $NMe_2$, considered whether the zincate was carrying out the deprotonation by alkyl or amido means.[158] By calculating the activation energies of the transition states from the two possible reaction pathways, it was found that alkyl basicity had a restrictively high activation energy ($\Delta E_a$ = +45.6 kcal mol$^{-1}$) compared to amido basicity ($\Delta E_a$ = +25.1 kcal mol$^{-1}$). To align these calculations with the empirical observation of overall alkyl basicity, a 2-step mechanism was proposed and evaluated, where the zincate initially acts as an amido base towards benzene generating $HNMe_2$ and new zincate [(TMEDA)Na($C_6H_5$)(Me)Zn(Me)]. This new zincate is then able to act as an alkyl base towards the newly formed amine $HNMe_2$, giving methane as a by-product along with [(TMEDA)Na($C_6H_5$)($NMe_2$)Zn(Me)] which is in good agreement with previously isolated intermediates. **Figure 5.2** summarises these findings, showing that the 2-step mechanism is more favoured with a lower barrier to activation ($\Delta E_a$ = +25.1 ($TS_1$) and +21.3 kcal mol$^{-1}$($TS_2$) shown by the green line) than the 1-step alkyl base mechanism ($\Delta E_a$ = +45.6 kcal mol$^{-1}$ shown by the blue line), with each pathway showing a gain in energy of 12.8 kcal mol$^{-1}$. Thus, the amido basicity is the

kinetically favoured reaction pathway and the alkyl basicity is the thermodynamic one, resulting in a 2-step mechanism to form the final product.

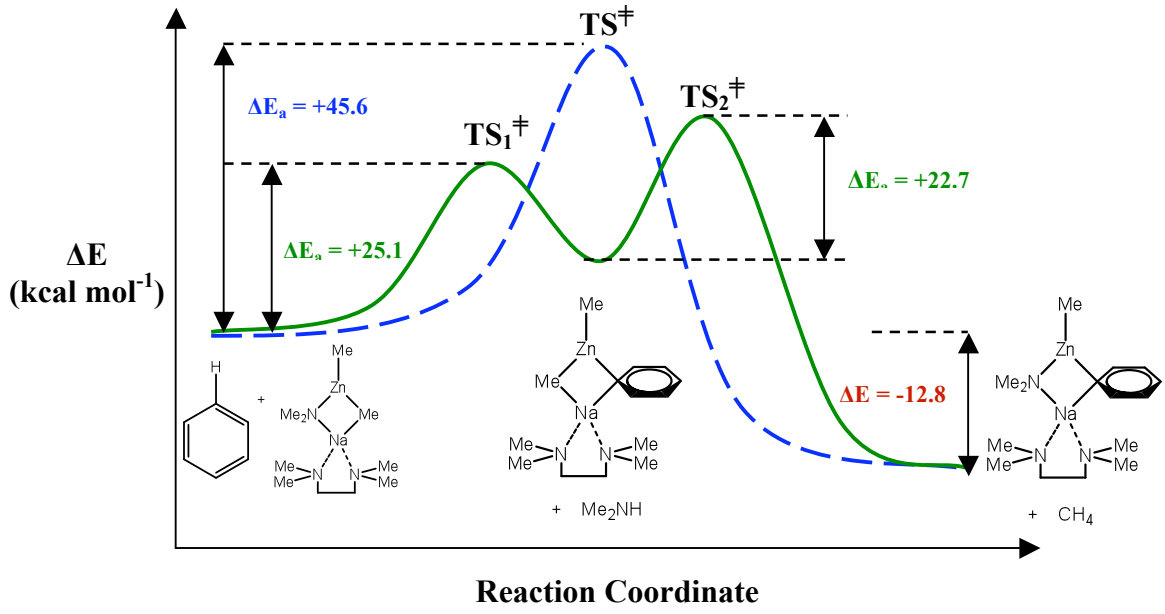


**Figure 5.2**: Energy profile for the reaction of [(TMEDA)Na(NMe$_2$)(Me)Zn(Me)] with benzene showing one-step (alkyl basicity) mechanism (blue), and two-step (amido then alkyl basicity) mechanism (green).

Similar DFT studies have also been carried out to model the reactions of lithium zincate [(THF)Li(TMP)(*t*Bu)Zn(*t*Bu)] (using the simplified base [(Me$_2$O)Li(NMe$_2$)(Me)Zn(Me)]) with *N*,*N*-diisopropylbenzamide (simplified to *N*,*N*-dimethylbenzamide),[159] methyl benzoate[160] and benzonitrile,[160] which demonstrate a similar kinetic preference for the zincate to react *via* a stepwise mechanism, with the zincate behaving in the first instance as an amido base to generate a kinetic [(TMEDA)NaZn(arenide)(alkyl)$_2$] intermediate and TMP(H) which can then react in turn to from the final metallated product [(TMEDA)NaZn(arenide)(TMP)(alkyl)] and isobutane. Whilst these theoretical studies strongly support the existence of a 2-step mechanism for these bimetallic bases, no tangible experimental evidence was offered to confirm this.[161] Further, as only simplified models were used in place of the real bimetallic systems, these can greatly underestimate the influence that steric factors may have in these reactions. For example, it has recently been reported that mixed alkyl-amido zincates, prepared

by combining Li($NMe_2$) and $ZnMe_2$ in THF, display no metallating ability towards aromatic substrates such as anisole, benzonitrile, and *N,N*-diisopropylbenzamide.[162]

In 2009 Hevia and co-workers presented indirect experimental evidence of the amido basicity and 2-step mechanism of zincates by the preparation and structural elucidation of putative intermediates $[(S)_xLi(C_6H_4OMe)(R)Zn(R)]$ (S = THF, TMEDA, PMDETA; R = Me, *t*Bu) by the cocomplexation of *ortho*-lithiated anisole and $ZnR_2$ (R = Me, *t*Bu) and subsequent reactivity towards TMP(H).[163] By examining in detail the reactivity of the isolated intermediates with TMP(H) the authors established that (when R = *t*Bu) isobutene was generated, confirming that one alkyl arm of the intermediate zincate does indeed react with TMP(H), as postulated by the theoretical calculations. The following year the first key reaction intermediates from the actual reaction conditions employed in the AMM*Zn* of $PhCF_3$ were elucidated, lending further evidence to the 2-step mechanism.[155]

### 5.1.2 Salt effects in organometallic chemistry

To complicate matters further, if the alkali metal zincate (or, indeed, any organometallic reagent) is synthesised using the metathesis method and used without purification, an excess of alkali metal salt (usually LiCl or $MgCl_2$) will be present in the reaction mixture. For example, in the preparation of "$LiZn(TMP)_3$" *via* metathesis, three equivalents of LiTMP react with $ZnCl_2$ forming the lithium zincate along with two equivalents of LiCl (**Scheme 5.2**).

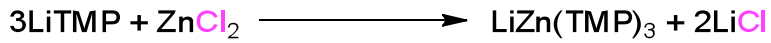


**Scheme 5.2**: Example of the synthesis of mixed-metal reagent $LiZn(TMP)_3$ and concomitant formation of 2 equivalents of LiCl *via* the metathesis method.

Usually the presence of the inorganic salt in the reaction media is not taken into consideration, but, far from being spectators, they can greatly influence the overall performance of the newly generated organometallic reagent. Thus, these salts can have either a positive or negative effect on many reactions (in terms of reactivity

and/or selectivity) prompting a recent review to make the analogy with "Jekyll and Hyde": in the metallation and electrophilic quench of the pyridine derivative shown in **Scheme 5.3** the presence of LiCl promotes enhanced reactivity and allows for a room temperature deprotonation. In contrast, and revealing the "Hyde" nature of LiCl, in the enantioselective phenylation by $ZnPh_2$ of aldehydes in the presence of an asymmetric catalyst only 2% ee is observed when the salt is present (from the metathesis preparation of starting material) whereas a 94% ee is accomplished in its absence (**Scheme 5.3**).[12]

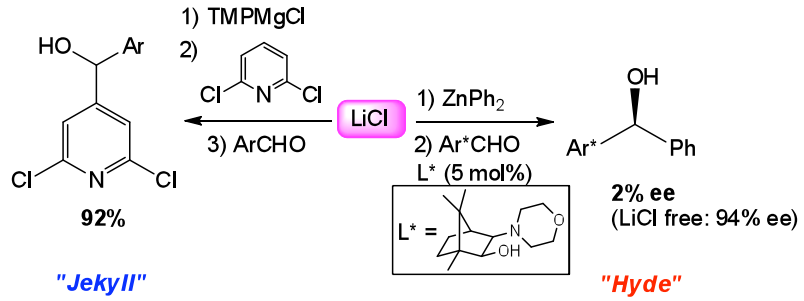


**Scheme 5.3**: "Jekyll and Hyde" nature of LiCl.

**Chapter 1** described the development by Knochel of the turbo-Grignard reagent with the stoichiometric addition of LiCl to a Grignard reagent resulting in enhanced metallating prowess when compared to the Grignard reagent alone. This can be extended to include zinc with the complex $[(TMP)_2Zn{\cdot}2MgCl_2{\cdot}2LiCl]$ able to perform C-H exchange of sensitive oxidiazoles and triazoles in excellent yield (**Scheme 5.4**).[164]

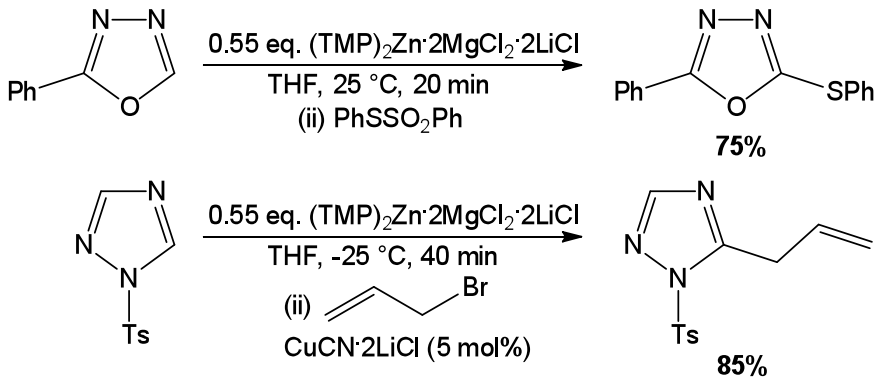


**Scheme 5.4**: Metallation of sensitive arenes by promotion of zinc amide by salts.

In the broader terms of organometallic chemistry, it has been shown by Collum that quantities of LiCl far less than stoichiometric can greatly accelerate the reaction of LDA in either *ortho*-lithiation or nucleophilic addition reactions. Remarkably, he has shown that 0.5 mol% of LiCl can affect a 100-fold acceleration of *ortho*-lithiation (with halogen based directing groups F, Cl or $CF_3$)[24] and 1 mol% can cause a 70-fold acceleration in the 1,4-addition of LDA with unsaturated esters.[165] Extensive kinetic studies by the same group have named the deaggregation of the LDA dimer, favoured by the inorganic salt, as the rate limiting step.[166]

With quantities as low as these able to have such a large effect on the course of reactions, then the presence and behaviour of these salts either as a by-product of a metathesis reaction, or even as a commercial impurity, should not be overlooked or discarded as "innocent bystander".

## 5.2 Application of new lithium zincate approaches in the functionalization of pyrazine

Amongst the extensive catalogue of N-heterocycles, diazines occupy a special place as scaffolds frequently present in numerous natural products, biologically active molecules, pharmaceuticals and materials.[167] Whilst in general deprotonative metallation is one of the most useful synthetic tools to functionalise heterocyclic molecules, for this particular family of π-deficient aza-heterocycles the choice of organometallic base capable of performing their efficient deprotonation can represent a major challenge. Regioselective control can be particularly problematic with non-substituted diazines which lack a directing group.[168] In spite of their enhanced acidity (in terms of p$K_a$ values) when compared to pyridine, the presence of two N atoms in the aryl rings greatly decreases the energy of their LUMO,[169] making these heterocycles more prone to nucleophilic addition than deprotonation when reacted with classical organolithium reagents such as BuLi. Using more sterically hindered secondary lithium amides such as LiTMP allows the lithiation of diazines in moderate yields, although these reactions require strict cryogenic conditions, *in situ* electrophilic interceptions and short reaction times in order to avoid side reactions

involving the highly reactive heteroaryl lithium generated intermediates.[170] While searching for improved synthetic alternatives to overcome these important drawbacks, a new generation of multimetallic multicomponent reagents has recently come to the fore which allow functionalization of diazines under mild conditions. Thus, Mongin has found that "Li(TMP)·Zn(TMP)$_2$" facilitates the deprotonation of naked diazines at room temperature[22] whereas Knochel and Dong have reported the use of (TMP)$_2$Mg·2LiCl in the presence of $ZnCl_2$ for the regioselective α-deprotonation of pyrazine and quinoxaline, where the zinc salt seems crucial to the success of the reaction.[171] Despite these relevant organic studies, which draw attention to the applications of alkali metal zincates for the functionalization of sensitive heterocycles, no information was provided regarding the constitution (either in solution or solid-state) of the organometallic intermediates involved in these reactions. Such realisation can provide important clues into how these processes work and the roles played by each metal and anionic component in the bimetallic reagent.

Thus, taking pyrazine as a case study, the reactivity of this molecule towards heteroleptic zincate [(THF)LiZn(TMP)(*t*Bu)$_2$] (**22**), homoleptic zincate [(PMDETA)LiZn(*t*Bu)$_3$] (**23**) and neutral organozinc Zn*t*Bu$_2$ was investigated. By preparing some these organometallic reagents *in situ via* salt metathesis reactions the activation effect of LiCl was assessed.

### 5.2.1 Di-deprotonation of pyrazine

In the first instance, the reaction of equimolar amounts of TMP-zincate **22** and pyrazine at 0 °C in THF was examined. **22** was prepared by adding a solution of Zn*t*Bu$_2$ in hexane to LiTMP (prepared *in situ* by reaction of BuLi and TMP(H)) and stirred for 10 min before addition of THF and cooling to -28 °C overnight to aid crystallisation. When pyrazine was added to isolated crystals of **22** a bright orange solution was rapidly formed, which on cooling deposited deep orange crystals of [2,5-{(THF)$_2$LiZn(TMP)(*t*Bu)}$_2$($C_4N_2H_2$)] (**24**) in 35% yield, resulting from the selective two-fold metallation of pyrazine at the 2,5-positions. This yield improved to

51% on using 2 equivalents of **22**. Furthermore, $^{1}$H NMR monitoring of the reaction in $d_8$-THF revealed that **24** is obtained quantitatively. **24** can be intercepted with iodine to generate 2,5-diiodopyrazine in a 68% isolated yield (**Scheme 5.5** and **Figure 5.3**).

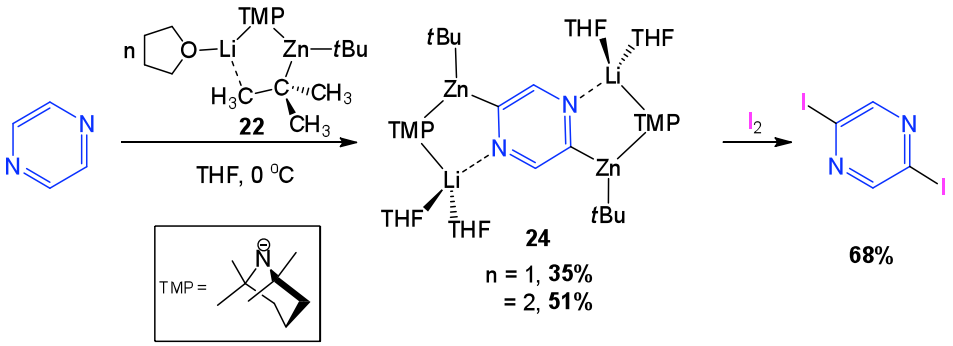


**Scheme 5.5**: Di-deprotonation of pyrazine with **22**.

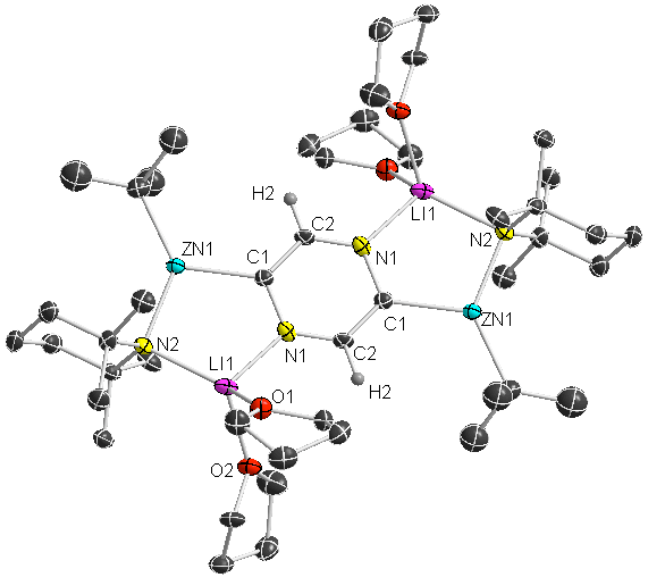


**Figure 5.3**: Molecular structure of **24**. Displacement ellipsoids shown at 50% probability level and hydrogen atoms omitted for clarity except those belonging to the aromatic ring. The unit cell of **24** contains two crystallographically independent molecules with identical connectivities. One molecule contains a disordered *t*Bu group, thus structural discussion will focus on the non-disordered molecule. Selected bond angles and distances, Zn1-C1 2.054(4) Å, Li1-N1 2.049(7) Å, Li1-N2 2.137(8) Å, C1-N1 1.364(5) Å, C1-C2 1.396(5) Å, C2-N1#1 1.339(5) Å; N2-Zn1-C12 134.05(15)°, N2-Zn1-C1 105.71(14)°, C12-Zn1-C1 120.00(16)°, C2#1-N1-C1 118.0(3)°, C2#1-N1-Li1 129.3(3)°,C1-Li1-N1 112.6(3)°.

$^{1}H$ and $^{13}C$ NMR experiments of **24** in $C_6D_6$ solutions established the regioselectivity of the reaction, as indicated by a singlet at 9.17 ppm in the $^{1}H$ NMR spectrum for the aromatic $C_4N_2H_2$ fragment and a resonance at 187.1 ppm for the metallated α-*C* in the $^{13}C$ NMR spectrum. Both appear significantly downfield compared to the corresponding chemical shifts observed for pyrazine (8.07 and 145.1 ppm respectively).

The unit cell of **24** contains two crystallographically independent molecules with identical connectivities. One molecule contains disordered *t*Bu groups, thus the structural discussion will focus on the non-disordered molecule. The centrosymmetric molecular structure of **24** (**Figure 5.3**) confirmed the two-fold deprotonated pyrazine ring substituted at the 2,5-positions by zinc atoms. Solvated by two THF molecules, Li interacts with the N lone pair of the heterocycle giving rise to a near planar arrangement with both metals lying slightly out of the $C_4N_2H_2$ ring. Bonded to a terminal *t*Bu group, trigonal planar Zn is connected to Li *via* a TMP bridge, closing a {ZnCNLiN} 5-membered ring which renders a unique three (5,6,5)-ring-fused structure. As far as we can ascertain, **24** represents the first example of a metallated pyrazine of any metal in the periodic table to be structurally characterised. Considering the inherent instability of α-metallated diazines, the entrapment of the dianion $\{C_4N_2H_2\}^{2-}$ present in **24** (which intuitively should be even more destabilised than monoanionic $\{C_4N_2H_3\}^{-}$) is unexpected; however, a closer look at the molecular structure of **24** provides important clues that help to rationalise these results. Thus, the synergic alliance between Li and Zn, which translates into two well-defined coordination modes for each metal, must be key to greatly minimising the repulsions between the electron clouds of the nitrogen lone pair (now involved in forming a dative bond with Li) and the negative charge of the carbanions (which attains extra stabilisation by generating a more covalent, and therefore significantly less polarised, Zn-C bond). Furthermore, the bulky anionic ligands TMP and *t*Bu group may also play an important role by facilitating the formation of a rigid tricyclic structure which provides a protective steric shelter for these newly formed Zn-C bonds (**Figure 5.4**).

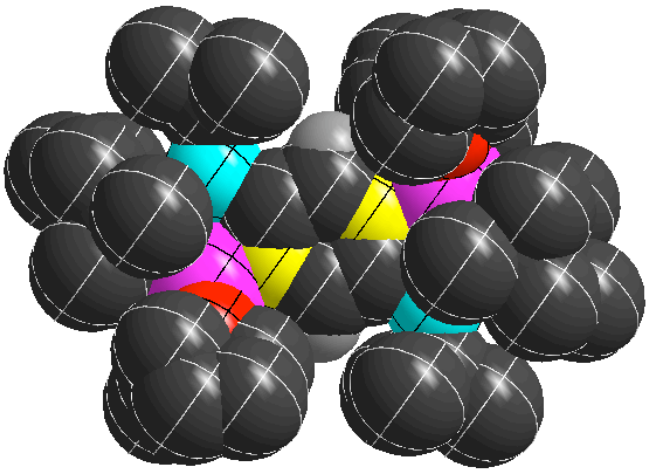

**Figure 5.4**: Space-filling model of **24**.

Hitherto, applications of mixed lithium-zinc combinations for the functionalization of pyrazine have been confined to α-monodeprotonation reactions,[22, 171] where it appears that the substrate is deprotonated by a polar reagent (such as LiTMP or $(TMP)_2Mg{\cdot}2LiCl$) followed by a fast *in situ* trapping by the zinc component present in the mixed-metal mixture to generate a more stabilised heteroarylzinc species.[23, 171] In contrast, using a preformed mixed-metal reagent (where Li and Zn are already in close proximity to each other)[156] switches the cooperative effects which allow the direct zincation of pyrazine affording an unusual regioselectivity for the reaction, not accessible with monometallic bases.[155] To effect this two-fold deprotonation (favoured even when 1 equivalent of **22** is employed), **22** has ultimately used one *t*Bu group, which reacts to form *t*BuH, although the TMP ligand may be involved at an intermediate stage, as demonstrated by other AMM*Zn* reactions.[163, 172]

### 5.2.2 Chemoselective C-H alkylation of pyrazine

To assess the significance of TMP as a constituent of the bimetallic reagent, homoleptic alkyl zincate [(PMDETA)LiZn(*t*Bu)$_3$] (**23**) was prepared by mixing a solution of Zn*t*Bu$_2$ in hexane with *t*BuLi for 1 hour, after which PMDETA was introduced. **23** was formed as a white powder and pyrazine was added at room temperature, forming a bright yellow oil, which was transferred to the freezer overnight. In contrast to **22**, **23** promotes the chemoselective addition of a *t*Bu group

to one α-C of the heterocycle at room temperature, causing its dearomatisation, to give colourless crystals of [(PMDETA)Li{$C_4N_2H_4$(*t*Bu)}Zn(*t*Bu)$_2$] (**25**) in a 76% yield (**Scheme 5.5** and **Figure 5.5**).

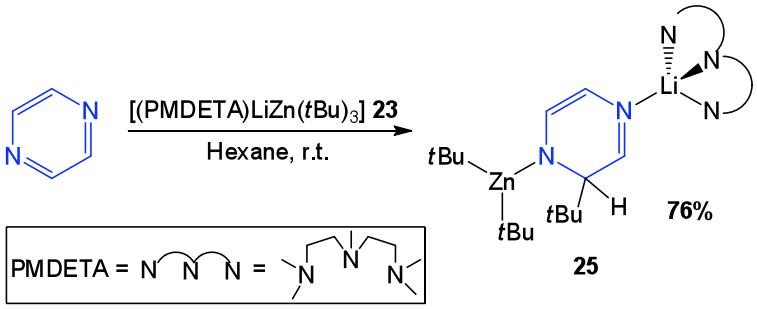


**Scheme 5.5**: Nucleophilic addition of *t*Bu to pyrazine with **23**.

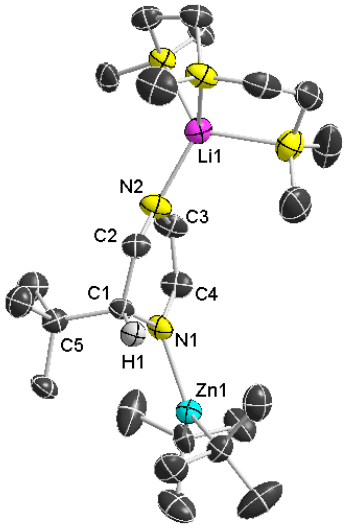


**Figure 5.5**: Molecular structure of **25**. Selected bond distances, N1-C1 1.480(4) Å, C1-C2 1.504(5) Å, C2-N2 1.281(4) Å, N1-C3 1.339(4) Å, C3-C4 1.362(5) Å, C3-N2 1.396(4) Å. Displacement ellipsoids shown at 50% probability level and hydrogen atoms omitted for clarity except that on the C that has experienced alkylation. Minor disorder in PMDETA also omitted for clarity.

The crystal structure of **25** (**Figure 5.5**) provided confirmation of the addition of the lithium-zincate **23** across one C=N bond of pyrazine in a 1,2-fashion, transferring a *t*Bu group to the α-C of the heterocycle (C1 in **Figure 5.5**) to generate a cyclic amide fragment bonded to Zn*t*Bu$_2$. The structure is completed by a PMDETA-

solvated Li which coordinates to the lone pair of the remaining pyridine-type N on the ring. Demonstrating its loss of aromaticity, the new heterocyclic ring is noticeably puckered and the C-C and C-N distances involving N1, C1, C2 and N2 show a more localised double/single bond pattern (N1-C1 1.480(3) Å, C1-C2 1.504(4) Å, C2-N2 1.281(4) Å), in comparison with those involving N1, C3, C4 and N2 (N1-C3 1.338(4) Å, C3-C4 1.362(5) Å and C3-N2 1.397(4) Å). Dearomatisation of related N-heterocycle pyridine with a monometallic magnesium species [HC{(Me)CN(2,6-*i*Pr$_2$C$_6$H$_3$)}$_2$Mg*n*Bu] has been reported giving a 1,2- and 1,4-dihydropyridide anion; however, the authors note that due to a combination of symmetry within the molecule and possible disorder, meaningful discussion of the bond lengths in their dearomatised 1,2-dihydropyridide species could not be defined.[173] The 1,4-dihydropyridide shows disparity between the double and single bonds of 1.336(3) Å and 1.493(3) Å respectively.[173] A search of the Cambridge Structural Database found no precedents for an alkylated diazine structure of zinc or lithium or indeed of any metal, comparable to **25**. Moreover, as far as can be garnered, compound **25** represents the first example of a structurally defined reaction intermediate of the nucleophilic addition of a zincate to a C=N of an organic molecule. Fitting its structure in the solid-state, NMR studies of $C_6D_6$ solutions of **25** confirmed the dearomatisation of the pyrazine ring (**Figure 5.6**) with a diagnostically relevant signal at 4.08 ppm from the α-H located on the newly generated sp$^3$ carbon.

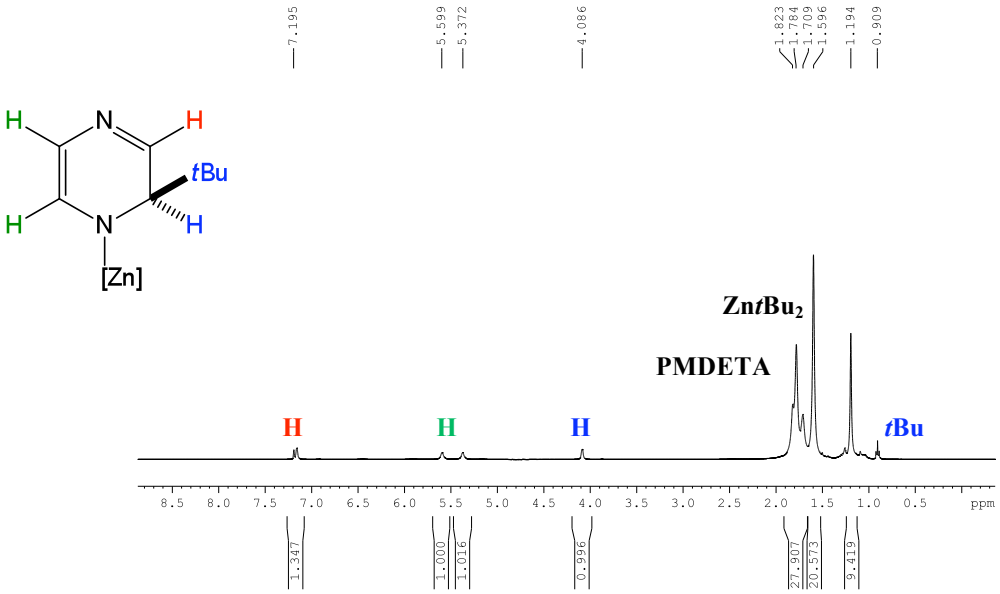


**Figure 5.6**: $^1$H NMR data of **25**.

The strikingly different reactivity exhibited by lithium zincates **22** and **23** is even more surprising taking into account their closely related constitutions, illustrating how chemical profiles of mixed-metallate reagents can be finely tuned by small modifications to the coordination sphere of the metals. Thus, despite the heteroleptic formulation of **22**, the presence of just one amido ligand seems sufficient to favour the two-fold deprotonation of pyrazine precluding the *t*Bu groups still on the zincate to be involved in a competing alkylation reaction as observed for **23**. Hydrolysis of **25** followed by aerobic oxidation furnished 2-*tert*-butyl pyrazine (**26**) as an oil (83% yield, **Scheme 5.6**).

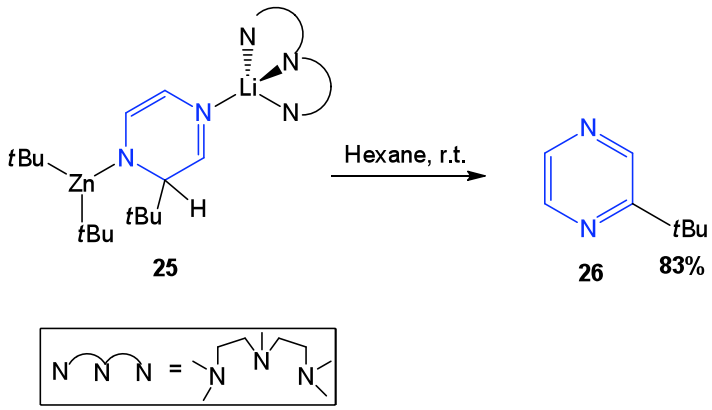


**Scheme 5.6**: Oxidation of **25** to form **26**.

The mild conditions (room temperature, stoichiometric conditions, short reaction times), chemoselectivity and high yield of this reaction is in sharp contrast with results using polar organolithium or Grignard reagents (usually requiring cryogenic conditions to yield the relevant products in low-moderate yields),[174] hinting at this dearomatising mixed-metal addition/oxidation approach as a potential new and improved route for direct C-H alkylation of electron-deficient heterocycles. In this regard, arylzinc compounds have recently been reported to participate in direct arylation processes of N-aromatic heterocycles; however, these reactions require the presence of Ni catalysts, high temperatures (80 – 130 °C) and long reaction times (20 h), an example of which is shown in **Scheme 5.7**.[175]

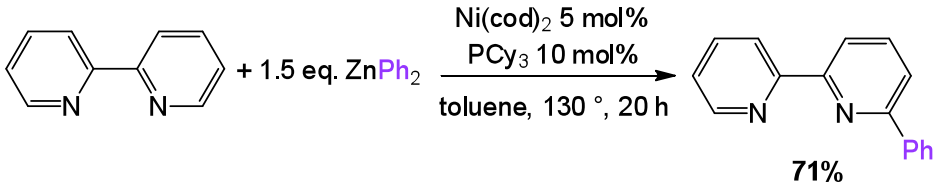


**Scheme 5.7**: Arylation of 2,2-bipyridine with $ZnPh_2$ in the presence of a Ni catalyst.

Adding neutral Zn*t*Bu$_2$ to pyrazine was insufficient to promote the addition of a *t*Bu group, leading to the isolation of the coordination complex [{Zn*t*Bu$_2$}$_3${C$_4$N$_2$H$_4$}$_4$] (**27**) in a 42% yield (**Scheme 5.8** and **Figure 5.7**) demonstrating the formation of **26** is a genuine example of cooperative bimetallic synthesis.

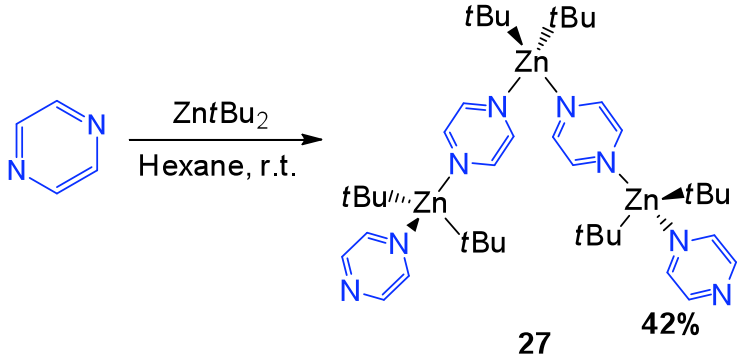


**Scheme 5.8**: Coordination product **27**.

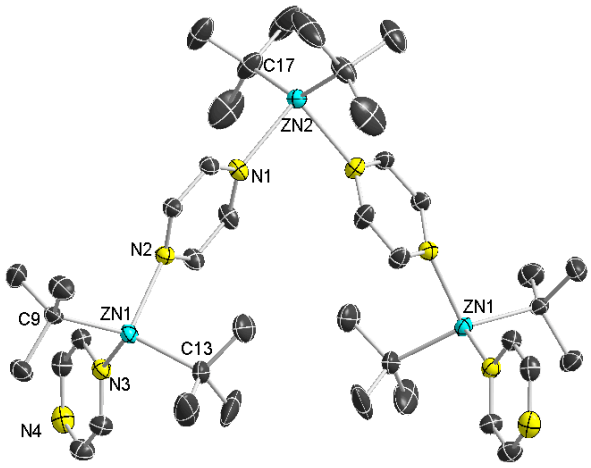


**Figure 5.7**: Molecular structure of **27**. Displacement ellipsoids shown at 50% probability level and hydrogen atoms omitted for clarity. Selected bond distances, Zn1-C9 2.015(2) Å, Zn1-C13 2.026(2) Å, Zn1-N3 2.2650(18) Å, Zn1-N2 2.2791(19) Å, Zn2-C17 2.013(2) Å, Zn2-N1 2.3087(19) Å; C9-Zn1-C13 136.36(10)°, C13-Zn1-N3 109.60(9)°, C17-Zn2-C17#1 137.65(17)°.

Exhibiting an open trinuclear arrangement, the crystal structure of **27** (**Figure 5.7**) shows that each Zn binds to two unchanged molecules of pyrazine which act as simple 2e-neutral donors through their N atoms (Zn1-N3 2.2650(18) Å), whereas the remaining two act as bridges through both N centres connecting central Zn2 with Zn1 (Zn1-N2 2.2791(19) Å, Zn2-N1 2.3087(19) Å). The Zn-C bond distances are slightly longer (average bond distance in **27** = 2.017 Å) than in the discrete linear Zn*t*Bu$_2$ molecule (bond distance 1.977(4) Å)[176] probably due to the increased steric hindrance around the tetrahedral zinc centre in **27** coupled with the 2e donation to zinc from the ligating nitrogen atoms. Compound **27** (prepared using sublimed Zn*t*Bu$_2$) appears stable in $d_8$-THF solution over a period of 3-4 days with singlets at 8.57 (broad) and 0.96 ppm in the $^1$H NMR corresponding to the pyrazine and *t*Bu groups respectively. Contrastingly, when the reaction was performed by adding pyrazine to an *in situ* mixture of 2 equivalents of *t*BuLi with $ZnCl_2$ a complicated mixture of organometallic species occurred, which after hydrolysis led to the isolation of 2-*tert*-butyl pyrazine (**26**) in a 52% yield. This suggests that LiCl (a by-product of the metathesis reaction) must have an activating effect on Zn*t*Bu$_2$ facilitating the alkylation of the heterocycle, in agreement with recent reports highlighting the enhanced kinetic reactivity of organozinc reagents in the presence of LiCl (*vide supra*).[12]

In order to gain some information on the constitution of the organometallic mixture of Zn*t*Bu$_2$ and LiCl, $^1$H-DOSY NMR studies were performed on Zn*t*Bu$_2$·*x*LiCl (*x* = 0-2) mixtures implying a significant increase in the size of the organometallic species present in solution (in terms of their diffusion coefficients) when increasing amounts of LiCl were added. As described previously, these DOSY NMR reactions were carried out in the presence of internal standards TMS, PhN and TPhN. The diffusion constants, *D*, decreased as the LiCl additions increased, indicating that the molecular species was increasing in size as the diffusion coefficient is inversely proportional to size as defined theoretically by the Stokes-Einstein relation (**Equation 5.1**) where *D* is the diffusion coefficient, $k_B$ is the Boltzmann constant, *T* is the temperature in K, $\eta$ is the viscosity of the solution and *r* is the radius of the molecular sphere).[177]

$$D = \frac{k_B T}{6\pi \eta r}$$

**Equation 5.1**: Stokes-Einstein equation

Thus, for organometallic mixtures Zn*t*Bu$_2$·*x*LiCl (*x* = 0-2) the diffusion constants are as follows: *x* = 0, *D* = 11.19 x $10^{-10}$ $m^2$ $s^{-1}$, *x* = 1, *D* = 8.77 x $10^{-10}$ $m^2$ $s^{-1}$, *x* = 2, *D* = 7.20 x $10^{-10}$ $m^2$ $s^{-1}$. **Figure 5.8** shows the diffusion constants of Zn*t*Bu$_2$·*x*LiCl (*x* = 0-2) (purple) compared with the standards (TMS, blue; PhN, red; TPhN, green). These DOSY NMR results coupled with the enhanced nucleophilic power of Zn*t*Bu$_2$·2LiCl can be attributed to the formation of a more reactive bimetallic halozincate resulting from cocomplexation of Zn*t*Bu$_2$ with LiCl.[178]

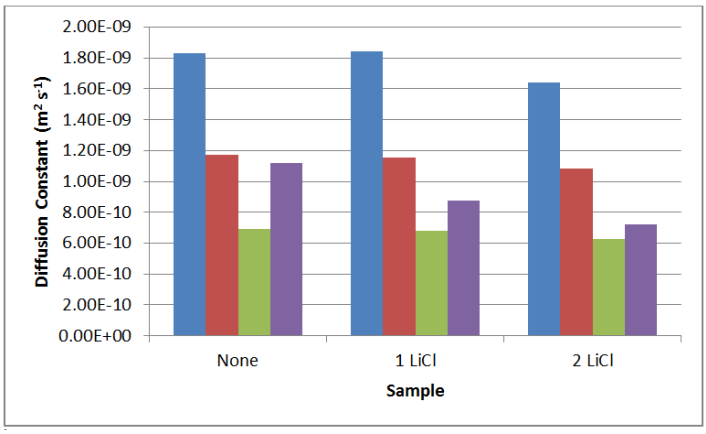


**Figure 5.8**: Diffusion constants for TMS (blue), PhN (red), TPhN (green) and sample in purple: diffusion constant decreases for the sample as the size of the zinc species increases.

To conclude this section, two mixed-metal methodologies for the selective functionalization (two-fold deprotonation or chemoselective C-H alkylation) of pyrazine using different but related lithium zincate reagents as the organometallic source have been uncovered. Furthermore, Zn*t*Bu$_2$ has been shown to be enhanced towards nucleophilic addition of pyrazine in the presence of LiCl (**Scheme 5.9**).

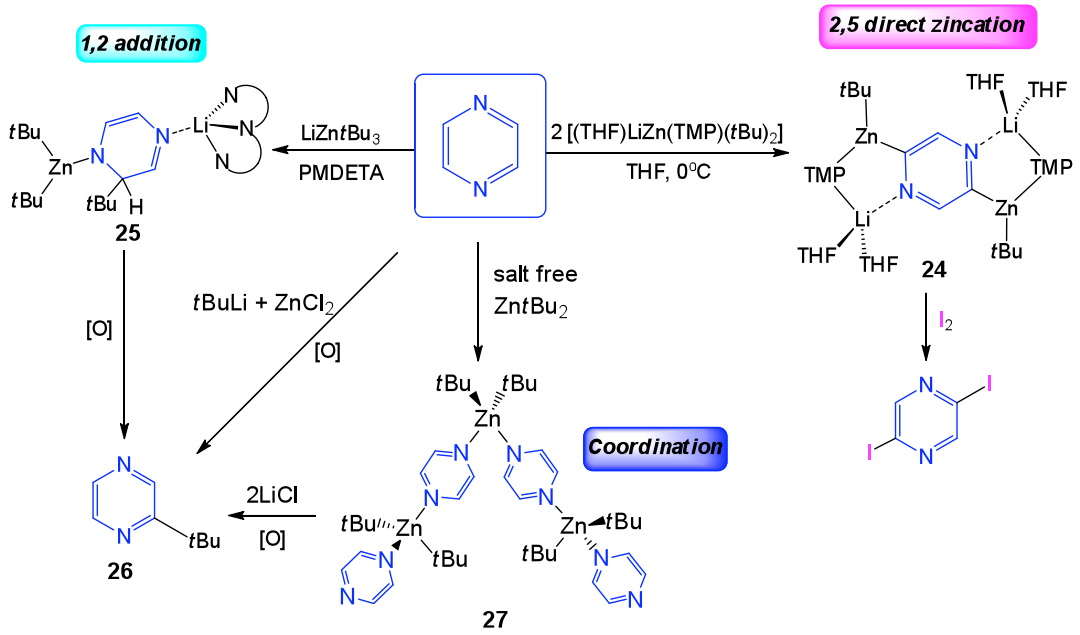


**Scheme 5.9**: Contrasting reactivities of related lithium zincates towards pyrazine.

## 5.3 Mild protocol for zinc-iodine exchange

Continuing the investigations on the cooperative synergy of lithium and zinc, and complementing the application of **22** towards C-H bond activation and **23** towards nucleophilic addition, a new mixed-metal reagent was designed and synthesised to promote direct zincation of aromatic molecules *via* metal-halogen exchange reactions. Metal-halogen exchange, a process which transforms a C-X bond (where X is usually Br or I) into a more polar, more reactive M-C bond, is a cornerstone methodology in synthesis. The regiospecific activation of the C-X bond into a carboanionic organometallic reagent facilitates the creation of C-C bonds (arguably one of the most important processes in synthetic chemistry) or other functionalisation as required. Illustrating the importance of this powerful methodology, Nicolaou employed iodine-magnesium exchange in the final stages of the total synthesis of the exceedingly complex antibiotic vancomycin (**Scheme 5.10**).[179] Halogen-metal exchange of the aryl iodide at -40 ºC yielded the corresponding Grignard reagent which was quenched with $B(OMe)_3$. Oxidation with basic $H_2O_2$ gave the phenol in 50% yield, with no significant change in stereochemistry observed during the transformation.

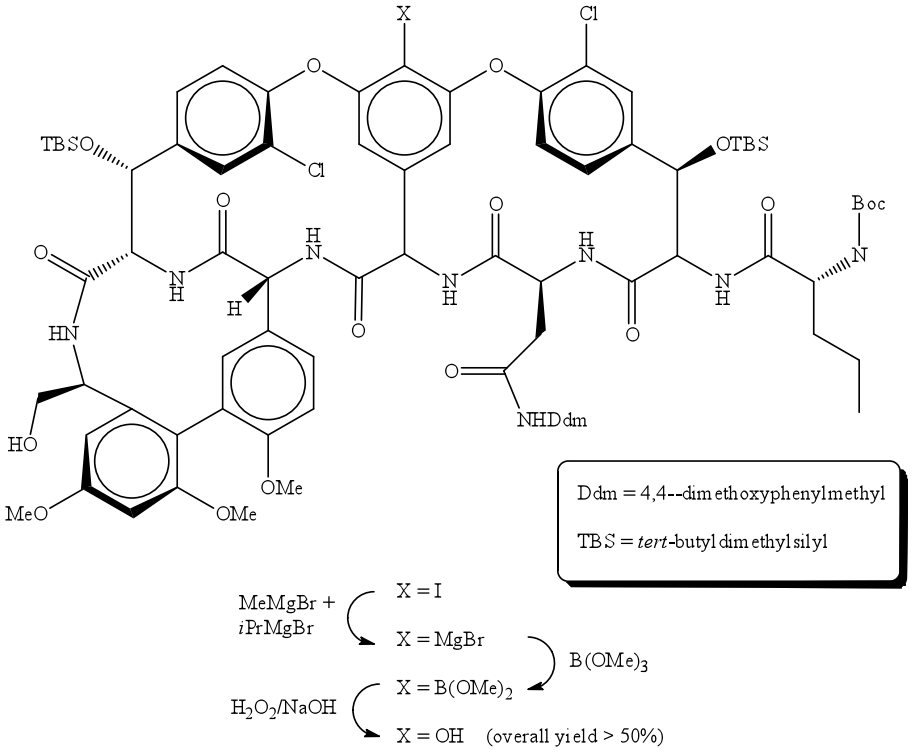


**Scheme 5.10**: Formation of a functionalised aryl magnesium in the total synthesis of vancomycin.

Recently, as outlined in **Chapter 1**, there has been a growing interest in the application of complex metallators as powerful reagents in halogen-metal exchange reactions. Thus, the development of methods that lead, for example, to the direct zincation or magnesiation of an aromatic molecule which can, in turn, be used in Pd or Ni-catalysed cross-coupling reactions *via* the Negishi[51] or Kumada[180] reactions respectively, attracts a lively attention from the research community. However, despite the importance of these reactions, very limited information is available regarding the organometallic intermediates generated *in situ*.

Within the context of M-X exchange reactions, dialkylzinc reagents have been generally overlooked when carrying out organic transformations due to their lower reactivity when compared to more polar organolithium or Grignard reagents; however, their exceptional functional group tolerance together with their ability to take part directly in Negishi Pd-catalysed cross-coupling reactions give dialkylzinc reagents a distinct advantage over their s-block congeners. Recent reports have

shown that trisalkyl- and tetraalkylzincates are effective in halogen-metal exchange reactions[52] whereas the inclusion of an amide functionality (resulting in a monoamido/dialkylzincate species) gives rise to a reagent specialised in performing metallation reactions.[156] Thus, formation of a zincate reagent incorporating an alkoxide ligand was attempted, based on the LIC-KOR superbase reagent. As the superbase pairs two s-block metals together in a 1:1 ratio, it was considered logical that pairing Li with a divalent metal would benefit from a 2:1 ratio of Li:Zn which would produce a higher order zincate that would be anticipated to be more activated towards exchange. When Li(acac) is used as an additive with diethyl zinc, nucleophilic addition reactions can be carried out which exhibit good functional group tolerance[50, 181] and, in the presence of a chiral ligand, can conduct the reaction asymmetrically.[181] From a structural viewpoint, previous studies mixing KO*t*Bu with $ZnEt_2$ in toluene confirmed the formation of a bimetallic complex, which is a dimer of {$Et_2ZnO$*t*BuK} (**Figure 5.9**).[182] Inspired by these results it was decided to test the activation effect that LiOR can have when added to $ZnR_2$ reagents.

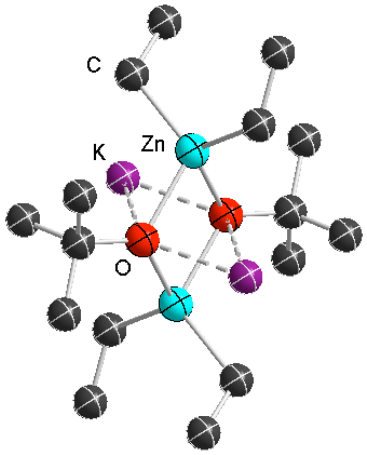


**Figure 5.9**: Evidence of a bimetallic zincate reagent from mixing a diorganozinc compound with an alkali metal alkoxide.[182]

$ZnEt_2$ was chosen as a zinc source because it is commercially available, cheap and widely used in synthesis; however, it lacks sufficient reactivity to perform zinc-iodine exchange reactions with aromatic halides. In this regard, 2-iodoanisole (**21**) was chosen as a test substrate for the zinc-iodine exchange as the methoxy group

serves as a good docking point for the bimetallic reagent. Addition of two molar equivalents of LiO*t*Bu to one equivalent of $ZnEt_2$ in THF followed by addition of two equivalents of 2-iodoanisole gave a milky solution which upon heating resulted in a clear solution. Storage at -28 ºC deposited a crop of clear crystals in 43% isolated yield (**Scheme 5.11**). Analysis of the crystals revealed them to be zincated anisole **28** (**Figure 5.10**). This pleasing result demonstrated a synergic activation was occurring, as neither diethylzinc or LiO*t*Bu are reactive enough to exchange with 2-iodoanisole, yet with the simple addition of lithium *tert*-butoxide to diethylzinc the reaction takes place smoothly at room temperature with both arms activated towards exchange. Using highly sterically demanding $Zn tBu_2$ resulted in a modest increase in crystalline yield of **28** to 51%.

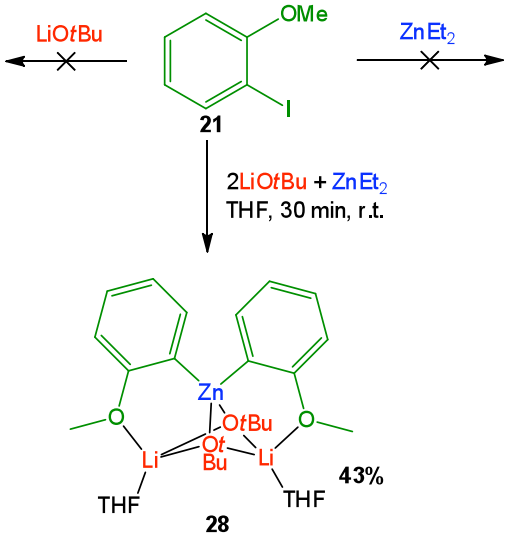


**Scheme 5.11**: Synergic reactivity of LiO*t*Bu and $ZnEt_2$ towards iodine-zinc exchange.

**28** is a CIP zincate containing two lithium atoms, one zinc atom and four anionic ligands. Two of the anionic ligands are butoxide groups from the addition of LiO*t*Bu to the reaction mixture; however, zinc is now coordinated by two aryl molecules, demonstrating that the Zn-I exchange process has taken place and confirming the synergic activation of $ZnEt_2$ by LiO*t*Bu. Thus, Zn has exchanged with I in two anisole molecules forming two new Zn-C bonds (average Zn-C bond distance of 2.021 Å is similar to other compounds in the literature containing *o*-zincated anisole[163, 183]) and completes its distorted tetrahedral coordination by bonding to

each oxygen of the butoxide bridges (sum of angles around Zn = 107.4º from 73.94(4)º [O4-Zn-O3] to 126.28(6)º [C12-Zn-C22]).

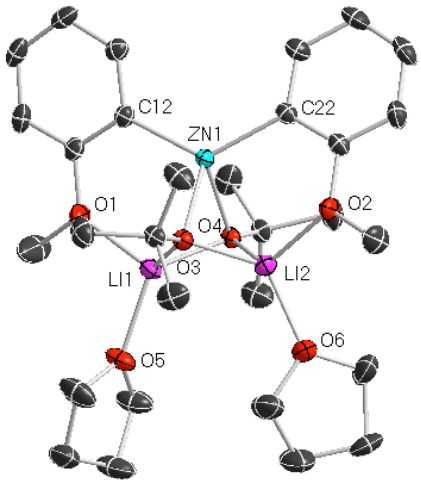


**Figure 5.10**: Molecular structure of **28**. Displacement ellipsoids are drawn at the 50% probability level. Hydrogen atoms and minor disorder in one molecule of THF omitted for clarity. Selected bond distances and angles, Zn-C22 2.0203(15) Å, Zn-C12 2.0217(15) Å, Zn-O3 2.0970(10) Å, Zn-O4 2.1066(10) Å, Li1-O4 1.907(3) Å, Li1-O3 1.921(3) Å, Li1-O5 2.002(3) Å, Li1-O1 2.034(3) Å; C22-Zn-C12 126.28(6)°, C22-Zn-O3 114.92(5)°, C12-Zn-O3 111.15(5)°, C22-Zn-O4 106.65(5)°, C12-Zn-O4 111.38(5)°, O3-Zn-O4 73.94(4)°, O4-Li1-O3 82.68(11)°, O4-Li1-O5 124.14(14)°, O3-Li1-O5 121.23(15)°, O4-Li1-O1 108.38(14)°, O3-Li1-O1 115.96(13)°, O5-Li1-O1 103.86(12)°.

Within the context of Zn-I exchange, a SSIP structure of the reaction intermediate from the treatment of 4-iodotoluene with magnesium zincate $[\{Mg_2Cl_3(THF)_6\}^+\{Zn\textit{t}Bu_3\}^-]$ has previously been defined where the zinc binds in a sigma fashion to three *p*-tolyl groups.[63] Li1 and Li2 are also tetrahedral bonding to four oxygen atoms: each butoxide bridge in the butterfly ring, the oxygen of the closest anisole molecule and finally solvated by a molecule of THF. The angles around each lithium are essentially similar, with an average angle around Li1 of 109.4º and around Li2 of 109.5º. Inspection of bond lengths reveals the longest interaction is between Li and the O of the anisole molecule with an average distance

of 2.056 Å, compared to an average distance of 1.981 Å to the THF oxygen and 1.916 Å to the butoxide oxygen. The most salient feature in the $^1$H NMR spectra (run in deuterated benzene solutions) is the change in the chemical shift of the anisole-related resonances from the free starting material **21** and the product **28**. The methoxy C$H_3$ signal shifts significantly downfield from 3.16 ppm in **21** to 3.66 ppm in **28**. The aryl resonances are also distinctly different, with a doublet now present at 8.28 ppm in **28** whereas the lowest resonance in **21** is a doublet at 7.67 ppm.

### 5.3.1 Electrophilic interception reactions

With a key intermediate of the halogen-metal exchange reaction isolated and structurally defined, the reaction was subjected to electrophilic quench with benzaldehyde (**Scheme 5.12**). A variety of conditions were explored, as shown in **Table 5.1** altering the alkyl group on the zinc and the alkali metal of the butoxide.

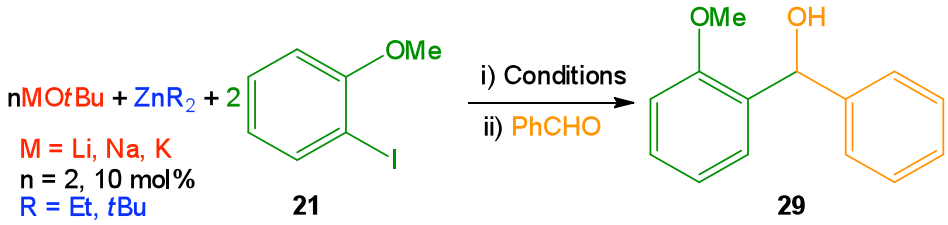


**Scheme 5.12**: General scheme for the synthesis of **29** under various conditions.

Employing a 2.5 hour reflux (entry 1) in the presence of $ZnEt_2$ with two equivalents of Li*O*t*Bu* showed a 1:1.5 conversion, with more of desired product **29** seen by $^1$H NMR than starting material, and a modest isolated yield of 15%. Increasing the reaction time to 24 hours at room temperature (entry 2) showed an increase to almost quantitative conversion and 37% isolated yield. Due to the lower than expected isolated yields, the scale of the reaction was increased at this point. The reaction was next carried out on a 2 mmol scale with a 4 hour stir time; however, the conversion after this time was disappointing with $^1$H analysis of the crude mixture confirming starting material to be the major product and the reaction was not purified further (entry 3). Increasing the scale to 5 mmol and employing the optimised conditions to date (stirring for 24 hours at room temperature) again gave a quantitative conversion

and this time an isolated yield of 32% was attained (entry 4). Employing a catalytic amount of Li*O*t*Bu disappointingly resulted in no reaction taking place (entry 5). The effect of the alkyl group bonded to the zinc moiety was next examined and the more reactive Zn*t*Bu$_2$ reagent was employed; however, in each of the conditions explored no advantage was observed over the commercially available ZnEt$_2$ reagent, hence this was not investigated further (entries 6 and 7). Turning to investigating the effect of the alkali metal present, Li*O*t*Bu was replaced by Na*O*t*Bu (entry 8) and K*O*t*Bu (entry 9). Sodium performed better than potassium (11% isolated yield versus 0% conversion observed with K and only starting material present in the $^1$H NMR). This low conversion with Na*O*t*Bu and complete lack of reactivity observed with K*O*t*Bu suggests that the mixed-metal species forms reluctantly with sodium *tert*-butoxide and does not form when potassium *tert*-butoxide is combined with ZnEt$_2$ in THF. Overall in the conditions explored ZnEt$_2$ with two equivalents of Li*O*t*Bu resulted in the best conversion.

**Table 5.1**: Conditions for the reaction of 2-iodoanisole and various bimetallic mixtures followed by quench with benzaldehyde.

| Entry | Reagent | Scale | Conditions[a] | Conversion SM:product[b] | Yield[c] |
|---|---|---|---|---|---|
| 1 | 2Li*O*t*Bu + ZnEt$_2$ | 1 mmol | 2.5 h reflux | 1:1.54 | 15% |
| 2 | 2Li*O*t*Bu + ZnEt$_2$ | 1 mmol | 24 h r.t. | 0:1 | 37% |
| 3 | 2Li*O*t*Bu + ZnEt$_2$ | 2 mmol | 4 h r.t. | 1:0.05[d] | - |
| 4 | 2Li*O*t*Bu + ZnEt$_2$ | 5 mmol | 24 h r.t. | 0:1 | 32% |
| 5 | Li*O*t*Bu (10 mol%) + ZnEt$_2$ | 2 mmol | 24 h r.t. | 1:0[d] | - |
| 6 | 2Li*O*t*Bu + Zn*t*Bu$_2$ | 2 mmol | 2.5 h r.t. | 1:0.75[d] | - |
| 7 | 2Li*O*t*Bu + Zn*t*Bu$_2$ | 2 mmol | 24 h r.t. | 1:0.65[d] | - |
| 8 | 2Na*O*t*Bu + ZnEt$_2$ | 2 mmol | 2.5 h reflux | 1:0.47 | 11% |
| 9 | 2K*O*t*Bu + ZnEt$_2$ | 2 mmol | 2.5 h reflux | 1:0[d] | - |

[a] General reaction conditions: Following the conditions shown, a slight excess of PhCHO was added and the suspension stirred for 24 h after which it was worked up following standard protocol. [b] Conversion estimated by $^1$H NMR integration of crude product. [c] Isolated yield of analytically pure product. [d] Not purified further.

This methodology is also applicable to magnesium, where the addition of two equivalents of Li*O*t*Bu to commercially available *n*Bu$_2$Mg is able to activate the

dialkyl magnesium reagent towards bromine-metal exchange, with crystals of intermediate **28a**, analogous to **28** formed (**Figure 5.11**). Although *n*$Bu_2$Mg is unable to carry out Mg-Br exchange on its own, the combination of the dialkyl magnesiate with Li*O*t*Bu* and resulting magnesiate is sufficiently reactive to perform the exchange and the C-Br bond (which is stronger than the C-I bond) is replaced with a C-Mg bond. Despite washing the crystals, unfortunately the $^1$H NMR showed some starting material still present as well as the *ortho*-magnesiated product. Structure **28a** is entirely analogous with that described above for structure **28**, hence discussion will be omitted for brevity. The main difference between related structures **28a** and **28** is a shortening in the M-C bond length (where M = Mg or Zn respectively) from an average Mg-C bond distance of 2.171 Å to an average Zn-C bond distance of 2.021 Å, due to the smaller radius of Zn.

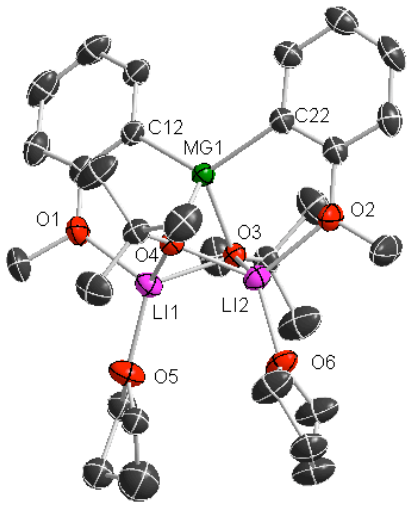


**Figure 5.11**: Mg-analogue of **28**. Displacement ellipsoids are drawn at the 50% probability level. Hydrogen atoms and minor disorder in one molecule of THF omitted for clarity. Selected bond distances and angles Li1-O5 1.947(4) Å, Li1-O3 1.950(4) Å, Li1-O4 1.965(4) Å, Li1-O1 2.032(4) Å, Mg-O4 2.0200(14) Å, Mg-O3 2.0251(14) Å, Mg-C12 2.170(2) Å, Mg-C22 2.172(2) Å; O5-Li1-O3 118.32(18)°, O5-Li1-O4 129.03(19)°, O3-Li1-O4 80.10(13)°, O5-Li1-O1 106.87(17)°, O3-Li1-O1 114.60(17)°, O4-Li1-O1 106.08(16)°, O4-Mg-O3 77.02(6)°, O4-Mg-C12 116.00(7)°, O3-Mg-C12 107.25(7)°, O4-Mg-C22 112.44(7)°, O3-Mg-C22 111.13(7)°, C12-Mg-C22 123.09(8)°.

### 5.3.2 Cocomplexation reactions of $ZnEt_2$ and Li*O*t*Bu*

In parallel studies, investigations were initiated into the structure of the active species carrying out the zinc-iodine exchange described for the preparation of **28**. Two molar equivalents of Li*O*t*Bu with one equivalent of $ZnEt_2$ in hexane were stirred for 30 minutes, after which four equivalents of THF were added. Storage at -28 ºC resulted in clear crystals, which were analysed by X-ray crystallography revealing a heterometallic cubane structure had formed, **30**, in 13% isolated yield (**Scheme 5.13**, **Figure 5.12**).

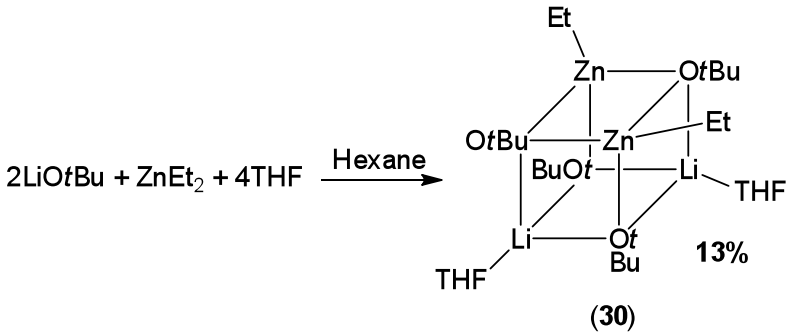


**Scheme 5.13**: Attempted preparation of the dialkoxo-dialkyl zincate species.

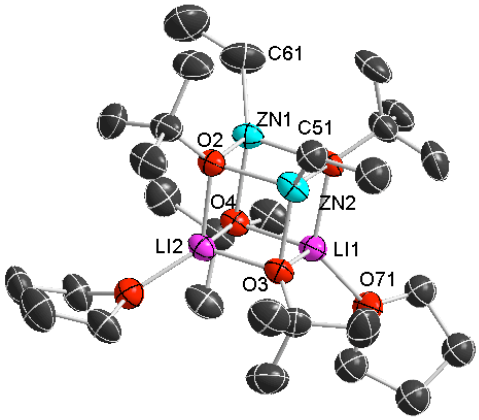


**Figure 5.12**: Molecular structure of **30**. Displacement ellipsoids are drawn at the 50% probability level. Hydrogen atoms and minor disorder in one Et and both THF molecules omitted for clarity.

The heterocubane structure of **30** is a triorganozincate dimer and could be considered a stacking of two {LiOZnO} rings, limited to an aggregate of this size due to the presence of the bulky *tert*-butoxide groups,[6] with the corners made up of alternating

metal and oxygen atoms. Each metal adopts a distorted tetrahedral geometry. Zn binds to three *tert*-butoxide moieties within the cube and one terminal ethyl group. Li also binds to three *tert*-butoxide groups and its coordination sphere is completed by interacting with a molecule of THF. The pseudo-cubane motif displayed by **30** has previously been reported for mixed alkyl/alkoxide species (both bimetallic Li-Zn and monometallic Zn species),[6, 184] and both the Me[184a] and *t*Bu[184c] analogues are known. The methyl analogue was synthesised from non-donor solvent and forms a polymer of cubes whereas the *tert*-butyl analogue was synthesised in the presence of THF and forms a discrete cube as per **30**. The most notable difference between the related Me and *t*Bu species with the Et one of **30** is the mode of synthesis. In both the Me and *t*Bu examples, *t*BuLi is used in place of Li*Ot*Bu and oxygen is then deliberately introduced leading to insertion between the M-*t*Bu bonds, demonstrating the oxophilic nature of mixed Li-Zn systems. The Li-O bond distances (mean 1.989 Å) and Zn-O bond distances (mean 2.049 Å) are slightly shorter than those in found in the related Me polymer (2.078 Å and 2.066 Å respectively), showing the discrete heterocubane to be more compact, but within the same order of those found in the *t*Bu example (2.004 Å and 2.047 Å respectively). Comparison of the Zn-O bond lengths in **30** with related homometallic cubane $[Zn_4(Et)_4(O\textit{t}Bu)_4]$ reveals the homometallic species to have slightly longer (weaker) bonds (mean 2.073 Å).[185]

The most salient feature of the $^1$H NMR of **30** is the appearance of only one singlet relating to the O*t*Bu group. Two *tert*-butoxide moieties are present, with one alkoxy group capping a $Li_2Zn$ triangle and another capping a $Zn_2Li$ triangle; however, at room temperature these are indistinguishable in $C_6D_6$, suggesting a rapid interconversion is occurring or the dimer aggregation is no longer retained.

Comparing the constitution of **30** with the stoichiometry of the reaction, it appears that a disproportionation reaction has taken place. A plausible reaction pathway is shown in **Scheme 5.14** which will involve the formation of EtLi. $^1$H NMR studies of the constitution of the species present in solution after crystallisation of **23** show the presence of a mixture of different organometallic compounds, suggesting that the solution chemistry of these bimetallic mixtures is extremely complex.

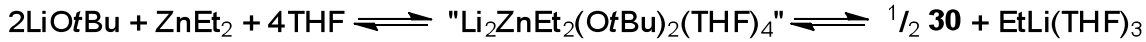


**Scheme 5.14**: Possible disproportionation to give **30**.

## 5.4 Conclusions

By isolating and characterising the organometallic intermediates of a number of key organic transformations (metallation, alkyl addition and metal-halogen exchange reactions) new insights have been garnered regarding the way subtle changes in the coordination environment of CIP lithium zincates can induce drastic changes in the reactivity pattern of these mixed-metal reagents. The reactivity of heteroleptic zincate [(THF)LiZn(TMP)(*t*Bu)$_2$] (**22**) towards pyrazine has been examined, showing that despite the presence of two nucleophilic *t*Bu groups the selective two-fold deprotonation of pyrazine is preferred to form the unprecedented 2,5-di-zincated pyrazine molecule. These results are in contrast with those observed when pyrazine is confronted by the homoleptic alkyl zincate [(PMDETA)LiZn(*t*Bu)$_3$] (**23**) where the chemoselective addition of a *t*Bu group to the α-C of the heterocycle takes place under mild reaction conditions. By trapping the bimetallic intermediates of these reactions the first structural insights into the constitution of the inorganic products resulting from the reactions of an organometallic reagent with pyrazine are provided. Additionally, the aggregation of LiCl and Zn*t*Bu$_2$ has been probed using $^1$H-DOSY NMR studies which suggest a lithium zincate aggregate is forming in solution that is shown to be sufficiently reactive to transfer a *t*Bu group to the pyrazine molecule, in contrast with Zn*t*Bu$_2$ alone which forms a coordination product. Switching to a monoalkoxo/dialkyl species (from cheap, commercially available starting materials) led to a novel route for halogen-metal exchange. Whilst the isolated yields are poor, quantitative conversion was determined by $^1$H NMR analysis and the low cost and mild reaction conditions of this reaction demonstrates it has potential to be a useful addition in M-X exchange reactions following some optimisation.

# Chapter 6: Applying mixed-metal chemistry to N-heterocyclic carbene chemistry

## 6.1 Introduction to N-heterocyclic carbene chemistry

The area of carbene chemistry is growing at a vast rate and shows no signs of waning. Whole tomes can be dedicated to this subject; however, for the sake of brevity this short introduction will concentrate on persistent N-heterocyclic carbenes as ligands, primarily with respect to main group elements, and forego any discussion on the reactive organometallic Fischer[186] or Schrock[187] carbenes.

Carbon has the electronic configuration $[He]2s^2 2p^2$ and normally uses all four valence electrons to form four valence bonds (tetravalent carbon) but in the case of carbenes only two valence bonds are formed (divalent carbon) leaving two electrons not used in bonding. These electrons can be placed in the two unused orbitals in the following ways: (a) one electron each is placed into the two empty orbitals with parallel spins giving a triplet carbene, (b) both electrons are placed in the same orbital giving a singlet carbene and (c) an excited state singlet carbene, where one electron is in each orbital, similar to the triplet carbene except now the electrons occupy opposite spins (**Figure 6.1**).[188]

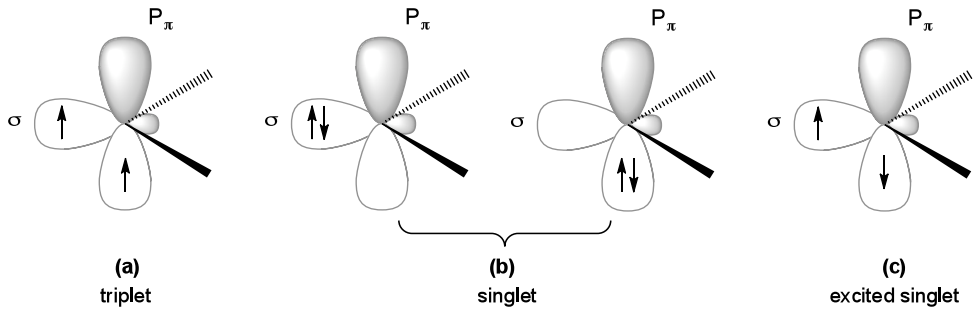


**Figure 6.1**: Possible configurations of carbenes.[188]

N-Heterocyclic carbenes (NHCs) are singlet carbenes that garner extra stability from the donation of the lone pairs from the nitrogen atoms adjacent to the carbene carbon into the vacant $p_\pi$ orbitals of the carbene centre (reducing the electron deficiency of

the carbene) in addition to the nitrogens acting as σ-acceptors which stabilises the carbene lone pair by the inductive effect of the electronegative nitrogen (**Figure 6.2**).[188]

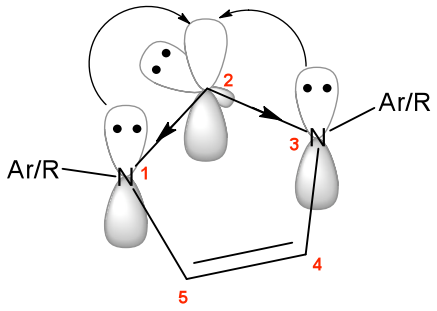


**Figure 6.2**: Electronic effect of the diamino N-heterocyclic carbene: π-donor, σ-acceptor.[188] IUPAC numbering system shown in red.

The combination of the resonance and inductive effects result in the stabilisation of these diaminocarbenes; however, before the first stable free crystallised carbene could be isolated, steric factors also had to be taken into account. Thus, in 1991 Arduengo was able to synthesise and characterise the first crystalline carbene by employing the highly sterically demanding adamantyl substituents on N. Carbene 1,3-bis-adamantylimidazol-2-ylidene was produced from the deprotonation of the corresponding imidazolium salt with NaH (**Scheme 6.1**).[189]

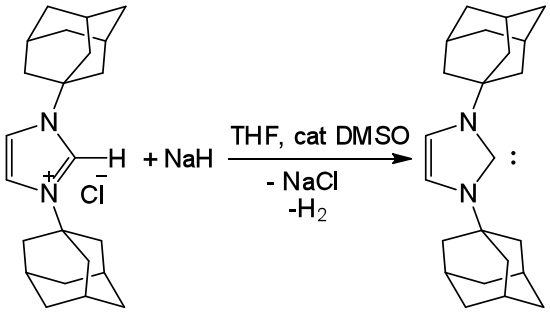


**Scheme 6.1**: Preparation of the adamantyl-substituted carbene.

This landmark discovery helped to elevate NHCs into the realm of the synthetic chemist as they were now much more easily handled and practical. NHC ligands have been shown to exhibit excellent attributes in respect to the C-C bond formation of Pd-catalysed cross-coupling reactions[190] and olefin metathesis reactions[191] due

to the strong binding of the NHC to the metal centre, which can increase the lifetime of the catalyst.[190] For example, the exchange of a phosphine ligand in Grubbs' catalyst to an NHC, giving the *2nd generation catalysts*, resulted in a catalyst that can efficiently promote olefin metathesis reactions at very low catalyst loading (0.05 mol%) (**Figure 6.3a**).[191] With respect to Pd-catalysed cross-coupling reactions, Organ and co-workers have been amongst the leaders in the field of catalyst development, notably with the design of the Pd-PEPPSI-NHC precatalyst complexes (PEPPSI = pyridine-enhanced precatalyst preparation, stabilisation and initiation), a number of which are now commercially available and exhibit enhanced reactivity, which is partially attributed to the increase in steric bulk around Pd (**Figure 6.3b**).[190]

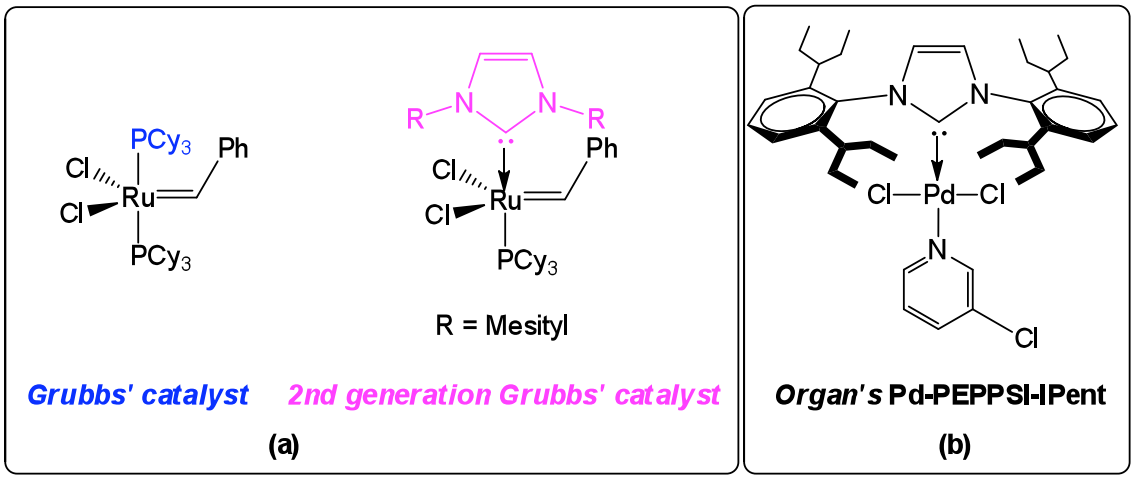


**Figure 6.3**: Incorporation of NHCs into catalysts for organic transformations.

Contrasting with the extensive applications of NHC complexes containing transition metals, the NHC chemistry of main group elements has received much less attention. Having stated that, there are several seminal reports of this important ligand being used to stabilise low-oxidation state main group molecules. Diatomic allotropes of the p-block have been reported for Si,[192] P,[193] and Ge,[194] (amongst others) generally by the reduction of a halogenated precursor with, for example, potassium graphite (**Figure 6.4**). The role of the ligand is to provide steric support to the newly generated element-element bonds, while at the same time being unreactive towards the alkali metal reduction method used in synthesising the allotropes. Of particular note is the recent report in *Science* of the NHC-stabilised boron-boron triple

bond.[195] This novel complex is stable at ambient temperature and was synthesised by the addition of 1,3-bis-(2,6-diisopropylphenyl)imidazol-2-ylidene (IPr) to tetrabromodiborane and the resulting adduct was reduced with four equivalents of sodium naphthalenide to give the triple bonded product (**Scheme 6.2**).

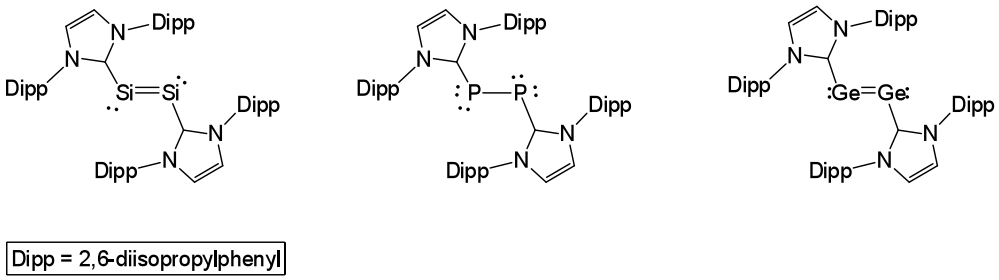


**Figure 6.4**: Low oxidation state main-group molecules stabilised by NHC ligands.

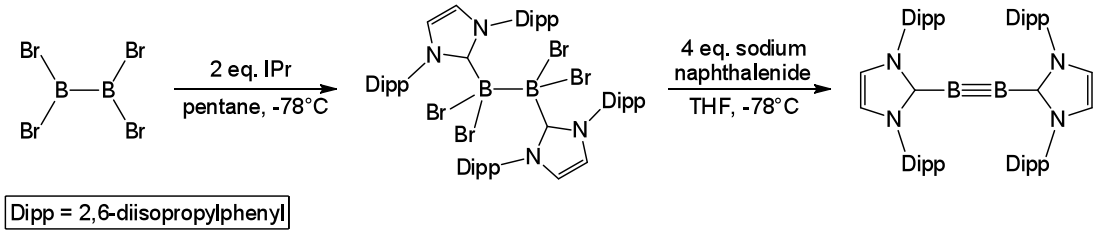


**Scheme 6.2**: Preparation of a boron-boron triple bond.[195]

Turning to the s-block, Alexakis *et al* have employed a functionalised NHC as a catalyst for asymmetric allylic alkylation reactions with Grignard reagents, although no structural intermediates were isolated. [196] Notably, the deft application of IPr as a trapping agent for oligomeric fragments of magnesium compounds has been reported by mixing IPr with Mg*n*$Bu_2$, which allowed the polymeric network of [$(IPr)_2$·*n*$Bu_8Mg_4$] to be elucidated (**Figure 6.5a**). This tetranuclear complex provides insight into the solvent-free structure of *n*$Bu_2$Mg, which has thus far remained elusive.[197] Another example of a tetranuclear Mg complex to be structurally defined and that is dependent on IPr is the striking magnesium hydride cluster synthesised by Hill and co-workers by adding 8 molar equivalents of $PhSiH_3$ to the mononuclear adduct [IPr·Mg$(HMDS)_2$] which gives [$(IPr)_2$·$Mg_4H_6(HMDS)_2$] which displays an andamatane-like $Mg_4H_6$ core, supported by two molecules of IPr and two HMDS fragments (**Figure 6.5b**).[198]

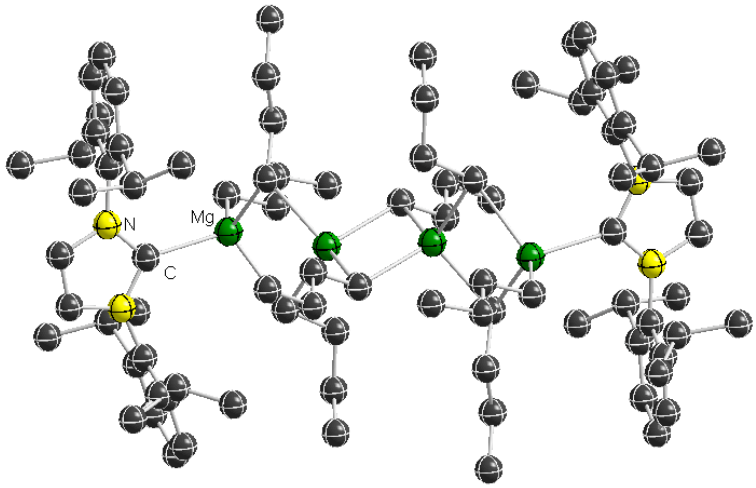


**(a)**

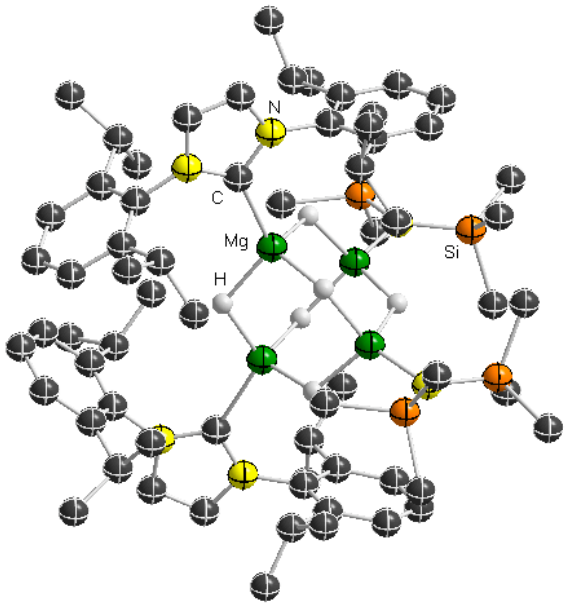


**(b)**

**Figure 6.5**: Tetranuclear Mg complexes stabilised by IPr. (**a**) $[(IPr)_2{\cdot}n Bu_8Mg_4]$.[197] (**b**) $[(IPr)_2{\cdot}Mg_4H_6(HMDS)_2]$.[198] Displacement ellipsoids are drawn at the 50% probability level. Hydrogen atoms, except attached to Mg, omitted for clarity.

### 6.1.1 Functionalization of the NHC molecule

A major advantage of NHC molecules is the ability to tune the sterics and electronics of the system by modifying the substituents on the N atoms or the backbone of the imidazole ring. Intuitively the sterics can be tuned by increasing/decreasing the bulk on the N-substituent. Remarkably, these changes can have a profound effect on the

stability of the carbene, as illustrated by the fact that the bis(chloro) analogue of 1,3-dimesityimidazol-2-ylidene (IMes) stable in air whereas IMes itself must be stored under an inert atmosphere.[199] With a multitude of fundamental organic transformations available utilising NHC-containing complexes, for example ring closing/ring opening polymerisation reactions,[200] the synthesis of aromatic compounds,[201] and the application of Grubbs' catalyst to non-metathetic reactions (hydrosilylations, cycloaddition reactions, cyclopropanation reactions amongst others),[202] a facile route to C4/C5 activation would be of great interest as a change in the electronics of the carbene molecule from backbone substitution could provide a more efficient catalyst.

In 2001 Crabtree reported the isolation of an Ir-based *abnormal* carbene (*a*NHC) where the carbenic position was at the C5 carbon (between one N and one C) instead of the normal carbene C2 position (between both N atoms) (**Scheme 6.3**).[203] The chelating nature of the carbene ligand favoured the formation of the *a*NHC at the C5 position, furthermore studies by the same group showed that the C5-bound *a*NHC to be more electron donating than the normal C2-bound NHC.[204]

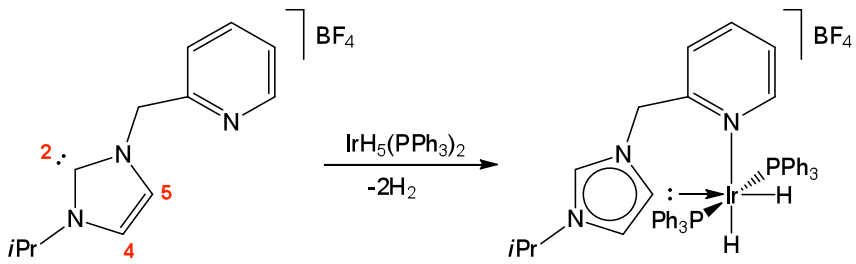


**Scheme 6.3**: Synthesis of an *abnormal* carbene.

The preparation of a stable metal-free *a*NHC was realised in 2009 when Bertrand *et al* chose an imidazolium salt with the C2 and C4 positions blocked by a phenyl group, leaving only the C5 position available for deprotonation by potassium amide KHMDS, as reported in *Science* (**Scheme 6.4**).[205] This methodology produced the *a*NHC in 68% yield and the resulting compound is stable both in the solid-state and in solution for a few days at room temperature. Heating the compound in benzene for

48 hours did cause the quantitative rearrangement to a more stable non-carbene molecule.

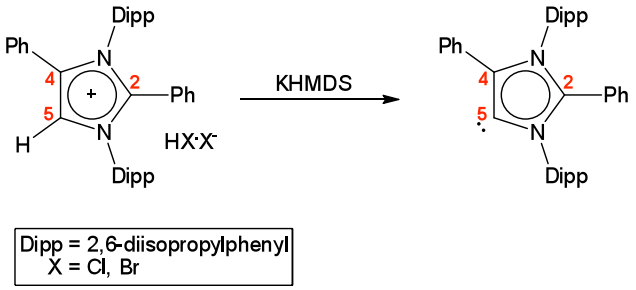


**Scheme 6.4**: Synthesis of a stable metal-free *abnormal* carbene.

This important discovery was closely followed by the synthesis of an anionic dicarbene (NHDC), where two carbene centres (C2 and C4) are found within one heterocylic imidazole ring.[206] Deprotonation of IPr by BuLi in THF resulted in a polymer that sees Li bonding to the C2 of one ring and the C4 of a neighbouring ring and also interacts with one molecule of THF. The dicarbene nature of the molecule was confirmed by the addition of a Lewis acid to the polymer, which gave crystals showing the Lewis acid coordinating to the C4 (*abnormal*) position with the Li present at the C2 (normal) position (**Scheme 6.5**). The functionalization of the C4 position was also demonstrated by the addition of TMSCl giving a C-Si bond.

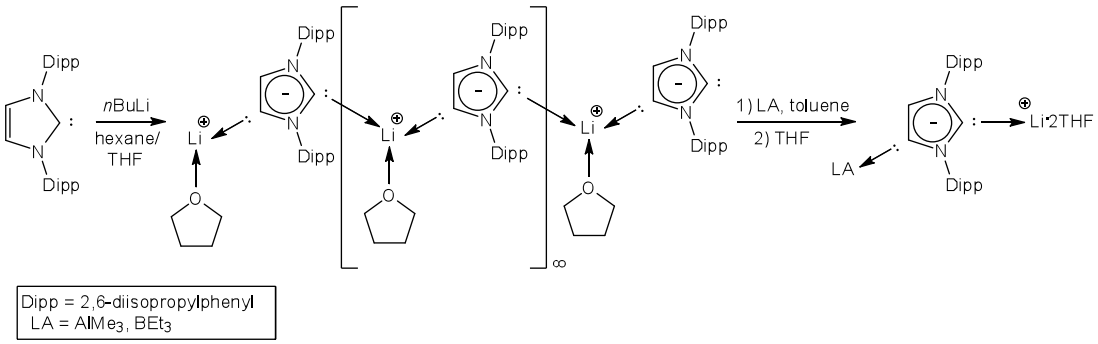


**Scheme 6.5**: Synthesis of an anionic dicarbene.

Manipulation of the reaction conditions can lead to the interconversion between the borane adduct shown above (when LA = $BEt_3$) and a mononuclear *abnormal* NHC by the protonation of the product at the C2 position, which can, in turn, undergo

lithiation back to the dinuclear dicarbene (**Scheme 6.6**).[207] A similar structure with an NHC ligand bridging between B and Li, this time with boron at the C2 position and lithium at the C4 position, has also been reported by the initial complexation of IPr with $BH_3$·THF (thereby "blocking" the carbene C2) followed by deprotonation by BuLi forming a C-Li bond at C4.[208] This highly polar bond allows for further functionalization of the imidazole ring and the incorporation of moieties that can affect the sterics and electronics of the carbene.

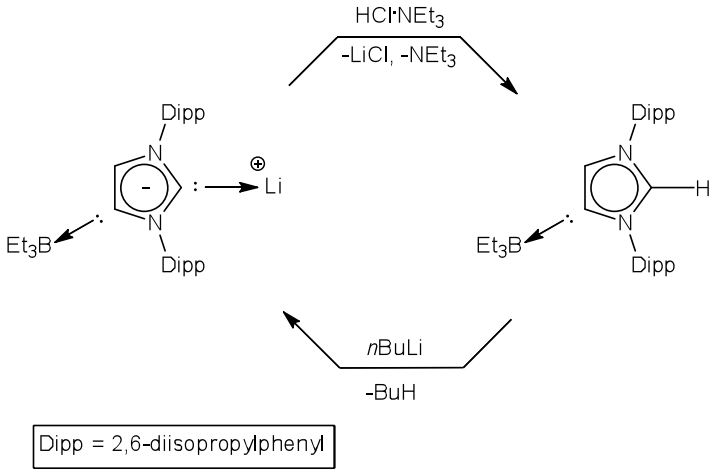


**Scheme 6.6**: Conversion between the *a*NHC and anionic dicarbene.

Of note is the fortuitous discovery by Bertrand of the C4 functionalisation of the imidazole ring whilst attempting to prepare a range of C2-substituted *a*NHC molecules. Employing a similar strategy to that used in his pioneering discovery of the first stable metal-free *a*NHC by blocking the C2 position, the author found that if an electrophile was added to IPr, giving the desired C2-adduct, deprotonation did not lead the expected *a*NHC but instead to the isomeric analogue with the electrophile at the C4 position and a normal carbene at C2.[209] **Table 6.1** details some of the electrophiles used.

**Table 6.1:** Addition of an electrophile to IPr and deprotonation.

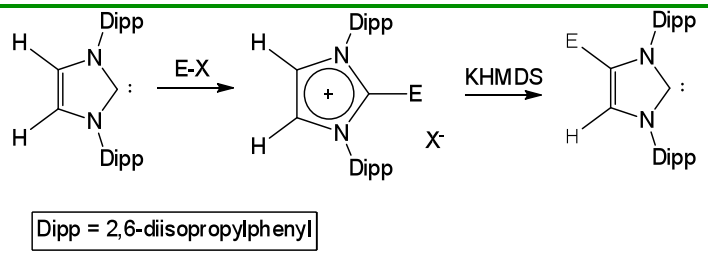


Dipp = 2,6-diisopropylphenyl

| E | X | Yield of salt/% | Yield of product/% |
|---|---|---|---|
| PhC(O) | Cl | 79 | 64 |
| Cl | Cl | 83 | 42 |
| Br | Br | 86 | 39 |
| $CF_3SO_2$ | $CF_3SO_3$ | 72 | 72 |
| $Me_3Si$ | $CF_3SO_3$ | 80 | 35 |
| $Ph_2P$ | Cl | 77 | 57 |

With regards mixed-metal systems, the first example of an NHC ligand bridging between two metals was described in 2006 by the Arnold group by deprotonating an amido-tethered NHC yttrium complex with potassium naphthalenide resulting in the bimetallic species shown in **Scheme 6.7** and **Figure 6.6**, which then forms a dimer. In the product, yttrium has migrated from its original C2 position (the normal carbenic centre) to C4 (the *abnormal* carbenic centre) with solvent-supported K now residing at the C2 position.[210]

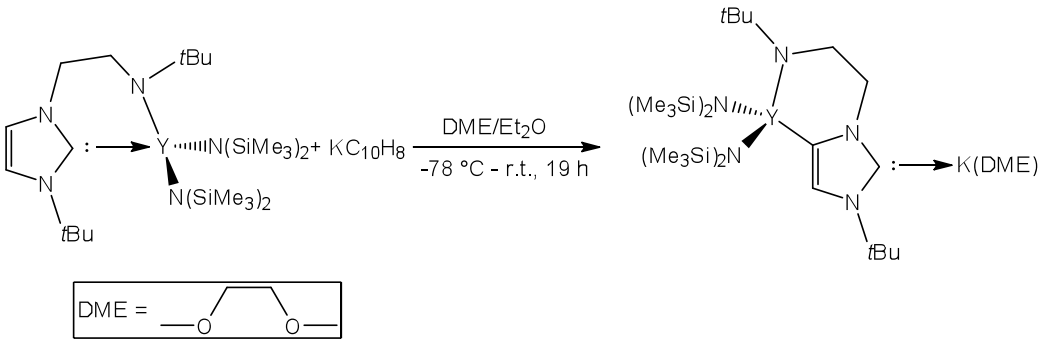


DME = O O

**Scheme 6.7**: Synthesis of an NHC-bridged Y/K complex.

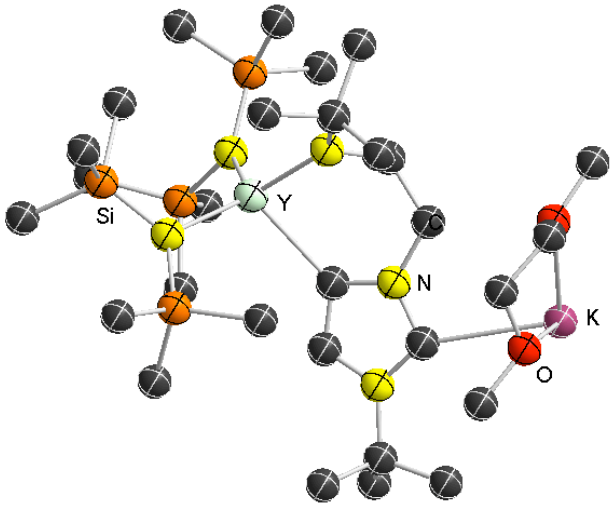


**Figure 6.6**: Monomeric structure of NHC-bridged Y/K complex. Displacement ellipsoids are drawn at the 50% probability level. Hydrogen atoms omitted for clarity. (Structure forms a dimer through K.)

In terms of s-block mixed-metal chemistry, only one report detailing any sort of 'ate complex incorporating NHC molecules is known. Hill and co-workers isolated a number of SSIP structures $[\{M^{I}(IPr)_2\}^{+}\{ M^{II}(HMDS)_3\}^{-}]$ (where $M^{I}$ = Li, Na, K; $M^{II}$ = Mg, Ca, Sr, Ba) by mixing equimolar amounts of a group 1 and group 2 amide with two molar equivalents of IPr.[211] A representative example is shown in **Scheme 6.8** and **Figure 6.7**, with the alkali metal sequestered by the IPr molecules and the group 2 centre ligated by the HMDS ligands.

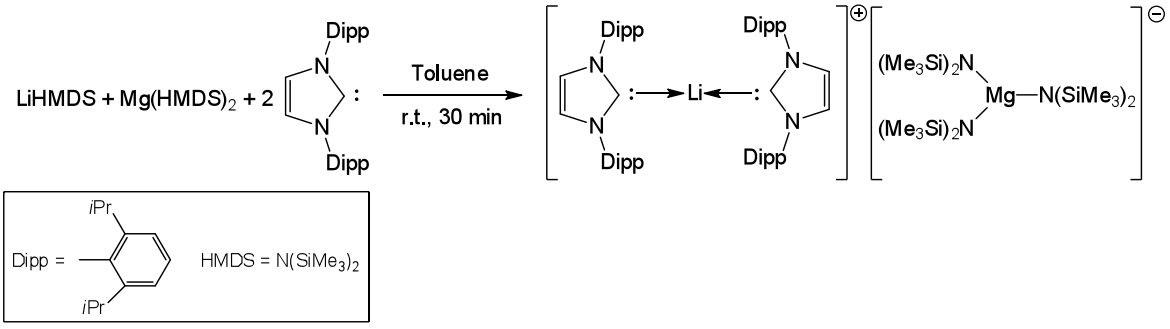


**Scheme 6.8**: Synthesis of SSIP lithium magnesiate $[\{Li(IPr)_2\}^{+}\{Mg(HMDS)_3\}^{-}]$.

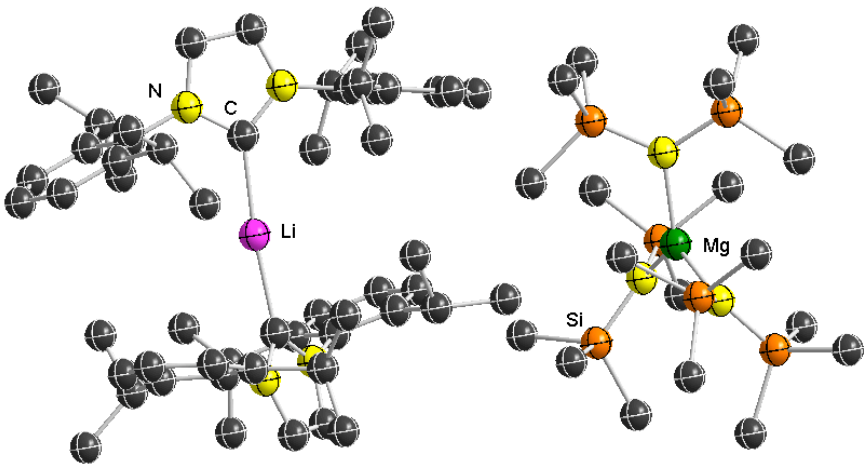


**Figure 6.7**: Molecular structure of $[\{Li(IPr)_2\}^+\{Mg(HMDS)_3\}^-]$. Displacement ellipsoids are drawn at the 50% probability level. Hydrogen atoms omitted for clarity.

In light of these very recent advances in N-heterocyclic chemistry, coupled with the importance of these molecules and the scarcity of studies involving mixed-metal systems, it seemed expedient for research towards the application of alkali metal zincates and magnesiates towards NHCs be carried out. This final chapter will now detail original research in this area.

## 6.2 Preparation of NHCs and complexation with dialkyl zinc species

Synthesis of the N-heterocyclic carbene starting materials was carried out according to literature procedures.[212] Aryl substituted imidazolin-2-ylidenes 1,3-bis-(2,6-diisopropylphenyl)imidazol-2-ylidene IPr, **31**, and 1,3-dimesityimidazol-2-ylidene IMes, **32**, were prepared by the addition of the appropriate amine (2 equivalents) to a glyoxal solution in water/isopropanol, yielding the diimine intermediate in good yield (average 80%). Cyclisation of the intermediate using chloromethylethyl ether gave the imidazolium salt in modest yield (average 50%) which could be deprotonated with KO*t*Bu to furnish the desired carbene in nearly quantitative yield (**Scheme 6.8**).[212a]

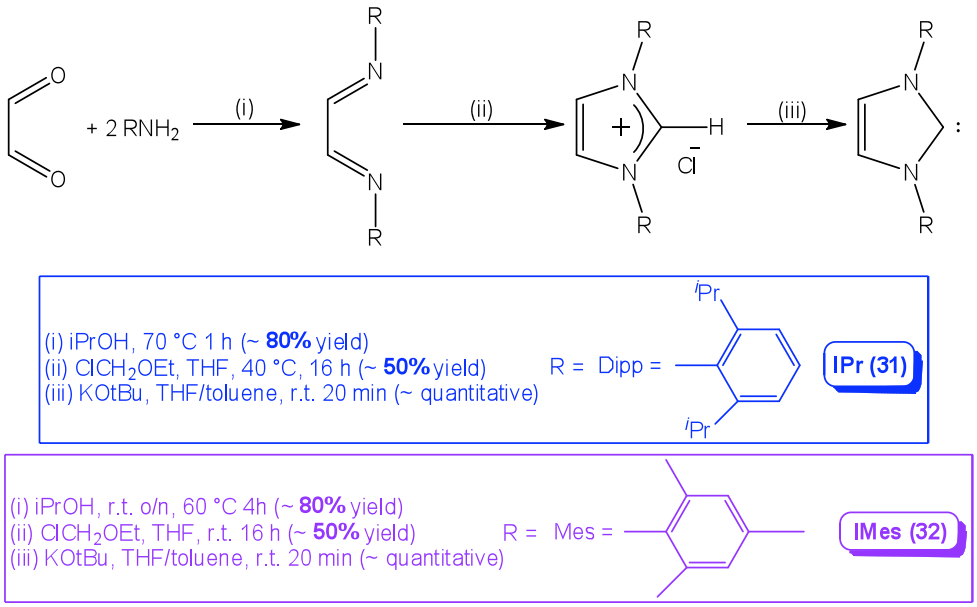


**Scheme 6.8**: Preparation of starting materials IPr (**31**) and IMes (**32**).

Alkyl substituted imidazolin-2-ylidene 1,3-di-*tert*-butylmidazole-2-ylidene IBu, **33**, was synthesised by adding 1 equivalent of *tert*-butylamine to paraformaldehyde in the first instance. Once a clear solution was obtained the mixture was cooled to 0 °C and a second equivalent of amine added. The solution was acidified with HCl and 1 equivalent of glyoxal added. Following an 18 h stir the imidazolium salt was extracted (average yield 65%), which could be deprotonated in a similar fashion to **31** and **32** in an average yield of 80% (**Scheme 6.9**).[212b] All carbene starting materials were able to be stored in the drybox (under Ar) indefinitely.

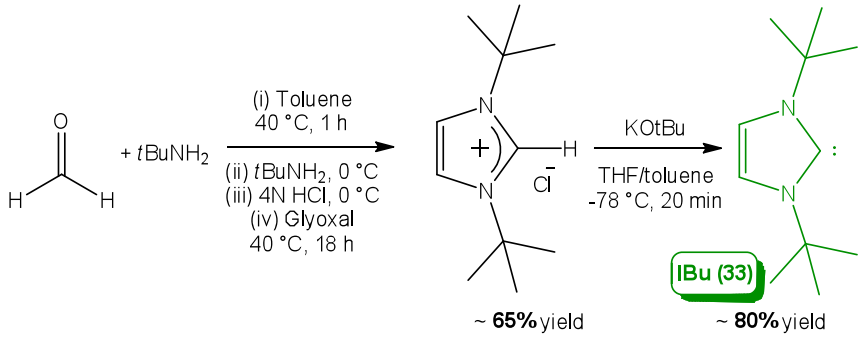


**Scheme 6.9**: Preparation of starting material IBu (**33**).

With the requisite carbenes prepared, attention initially focussed on the synthesis of NHC adducts of **31**, **32** and **33** with $ZnR_2$, where R = Me or *t*Bu. Zn*t*Bu$_2$ was

prepared from the metathesis reaction of $ZnCl_2$ with two equivalents of *t*BuLi in ether. Following filtration of LiCl through celite and glass wool, the solution was concentrated *in vacuo* and purified by sublimation in good yields (typical yield 79% on a 40 mmol scale). $ZnMe_2$ was used as purchased. **Table 6.2** summarises the reaction conditions and yields for each of the carbene-metal complexes from the reaction of $ZnMe_2$ or $Zn$*t*$Bu_2$ with IPr, IMes or IBu and **Figure 6.8** shows the X-ray crystal structures.

**Table 6.2:** Synthesis of NHC-$ZnR_2$ species **34-39**.

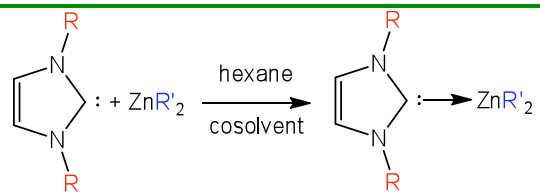


| R | R' | Product | Cosolvent | Scale and yield |
|---|---|---|---|---|
| Dipp | Me | IPr·$ZnMe_2$ **34** | Toluene | 0.5 mmol, 16% |
| Dipp | *t*Bu | IPr·Zn*t*$Bu_2$ **35** | THF | 7.0 mmol, 76% |
| Mes | Me | IMes·$ZnMe_2$ **36** | Toluene | 0.5 mmol, 17% |
| Mes | *t*Bu | IMes·Zn*t*$Bu_2$ **37** | None | 2 mmol, 69% |
| *t*Bu | Me | IBu·$ZnMe_2$ **38** | None | 1 mmol, 32% |
| *t*Bu | *t*Bu | IBu·Zn*t*$Bu_2$ **39** | None | 2 mmol, 31% |

Structures **34-39** were prepared by stirring the relevant carbene with dialkyl zinc in noncoordinating hexane. Complexes **37-39** were soluble in this solvent and the crystallised on cooling in the freezer whereas complexes **34-36** were insoluble in hexane alone. $ZnMe_2$ analogues **34** and **36** were solubilised by the addition of toluene and **35** by THF and all crystallised at -28 °C. Although the isolated crystalline yields of **34** and **36** were very low, analysis of the filtrate showed no other organometallic species to be present. The structure of each complex was confirmed by single crystal diffraction and all compounds are monomeric. **Table 6.3** shows selected bond lengths and angles. The carbene-zinc bond lengths show little disparity depending on the NHC or dialkyl zinc species used, with a difference of only 0.0124

Å between the closest (**36** = 2.106(2) Å) and longest contacts (**34** and **38** = 2.1184(18) Å). Similarly, the Zn-$C_{Me}$ contacts are within the same range regardless of the identity of the NHC complexed (from 1.996(2) Å to 2.007(2) Å), as are the Zn-$C_{t\text{Bu}}$ contacts (from 2.029 Å to 2.045(4) Å) although these bond lengths are on average 0.03 Å longer than the Me analogues. The average Zn-$C_{t\text{Bu}}$ bond length in **35**, **37** and **39** (2.034 Å) is longer than in the discrete Zn*t*Bu$_2$ monomer (1.977(4) Å).[176] In all cases the dative carbene-zinc bond is longer than the anionic carbon-zinc bond, as would be expected. **34-39** represent, as far as we can ascertain, the first examples of any NHC compound to be complexed with $ZnMe_2$ or Zn*t*Bu$_2$, although one report does detail the synthesis of the complexation of $ZnEt_2$ with adamantyl-substituted NHC 1,3-bis-adamantylimidazol-2-ylidene, with a carbene-zinc bond distance of 2.096(3) Å.[213] A search of the Cambridge Structural Database shows this area to be largely unexplored, as only a handful of Zn-carbene complexes have been structurally characterised, and only the dialkyl zinc adduct previously reported is the aforementioned adamantyl-substituted NHC/$ZnEt_2$ species.[213]

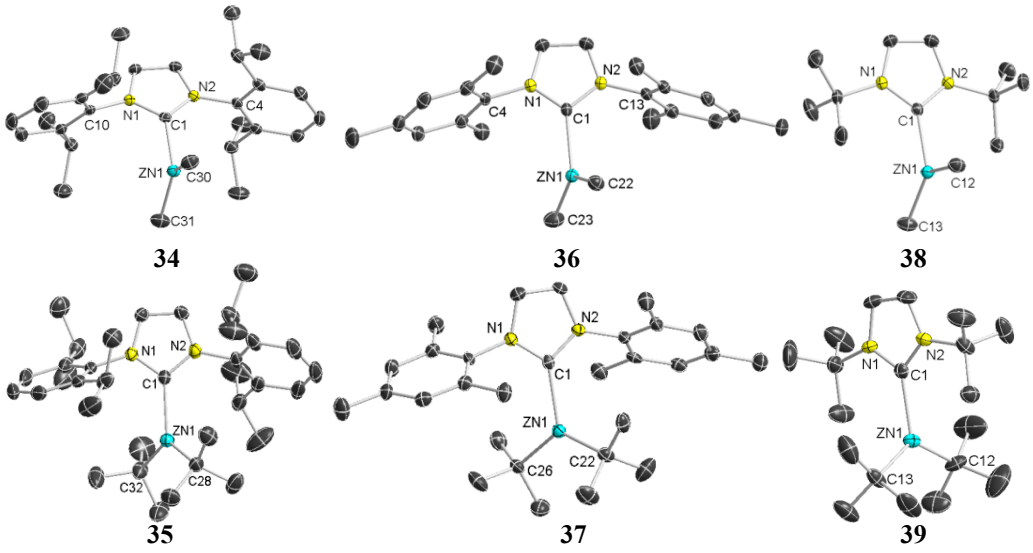


**Figure 6.8**: Molecular structures of **34-39**. Displacement ellipsoids are drawn at the 50% probability level. Hydrogen atoms omitted for clarity. The unit cell of **37** contains two crystallographically independent molecules with identical connectivities and two molecules of free IMes: only one zinc adduct shown.

**Table 6.3:** Selected bond lengths (Å) and angles (°) for **34**-**39**.

| Complex | Zn-C1 | Zn-$C_{Me/tBu}$ | N-C-N | N-C-Zn |
|---|---|---|---|---|
| IPr·$ZnMe_2$ **34** | 2.1184(18) | 1.998(2), 2.0010(19) | 103.95(15) | 126.91(13), 128.46(13) |
| IPr·Zn*t*$Bu_2$ **35** | 2.118(2) | 2.030(2), 2.032(2) | 103.20(16) | 128.19(14), 128.10(14) |
| IMes·$ZnMe_2$ **36** | 2.106(2) | 1.996(2), 2.003(2) | 103.26(16) | 125.38(13), 130.79(14) |
| IMes·Zn*t*$Bu_2$ **37** | 2.110(3) | 2.029(3), 2.038(3) | 103.9(2) | 127.0(2), 129.0(2) |
| IBu·$ZnMe_2$ **38** | 2.1184(19) | 2.005(2), 2.007(2) | 104.36(16) | 127.09(14), 127.52(14) |
| IBu·Zn*t*$Bu_2$ **39** | 2.113(4) | 2.030(4), 2.045(4) | 103.5(3) | 128.4(3), 128.1(3) |

Spectral analyses were carried out by $^{1}H$ and $^{13}C$ NMR spectroscopy (see **Table 6.4** for selected NMR chemical shifts of the free carbenes **31-33** and complexes **34-39**). The most pertinent chemical shift is that of the carbene itself in the $^{13}C$ spectra, but regrettably this could not be detected for the IPr and IMes complexes **34-37**. In contrast, the carbene signal in the $^{13}C$ spectra of the IBu complexes **38** and **39** is easily observed, which could be the result of changing from an electron withdrawing arene substituent on N (in the IPr and IMes adducts) to the inductive alkyl *t*Bu group. The carbene resonance is shifted substantially upfield in complex **39** (183.02 ppm) compared to free IBu **33** (213.40 ppm, Δδ 30.38 ppm) which is consistent with that reported for the adamantyl-substituted $ZnEt_2$ adduct.[213] The change in the resonance in the $^{13}C$ spectra of the imidazole backbone is far less pronounced, with a modest change of 2.28 ppm between free IBu **33** (115.60 ppm) and complex **39** (117.88 ppm); a pattern which is also observed with the free IPr (**31**) and IMes (**32**) species and their respective adducts (largest Δδ observed with IPr = 1.81 ppm and IMes = 1.69 ppm). In the $^{1}H$ NMR spectra, complexation with the dialkyl zinc reagent resulted in an upfield shift of the signal relating to the imidazole C*H cf* the free carbene, with the exception of **35** where both the free carbene and the adduct resonate at 6.63 ppm.

Despite concentrated samples of **34-37** undergoing extended $^{13}C$ NMR analyses, the elusive carbene signal was never observed. A possible explanation could be if the dialkyl zinc was not well bound to the carbene the dialkyl zinc was associating and disassociating in solution (**Scheme 6.10**). A similar observation has been reported

by Mulvey *et al* in the solution analyses of [IPr·*n*BuMgTMP] where resonances belonging to both the adduct and also the free starting materials were present and the authors propose an equilibrium is taking place.[197] As only one set of resonances are observed with **35**, that would suggest that in solution the equilibrium shown in **Scheme 6.10** is more rapid than the [IPr·*n*BuMgTMP] example.

**Table 6.4**: Selected $^{1}$H and $^{13}$C NMR chemical shifts (ppm δ) for **31-39** in $C_6D_6$ except **38** which is in $d_8$-THF.

| Complex | $\delta^{1H}C\boldsymbol{H}_{imidazole}$ | $\delta^{13C}\boldsymbol{C}H_{imidazole}$ | $\delta^{13C}C_{carbene}$ |
|---|---|---|---|
| IPr **31** | 6.63 | 121.49 | 220.52 |
| IMes **32** | 6.81 | 120.38 | 220.01 |
| IBu **33** | 6.75 | 115.6 | 213.4 |
| IPr·$ZnMe_2$ **34** | 6.47 | 122.88 | - |
| IPr·Zn*t*$Bu_2$ **35** | 6.63 | 123.30 | - |
| IMes·$ZnMe_2$ **36** | 6.12 | 121.29 | - |
| IMes·Zn*t*$Bu_2$ **37** | 6.17 | 122.07 | - |
| IBu·$ZnMe_2$ **38** | 7.73 | 117.32 | 186.88 |
| IBu·Zn*t*$Bu_2$ **39** | 6.39 | 117.88 | 183.02 |

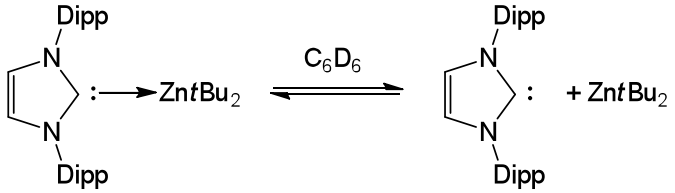


**Scheme 6.10**: Possible equilibrium of **35** in $C_6D_6$ solution.

To explore this possibility, and taking advantage of the volatility of free Zn*t*$Bu_2$, a proton NMR was collected of [IPr·Zn*t*$Bu_2$] (**35**) and then the sample was placed under vacuum for 5 hours and a second NMR collected. After 5 hours the relative integration of IPr to *t*$Bu_2$ had dropped from a 1:1 ratio to 1:0.5 suggesting that the dialkyl zinc species is not tightly bound to the carbene as some Zn*t*$Bu_2$ is lost under vacuum.

Furthermore, theoretical calculations at the Density Functional Theory (DFT) level using the B3LYP method and the 6-311G(d,p) basis set were used to predict the energy of the reaction of IPr with Zn*t*Bu$_2$ (for full details of DFT calculations see **Appendix**). **Table 6.5** shows a comparison of the main geometric parameters of **35** and model IPr·Zn*t*Bu$_2$ (**I**) (**Figure 6.9**) calculated by DFT studies.

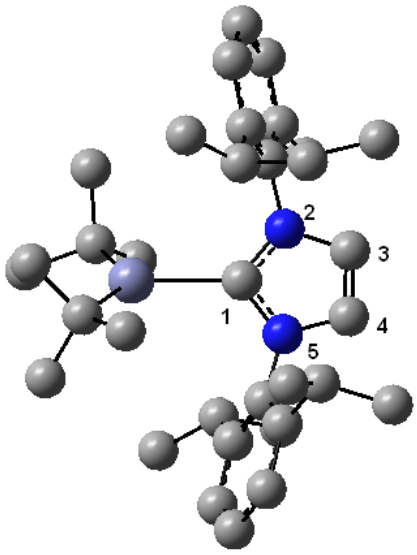


**Figure 6.9**: Optimised geometry model of IPr·Zn*t*Bu$_2$ (**I**) calculated by DFT studies.

**Table 6.5**: Comparison of selected bond lengths (Å) and angles (°) of **35** *cf* **I**.

| | **35** | **I** |
|---|---|---|
| **Zn-C$_{tBu}$** | 2.032(2), 2.030(2) | 2.043, 2.036 |
| **Zn-C$_1$** | 2.118(2) | 2.242 |
| **C$_1$-N$_{2/5}$** | 1.363(2) | 1.370, 1.370 |
| **N$_2$-C$_3$/N$_5$-C$_4$** | 1.390(3), 1.392(3) | 1.392, 1.392 |
| **C$_3$-C$_4$** | 1.335(3) | 1.348 |
| **C$_{tBu}$-Zn-C$_{tBu}$** | 126.14(10) | 129.9 |
| **C$_{tBu}$-Zn-C$_1$** | 120.08(8), 113.75(9) | 117.4, 112.7 |
| **Zn-C$_1$-N$_2$** | 128.19(14) | 128.7 |
| **N$_5$-C$_1$-N$_2$** | 103.20(16) | 103.4 |

As shown in **Table 6.5** a good correlation was observed between the geometrical parameters calculated for model **I** and structure **35**. Thus, the calculated energy for

the reaction of IPr with Zn*t*Bu$_2$ is found to be only -0.32 kcal mol$^{-1}$. This very low energy of complexation supports the observation that the dialkyl zinc species is not strongly bound to the carbene in solution.

## 6.3 Direct C4 zincation of IPr

Having previously explored the cooperative effects of Li and Zn with respect to the deprotonation of and nucleophilic addition to pyrazine as well as within the context of direct zinc-iodine exchange reactions with aromatic halides (see **Chapter 5**), these mixed-metal species were next brought together with IPr. Due to the lack of studies of NHC ligands with zincate reagents it was unknown if the carbene would coordinate to Li or Zn, if it would undergo deprotonation (as lithium zincates have been shown to promote direct zincations of aromatic molecules),[163, 172] or indeed if no reaction at all would take place. Addition of IPr to a solution of [(THF)LiZn(TMP)(*t*Bu)$_2$] (**22**) in hexane gave an oil, which solubilised with the introduction of THF as a cosolvent. Unfortunately, despite various solvent systems being attempted, crystals suitable for X-ray diffraction could not be obtained and $^1$H NMR analysis of the crude product showed a complex mixture of products. The Na congener of **22**, where the THF-coordinated Li is replaced by TMEDA-solvated Na [(TMEDA)Na(TMP)(*t*Bu)Zn(*t*Bu)] (**40**), displays excellent metallating ability, including the smooth deprotonation of benzene,[214] as well as a number of other substrates, for example toluene,[215] anilines,[216] benzonitriles,[217] benzamides,[218] carbamates,[218b] naphthalene and[219] aromatic ethers, [220] and so it was prepared and applied to IPr.

### 6.3.1 Zincation of IPr with a sodium zincate reagent

Preparation of sodium zincate base **40** began with the synthesis of BuNa from NaO*t*Bu mixed with BuLi in hexane. This was prepared in bulk in up to 40 mmol scale with a typical yield of 82%. NaTMP (prepared by addition of amine TMP(H) to BuNa in hexane) was added to a solution of Zn*t*Bu$_2$ in hexane. Addition of a

stoichiometric amount of donor solvent TMEDA gave a clear solution from which sodium zincate **40** crystallised at -28 °C in a typical yield of 81% (**Scheme 6.11**).

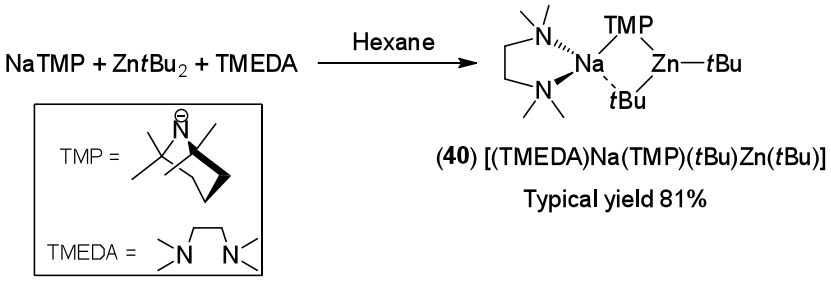


**Scheme 6.11**: Synthesis of monoamido/dialkyl sodium zincate **40**.

With sodium zincate **40** isolated as a crystalline solid, equimolar amounts of **40** and IPr were reacted in hexane. Following a 30 minute stir all volatiles were removed from the cream suspension and the solid product dissolved in THF. Cooling the solution in the freezer led to a crop of crystals of $[(THF)_3Na(IPr^*)Zn(tBu)_2]$ **41** (IPr* = :C{[N(2,6-$i$Pr$_2$C$_6$H$_3$)]$_2$CHC}) in 86% yield (**Scheme 6.12** and **Figure 6.10**).

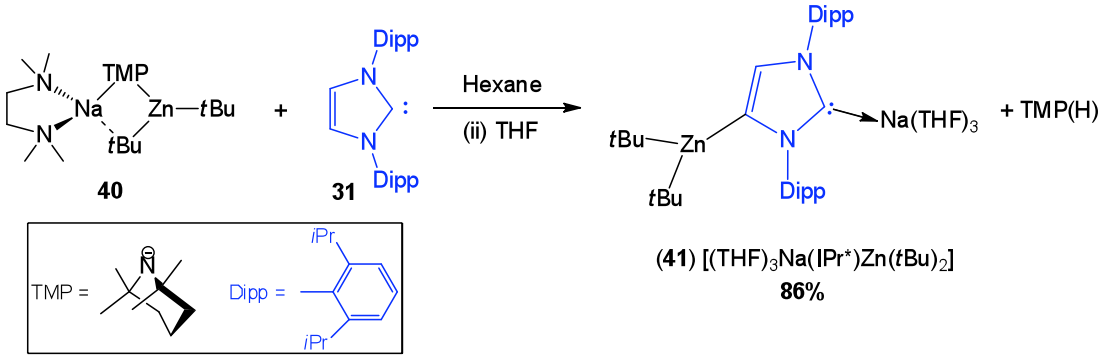


**Scheme 6.12**: Zincation of IPr by **40**.

X-ray crystallography revealed the bimetallic constitution of **41** where both metals are connected by a bridging NHC ligand which has been deprotonated at the C4 position of the imidazole ring. The NHC ligand coordinates asymmetrically through its normal C2 position to Na and its "abnormal" C4 position to Zn. Na is tetracoordinated and solvated by three molecules of THF. Zinc is trigonal planar (sum of angles 359.69°) and bonds to three carbon atoms, with little disparity

between the *t*Bu ligands (Zn-C(32) 2.033(3) Å and Zn-C(16) 2.056(3) Å) and the imidazole ring (Zn-C(2) 2.058(3) Å). The Zn-$C_{backbone}$ distance (2.058(3) Å) is significantly shorter than the Zn-$C_{carbene}$ distance observed in [IPr·Zn*t*Bu$_2$] **35** (2.118(2) Å) and also shorter than the closest Zn-$C_{carbene}$ bond distance reported 2.096(3) Å.[213] Indeed, at 2.058(3) Å, the Zn-$C_{backbone}$ distance is of the order expected from a Zn-$C_{aryl}$ bond distance.[31, 155, 221]

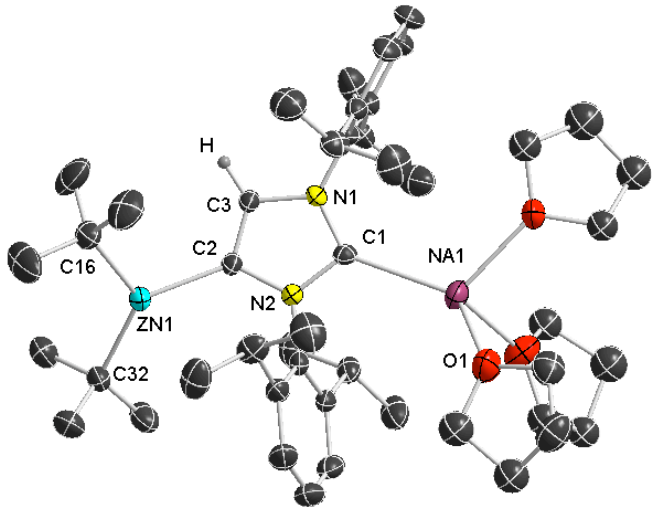


**Figure 6.10**: Molecular structure of **41**. Displacement ellipsoids are drawn at the 50% probability level. Hydrogen atoms, except on the backbone of the imidazole ring, and minor disorder in THF molecules omitted for clarity. Selected bond distances and angles, Zn1-C32 2.033(3) Å, Zn1-C16 2.056(3) Å, Zn1-C2 2.058(3) Å, Na1-C1 2.501(3) Å, N1-C1 1.359(4) Å, N1-C3 1.403(4) Å, N1-C4 1.442(4) Å, N2-C1 1.379(4) Å, N2-C2 1.416(4) Å, N2-C22 1.432(3) Å, C3-C2 1.338(4) Å, C32-Zn1-C16 122.01(13)°, C32-Zn1-C2 127.33(12)°, C16-Zn1-C2 110.25(12)°, C1-N1-C3 111.7(2)°, C1-N1-C4 124.4(2)°, C3-N1-C4 123.1(2)°, C1-N2-C2 115.3(2)°, C1-N2-C22 121.1(2)°, C2-N2-C22 123.6(2)°, N1-C1-N2 101.0(2)°, N1-C1-Na1 136.4(2)°, N2-C1-Na1 122.5(2)°, C2-C3-N1 109.9(3).

**41** displays several novel features. It is the first example of an NHC CIP structure containing sodium; indeed, only one other report detailing any sort of Na-NHC interaction could be found where Hill and co-workers isolate three SSIP structures [{Na(IPr)$_2$}$^+${M(HMDS)$_3$}$^-$] (where M = Mg, Ca, Sr). As these structures constituted the first Na-carbene complexes, Hill notes that the "narrow range of Na-C distances

observed (2.439(6)-2.452(2) Å) is typical of sodium to NHC interactions",[211] however, the Na-C distance in **41** is slightly longer (Na-C(1) 2.510(3) Å) probably due to the tetracoordination of Na from the three solvating THF molecules compared to Hill's SSIP sodium cation that is ligated by only two IPr molecules. Furthermore, **41** is distinctive by displaying the direct zincation of an NHC with zinc occupying the position classed as *abnormal* (albeit anionically), in what we believe to be the first example of a direct zincation of any NHC molecule.

Analysis of **41** by multinuclear NMR was originally conducted in $C_6D_6$ but the proton spectrum was broad and the resonance for the carbene carbon in the $^{13}C$ NMR spectrum was, again, difficult to identify. Pleasingly, in this instance, changing to $d_8$-THF gave well resolved $^{1}H$ and $^{13}C$ spectra and a diagnostic carbene signal at 201.44 ppm, which is significantly upfield compared to that observed with free carbene **31** (221.08 ppm), similar to the change noted in free IBu **33** (213.4 ppm) to Zn-coordinated IBu **39** (183.02) (*vide supra*). In starting material **31** only one septet (integrating to four hydrogens) and two doublets (each integrating to twelve hydrogens) are observed for the methine and methyl groups of the Dipp groups respectively; in **41** two distinct septets integrating to two hydrogens each for the methine and four sets of doublets (six protons each) for the methyl protons of the Dipp groups are observed, indicating the loss of symmetry in the NHC ligand, with the Dipp attached to N1 now clearly defined from that attached to N2. Another notable change in the proton NMR is the upfield shift in the imidazole C*H* backbone: in **31** this resonates at 7.17 ppm (integrating to two hydrogens) but in **41** it shifts to 6.66 ppm and now integrates to one hydrogen as one has been lost during the reaction. **Figure 6.11** shows the $^{1}H$ NMR spectra in $d_8$-THF of free carbene **31** and zincated product **41**.

Selected geometric parameters of the imidazole ring of Zn*t*Bu$_2$ adduct **35**, zincated species **41** and the lithiated anionic dicarbene reported by Robinson [{(THF)Li(IPr*)}$_\infty$][206] (*vide supra*) are shown in **Table 6.6**. The N-C distances in **41** are similar to the dicarbene, both showing one bond length longer than the other (1.379(4) Å *vs* 1.359(4) in **41** and 1.375(3) *vs* 1.361(3) in the dicarbene) in contrast

to **35** where both bond lengths essentially the same (1.363(2) Å and 1.361(2) Å). Having stated that, **41** differs from the dicarbene by displaying a shorter (stronger) C=C bond distance (1.338(4) Å *cf* 1.356(4) Å) more akin to **35** (1.335(3) Å).

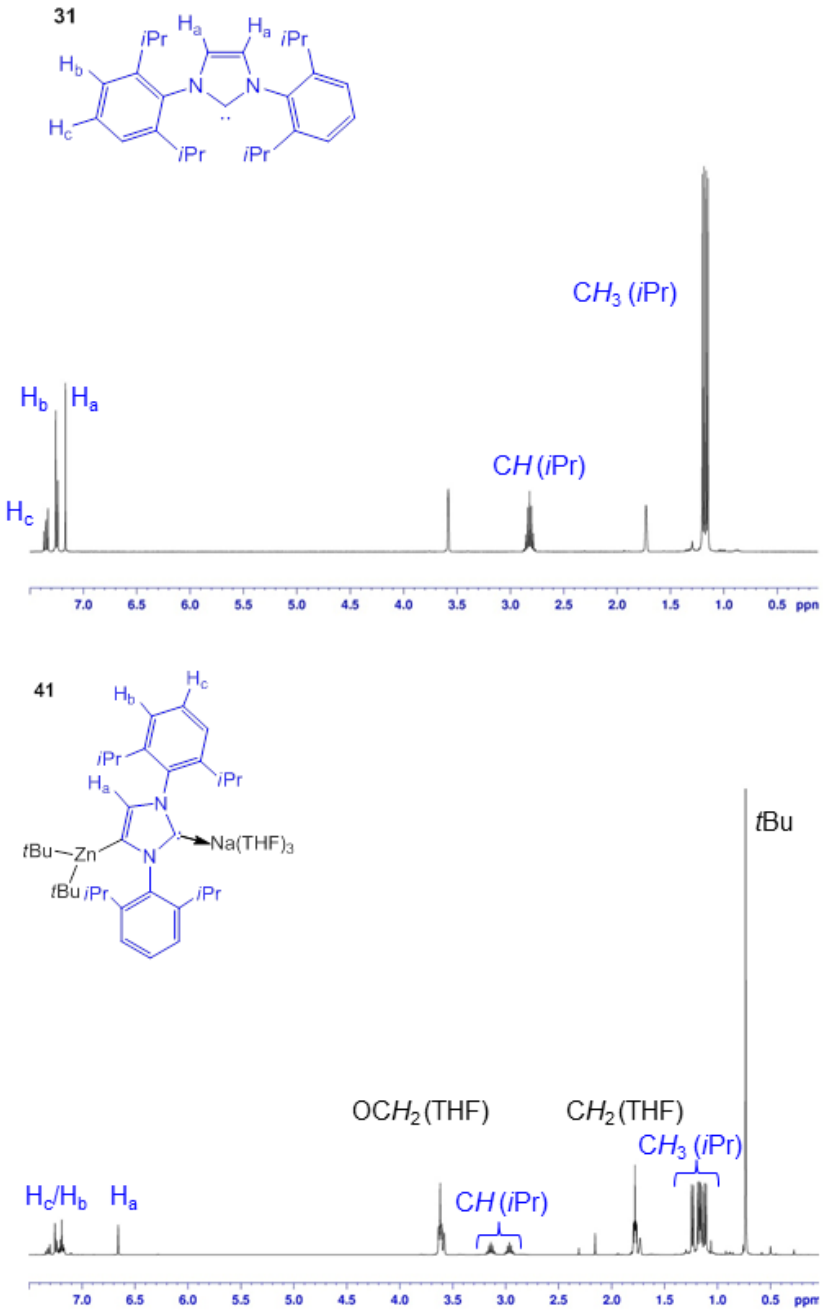


**Figure 6.11**: Comparison of the $^{1}$H NMR data of free carbene **31** and zincated species **41** in $d_8$-THF.

**Table 6.6**: Selected bond angles (°) and bond distances (Å) for **35**, **41** and lithiated anionic dicarbene.

| 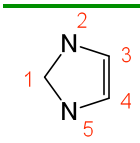 | **35** | **41** | **NHDC**[206] |
|---|---|---|---|
| $N_{2/5}$-$C_1$ | 1.363(2), 1.361(2) | 1.379(4), 1.359(4) | 1.375(3), 1.361(3) |
| $N_2$-$C_3$/$N_5$-$C_4$ | 1.390(3), 1.392(3) | 1.403(4), 1.416(4) | 1.399(4), 1.442(4) |
| $C_3$-$C_4$ | 1.335(3) | 1.338(4) | 1.356(4) |
| $N_5$-$C_1$-$N_2$ | 103.20(16) | 101.0(2) | 100.5(2) |

To gain greater understanding of the structure of **41**, theoretical calculations at the DFT level using the B3LYP method and the 6-311G(d,p) basis set were carried out (for full details of DFT calculations see **Appendix**). DFT calculations predict the reaction of bimetallic base **40** with IPr (**31**) to be exothermic, with a gain in energy of -23.99 kcal $mol^{-1}$. **Table 6.7** shows a comparison of the main geometric parameters of **41** and model $[(THF)_3Na(IPr^*)Zn(tBu)_2]$ (**II**) (**Figure 6.12a**) calculated by DFT studies. **Figure 6.12b** shows the location of the highest occupied molecular orbital.

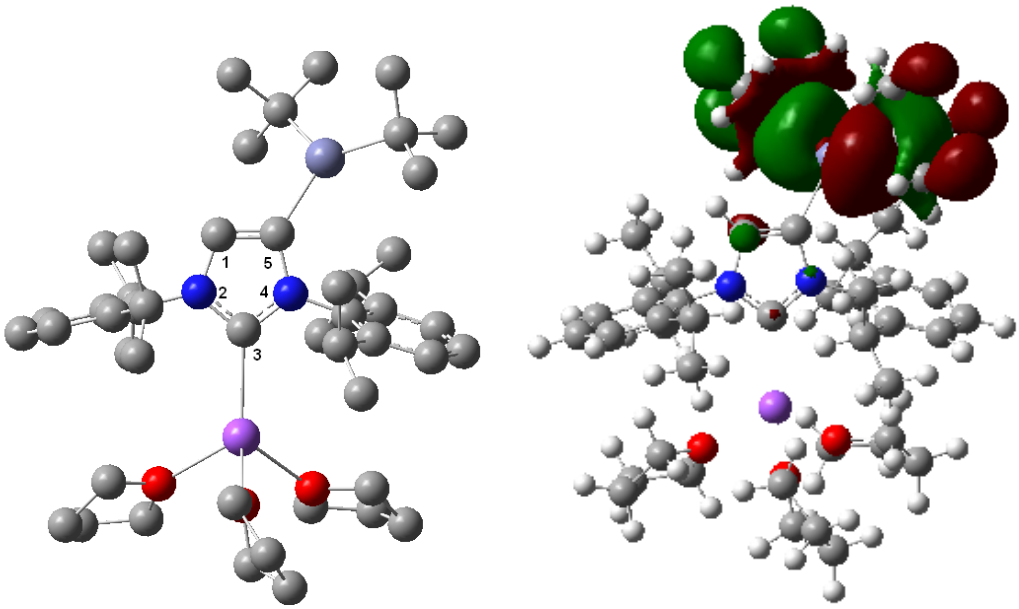

**(a)** **(b)**

**Figure 6.12**: (**a**) Optimised geometry model of $[(THF)_3Na(IPr^*)Zn(tBu)_2]$ (**II**) calculated by DFT studies and (**b**) HOMO of **II**.

**Table 6.7**: Comparison of selected bond lengths (Å) of **41** *cf* **II**.

| | **41** | **II** |
|---|---|---|
| **$C_1$-$N_2$** | 1.403(4) | 1.404 |
| **$C_3$-$N_2$** | 1.359(4) | 1.362 |
| **$C_1$-$C_5$** | 1.338(4) | 1.364 |
| **$C_5$-$N_4$** | 1.416(4) | 1.424 |
| **$C_3$-$N_4$** | 1.379(4) | 1.373 |
| **Zn-$C_5$** | 2.058(3) | 2.127 |
| **Zn-$C_{tBu}$** | 2.033(3), 2.056(3) | 2.051, 2.073 |
| **Na-$C_3$** | 2.501(3) | 2.500 |

On the whole there is good agreement between most of the calculated values of **II** and solid-state structure **41**, although there is a fairly large discrepancy found for the Zn-$C_{backbone}$ bond distance (2.0583(3) Å found experimentally, 2.127 Å predicted). In **II** the HOMO rests on the Zn*t*$Bu_2$ fragment which is in contrast to the lithium anionic dicarbene where two strongly polarised Li-C bonding orbitals are observed.[206] In view of the theoretical and structural studies, it appears that **41** can best be described as an anionic carbene, rather than an anionic dicarbene, with the negative charge localised in the C4 position of the imidazole ring which forms a strong σ-bond with Zn.

Remarkably, in forming **41** sodium zincate **40** has acted as an amido base, with the loss of TMP(H) and two *t*Bu groups remaining in the product. This is in contrast to other applications of this reagent, where the generation of the amine is the kinetic product which subsequently reacts with the intermediate, giving an overall thermodynamic alkyl base (see discussion in **Chapter 5.1.1** and **Scheme 6.13**), which is not observed on reaction with the NHC.

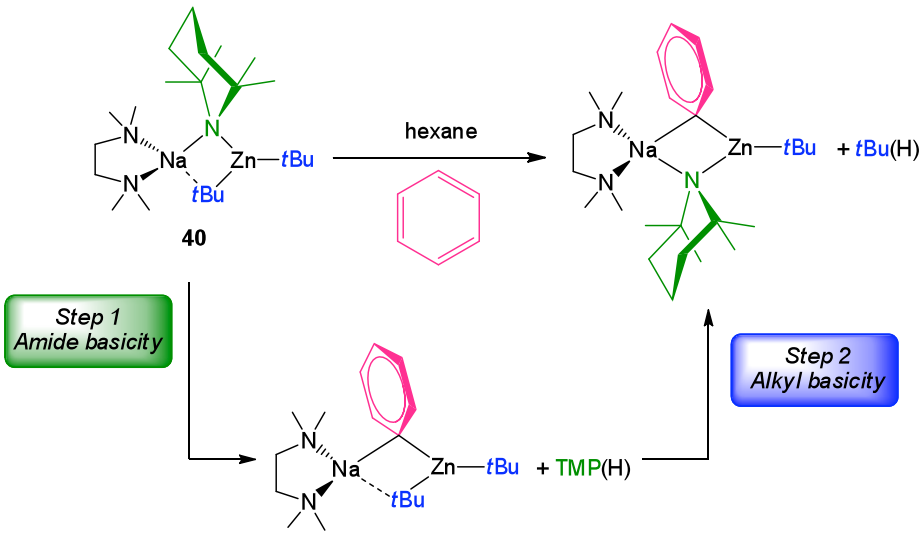


**Scheme 6.13**: Two-step mechanism in the metallation of benzene by **40**.[155]

This may be due to the relative separation of the Na and Zn in **41**, with three atoms separating them, compared to previously isolated intermediates using **40** as a base where the metals are bridged by only one atom. Having stated that, two anionic *t*Bu arms are still present on **41** and a reaction was carried out to test their basicity.

Thus, two equivalents of **31** were introduced to **40** and the reaction mixture stirred overnight, after which the solvent was changed to toluene and the reaction continued for 72 hours. Crystallisation from a hexane/THF mixture gave product **42** in 44% yield (**Scheme 6.14** and **Figure 6.13**).

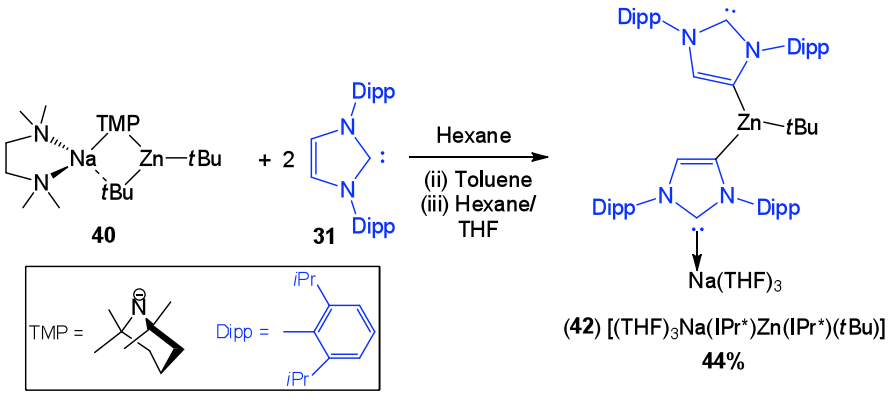


**Scheme 6.14**: Zincation of two molecules of IPr by **40**.

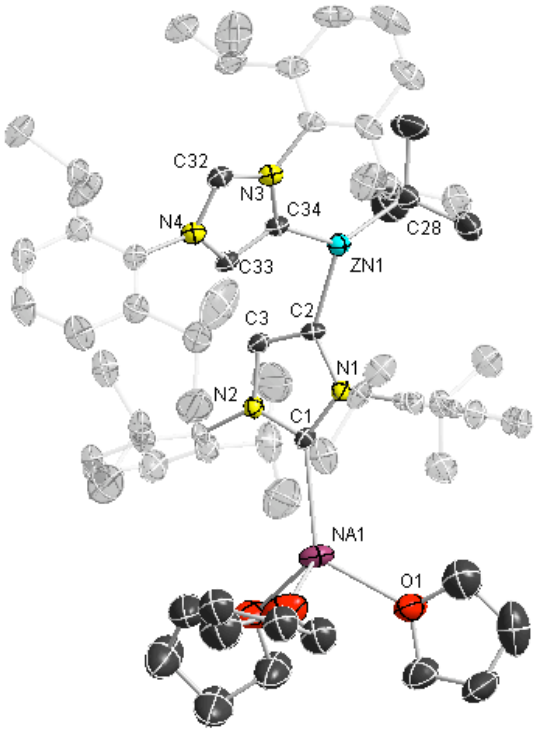


**Figure 6.14**: Molecular structure of **42**. Displacement ellipsoids are drawn at the 50% probability level. Hydrogen atoms and minor disorder in THF molecules omitted for clarity. The Dipp groups have been faded for clarity. Selected bond distances and angles, Na1-C1 2.534(3) Å, Zn1-C34 2.006(3) Å, Zn1-C28 2.017(3) Å, Zn1-C2 2.063(3) Å, N1-C1 1.370(4) Å, N1-C2 1.410(4) Å, N1-C16 1.442(4) Å, N2-C1 1.352(4) Å, N2-C3 1.395(4) Å, N2-C4 1.440(4) Å, N3-C32 1.367(4) Å, N3-C34 1.416(4) Å, N3-C35 1.441(4) Å, N4-C32 1.374(4) Å, N4-C33 1.396(4) Å, N4-C47 1.438(4) Å, C2-C3 1.337(4) Å, C33-C34 1.344(4) Å, C34-Zn1-C28 136.03(13)°, C34-Zn1-C2 105.54(11)°, C28-Zn1-C2 117.68(13)°, N2-C1-N1 101.4(2)°, N3-C32-N4 100.8(2)°.

Confirmation of the constitution of **42** by single crystal diffraction shows it to be similar to **41**, containing two IPr* fragments which have been deprotonated at the C4 position of the imidazole ring, and one remaining *t*Bu arm on Zn. As with **41**, in **42** sodium interacts with the normal C2 position of one of the IPr* fragments (2.534(3) Å) and three THF molecules. As stated, only one *t*Bu group remains on Zn with its coordination now filled by two molecules of deprotonated IPr in a trigonal planar geometry (sum of angles 359.25°). In the solid-state structure one C2 carbene position is occupied by Na, however the second carbene position is "free". Inspection of the bond lengths and angles of the imidazole ring in **42** show no real

differences depending on whether the carbene is coordinated or not, and the values are also in good agreement with mono-IPr species **41** (**Table 6.8**).

**Table 6.8**: Selected bond angles (°) and bond distances (Å) for the Na-coordinated carbene IPr fragment of **42**, the free carbene IPr fragment of **42** and **41**.

| 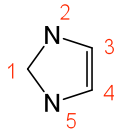 | **42** (Na-coordinated carbene) | **42** (free carbene) | **41** |
|---|---|---|---|
| $\mathbf{N_{2/5}\text{-}C_1}$ | 1.370(4), 1.352(4) | 1.374(4), 1.367(4) | 1.379(4), 1.359(4) |
| $\mathbf{N_2\text{-}C_3/N_5\text{-}C_4}$ | 1.395(4), 1.410(4) | 1.396(4), 1.416(4) | 1.403(4), 1.416(4) |
| $\mathbf{C_3\text{-}C_4}$ | 1.337(4) | 1.344(4) | 1.338(4) |
| $\mathbf{N_5\text{-}C_1\text{-}N_2}$ | 101.4(2) | 100.8(2) | 101.0(2) |

Analysis by $^{1}$H NMR spectroscopy in $d_8$-THF reveals similar spectra for **42** *cf* **41** and deviation only notably occurs in terms of integration, in line with what would be expected in the final product due to the stoichiometry of **41** compared to **42**. Of note is the presence of two inequivalent carbene centres in the solid-state structure of **42** with one bound to sodium and one free. Only one carbene signal is observed in the deuterated THF $^{13}$C spectrum which suggests that on the NMR timescale sodium is migrating between the carbene positions. Taking into account the chemical shifts, the carbene signal of **42** resonates at 209.57 ppm which is almost the median point of free carbene **31** (221.07 ppm) and single carbene product **41** (201.44 ppm) lending weight to the hypothesis that in solution the sodium moves between the carbene positions and an average chemical shift is observed.

Attempts to activate the final *t*Bu arm were unsuccessful and reactions performed with three equivalents of base **40** with IPr **31** gave a mixture of **42** and **31** when analysed by X-ray crystallography, most likely due to the significant steric shielding of the zinc from two highly sterically demanding deprotonated NHCs.

### 6.3.2 Zincation of IPr with a potassium zincate reagent

Moving down the s-block again, the K analogue of **40** was prepared by the cocomplexation of PMDETA-solvated KTMP and Zn*t*Bu$_2$ giving [(PMDETA)K(TMP)(*t*Bu)Zn(*t*Bu)] **43** in average yields of 70% (**Scheme 6.15**).[222]

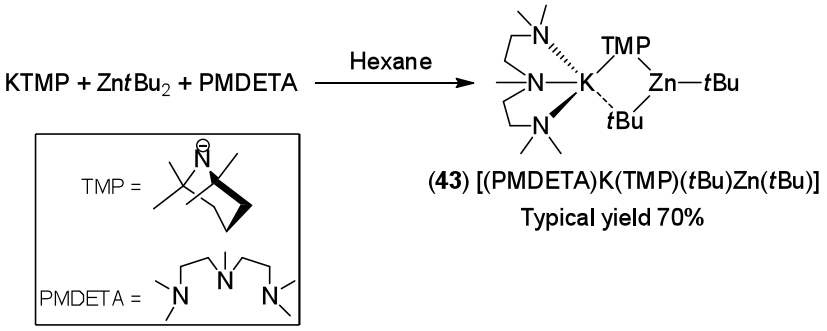


**Scheme 6.15**: Synthesis of mixed-metal potassium zincate **43**.[222]

Crystalline **43** was dissolved in hexane and **31** added, giving a yellow suspension. After stirring for 30 minutes THF was introduced giving a straw coloured solution that deposited crystals of **44** in 35% yield (**Scheme 6.16** and **Figure 6.15**).

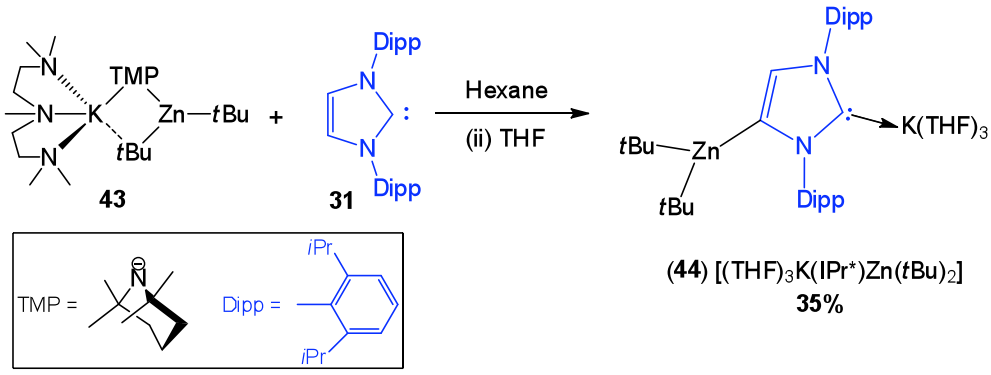


**Scheme 6.16**: Zincation of IPr by potassium zincate **43**.

Displaying a similar motif to that described for sodium congener **41**, the crystal structure of **44** exhibits a molecule of deprotonated IPr bridging between potassium in the carbenic position (K1-C1 2.831(6) Å) and Zn bonded to the C4 position of the imidazole backbone (Zn1-C2 2.050(5) Å). The environment around Zn is almost identical to that of **41** (**Table 6.9**), however by moving to the larger, more

electropositive potassium atom, the alkali metal is no longer satiated by interacting with the carbene electrons and three molecules of THF and it rests closer to one of the Dipp pendant arms than the other which translates into a significantly smaller angle observed between N2-C1-K1 (112.0 (4)°) than N1-C1-K1 (145.74 (4)°) which allows K to interact with the *ipso* carbon of the pendant group on N2 (K1-C16 3.427 (5) Å), which is within the range expected of potassium-π interactions).[142, 146a, 223]

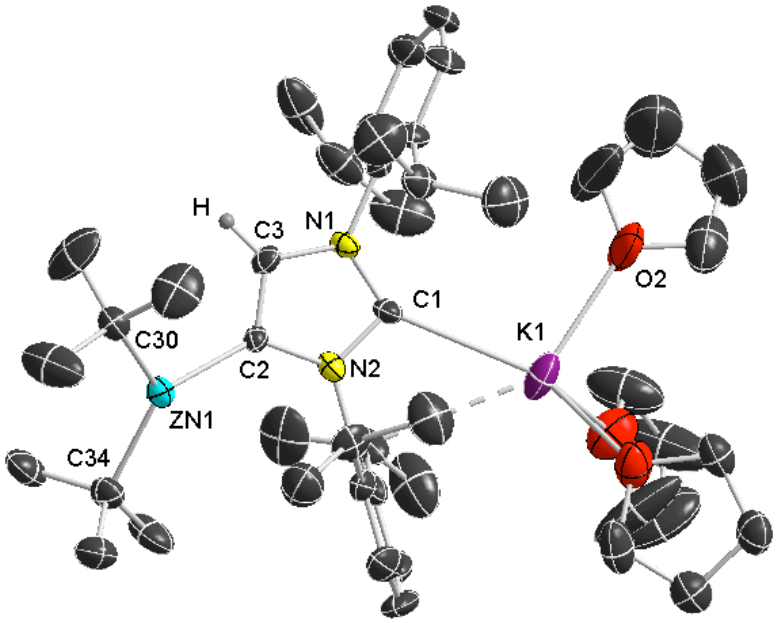


**Figure 6.15:** Molecular structure of **44**. Displacement ellipsoids are drawn at the 50% probability level. Hydrogen atoms and minor disorder in two THF molecules omitted for clarity. Selected bond distances and angles; K1-C1 2.831(6) Å, K1-C16 3.427(5) Å, Zn1-C2 2.050(5) Å, Zn1-C34 2.029(5) Å, Zn1-C30 2.065(6) Å, C1-N1 1.346(7) Å, C1-N2 1.372(6) Å, N1-C3 1.409(6) Å, N2-C2 1.414(6), C3-C2 1.346(6); N2-C1-K1 112.0(4)°, N1-C1-K1 145.74(4)°, N1-C1-C2 100.9(5)°, C34-Zn1-C2 126.1(2), C34-Zn1-C30 122.3(2), C2-Zn1-C30 122.3(2).

**Table 6.9**: Selected bond angles (°) and bond distances (Å) for the Zn environments of potassium zinc compound **44** and sodium zinc compound **41**.

| | **44** | **41** |
|---|---|---|
| **Zn-$C_{backbone}$** | 2.050(5) | 2.058(3) |
| **Zn-$C_{tBu}$** | 2.029(5), 2.065(6) | 2.033(3), 2.056(3) |
| **$C_{tBu}$ -Zn-$C_{backbone}$** | 111.3(2), 126.1(2) | 110.25(12), 127.33(12) |
| **$C_{tBu}$ -Zn-$C_{tBu}$** | 122.3(2) | 122.01(13) |

The scarcity of K-NHC containing structures is not as pronounced as with Na, however there is still very little reported in this area.[210, 224] The same publication that details SSIP Na-NHC interactions (*vide supra*) also reports similar SSIP structures of K $[\{K(IPr)_2\}^+\{M(HMDS)_3\}^-]$ (where M = Mg, Ca, Sr, Ba) with a K-NHC average contact of 2.845 Å.[211] Spectral analyses of **44** were almost identical to **41** with the presence of K varying the chemical shifts in the $^1$H NMR a negligible amount, for example, the C*H*$_{imidazole}$ is a singlet at 6.66 ppm in **41** and 6.60 ppm in **44**. The only notable difference occurs in the $^{13}$C spectra, where the $C_{carbene}$ bonded to the alkali metal appears at 209.16 ppm in **44** compared to 201.44 in **41**. In the mixed potassium/yttrium NHC complex (*vide supra*, **Scheme 6.7** and **Figure 6.6**) the K-$C_{carbene}$ signal is at 199.22 ppm in $d_8$-THF, which is more upfield than in **44** (209.16 ppm), although it should be noted that the NHC is different, with a pendent arm that chelates to the yttrium, and the complex forms a dimer.

### 6.3.2.1 Electrophilic quench reaction

As previously mentioned, the advantage of using mixed-metal systems **40** and **43** is that the zincated NHC products (**41** and **44** respectively) can be readily synthesised at room temperature under ambient conditions. The presence of Zn on the imidazole backbone allows the system to be further functionalised, for example by the addition of an electrophile. To test the applicability of bimetallic NHC product **44** towards electrophilic attack, crystals of the compound were dissolved in THF and cooled to 0 °C and TMSCl added dropwise. The solution immediately became a rich yellow

colour which faded after a few minutes. After stirring for 5 days, hexane was added and storage in the freezer gave crystals of **45** (**Scheme 6.17** and **Figure 6.16**).

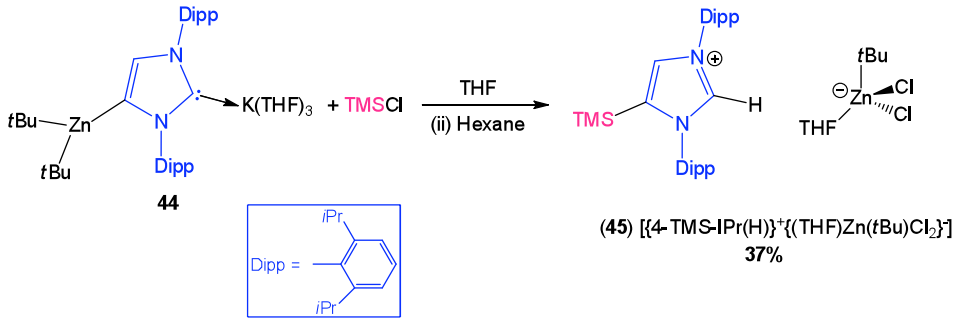


**Scheme 6.17**: Electrophilic quench of **44**.

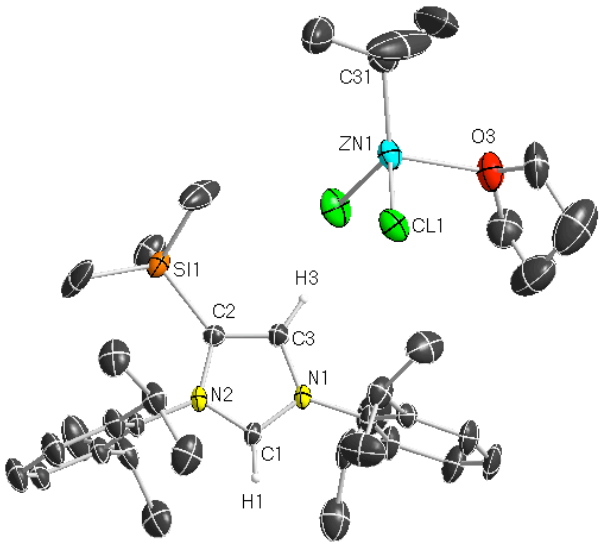


**Figure 6.16**: Molecular structure of **45**. Displacement ellipsoids are drawn at the 50% probability level. Two molecules of cocrystallised THF and hydrogen atoms except those on the imidazole ring have been omitted for clarity.

Structure **45** was elucidated by X-ray diffraction; however, the crystals of **45** were twinned which precludes meaningful discussion of the bond parameters although connectivity is definite. **45** is a salt, with the organic fragment bearing a positive charge and an anionic organometallic component with Zn in a distorted tetrahedron bonding to two chlorine atoms, one alkyl ligand and a solvating molecule of THF. How **45** is formed is not precisely known, but we suspect that a proton is abstracted from the solvent or serendipitous traces of water in the reaction mixture. The constitution of the anionic fragment appears unusual, however the "scrambling" of

alkyl and halide substituents in solution has previously been reported.[225] Unfortunately, despite washing the crystals with hexane, the $^{1}$H NMR shows more than one product present (albeit **45** is the major product). That notwithstanding, this experiment shows that, in principle, these zincated NHC products are suitable intermediates for fine tuning the electronic and steric environment of the carbene by the addition of electrophiles, as pleasingly the Zn-C bond of the imidazole ring has been successfully replaced by a new C-Si bond. In addition, the formation of the new C-Si at the C4 position of the imidazole ring is in contrast to that observed when Robinson treats Li/B anionic dicarbene with TMSCl where a new C-Si bond is formed a the C2 position (**Scheme 6.18**).[207] This differing reactivity also supports the classification of our mixed-metal systems as normal carbenes at the C2 position and anions at the C4 position.

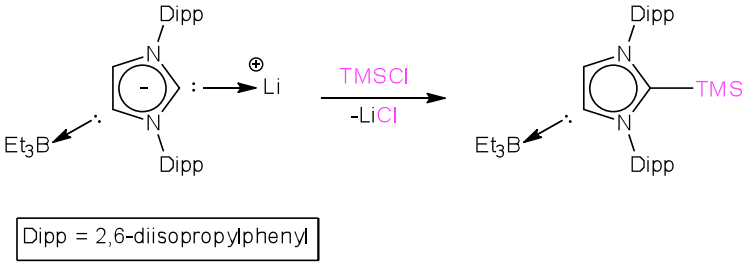


**Scheme 6.18**: Reaction of an anionic dicarbene with TMSCl.[207]

## 6.4 Application of 41 as a transmetallating reagent: synthesis of novel {MIPr*M} complexes

Encouraged by the selective functionalisation of IPr using bimetallic bases, attention then focussed on assessing the ability of these newly functionalised compounds to transfer their IPr* to other metal fragments. Towards this end, NHC-bridged sodium zincate **41** was reacted with one equivalent of Zn*t*Bu$_2$ in hexane (**Scheme 6.19**). Following a 15 minute stir the reaction mixture was placed in the freezer and crystals of [{Na(THF)$_6$}$^+${(*t*Bu)$_2$Zn(IPr*)Zn(*t*Bu)$_2$}$^-$] **46** (**Figure 6.17**) were isolated in a 30% yield.

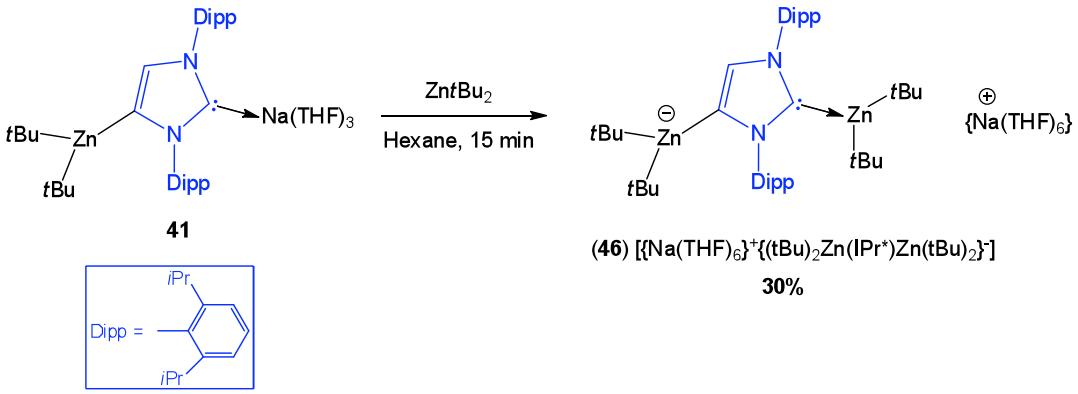


**Scheme 6.19**: Synthesis of homometallic binuclear structure **46**.

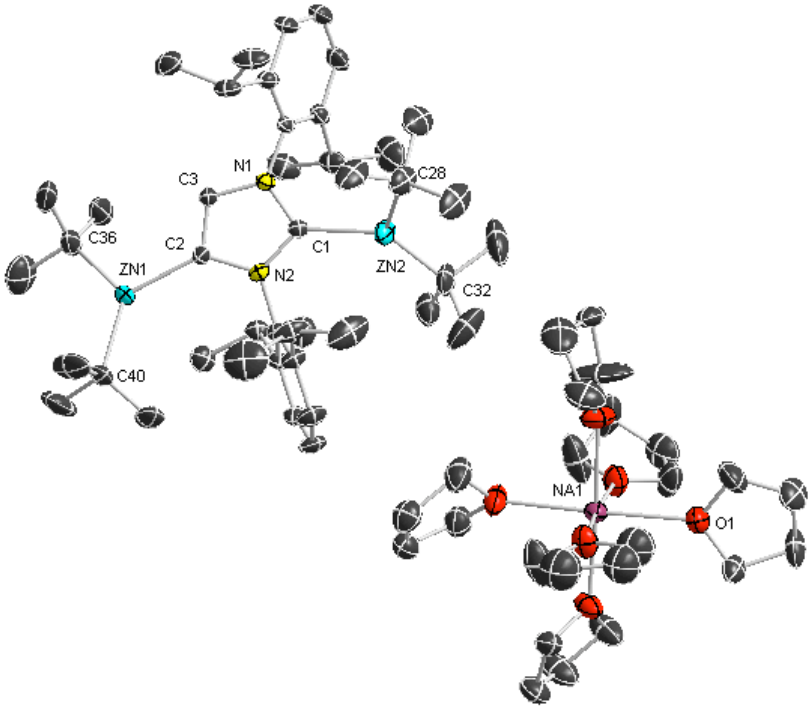


**Figure 6.17**: Molecular structure of **46**. Displacement ellipsoids are drawn at the 50% probability level. One molecule of cocrystallised THF, hydrogen atoms and minor disorder in four molecules of THF and one *t*Bu group omitted for clarity. Selected bond lengths and angles; Zn2-C1 2.114(3) Å, Zn1-C2 2.058(3) Å, Zn2-C28 2.047(4) Å, Zn2-C32 2.030 (4) Å, Zn1-C40 2.058(4) Å, N1-C1 1.395(4) Å, N1-C3 1.394(4) Å, C2-C3 1.362(4) Å, N2-C2 1.423(4) Å, N2-C1 1.367 Å; N1-C1-N2 103.0(3)°.

SSIP **46** now has a Zn*t*Bu$_2$ molecule at the normal C2 position (replacing sodium) and at the C4 position, with a deprotonated IPr molecule bridging between the two Zn*t*Bu$_2$ fragments. The charge is balanced by a hexacoordinated Na surrounded by

THF molecules. Structure **46** is reminiscent of the NHDC-borane complex reported by Robinson [{Li(THF)$_3$}$^+${(H$_3$B(IPr*)BEt$_3$}$^-$] which places a BEt$_3$ at the C4 and BH$_3$ at the C2 position that interacts with a THF trisolvated Li.[226] Although the NHDC-borane complex is classed as an anionic dicarbene, **46** is better regarded as having a normal carbene at the C2 position with a Zn(2)-C(1) bond distance of 2.114(3) Å and forming a strong σ-bond between the carbon of the backbone and zinc with a distance of 2.058 (3) Å (Zn(1)-C(2)) which is of the same order as the bonds formed by Zn with the *t*Bu ligands: Zn(2)-C(28) 2.047(4) Å, Zn(2)-C(32) 2.030(4) Å and Zn(1)-C(40) 2.058(4) Å (note that Zn(1)-C(36) is omitted due to disorder in that *t*Bu group). The effect of the Zn substitution in **46** with respect to the imidazole ring is compared with precursor **41** in **Table 6.10**, with both structures displaying similar trends. Having stated that, of note is the lengthening of the C=C bond distance in **46** (1.362(4) Å) compared to **41** (1.338(4) Å) which suggests a higher degree of delocalisation is present in **46**. Furthermore, comparison of diagnostic resonances of **46** and **41** by $^1$H and $^{13}$C NMR spectroscopy (**Table 6.10**) reveals a slight downfield shift for all signals of **46** except the carbene signal where changing from Na (201.44 ppm) to the more carbophilic Zn (187.88 ppm) sees an upfield shift of 13.56 ppm.

**Table 6.10**: Selected bond angles (°) and bond distances (Å) of the imidazole ring and NMR chemical shifts (ppm δ) in d$_8$-THF for **46** and **41**.

| 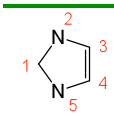 | **46** | **41** |
|---|---|---|
| **$N_{2/5}$-$C_1$** | 1.367(4), 1.359(4) | 1.379(4), 1.359(4) |
| **$N_2$-$C_3$/$N_5$-$C_4$** | 1.394(4), 1.423(4) | 1.403(4), 1.416(4) |
| **$C_3$-$C_4$** | 1.362(4) | 1.338(4) |
| **$N_5$-$C_1$-$N_2$** | 103.0(3) | 101.0(2) |
| **δ$^{1H}$C*H*$_{iPr}$** | 3.38, 3.23 | 2.95, 3.16 |
| **δ$^{1H}$C*H*$_{imidazole}$** | 6.88 | 6.66 |
| **δ$^{13C}$Zn*C*$_{backbone}$** | 160.85 | 159.49 |
| **δ$^{13C}$*C*:** | 187.88 | 201.44 |

The synthesis of **46** can alternatively be carried out by deprotonating adduct [IPr˙Zn*t*Bu$_2$] **35** directly with sodium zincate **40**, demonstrating this methodology is compatible with coordinated carbenes (**Scheme 6.20**).

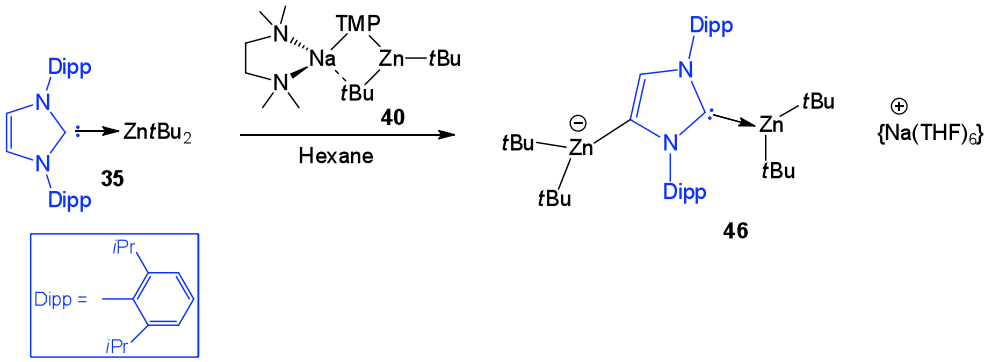


**Scheme 6.20**: Alternative synthetic route to **46**.

Au was also chosen as a metal of interest due to the impressive use of Au(I)-NHC complexes in catalysis, where they have been shown to facilitate a plethora of organic transformations (e.g. hydroamination, C-H activation, alkyne hydration and polymerisation reactions, to name but a few).[227] In addition, the medicinal value of Au-NHC complexes has been investigated with respect to their antimicrobial and antitumour properties.[228] Preparation of [ClAu(NHC)] complexes is generally carried out by mixing the free carbene with [AuCl] (**Scheme 6.21a**), reacting the free carbene with [ClAu(SMe$_2$)] (**Scheme 6.21b**) or by transmetallation of [ClAu(SMe$_2$)] with a Ag(I)-NHC complex (**Scheme 6.21c**).[229] In an extensive systematic study of the preparation of [ClAu(NHC)] complexes, Nolan and co-workers report the direct addition pathway (**Scheme 6.21a**) gave poor yields and by-products and although the exchange reaction pathway (**Scheme 6.21b**) generally improved the yields, a mixture of products was still obtained. Using the exchange method the reaction was unsuccessful when the NHC employed was IMes. The most applicable method was transmetallation where there was no need to generate the free carbene and no decomposition to metallic gold was observed.[229]

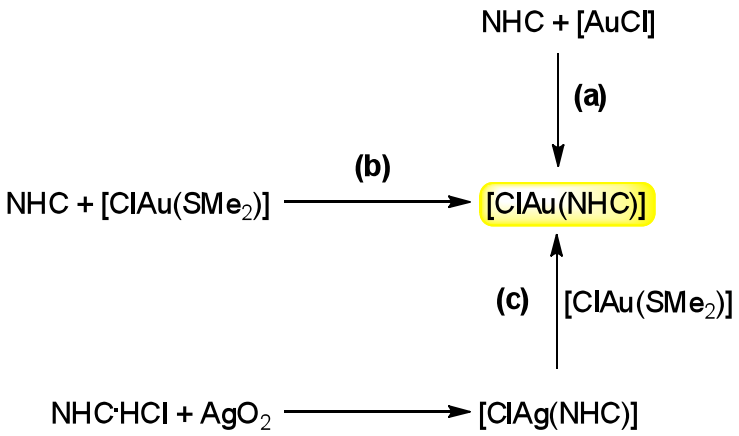


**Scheme 6.21**: General preparative pathways in the synthesis of Au-NHC complexes.

Thus, we next attempted a transmetallation reaction of **41** with two equivalents of [ClAu($PPh_3$)][230] which gave the novel product [ClAu(IPr*)Au($PPh_3$)] **47** in 61% yield (**Scheme 6.22** and **Figure 6.18**). Remarkably, now both Na and Zn have been replaced by Au atoms. The C2 position of IPr* is bonded to a [AuCl] fragment, replacing the $PPh_3$ in the precursor, whereas the C4 carbon of IPr* is now directly bonded to a {$AuPPh_3$} fragment, replacing the Cl in the precursor. This gives rise to a novel diaurate complex where both Au centres are connected by a bridging deprotonated NHC.

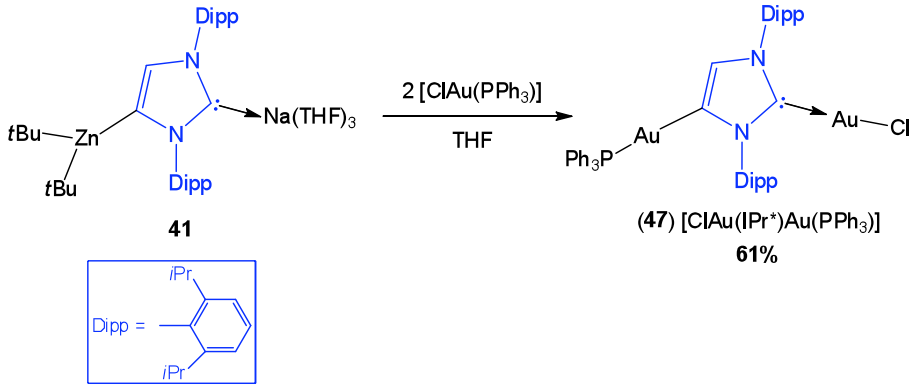


**Scheme 6.22**: Synthesis of homometallic binuclear structures **47**.

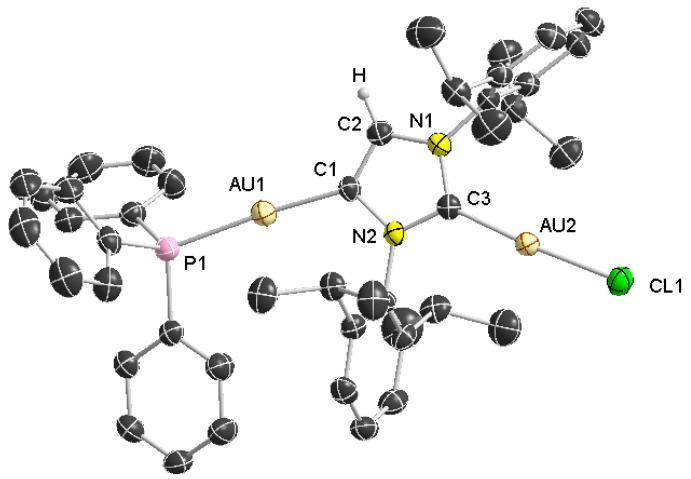


**Figure 6.18**: Molecular structure of **47**. Displacement ellipsoids are drawn at the 50% probability level. Hydrogen atoms have been omitted for clarity. Selected bond lengths and angles; Au2-C3 1.975(5) Å, Au1-C2 2.022(5) Å, C3-N1 1.351(6) Å, C2-N1 1.389(7) Å, C1-C2 1.362(7) Å, C1-N2 1.421(6) Å, C3-N2 1.359(6) Å; C3-Au2-Cl1 176.23(15)°, C1-Au1-P1 175.13(15)°, N2-C3-N1 104.4(4)°.

Only one example of an abnormally bound Au is present in the literature, which was used as "proof of concept" by Bertrand after the isolation of the first stable abnormal carbene (*i.e.* with the C2 position blocked) which was then complexed with Au and displays a Au-C4 bond distance of 1.981 Å.[205] In contrast, the number of normally bound Au carbenes numbers in the hundreds, as would be expected due to the importance of these compounds in catalysis and medicinal applications.[227-228] The related complex [(IPr)AuCl] was reported by Nolan[229] and has a Au-$C_{carbene}$ bond distance of 1.942(3) Å, which is slightly shorter than the Au-C bond distance at the C2 (normal) position in **47** (Au(2)-C(3) 1.975(5) Å) and considerably shorter than the gold-carbon interaction at the *abnormal* position (Au(1)-C(1) 2.022(5) Å). In addition the Au-$C_{abnormal}$ bond distance in **47** is longer (Au(1)-C(1) 2.022(5) Å) than Bertrand's compound (1.981 Å). Having stated that, both gold-carbon bond distances present in **47** are within the range of carbene-Au complexes reported.[231] In line with other Au(I) complexes, the gold atoms in **47** both display a two-coordinate geometry, only slightly deviating from linearity: C(3)-Au(2)-Cl(1) 176.23(15)° and C(1)-Au(1)-P(1) 175.13(15)°. A comparison of the bond distances and angles the imidazole ring of **47** with dizinc complex **46** and precursor **41** are

presented in **Table 6.11**. As was noted with complex **46**, complex **47** also shows a lengthening of the C=C backbone (1.362(7) Å) when compared to precursor **41** (1.338(4) Å) which indicates there is more delocalisation in the ring. **47** also displays an increase in the N-C-N bond angle from **41** (101.0(2)°) to 104.4(4)° in **47**.

**Table 6.11**: Selected bond angles (°) and bond distances (Å) of the imidazole ring **47**, **46** and **41**.

| 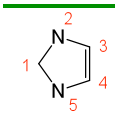 | **47** | **46** | **41** |
|---|---|---|---|
| **$N_{2/5}$-$C_1$** | 1.359(6), 1.351(6) | 1.367(4), 1.359(4) | 1.379(4), 1.359(4) |
| **$N_2$-$C_3$/$N_5$-$C_4$** | 1.389(7), 1.421(6) | 1.394(4), 1.423(4) | 1.403(4), 1.416(4) |
| **$C_3$-$C_4$** | 1.362(7) | 1.362(4) | 1.338(4) |
| **$N_5$-$C_1$-$N_2$** | 104.4(4) | 103.0(3) | 101.0(2) |

Although carbene complexes containing more than one gold atom have been reported in the literature,[232] structure **47** is unique on account of the two gold atoms being bridged by a deprotonated NHC molecule. A recent report states that "*two metals are better than one*"[231d] in Au catalysis which indicates that complex **47** could be of great interest in this area.

## 6.5 Deprotonation vs cocomplexation reactions of homoleptic alkyl lithium zincates and sodium magnesiates

### 6.5.1 Reaction of [IPr·Zn*t*Bu$_2$] (35) with *t*BuLi: stabilisation of LiZn*t*Bu$_3$

The synthesis of **46** shows that bimetallic base **40** can selectively metallate the NHC complex [IPr·Zn*t*Bu$_2$] (**35**) (see **Scheme 6.20**). We then decided to assess if conventional homometallic *t*BuLi could also promote the deprotonation, in this case leading to a lithiation of **35**. A two-step reaction was therefore attempted, by reacting [IPr·Zn*t*Bu$_2$] **35** with *t*BuLi in hexane (**Scheme 6.23**). As Robinson had reported the smooth deprotonation of free carbene **31** by *n*BuLi,[206] it was

anticipated that *t*BuLi would also carry out the reaction and a Li analogue similar to **41** and **44** would be obtained. Surprisingly, analysis of product **48** by $^{1}$H NMR spectroscopy revealed both protons of the backbone to be present, further still, it confirmed an increase in *t*Bu protons from the starting material (from eighteen protons in **35** to twenty seven in **48**). Accompanying the increase in the amount *t*Bu protons, a change in the chemical shift was also observed from a singlet at 1.10 ppm [18H] in **35** to a singlet at 1.94 ppm [27H] in **48**. The presence of a singlet for the *t*Bu protons in **48** suggests that on the NMR timescale all *t*Bu groups are equivalent. **Table 6.12** shows a selection of the chemical shift data of **35** and **48**.

**Table 6.12**: Selected NMR chemical shifts (ppm δ) in $C_6D_6$ for **35** and **48**.

| | **35** | **48** |
|---|---|---|
| $\delta^{1H}CH_{3(iPr)}$ | 0.96, 1.35 | 0.96, 1.26 |
| $\delta^{1H}CH_{3(tBu)}$ | 1.10 | 1.95 |
| $\delta^{1H}CH_{(iPr)}$ | 3.06 | 2.64 |
| $\delta^{1H}CH_{(backbone)}$ | 6.63 | 6.47 |
| $\delta^{1H}CH_{(Ar)}$ | 7.12, 7.19 | 7.07, 7.21 |

The structure was confirmed by single crystal X-ray diffraction and shows **48** to be a trisalkyllithium zincate with the carbene now coordinating to the lithium atom (**Figure 6.19**). Two alkyl groups bridge between the metals and the final alkyl group is terminal on zinc. Unfortunately, the crystal was weakly diffracting and gave poor data, as such no meaningful discussion can be entered in to with regards bond angles and lengths; however, the connectivity is definite.

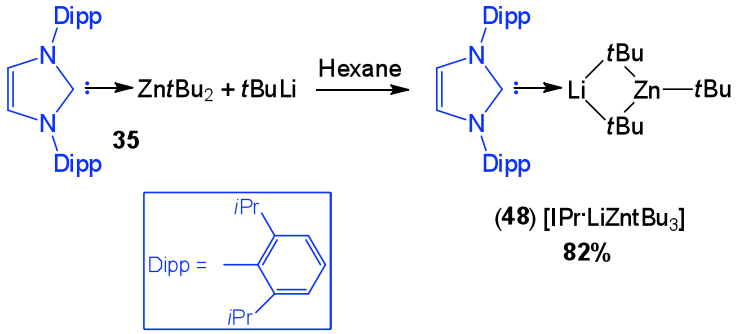


**Scheme 6.23**: Synthesis of trisalkyllithium zincate **48**.

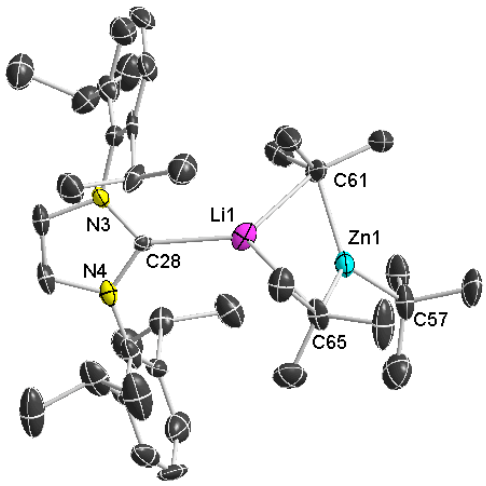


**Figure 6.19**: Molecular structure of **48**. Displacement ellipsoids are drawn at the 50% probability level. Hydrogen atoms have been omitted for clarity. The unit cell of **48** contains two crystallographically independent molecules with identical connectivities.

The formation of **48** suggests that the cocomplexation product must be favoured over deprotonation of the carbene, furthermore these results also provide the first insights into the structure of mixed-metal fragment "LiZn*t*Bu$_3$", a species which has been previously used in several organic transformations but the real constitution of which has thus far proved elusive.[9] In THF solutions Uchiyama has shown that LiZn*t*Bu$_3$ disproportionates to Zn*t*Bu$_2$ and the higher order zincate Li$_2$Zn*t*Bu$_4$ (**Scheme 6.24**)[9] however the presence of IPr in bulk hexane allows for the trapping of LiZn*t*Bu$_3$.

$$2\ \mathrm{LiZn}t\mathrm{Bu}_3 \rightleftharpoons \mathrm{Li}_2\mathrm{Zn}t\mathrm{Bu}_4 + \mathrm{Zn}t\mathrm{Bu}_2$$

**Scheme 6.24**: Disproportionation of LiZn*t*Bu$_3$ in THF solutions.[9]

### 6.5.2 Reaction of [IPr·Zn*t*Bu$_2$] (35) with BuNa: indirect zincation of IPr

In contrast, when **35** is exposed to BuNa in hexane and crystallised with THF as a cosolvent, **41** is produced in an isolated yield of 66%, confirmed by $^1$H NMR and X-ray diffraction (**Scheme 6.25**). Deprotonation of the backbone has occurred, with the loss of Bu(H) and sodium coordinates to the carbene position, solvated by three molecules of THF, and zinc bonds to the backbone of the deprotonated imidazole

ring. This can be rationalised in terms of initial deprotonation of the C4 position by the more aggressive base BuNa, followed by a redistribution to the positions occupied by the metals according to their carbophilicity. The differing reactivity of *t*BuLi and BuNa towards **35** is shown in **Figure 6.20**.

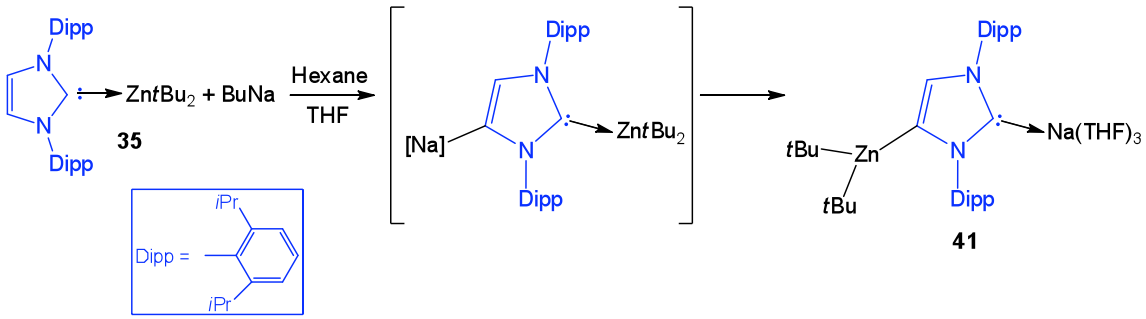


**Scheme 6.25**: Deprotonation of **35** with BuNa.

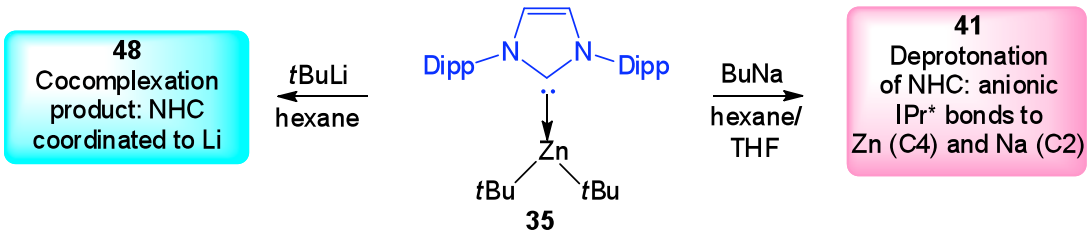


**Figure 6.20**: Deprotonation vs cocomplexation of **35**.

### 6.5.3 Reaction of IPr with sodium magnesiate 12: redistribution and coordination

As there are very few previous reports in the literature of any mixed-metal magnesiate complex containing an NHC, and no reports of a CIP, attention turned at this point towards applying IPr **31** to the unsolvated 2D polymeric network [$NaMgR_3$] (R = $CH_2SiMe_3$) **12** (*vide supra*). Mixing an *in situ* preparation of **12** with an equimolar amount of **31** in a solution of hexane and benzene gave a clear, straw solution (**Scheme 6.26**). Crystallisation from neat hexane in the freezer gave a crop of crystals of **49** in a 13% isolated yield (with a maximum possible yield of 50%). Remarkably, no metallation of the carbene has occurred, and instead a coordination adduct [$IPr_2Na_2MgR_4$] is obtained containing a higher order magnesiate unit resulting from a redistribution process (*vide supra*). Surprisingly, although this synthesis is reproducible, attempts to synthesise **49** rationally (*i.e.* a 2:1:2 ratio of IPr,

$MgR_2$ and NaR) gave an insoluble solid. Product **49** is a bimetallic trinuclear sodium magnesiate that exhibits the "Weiss motif", with each sodium and magnesium bridged by two alkyl groups and the alkali metal capped with a molecule of IPr (**Figure 6.21**).

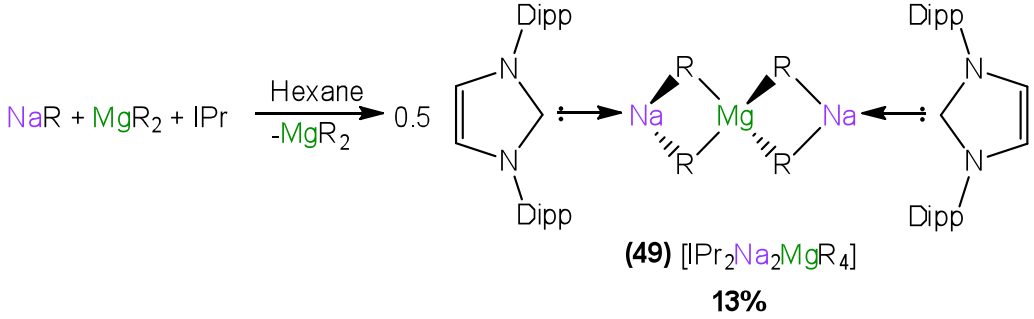


**Scheme 6.26**: Synthetic route to **49**.

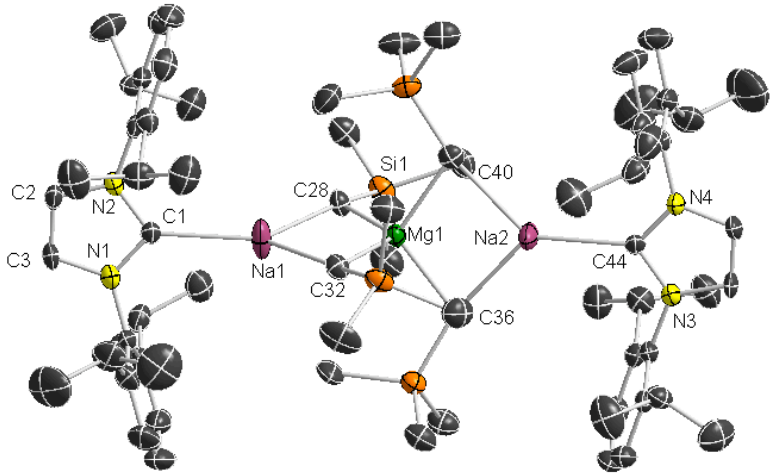


**Figure 6.21**: Molecular structure of **49**. Displacement ellipsoids are drawn at the 50% probability level. Hydrogen atoms except have been omitted for clarity. The unit cell of **49** contains two crystallographically independent molecules with identical connectivities. Selected bond distances and angles: Na1-C1 2.445(4) Å, Na1-C32 2.506(4) Å, Na1-C28 2.568(5) Å, Na2-C44 2.415(4) Å, Na2-C40 2.507(4) Å, Na2-C36 2.515(4) Å, Mg1-C40 2.255(5) Å, Mg1-C32 2.256(4) Å, Mg1-C28 2.263(4) Å, Mg1-C36 2.264(4) Å, C1-Na1-C32 135.43(15)°, C1-Na1-C28 128.75(14)°, C32-Na1-C28 95.44(14)°, C44-Na2-C40 132.23(15)°, C44-Na2-C36 130.77(14)°, C40-Na2-C36 96.53(15)°, C40-Mg1-C32 107.23(17)°, C40-Mg1-C28 107.64(17)°, C32-Mg1-C28 112.35(16)°, C40-Mg1-C36 112.05(16)°, C32-Mg1-C36 110.53(17)°, C28-Mg1-C36 107.07(17)°, C1···Na1···Mg1 175.09(12)°, Na1···Mg1···Na2 176.32(7)°, Mg1···Na2···C44 171.17(13)°.

In **49** Mg is surrounded by four anionic R groups in an almost perfect tetrahedral geometry, with an average angle around Mg1 and Mg2 of 109.5° and a $\tau_4$ (*vide supra*) value of 0.96 and 0.95 respectively. Sodium displays a very rare planar three coordinate geometry (Na1 sum of angles 359.63°, Na2 sum of angles 359.53°); however the angles are not equivalent, with a much greater angle observed for $C_{carbene}$-$Na_{1/2}$-$C_R$ (average 139.75°) compared to $C_R$-$Na_{1/2}$-$C_R$ (average 95.98°). **49** displays and almost linear arrangement along C1···C44···Na1···Mg1···Na2···C44, as evidenced by C1···Na1···Mg1 = 175.09(12)°, Na1···Mg1···Na2 = 176.32(7)° and Mg1···Na2···C44 = 171.17(13)°. The carbene-sodium bond distances (average 2.436 Å) are slightly shorter than in the Na-Zn species **41** and **42** (2.510(3) Å, 2.534(3) Å) and are more of the order of those reported by Hill for [{Na(IPr)$_2$}$^+${Mg(HMDS)$_3$}$^-$] (2.439(6)-2.452(2) Å).[211] Analysis by $^1$H and $^{13}$C NMR in $C_6D_6$ is entirely as would be predicted with the C$H_2$ that bridges between Na and Mg resonating upfield at -1.91 ppm and the C$H_3$ of the R group at 0.20 ppm. The IPr fragment displays the normal pattern in the $^1$H NMR spectrum (**Figure 6.22**) and the carbene resonance is observed in the $^{13}$C spectra at 202.95 ppm, shifting distinctly upfield from free carbene **31** (220.52 ppm).

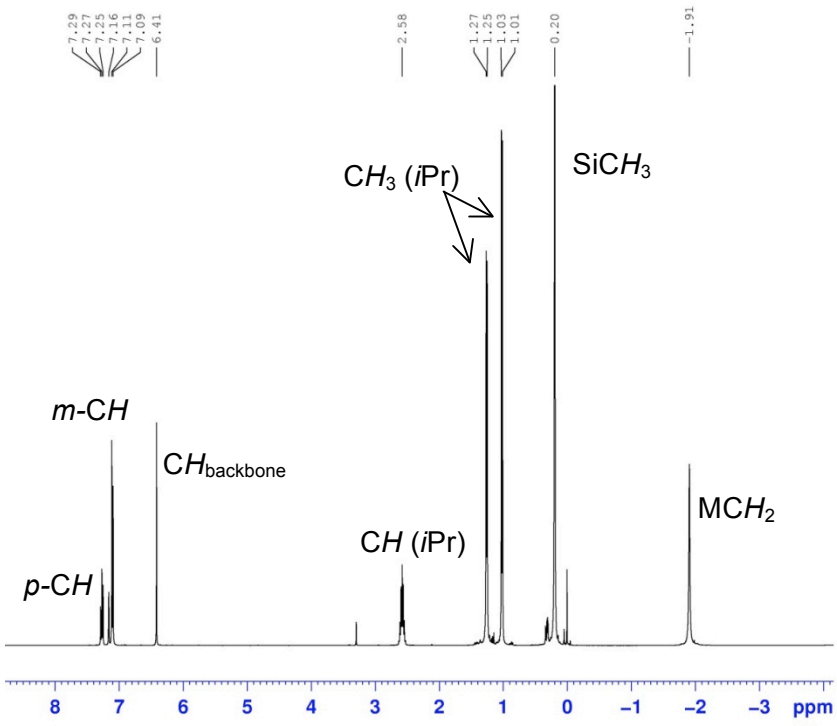


**Figure 6.22**: $^1$H NMR spectrum of **49** in $C_6D_6$.

As with the TMEDA- and PMDETA-solvated analogues of the tetraalkyl magnesiate (**8** and **9** respectively), in the preparation of **49** a reorganisation has taken place from the trisalkyl magnesiate precursor to the higher order magnesiate on crystallisation. As was previously noted, when Na was only tetracoordinated in **8**, additional electrostatic interaction took place with the Me group of a bridging R group, in order to fill the coordination sphere of sodium. When PMDETA was present and Na was pentacoordinated this was no longer necessary. Surprisingly, in compound **49**, sodium is only tricoordinate, but forms no additional interactions with the bridging alkyl groups. A comparison of key bond angles, bond distances and the $^{1}$H NMR spectra of **49**, **8** and **9** are presented in **Table 6.13**.

**Table 6.13**: Selected bond angles (°), bond distances (Å) and NMR chemical shifts (ppm δ) in $C_6D_6$ for **49**, **8** and **9**.

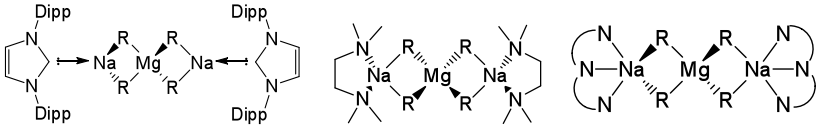


| | **49** | **8** | **9** |
|---|---|---|---|
| **CN of Na** | 3 | 4 | 5 |
| **Average Na-$C_R$** | 2.513 | 2.602 | 2.711 |
| **Average Na-$C_{carbene}$** | 2.436 | - | - |
| **Average Mg-$C_R$** | 2.268 | 2.265 | 2.289 |
| **Na···Mg···Na** | 176.34 | 156.72 | 174.69 |
| **Na···C···Si** | 130.50, 131.91 | 96.54, 166.29 | 151.93, 154.41 |
| **$\delta^{1H}$M-C*H*$_2$** | -1.91 | -1.78 | -1.90 |
| **$\delta^{1H}$Si-C*H*$_3$** | 0.20 | 0.47 | 0.52 |

These data imply that the steric and electronic protection of the alkali metal is similar for the monodentate carbene ligand as it is for the tridentate PMDETA, as these entries display the most similarity. Additionally, the anchoring $[MgR_4]^{2-}$ shows little change in Mg-C bond distances regardless of the donor employed.

### 6.5.4 Indirect magnesiation of IPr

In an effort to explore the reaction of a sodium analogue similar to the anionic dicarbene reported by Robinson by the addition of BuLi to **31**,[206] BuNa was added to the carbene in hexane and the solution stirred. Within 1 h a solid crashed out of solution that was insoluble in neat toluene, THF, TMEDA, PMDETA or pyridine. As $MgR_2$ (R = $CH_2SiMe_3$) had previously been successfully employed in the trapping of the potassium enolate formed during the cleavage of THF (see **Chapter 4.1**, compound **19**), the same strategy was attempted here. Thus, following a 1 hour stir of **31** with BuNa, $MgR_2$ was added and the suspension stirred overnight. Now, addition of THF led to a clear solution that produced crystals of **50** in the freezer overnight in 58% yield (**Scheme 6.27** and **Figure 6.23**).

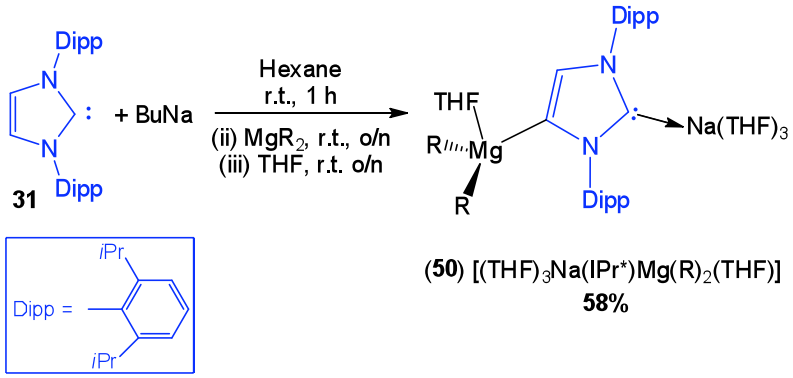


**Scheme 6.27**: Synthesis of sodium magnesiate **50**.

Analysis by single crystal X-ray diffraction revealed **50** to be a sodium magnesiate, bridged by a deprotonated molecule of IPr. **50** bears a strong resemblance to sodium zincate **41**. In **50** and **41** sodium is ligated by the carbene carbon of the imidazole ring and is further coordinated by three molecules of THF. Whereas in **41** a zinc atom bonds to the imidazole backbone and two molecules of *t*Bu, in **50** magnesium now binds to the ring and two anionic R groups. Perhaps due to the more oxophilic nature of Mg compared to Zn, Mg also is further ligated by a molecule of THF, making Mg tetracoordinate.

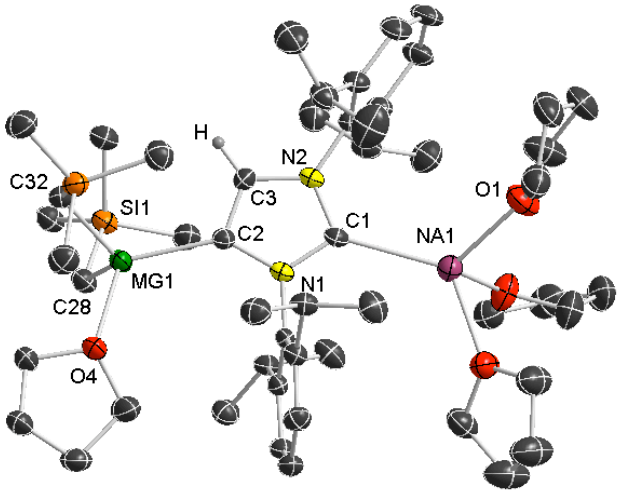


**Figure 6.23**: Molecular structure of **50**. Displacement ellipsoids are drawn at the 50% probability level. Hydrogen atoms and minor disorder in one THF molecule omitted for clarity. Selected bond distances and angles Mg1-C2 2.211(3) Å, Mg1-C32 2.179(3)Å, Mg1-C28 2.184(3) Å, Na1-C1 2.468(3) Å, N2-C1 1.364(3) Å, N2-C3 1.402(3) Å, N1-C1 1.373(3) Å, N1-C2 1.418(3) Å, C3-C2 1.359(3) Å, N2-C1-N1 101.0(2)°.

The Mg-$C_{backbone}$ bond distance is marginally longer (Mg1-C2 2.211 (3) Å) than the Mg-$C_R$ bond distances (average 2.182 Å) but still within the range of an anionic bond distance. In the related structure where $MgR_2$ coordinates to the normal carbene centre of IPr, the reported Mg-$C_{carbene}$ distance is 2.267 (3) Å:[233] indeed, the range of Mg-NHC complexes for monomeric, three coordinate systems lies between 2.254-2.285 Å, which are all longer than the Mg-$C_{backbone}$ bond distance in **50**. A comparison of the bond distances and angles of the imidazole ring in structures **50**, **41** and Robinson's lithiated NHDC[206] are shown in **Table 6.14**. While the C=C distance in **50** (1.359 (3) Å) is more similar to the NHDC (1.356(4) Å) implying a delocalised system, the N-$C_{backbone}$ distances between **50** and **41** are very similar (1.402(3) Å, 1.418(3) Å and 1.403(4) Å, 1.416(4) Å respectively), and the N-C-N angle is identical (101.0(2)°). Analysis of **50** by $^{1}H$ and $^{13}C$ NMR spectroscopy shows no surprises. The diagnostically relevant signal in the $^{13}C$ spectra for the carbene resonates at 200.19 ppm in **50**, which is very similar to the shift found in **41** (201.44 ppm) and only a relatively small variation in the M-C4 resonance is observed changing from 163.90 ppm in **50** when M = Mg to 159.49 ppm when M = Zn.

**Table 6.14**: Selected bond angles (°) and bond distances (Å) for the imidazole ring of magnesiate **50**, zincate **41** and Robinson's lithiated NHDC and NMR chemical shifts (ppm δ) in $d_8$-THF.[206]

| 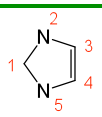 | **50** | **41** | **NHDC**[206] |
|---|---|---|---|
| $\mathbf{N_{2/5}\text{-}C_1}$ | 1.373(3), 1.364(3) | 1.379(4), 1.359(4) | 1.375(3), 1.361(3) |
| $\mathbf{N_2\text{-}C_3/N_5\text{-}C_4}$ | 1.402(3), 1.418(3) | 1.403(4), 1.416(4) | 1.399(4), 1.442(4) |
| $\mathbf{C_3\text{-}C_4}$ | 1.359(3) | 1.338(4) | 1.356(4) |
| $\mathbf{N_5\text{-}C_1\text{-}N_2}$ | 101.0(2) | 101.0(2) | 100.5(2) |
| $\mathbf{\delta^{1H}C\mathit{H}_{\mathit{i}Pr}}$ | 2.95, 3.08 | 2.95, 3.16 | |
| $\mathbf{\delta^{1H}C\mathit{H}_{imidazole}}$ | 6.55 | 6.66 | |
| $\mathbf{\delta^{13C}ZnC_{backbone}}$ | 163.90 | 159.49 | |
| $\mathbf{\delta^{13C}\mathit{C}:}$ | 200.19 | 201.44 | |

## 6.6 Conclusions

A systematic structural, spectroscopic and theoretical study has been undertaken to assess the impact of applying mixed-metal chemistry to the area of N-heterocyclic carbenes. The groundwork to this study began with the synthesis and characterisation of a family of dialkyl zinc complexed NHCs **34-39**, with $ZnR_2$ (R = Me or *t*Bu) complexing in turn with IPr, IMes and IBu. Building on this, sodium zincate **40** and potassium zincate **43** were introduced to IPr which led to the smooth, room temperature deprotonation of the carbene ring giving novel zincated species **41** and **44** respectively. The "proof of concept" for the forward functionalization of these complexes was carried out by reacting with an electrophile, showing that the backbone can be amended to alter the sterics and electronics of the carbene system. Studies were also conducted into the formation of homometallic binuclear systems, where the metal at the C2 and C4 positions were the same. The unique bis-zinc **46** and bis-gold **47** species were thus synthesised and fully characterised. Remarkably, *t*BuLi is not able to perform the deprotonation of IPr when coordinated to Zn, instead the formation of an adduct between IPr and newly formed $LiZnt Bu_3$ is preferred, showing a greater tendency of *t*BuLi to form a zincate rather than acting as a base

towards IPr, giving the first glimpse of the "LiZn*t*Bu$_3$" fragment in **48**. IPr was also able to deaggregate and trap the higher order magnesiate "Na$_2$MgR$_4$" (R = CH$_2$SiMe$_3$) by complexing with the alkali metal **49**. In contrast, if IPr is confronted with BuNa and MgR$_2$ sequentially deprotonation occurs giving rise to magnesiated product **50**. A summary is shown in **Figure 6.24**.

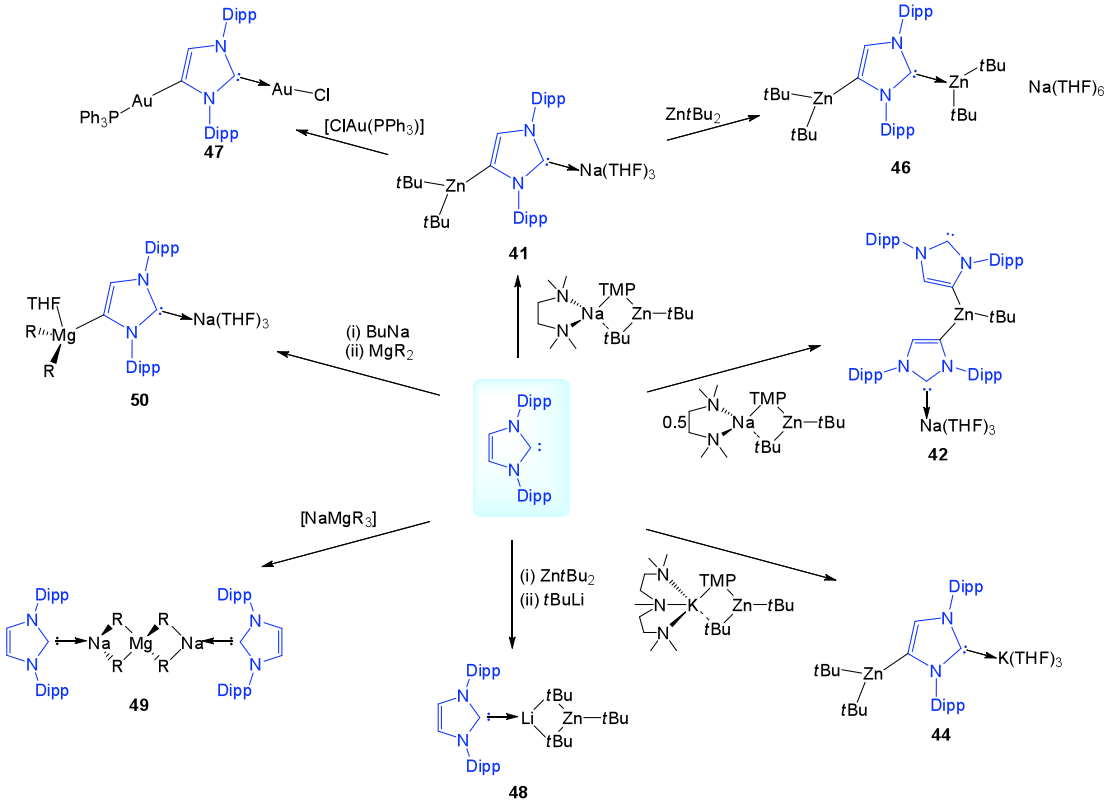


**Figure 6.24**: Summary of the reactions explored with IPr.

## Chapter 7: Conclusions and future work

New structural and synthetic insights in the area of magnesiate and zincate chemistry have been presented. A systematic study of the cocomplexation reactions of homometallic alkyls $M^IR$ ($M^I$ = Li, Na and K) and $MgR_2$ (R = $CH_2SiMe_3$) in the presence of several Lewis bases, including TMEDA and THF, two of the most commonly used donor molecules in organic synthesis for the activation of organometallic reagents such as BuLi or RMgX, has been undertaken. Structural characterisation and spectroscopic solution studies of several alkali metal magnesiates revealed the complex chemistry that this important family of mixed-metal reagents can display in solution and sheds new light on the effect that donor solvents play in the structure/constitution of these bimetallic reagents.

The control of the donor ligand on the structural outcome was examined by the application of monodentate, didentate (chelating and non-chelating) and tridentate ligands with solution mixtures of $M^IMgR_3$. Monodentate THF-coordinated [{(THF)$LiMgR_3$}$_\infty$] (**2**) provided an unusual structure with an infinite chain constructed of electron deficient M-C bonds obtained. Characterisation in deuterated benzene solution (including $^1$H-DOSY NMR and HOESY experiments) revealed a much more deaggregated structure is probably present where the alkali metal interacts with a molecule of the solvent and THF remains coordinated to Mg. In contrast, the dioxane-containing polymers, **3** and **4** are formed as a consequence of the ability of this donor to act as a 1,4-bridge through its two oxygen atoms, linking {$LiMgR_3$} or {$LiMgR_3$}$_2$ units to afford **3** and **4** respectively.

The use of didentate TMEDA allows the formation of discrete molecular structures, where TMEDA induces a redistribution process of the mixed-metal precursor to form the higher order tetraorganomagnesiate [$(TMEDA)_2M^I_2MgR_4$] ($M^I$ = Li (**5**), Na (**8**) and K (**10**)) along with $MgR_2$, representing a rare example of a homologous series. The compound of Li, **5**, has a coordination number of 4 and an almost linear arrangement of Li···Mg···Li. Na compound **8** attains a coordination number of 5 through electrostatic interactions and potassium structure **10** induces severe bending

of the most common linear arrangement to allow the larger cation to each form three σ-bonds with the bridging carbanionic ligands. On the other hand, PMDETA is found to form monomeric trisalkyl magnesiate complex [(PMDETA)LiMgR$_3$] (**6**) which, exhibiting an unusual open structural motif can be envisaged as an intermediate between a solvent-separated ion pair and a contacted ion pair magnesiate structure. This compound can react with dry $O_2$ to yield the novel [{(PMDETA)$_2$Li$_2$Mg(CH$_2$SiMe$_3$)$_3$}$^+${Mg$_3$(CH$_2$SiMe$_3$)$_6$(OCH$_2$SiMe$_3$)}$^-$] (**7**) which represents to the best of our knowledge the first example of a cationic lithium magnesiate moiety. In contrast, the use of tridentate donor PMDETA with the sodium and potassium mixture led to the higher order magnesiate which displays an almost linear M···Mg···M arrangement [(PMDETA)$_2$M$^I_2$MgR$_4$] (M$^I$ = Na (**9**) and K (**11**)).

Moving forward, the application of stronger/weaker ligands could be applied to ascertain their effect on the overall constitution of the structures and studies could be extended to other donor molecules or N-heterocyclic carbenes. For example, a tetradentate donor, such as Me$_6$TREN (tris(*N*,*N*-dimethyl-2-aminoethyl)amine) could be employed to gauge the effect of increased donor availability on the resulting structures. The structural studies outlined in **Chapters 2-3** concentrated on homoalkyl magnesiates yet little is known with regards other mixed-metal reagents, such as zincates, gallates, aluminates or manganates, and work could be done to explore these structures using a similar cocomplexation approach.

The novel structures of the solvent-free trialkylmagnesiate species [{NaMgR$_3$}$_\infty$] **12** and [{KMgR$_3$}$_\infty$] **16** have been uncovered. These unique polymeric structures display unprecedented 2D networks in the solid-state, held together exclusively through electron deficient M-C bonds. Furthermore, **16** represents the first structural analysis of a homoalkyl potassium magnesiate to be characterised. Solution studies carried out using $^1$H-DOSY have revealed that these polymeric structures undergo deaggregation and do not retain their solid-state structures in solution. Attempted synthesis of the unsolvated higher order sodium magnesiate {Na$_2$MgR$_4$} **14** revealed that **14** is in equilibrium with NaMgR$_3$ and NaR and led to the fortuitous

crystallisation of homometallic species [{(NaR)$_4$}$_\infty$] **13** which was exposed as a polymer of tetramers by Xray crystallography. The affinity of K to form π-interactions was demonstrated by introducing benzene to **16** giving chain structure [{($C_6H_6$)KMgR$_3$}$_\infty$] **17**. Also, the exclusive club of metallocene-K structures was added to by the addition of ferrocene to [{(ferrocene)KMgR$_3$}$_\infty$] (**18**) resulting in an elaborate three-dimensional structure.

The two-pronged consideration of structure controlling reactivity has been probed by studying the contrasting reactivities of the structurally defined potassium magnesiate reagents [{($C_6H_6$)KMgR$_3$}$_\infty$] (**17**) and [(PMDETA)$_2$K$_2$MgR$_4$] (**11**). Studies have shown polymeric reagent **17** is unable to carry out deprotonative metallation at ambient temperature with respect to thiophene and anisole whereas **11** gave yields of 87% and 81% respectively after addition of four equivalents of substrate and electrophilic quench with iodine. These results show the potential synthetic application of **11** which selectively deprotonate a number of aromatic substrates under mild conditions, contrasting with related K-based reagent LIC-KOR, where cryogenic conditions must be strictly adhered to. In further studies, the reactivity potassium magnesiates could be probed with regards other organic molecules, including N-heterocyclic molecules with -OMe, -$CO_2$R or -$CONR_2$ groups to assess the regioselectivity and efficiency of the deprotonation reaction. The quenching protocol could also be expanded, with Pd-catalysed cross-coupling reactions attempted. Also, as ArMgX can react with alkyl halides under Fe(III) salt catalysis conditions to yield the relevant aryl-alkyl coupling products, investigations could be carried out to assess the effect of this chemistry with relation to potassium magnesiates and the potential transmetallating power of the magnesiate with the Fe catalyst. A comparison of the reactivity of the homologous series [(TMEDA)$_2$M$_2$MgR$_4$] (M = Li, Na, K) towards substrates could also be carried out to assess the effect of the alkali metal on these organic transformations.

Within the context of zincate reagents, the organometallic intermediates of a number of key organic transformations (metallation, alkyl addition and metal-halogen exchange reactions) have been isolated and characterised which provide new insights

regarding the way subtle changes in the coordination environment of CIP lithium zincates can induce drastic changes in the reactivity pattern of these mixed-metal reagents. The reactivity of heteroleptic zincate [(THF)LiZn(TMP)(*t*Bu)$_2$] (**22**) towards pyrazine has been examined, showing that despite the presence of two nucleophilic *t*Bu groups the selective two-fold deprotonation of pyrazine is preferred to form the unprecedented 2,5-di-zincated pyrazine molecule. These results are in contrast with those observed when pyrazine is confronted by the homoleptic alkyl zincate [(PMDETA)LiZn(*t*Bu)$_3$] (**23**) where the chemoselective addition of a *t*Bu group to the α-C of the heterocycle takes place under mild reaction conditions. By trapping the bimetallic intermediates of these reactions the first structural insights into the constitution of the inorganic products resulting from the reactions of an organometallic reagent with pyrazine are provided. As only pyrazine has thus far been investigated under these conditions, these studies could be extended to other electron-deficient heterocycles. Building on this, the development of novel alkylating or, even more interestingly, arylating reagents which can allow the chemoselective C-H arylation of diazines using "LiZnAr$_3$" reagents could be probed.

Additionally, the effect of adding LiCl to Zn*t*Bu$_2$ has been probed with $^1$H-DOSY NMR studies suggesting a lithium zincate aggregate is forming in solution which is sufficiently reactive to transfer a *t*Bu group to the pyrazine molecule, in contrast with Zn*t*Bu$_2$ alone which forms a coordination product. Switching to a monoalkoxo/dialkyl species (from cheap, commercially available starting materials) led to a novel route for halogen-metal exchange, demonstrating the activating power of LiO*t*Bu towards ZnEt$_2$ and Bu$_2$Mg. Despite low isolated yields, analysis by $^1$H NMR showed the reaction to be quantitative and the low cost and mild reaction conditions of this reaction demonstrates it has potential to be a useful addition in M-X exchange reactions following some optimisation, for example, by altering the solvent, for example to an NMP/THF mixture (NMP = N-methyl pyrrolidone). Precedents in the literature have shown that the use of polar NMP can greatly activate homometallic reagents such as Zn*i*Pr$_2$ towards Zn-I exchange reactions. Further work can to be carried out to assess the scope of this reaction in terms of the substrates that can undergo the exchange.

With respect to NHC chemistry the field is ripe and almost completely unharvested. A systematic study has been undertaken to assess the impact of applying mixed-metal chemistry to the area of N-heterocyclic carbenes. The groundwork to this study began with the synthesis and characterisation of a family of dialkyl zinc complexed NHCs **34-39**, with $ZnR_2$ (R = Me or *t*Bu) complexing in turn with IPr, IMes and IBu. Building on this, sodium zincate **40** and potassium zincate **43** were introduced to IPr which led to the smooth, room temperature deprotonation of the carbene ring giving novel zincated species **41** and **44** respectively where the NHC is acting as a bridge between Zn (C4) and the alkali metal (C2). Structural and theoretical studies suggest that **41** can be envisaged as an anionic variation of neutral IPr, contrasting with previous studies where the lithiation of IPr generates an anionic dicarbene. The "proof of concept" for the forward functionalization of these complexes was carried out by reacting with TMSCl, which replaced Zn at the C4 position, showing that the backbone can be amended to alter the sterics and electronics of the carbene system. Moving forward, the application of a range of mixed-metal reagents could be applied to the carbene molecule (such as lithium aluminates or magnesium zincates) and quenched with a number of electrophiles. Pd-catalysed cross-coupling reactions would be a deft reaction to attempt, with the creation of a new C-C bond on the backbone of the carbene and its effect on the electronic and steric environment of the new carbene assessed in organic transformations, such as metathesis reactions. A protocol could be developed for the effective quenching of **41**, leading to a library of novel C4 substituted carbenes.

Studies were also conducted into the formation of homometallic binuclear systems, where the metal at the C2 and C4 positions were the same. The unique bis-zinc **46** species was synthesised by addition of $Zn(tBu)_2$ to **41**. Transmetallation of **41** to a transition metal was demonstrated by the addition of $[ClAu(PPh_3)]$, which resulted in the novel bis-gold species **47**, where two gold atoms are bridged by an NHC. The catalytic activity of the unique bis-gold species should be ascertained. Furthermore, the transmetallation with other transition metal fragments could be carried out, such as $[Cl_2Pd(COD)]$ (COD = cyclooctadiene) or $[Cl_2Pd(PPh_3)_2]$. This can also have

important implications in catalysis as NHC-Pd complexes have recently been shown to be effective catalysts in Negishi cross-coupling reactions.

In addition, investigations into the reaction of BuM (M = Li, Na) with [IPr·Zn*t*Bu$_2$] (**35**) showed differing reaction pathways depending on the identity of the alkali metal employed. Thus, mixing **35** with *t*BuLi in hexane led to the complexation product [IPr·ZnLi*t*Bu$_3$] **48**, which is the first glimpse at the elusive species "LiZn*t*Bu$_3$". In contrast, mixing **35** with BuNa led to the deprotonation product **41**. IPr was also able to deaggregate and trap the higher order magnesiate "Na$_2$MgR$_4$" (R = CH$_2$SiMe$_3$) by complexing with the alkali metal **49**, whereas stepwise addition of NaR to the carbene followed by introduction of MgR$_2$ led to the deprotonated carbene [(THF)$_3$Na(IPr*)Mg(R)$_2$(THF)] **50** resulting from direct sodiation of IPr followed by transmetallation with MgR$_2$. This stepwise reaction could be exploited to synthesise a number of bimetallic NHC-bridged compounds, by firstly deprotonating the carbene with an organoalkali metal reagent MR (M = Li, Na, K) and then treating with a second, less polar metal reagent, for example Al or Ga, leading to novel metallated carbene molecules.

# Chapter 8: General experimental techniques & procedures

## 8.1 General Experimental Techniques

### 8.1.1 Schlenk Techniques

Due to the sensitivity of all the organometallic starting materials and products to both oxygen and moisture, all manipulations were performed under a dry and inert atmosphere, typically under an argon blanket. The majority of the synthetic work described was carried out using high vacuum, Schlenk techniques on a vacuum/argon double manifold (**Figure 8.1**) and an argon filled glove box (**Figure 8.2**).

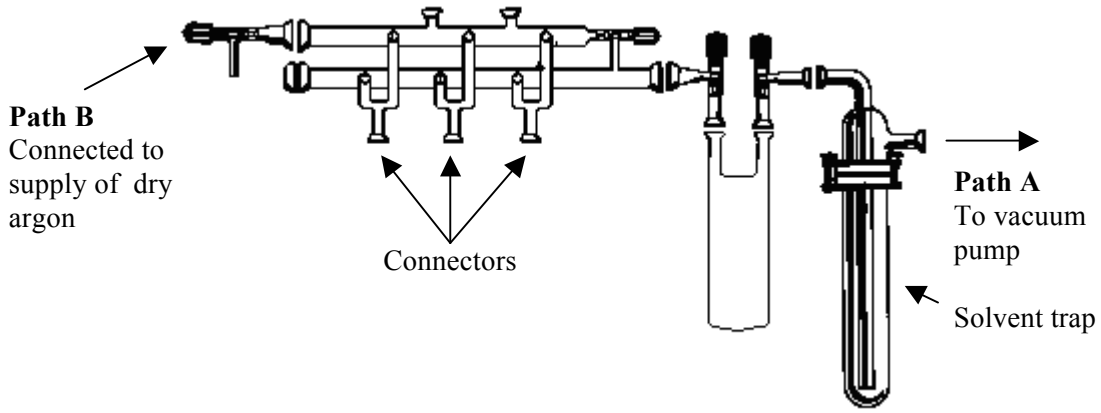


**Figure 8.1**: Standard Schlenk line

The Schlenk line follows two independent paths. Path A is connected to a vacuum pump and path B is connected to a supply of dry oxygen-free argon. Independent positions link the Schlenk line to the appropriate apparatus (usually a Schlenk tube). At each position glass taps allow for the position to be switched to either vacuum or argon, allowing the evacuation of the apparatus or the influx of gas, respectively. Taps and joints within the system are lubricated with high vacuum grease and gas overpressure is prevented by the addition of outlet oil Deschel bottle. In order to prevent contamination of the vacuum pump by solvents removed from the reaction media a Dewar flask filled with liquid nitrogen is placed around the vacuum trap.

Prior to each experiment air was expelled from the Schlenk tube *in vacuo* and substituted with inert argon gas. This evacuation and inert gas flushing was repeated thrice to ensure that all oxygen had been removed from the apparatus.

### 8.1.2 Glove box

The manipulation of all solid material, for example the determination of weights of reactants and products, and the preparation of NMR samples, was also carried out under an inert atmosphere. A standard glove box (or dry box) was used to provide a sealed, inert atmosphere for this function (**Figure 8.2**).


**Figure 8.2**: Standard glove box

The glove box comprises of two main chambers. The larger chamber, which contains a plastic window and two gloves, is the working area. This chamber is kept full of dry argon and is where all the manipulations of solid chemicals take place. The second chamber is a port which has an outer door and an inner door (connected to the main chamber), allowing transfer of apparatus and chemicals into, and out of, the glove box. Items are placed in the port, which is then evacuated to remove air and moisture, followed by the re-filling of the port with dry argon gas. As with the Schlenk line this process is carried out three times as standard practice to ensure that negligible quantities of air and moisture are present. After this the inner door of the port can be opened and the contents transferred to the main chamber to be used. The

gas in the glove box is constantly circulated over a scrubber, which removes and air or water which may be present.

### 8.1.3 Solvent Purification

As a result of the sensitivity of the reactants and products to air and moisture, all solvents were dried and de-gassed before use. All of the solvents used in this report were distilled over nitrogen, in the presence of sodium and benzophenone.[185] These substances act as self-indicators for ensuring the removal of air and water from the solvent. The reaction of sodium with benzophenone gives a ketyl radical, which gives an intense blue colour. This species is incredibly reactive towards oxygen and water, and results in the formation of colourless or yellow products. The colour change is a simple test for determining the presence of oxygen and water. The dried solvent was then removed using a glass syringe and needle, pre-flushed thrice with argon prior to use. The addition of solvent to the apparatus was carried out under a positive pressure of argon to prevent the entry of air into the system.

### 8.1.4 Analytical Procedures

All $^{1}H$ NMR spectroscopic analysis were carried out a Bruker AVANCE-400 NMR spectrometer operating at 400.13 MHz under TopSpin (version 2.0, Bruker Biospin, Karlsruhe). The $^{13}C\{^{1}H\}$ NMR spectra were carried out on the same instrument, operating at 100.62 MHz, and all were proton decoupled. The $^{7}Li$ NMR spectra were recorded at 155.50 MHz. Abbreviations of NMR patterns are as follows: s (singlet), d (doublet), t (triplet), m (multiplet) and br (broad peak).

Gas chromatography was carried out using a Perkin Elmer Clarus 500 2 Gas Chromatograph and data was interpreted using Total Chrom computer software. G.C. analysis: (i) Elite-cyclodex B column; (ii) carrier gas, $H_2$: 2 mL $min^{-1}$; (iii) injector/detector temperature, 230 °C; (iv) initial oven temperature, 60 °C; (v) temperature gradient, 60-150 °C 4 °C $min^{-1}$, 150-230 °C 15 °C $min^{-1}$; (vi) final oven temperature, 230 °C; and (vii) detection method, FID.

The X-ray crystallographic data were recorded on Nonius Kappa CCD diffractometers at 150 K, and Oxford Diffraction (now Agilent Technologies) Xcalibur and Gemini diffractometers at 123 K using MoKα and CuKα radiation (λ = 0.71073 and 1.54180 Å, respectively). The structures were solved by direct methods and refined on all unique $F^2$ values.[234]

## 8.2 Preparation of Starting Materials

### 8.2.1 Preparation of [Mg(CH$_2$SiMe$_3$)$_2$]

To an oven-dried 500 mL round bottom flask were added Mg turnings (4.00 g, 0.136 mol) and $Et_2O$ (100 mL). $ClCH_2SiMe_3$ (19 mL, 0.136 mol) was suspended in $Et_2O$ (50 mL) and added drop wise. The resulting grey solution was refluxed for 1 hour. To the cooled suspension was added 1,4-dioxane (9 mL, 0.106 mol) and the pale grey mixture stirred for 3 days. The suspension was then filtered through celite and glass wool and washed with $Et_2O$ (2 x 40 mL) giving a pale straw filtrate. Removal of the solvent *in vacuo* afforded a white solid which was purified by sublimation at 175 ºC ($10^{-2}$ torr) to furnish pure $Mg(CH_2SiMe_3)_2$ (typical yield 8.5-9.5 g, 63-70%). $^1$H NMR (400.13 MHz, 298 K, $d_8$-THF) δ -1.77 (s, 2H, C*H*$_2$), -0.11 (s, 9H, C*H*$_3$).

### 8.2.2 Preparation of [NaCH$_2$SiMe$_3$]

To a suspension of Na$O^t$Bu (0.86 g, 10 mmol) in hexane (40 mL) at 0 ºC was added drop wise $LiCH_2SiMe_3$ (10 mL of a 1 M solution of $LiCH_2SiMe_3$ in hexane). The reaction was stirred overnight. The resultant peach suspension was filtered, washed with hexane (2 x 20 mL) and dried under vacuum to afford a white solid (typical yield 0.82 g, 75%). $^1$H NMR (400.13 MHz, 298 K, $C_6D_6$) δ -2.45 (s, 2H, C*H*$_2$), 0.14 (s, 9H, C*H*$_3$).

### 8.2.3 Preparation of [KCH$_2$SiMe$_3$]

To a suspension of K$O^t$Bu (2.75 g, 25 mmol) in hexane (50 mL) at 0 ºC was added drop wise $LiCH_2SiMe_3$ (25 mL of a 1 M solution of $LiCH_2SiMe_3$ in hexane). The reaction was stirred overnight. The resultant off-white suspension was filtered, washed with hexane (2 x 20 mL) and dried under vacuum to afford a white solid

(typical yield 2.49 g, 79%). $^{1}$H NMR (400.13 MHz, 298 K, $C_6D_6$) δ -2.20 (s, 2H, C$H_2$), -0.20 (s, 9H, C$H_3$).

## 8.3 Synthesis of Products

### 8.3.1 Synthesis of [LiMg(CH$_2$SiMe$_3$)$_3$] (1)

To a solution of LiCH$_2$SiMe$_3$ (1 mL of a 1 M solution in hexane, 1 mmol) in hexane (15 mL) Mg(CH$_2$SiMe$_3$)$_2$ (0.20 g, 1 mmol) was added and the resulting suspension was heated gently affording a clear solution. Slow cooling resulted in the formation of clear, colourless crystals were isolated (0.28 g, 96%). $^{1}$H NMR (400.13 MHz, 298 K, $C_6D_6$) δ -1.36 (6H, s, SiC$H_2$), 0.25 (27H, s, Si(C$H_3$)$_3$). $^{13}$C {$^{1}$H} NMR (100.62 MHz, 298 K, $C_6D_6$) δ -2.21 (Si*C*H$_2$), 4.16 (Si(*C*H$_3$)$_3$). $^{7}$Li NMR (155.50 MHz, 298 K, $C_6D_6$) δ 0.38.

### 8.3.2 Synthesis of [{(THF)LiMg(CH$_2$SiMe$_3$)$_3$}$_\infty$] (2)

To a solution of LiCH$_2$SiMe$_3$ (1 mL of a 1 M solution in hexane, 1 mmol) in hexane (15 mL) Mg(CH$_2$SiMe$_3$)$_2$ (0.20 g, 1 mmol) was added and the resulting suspension was stirred for 1 h affording a clear solution. THF (0.08 mL, 1 mmol) was then added and the clear solution was frozen in liquid nitrogen before transferring to the freezer (-28 °C). Clear, colourless crystals formed after 18 h which were isolated (0.04 g, 11%). $^{1}$H NMR (400.13 MHz, 298 K, $C_6D_6$) δ -1.31 (6H, s, SiC$H_2$), 0.35 (27H, s, Si(C$H_3$)$_3$), 1.15 (4H, m, C$H_2$, THF), 3.40 (4H, m, OC$H_2$, THF). $^{13}$C {$^{1}$H} NMR (100.62 MHz, 298 K, $C_6D_6$) δ -3.33 (Si*C*H$_2$), 4.37 (Si(*C*H$_3$)$_3$), 25.02 (*C*H$_2$, THF), 68.90 (O*C*H$_2$, THF). $^{7}$Li NMR (155.50 MHz, 298 K, $C_6D_6$) δ 1.24.

### 8.3.3 Synthesis of [{(dioxane)$_2$LiMg(CH$_2$SiMe$_3$)$_3$}$_\infty$] (3)

To a solution of LiCH$_2$SiMe$_3$ (2 mL of a 1 M solution in hexane, 2 mmol) in hexane (15 mL) Mg(CH$_2$SiMe$_3$)$_2$ (0.40 g, 2 mmol) was added and the resulting suspension was stirred for 1 hour affording a clear solution. 1,4-Dioxane (0.17 mL, 2 mmol) was added drop wise, resulting in a white suspension which was stirred for 30 minutes. The volume was reduced *in vacuo* to approximately 5 mL. Addition of toluene (2 mL) and gentle heating gave a clear solution which was left to slowly.

Small, colourless crystals were isolated (0.28 g, 30%). $^{1}$H NMR (400.13 MHz, 298 K, $C_6D_6$) δ -1.51 (6H, s, SiC*H*$_2$), 0.35 (27H, s, Si(C*H*$_3$)$_3$), 3.30 (16H, s, OC*H*$_2$, dioxane). $^{7}$Li NMR (155.50 MHz, 298 K, $C_6D_6$) δ 1.25. $^{13}$C {$^{1}$H} NMR could not be collected due to poor solubility.

### 8.3.4 Synthesis of [{(dioxane)$Li_2Mg_2(CH_2SiMe_3)_6$}$_\infty$] (4)

To a solution of $LiCH_2SiMe_3$ (2 mL of a 1 M solution in hexane, 2 mmol) in hexane (15 mL) $Mg(CH_2SiMe_3)_2$ (0.40 g, 2 mmol) was added and the resulting suspension was stirred for 1 hour affording a clear solution. 1,4-Dioxane (43 μL *via* microsyringe, 0.5 mmol) was added drop wise, resulting in the formation of a white precipitate which was stirred for 18 h. Addition of toluene (4 mL) and gentle heating gave a clear solution which was left to cool slowly. Small, colourless crystals were isolated (0.34 g, 50%). $^{1}$H NMR (400.13 MHz, 298 K, $C_6D_6$) δ -1.47 (s, 6H, SiC*H*$_2$), 0.28 (s, 27H, Si(C*H*$_3$)$_3$), 3.21 (s, 4H, OC*H*$_2$, dioxane). $^{7}$Li NMR (155.50 MHz, 298 K, $C_6D_6$) δ 0.32 (s). The relative low solubility and stability of **4** over prolonged periods of time in $C_6D_6$ solutions precluded the collection of its $^{13}$C {$^{1}$H} NMR spectrum.

### 8.3.5 Synthesis of [$(TMEDA)_2Li_2Mg(CH_2SiMe_3)_4$] (5)

To a solution of $LiCH_2SiMe_3$ (1 mL of a 1 M solution in hexane, 1 mmol) in hexane (15 mL) $Mg(CH_2SiMe_3)_2$ (0.20 g, 1 mmol) was added and the resulting suspension was stirred for 30 m affording an almost clear solution. TMEDA (0.15 mL, 1 mmol) was then added giving a clear solution which was transferred to the freezer (-28 °C). After 18 h colourless crystals suitable for X-ray diffraction were deposited (0.14 g, 23%, which could be increased to 56% when prepared with the stoichiometry LiR:2MgR$_2$:2TMEDA). $^{1}$H NMR (400.13 MHz, 298 K, $C_6D_6$) δ -1.99 (2H, s, SiC*H*$_2$), 0.46 (9H, s, Si(C*H*$_3$)$_3$), 1.65 (2H, s, NC*H*$_2$, TMEDA), 2.02 (6H, s N(C*H*$_3$)$_2$, TMEDA). $^{13}$C {$^{1}$H} NMR (100.62 MHz, 298 K, $C_6D_6$) δ -3.19 (Si*C*H$_2$), 5.71 (Si(*C*H$_3$)$_3$), 46.41 (*C*H$_3$, TMEDA), 56.91 (*C*H$_2$, TMEDA). $^{7}$Li NMR (155.50 MHz, 298 K, $C_6D_6$) δ 0.82.

### 8.3.6 Synthesis of [(PMDETA)LiMg($CH_2SiMe_3$)$_3$] (6)

To a solution of $LiCH_2SiMe_3$ (1 mL of a 1 M solution in hexane, 1 mmol) in hexane (15 mL) $Mg(CH_2SiMe_3)_2$ (0.20 g, 1 mmol) was added and the resulting suspension was stirred for 1 hour affording a clear solution. PMDETA (0.21 mL, 1 mmol) was then added giving a slightly cloudy solution. Gentle heating gave a clear solution and the Schlenk tube was transferred to the freezer (-28 °C). After 4 days colourless crystals suitable for X-ray diffraction were deposited. Due to the fast formation of an oil at room temperature, an accurate yield has not been obtained; however the NMR of the oil showed no other species were present, supporting that the formation of **6** is quantitative. $^1$H NMR (400.13 MHz, 298 K, $C_6D_6$) δ -1.31 (6H, s, SiC$H_2$), 0.42 (27H, s, Si(C$H_3$)$_3$), 1.73-1.94 (23H, br overlapping m, PMDETA). $^{13}$C {$^1$H} NMR (100.62 MHz, 298 K, $C_6D_6$) δ -3.28 (Si$CH_2$), 5.39 (Si($CH_3$)$_3$), 44.91 ($CH_3$, PMDETA), 45.83 (($CH_3$)$_2$, PMDETA), 53.14 ($CH_2$, PMDETA), 57.04 ($CH_2$, PMDETA). $^7$Li NMR (155.50 MHz, 298 K, $C_6D_6$) δ 0.76.

### 8.3.7 Synthesis of [{(PMDETA)$_2$Li$_2$Mg($CH_2SiMe_3$)$_3$}$^+${Mg$_3$($CH_2SiMe_3$)$_6$($OCH_2SiMe_3$)}$^-$] (7)

To a solution of $LiCH_2SiMe_3$ (1 mL of a 1 M solution in hexane, 1 mmol) in hexane (15 mL) $Mg(CH_2SiMe_3)_2$ (0.40 g, 2 mmol) was added and the resulting suspension was stirred for 1 h affording a clear solution. PMDETA (0.21 mL, 1 mmol) was then added giving a slightly cloudy solution. A drying tube was fitted to the Schlenk tube for 30 minutes. Gentle heating gave a clear solution with a yellow oil deposited at the bottom of the Schlenk tube. The Schlenk tube was transferred to the freezer (-28 °C) overnight. Colourless crystals formed (0.23 g, 34%). $^1$H NMR (400.13 MHz, 298 K, $C_6D_6$) δ -1.11 (18H, overlapping m, br, SiC$H_2$), 0.45 (91H, overlapping m, Si(C$H_3$)$_3$), 1.80 (43H, overlapping m, NC$H_2$, N(C$H_3$)$_2$, and N(C$H_3$) PMDETA), 3.93 (2H, s, OC$H_2$). $^7$Li NMR (155.50 MHz, 298 K, $C_6D_6$) δ 0.20. The relative low solubility of **7** in $C_6D_6$ solution precluded the collection of a meaningful $^{13}$C {$^1$H} NMR spectrum.

### 8.3.8 Synthesis of $[(TMEDA)_2Na_2Mg(CH_2SiMe_3)_4]$ (8)

To a suspension of $NaCH_2SiMe_3$ (0.22 g, 2 mmol) in hexane (15 mL) $Mg(CH_2SiMe_3)_2$ (0.20 g, 1 mmol) was added and the suspension stirred for 1 hour. TMEDA (0.30 mL, 2 mmol) was then added and the almost clear solution transferred to the freezer (-28 °C). After 16 hours a crop of clear, colourless crystals was isolated (0.35 g, 54%). $^1$H NMR (400.03 MHz, 298 K, $C_6D_6$) δ -1.78 (2H, s, SiC$H_2$), 0.47 (9H, s, Si(C$H_3$)$_3$), 1.67 (2H, s, NC$H_2$, TMEDA), 1.92 (6H, s, N(C$H_3$)$_2$, TMEDA). $^{13}$C {$^1$H} NMR (100.62 MHz, 298 K, $C_6D_6$) δ -3.14 (Si*C*H$_2$), 5.63 (Si(*C*H$_3$)$_3$), 45.80 (N(*C*H$_3$)$_2$, TMEDA), 56.76 (N*C*H$_2$, TMEDA).

### 8.3.9 Synthesis of $[(PMDETA)_2Na_2Mg(CH_2SiMe_3)_4]$ (9)

To a suspension of $NaCH_2SiMe_3$ (0.055 g, 0.5 mmol) in hexane (10 mL) $Mg(CH_2SiMe_3)_2$ (0.1 g, 0.5 mmol) was added and the suspension stirred for 1 hour. PMDETA (0.10 mL, 0.5 mmol) was then added giving a slightly cloudy solution. Gentle heating gave a clear solution which was left to cool slowly. After 16 hours a crop of large crystals was isolated (0.05 g, 26%). $^1$H NMR (400.13 MHz, 298 K, $C_6D_6$) δ -1.90 (8H, s, SiC$H_2$), 0.52 (36H, s, Si(C$H_3$)$_3$), 1.82 (16H, s, NC$H_2$, PMDETA), 2.07 (30H, s, NC$H_3$, PMDETA). $^{13}$C {$^1$H} NMR (100.62 MHz, 298 K, $C_6D_6$) δ -3.73 (Si*C*H$_2$), 6.09 (Si(*C*H$_3$)$_3$), 44.35 (*C*H$_3$, PMDETA), 45.81 ((*C*H$_3$)$_2$, PMDETA), 54.30 (*C*H$_2$, PMDETA), 57.10 (*C*H$_2$, PMDETA).

### 8.3.10 Synthesis of $[(TMEDA)_2K_2Mg(CH_2SiMe_3)_4]$ (10)

To a suspension of $KCH_2SiMe_3$ (0.24 g, 2 mmol) in hexane (15 mL) $Mg(CH_2SiMe_3)_2$ (0.20 g, 1 mmol) was added and the suspension stirred for 1 hour. TMEDA (0.30 mL, 2 mmol) was then added and the almost clear solution transferred to the freezer (-28 °C). After 16 hours a crop of peach crystals was isolated (0.41 g, 60%). $^1$H NMR (400.03 MHz, 298 K, $C_6D_6$) δ -1.74 and -1.70 (2H, overlapping s, SiC$H_2$), 0.40 and 0.41 (9H, overlapping s, Si(C$H_3$)$_3$), 1.93 and 1.94 (8H, overlapping s, TMEDA). $^{13}$C {$^1$H} NMR (100.62 MHz, 298 K, $C_6D_6$) δ -0.03 (Si*C*H$_2$), 1.67 (Si*C*H$_2$), 5.64 (Si(*C*H$_3$)$_3$), 45.53 (N(*C*H$_3$)$_2$, TMEDA), 57.31 (N*C*H$_2$, TMEDA).

### 8.3.11 Synthesis of $[(PMDETA)_2K_2Mg(CH_2SiMe_3)_4]$ (11)

To a suspension of $KCH_2SiMe_3$ (0.12 g, 1 mmol) in hexane (15 mL) $Mg(CH_2SiMe_3)_2$ (0.2 g, 1 mmol) was added and the suspension stirred for 1 hour. PMDETA (0.10 mL, 0.5 mmol) was then added giving a clear solution with a yellow oil deposited at the bottom of the Schlenk. The Schlenk was transferred to the freezer (-28 °C) overnight. A crop of clear, colourless crystals was isolated (0.20 g, 50%). $^1$H NMR (400.13 MHz, 298 K, $C_6D_6$) δ -1.56 (8H, s, SiC*H*$_2$), 0.47 (36H, s, Si(C*H*$_3$)$_3$), 1.72-1.76 (16H, m, NC*H*$_2$, PMDETA), 1.83 (6H, s, NC*H*$_3$, PMDETA), 1.91 (24H, s, N(C*H*$_3$)$_2$, PMDETA). $^{13}$C {$^1$H} NMR (100.62 MHz, 298 K, $C_6D_6$) δ 0.00 (Si*C*H$_2$), 5.34 (Si(*C*H$_3$)$_3$), 44.09 (*C*H$_3$, PMDETA), 46.05 ((*C*H$_3$)$_2$, PMDETA), 54.83 (*C*H$_2$, PMDETA), 56.63 (*C*H$_2$, PMDETA).

### 8.3.12 Synthesis of $[\{NaMg(CH_2SiMe_3)_3\}_\infty]$ (12)

To a suspension of $NaCH_2SiMe_3$ (0.11 g, 1 mmol) in hexane (15 mL) $Mg(CH_2SiMe_3)_2$ (0.20 g, 1 mmol) was added and the resulting suspension stirred for 1 hour. 2 mL of toluene were then introduced and the mixture was gently heated. The resulting colourless solution was allowed to cool slowly to room temperature affording a crop of colourless crystals (0.15 g, 49%). $^1$H NMR (400.13 MHz, 298 K, $C_6D_6$) δ (ppm) -1.71 (6H, s, SiC*H*$_2$), 0.28 (27H, s, Si(C*H*$_3$)$_3$). $^{13}$C {$^1$H} NMR (100.62 MHz, 298 K, $C_6D_6$) δ (ppm) -2.16 (Si(*C*H$_3$)$_3$), 4.54 (Si*C*H$_2$).

### 8.3.13 Reaction of $2NaCH_2SiMe_3$ with $Mg(CH_2SiMe_3)_2$: preparation of (13)

To a suspension of $NaCH_2SiMe_3$ (0.11 g, 1 mmol) in hexane (15 mL) $Mg(CH_2SiMe_3)_2$ (0.10 g, 0.5 mmol) was added and the resulting suspension was stirred for 1 hour. 5 mL of toluene were then introduced and the mixture was gently heated. The resulting colourless solution was allowed to cool slowly to room temperature depositing colourless crystals. Analysis of these crystals by X-ray crystallography revealed that the constitution of some of these crystals was **12** while some were found to be **13**.

### 8.3.14 Synthesis of $[Na_2Mg(CH_2SiMe_3)_4]$ (14)

To a suspension of $NaCH_2SiMe_3$ (0.11 g, 1 mmol) in hexane (15 mL) $Mg(CH_2SiMe_3)_2$ (0.10 g, 0.5 mmol) was added and the resulting suspension was stirred for 1 hour after which all solvent was removed and the resulting solid analysed by NMR spectroscopy. $^1$H NMR (400.13 MHz, 298 K, $C_6D_6$) δ (ppm) -1.88 (2H, s, Si$CH_2$), 0.22 (9H, s, Si($CH_3$)$_3$). $^{13}$C {$^1$H} NMR (100.62 MHz, 298 K, $C_6D_6$) δ (ppm) 0.01 (Si($CH_3$)$_3$), 7.10 (Si$CH_2$).

### 8.3.15 Synthesis of $[\{NaMg(CH_2SiMe_3)_2(OCH_2SiMe_3)\}_\infty]$ (15)

To a stirred suspension of $NaCH_2SiMe_3$ (0.11 g, 1 mmol) in hexane (15 mL) $Mg(CH_2SiMe_3)_2$ (0.20 g, 1 mmol) was added and the resulting white suspension was stirred at room temperature for 1 h. The volume was reduced by approximately half under reduced pressure and 3 mL of benzene were then introduced and the mixture was gently heated. A drying tube was fitted for 1 h and the reaction was stirred overnight. The solvent was removed *in vacuo* and 5 mL of hexane were added with gentle heating. Allowed to cool slowly to room temperature, the resulting colourless solution afforded a crop of colourless crystals: 0.03 g, 15%. $^1$H NMR (400.03 MHz, 298 K, $C_6D_6$) δ (ppm) -2.12 (4H, s, Si$CH_2$), -0.04 (9H, s, Si($CH_3$)$_3$), -0.35 (18H, s, OSi($CH_3$)$_3$), 3.43 (2H, s, O$CH_2$). $^{13}$C {$^1$H} NMR (100.62 MHz, 298 K, $C_6D_6$) δ (ppm) -6.00 (M$CH_2$), -2.61 (OCH$_2$Si($CH_3$)$_3$), 4.65 (MCH$_2$Si($CH_3$)$_3$), 55.37 (O$CH_2$).

### 8.3.16 Synthesis of $[\{KMg(CH_2SiMe_3)_3\}_\infty]$ (16)

To a suspension of $KCH_2SiMe_3$ (0.12 g, 1 mmol) in hexane (15 mL) $Mg(CH_2SiMe_3)_2$ (0.20 g, 1 mmol) was added and the resulting suspension stirred for 1 hour. 2 mL of toluene were then introduced and the mixture was gently heated. The resulting colourless solution was allowed to cool slowly to room temperature affording a crop of colourless crystals of **x** was isolated (0.16 g, 49%). $^1$H NMR (400.13 MHz, 298 K, $C_6D_6$) δ (ppm) -1.68 (6H, s, Si$CH_2$), 0.35 (27H, s, Si($CH_3$)$_3$). $^{13}$C {$^1$H} NMR (100.62 MHz, 298 K, $C_6D_6$) δ (ppm) -0.04 (Si($CH_3$)$_3$), 4.74 (Si$CH_2$).

### 8.3.17 Synthesis of [{($C_6H_6$)KMg($CH_2SiMe_3$)$_3$}$_\infty$] (17)

To a suspension of $KCH_2SiMe_3$ (0.12 g, 1 mmol) in hexane (15 mL) $Mg(CH_2SiMe_3)_2$ (0.20 g, 1 mmol) was added and the resulting suspension stirred for 1 hour. The solution was concentrated *in vacuo* (to approx. 8 mL) and benzene (4 mL) added. Gentle heating resulted in a clear colourless solution which was allowed to cool slowly to room temperature. A crop of clear colourless crystals was isolated (0.18 g, 45%). $^1$H NMR (400.13 MHz, 298 K, $d_8$-toluene) δ -1.72 (6H, s, SiC$H_2$), 0.28 (27H, s, Si(C$H_3$)$_3$), 7.13 (2H, C*H*, benzene).

### 8.3.18 Synthesis of [{($Cp_2Fe$)KMg($CH_2SiMe_3$)$_3$}$_\infty$] (18)

To a suspension of $KCH_2SiMe_3$ (0.12 g, 1 mmol) in hexane (15 mL) $Mg(CH_2SiMe_3)_2$ (0.20 g, 1 mmol) was added and the resulting suspension stirred for 1 hour. Ferrocene (0.18 g, 1 mmol) was then added and the resulting orange suspension was stirred overnight. Toluene (1 mL) was introduced giving a clear orange solution. Transferring the schlenk to the freezer (-28 °C) overnight gave a crop of yellow crystals which was isolated (0.22 g, 26%). $^1$H NMR (400.13 MHz, 298 K, $C_6D_6$) δ (ppm) -1.67 (6H, s, SiC$H_2$), 0.36 (27H, s, Si(C$H_3$)$_3$), 4.01 (4H, s, C*H* (Cp)). $^{13}$C {$^1$H} NMR (100.62 MHz, 298 K, $C_6D_6$) δ (ppm) -0.00 (Si(*C*H$_3$)$_3$), 4.74 (Si*C*H$_2$), 68.06 (*C*H (Cp)).

### 8.3.19 Synthesis of [{(THF)$_3$K(μ-$CH_2SiMe_3$)(μ-OCH=$CH_2$)Mg($CH_2SiMe_3$)}$_2$] (19)

THF (10 mL) was added to $KCH_2SiMe_3$ (0.12 g, 1 mmol) giving a bright yellow solution. After 5 minutes $Mg(CH_2SiMe_3)_2$ (0.2 g, 1 mmol), paling the solution to a straw colour, and stirred for 30 minutes. The schlenk contents were concentrated to approximately 3 mL and hexane (3 mL) added and the solution transferred to the freezer. Storage for 3 days at -28 °C gave no solid and so all volatiles were removed and hexane added (3 mL) followed by THF (0.3 mL) and the reaction removed to the freezer which gave a crop of crystals overnight (0.10 g, 20%). $^1$H NMR (400.13 MHz, 298 K, $C_6D_6$) δ -1.98 (4H, s, SiC$H_2$), 0.38 (18H, s, Si(C$H_3$)$_3$), 1.37 (2H, m, C$H_2$, THF), 3.50 (2H, m, OC$H_2$, THF), 3.82 (1H, d, alkene =C$H_2$ $^3J$ = 5.6 Hz), 4.04 (1H, d, alkene =C$H_2$ $^3J$ = 14.0 Hz), 6.86 (1H, dd, alkene =C*H* $^3J$ = 5.6, 14.0 Hz). $^{13}$C

{$^1$H} NMR (100.62 MHz, 298 K, $C_6D_6$) δ -3.83 (Si*C*$H_2$), 4.84 (Si(*C*$H_3$)$_3$), 25.41 (*C*$H_2$, THF), 68.93 (O*C*$H_2$, THF), 88.57 (=*C*$H_2$), 153.71 (=*C*H).

### 8.3.20 Attempted preparation of 20 with 17

To a suspension of $KCH_2SiMe_3$ (0.12 g, 1 mmol) in hexane (15 mL) $Mg(CH_2SiMe_3)_2$ (0.20 g, 1 mmol) was added and the resulting suspension stirred for 1 hour. 2 mL of benzene were then introduced and the mixture was gently heated. Thiophene (0.24 mL, 3 mmol) was then introduced and the clear solution stirred for 1 h at room temperature before $I_2$ (7 mL of a 1 M solution in THF, 7 mmol) was added and stirred overnight. The reaction was quenched with $NH_4Cl$ and sodium thiosulfate then extracted with DCM. The combined organic phase was washed with brine, dried over sodium sulfate and concentrated. Crude $^1$H NMR and GC analysis showed no starting material or product present.

### 8.3.21 Attempted preparation of 21 with 17

To a suspension of $KCH_2SiMe_3$ (0.06 g, 0.5 mmol) in hexane (10 mL) $Mg(CH_2SiMe_3)_2$ (0.10 g, 0.5 mmol) was added and the resulting suspension stirred for 1 hour. 2 mL of benzene were then introduced and the mixture was gently heated. Anisole (0.054 mL, 0.5 mmol) was then introduced and the clear solution stirred for 1 h at room temperature before $I_2$ (4 mL of a 1 M solution in THF, 4 mmol) was added and stirred overnight. The reaction was quenched with $NH_4Cl$ and sodium thiosulfate then allowed to settle. An aliquot of the organic phase was diluted with $Et_2O$ and analysed by gas chromatography showing only starting material.

### 8.3.22 General procedure for the attempted preparation of 21 with an *in situ* mixture of KR:$MgR_2$:PMDETA

To a suspension of $KCH_2SiMe_3$ (0.06 g, 0.5 mmol) in hexane (10 mL) $Mg(CH_2SiMe_3)_2$ (0.10 g, 0.5 mmol) was added and the suspension stirred for 1 hour. PMDETA (0.11 mL, 0.5 mmol) was then added giving a clear peach solution. Anisole was then introduced at r.t. giving an instant suspension that was stirred for 1 h before $I_2$ (4 mL of a 1 M solution in THF, 4 mmol) was added and stirred

overnight. The reaction was quenched with $NH_4Cl$ and sodium thiosulfate then allowed to settle. An aliquot of the organic phase was diluted with $Et_2O$ and analysed by gas chromatography.

Following the **General Procedure**, data are presented as (a) equivalents of anisole and (b) conversion (SM:Product).

***Entry 1*** (a) 1 eq. (0.054 mL, 0.5 mmol) and (b) 100:0

***Entry 2*** (a) 2 eq. (0.11 mL, 1 mmol) and (b) 100:0

***Entry 3*** (a) 3 eq. (0.16 mL, 1.5 mmol) and (b) 100:0

### 8.3.23 Synthesis of 2-iodoanisole (21)

To a suspension of $KCH_2SiMe_3$ (0.12 g, 1 mmol) in hexane (10 mL) $Mg(CH_2SiMe_3)_2$ (0.10 g, 0.5 mmol) was added and the suspension stirred for 1 hour. PMDETA (0.21 mL, 1 mmol) was then added giving a clear peach solution. Anisole (0.22 mL, 2 mmol) was then introduced at r.t. giving an instant suspension that was stirred for 1 h before $I_2$ (4 mL of a 1 M solution in THF, 4 mmol) was added and stirred overnight. The reaction was quenched with $NH_4Cl$ and sodium thiosulfate then allowed to settle. An aliquot of the organic phase was diluted with $Et_2O$ and analysed by gas chromatography showing a conversion of 19:81 starting material:product.

### 8.3.24 General procedure for metallation of organic substrates and iodine quench with an *in situ* mixture of 11

To a suspension of $KCH_2SiMe_3$ (0.12 g, 1 mmol) in hexane (10 mL) $Mg(CH_2SiMe_3)_2$ (0.10 g, 0.5 mmol) was added and the suspension stirred for 1 hour. PMDETA (0.21 mL, 1 mmol) was then giving a clear peach solution. 4 equivalents of organic substrate were then introduced at temperature, T, and stirred for 1 h before $I_2$ (4 mL of a 1 M solution in THF, 4 mmol) was added and stirred overnight. The reaction was quenched with $NH_4Cl$ and sodium thiosulfate then allowed to settle. An aliquot of the organic phase was diluted with $Et_2O$ and analysed by gas chromatography.

Following the **General Procedure**, data are presented as (a) organic substrate (b) temperature, T and (c) conversion to product/%.

***Entry 1*** (a) 4-Methoxypyridine (0.20 mL, 2 mmol) (b) 0 °C and (c) >99

***Entry 2*** (a) Trifluorotoluene (0.25 mL, 2 mmol) (b) 0 °C and (c) >99 (22:78

*ortho*:*meta*)

(a) Trifluorotoluene (0.25 mL, 2 mmol) (b) r.t. and (c) >99 (68:32 *ortho*:*meta*)

***Entry 3*** (a) *N*,*N*-diisopropylbenzamide (0.41 g, 2 mmol) (b) 0 °C and (c) 98

(a) *N*,*N*-diisopropylbenzamide (0.41 g, 2 mmol) (b) r.t. and (c) 56

***Entry 4*** (a) Methylbenzimidazole (0.26 g, 2 mmol) (b) 0 °C and (c) 90

(a) Methylbenzimidazole (0.26 g, 2 mmol) (b) r.t. and (c) 64

***Entry 5*** (a) Anisole (0.22 mL, 2 mmol) (b) 0 °C and (c) 42

(a) Anisole (0.22 mL, 2 mmol) (b) r.t. and (c) 81

***Entry 6*** (a) Thiophene (0.16 mL, 2 mmol) (b) 0 °C and (c) 65

(a) Thiophene (0.16 mL, 2 mmol) (b) r.t. and (c) 87

***Entry 7*** (a) Pyrazine-*N*-oxide (0.19 g, 2 mmol) (b) 0 °C and (c) 0

***Entry 8*** (a) Pyridazine (0.16 g, 2 mmol) (b) 0 °C and (c) 0

***Entry 9*** (a) Pyrazine (0.16 g, 2 mmol) (b) 0 °C and (c) 0

***Entry 10*** (a) Chlorobenzene (0.20 mL, 2 mmol) (b) 0 °C and (c) 0

(a) Chlorobenzene (0.20 mL, 2 mmol) (b) r.t. and (c) 0

***Entry 11*** (a) 4-Trifluoromethyl pyridine (0.23 mL, 2 mmol) (b) 0 °C and (c) 0

(a) 4-Trifluoromethyl pyridine (0.23 mL, 2 mmol) (b) r.t. and (c) 0

### 8.3.25 Preparation of [(THF)Li(μ-TMP)(μ-*t*Bu)Zn(*t*Bu)] (22)[221]

A solution of $t$Bu$_2$Zn (0.36 g, 2 mmol) in hexane (5 mL) was transferred by cannula to a solution of LiTMP [prepared *in situ* by reaction of BuLi (1.25 mL of a 1.6 M solution in hexane, 2 mmol) and TMP(H) (0.34 mL, 2 mmol)]. The colourless solution was allowed to stir for 10 min and THF (0.16 mL, 2 mmol) was then introduced. The solution was concentrated by removing some solvent under vacuum and placed in the freezer (-28 °C). A crop of colourless crystals was deposited overnight (typical yield: 0.64 g, 80%). $^1$H NMR (400.13 MHz, 298 K d$_8$-THF) δ ppm: 0.90 (s, 18H, *t*Bu), 1.01 (s, 12H, C*H*$_3$-TMP), 1.20 (m, 4H, β-TMP), 1.66 (m, 2H, γ-TMP), 1.79 (m, 4H, THF), 3.69 (m, 4H, THF). $^{13}$C {$^1$H} (100.62 MHz, 298 K, d$_8$-THF) δ ppm: 20.40 (γ-TMP), 22.02 (q *t*Bu), 26.39 (THF), 34.87 (*C*H$_3$-TMP), 36.39 (*C*H$_3$, *t*Bu), 41.57 (β-TMP), 53.10 (α-TMP), 68.39 (THF). $^7$Li (155.50 MHz, 298 K, d$_8$-THF) δ ppm: 2.86.

### 8.3.26 Synthesis of [2,5-{(THF)$_2$LiZn(TMP)(*t*Bu)}$_2$($C_4N_2H_2$)] (24)

To a solution of **22** (0.8 g, 2 mmol) in 3 mL of THF at 0 °C was added 1,4-pyrazine (0.08 g, 1 mmol) giving an instant bright orange coloured solution. The reaction was allowed to stir at 0 °C for 5 minutes before 1.5 mL of hexane were added and the solution transferred to the refrigerator (-5 °C) to crystallise. After 24 hours a crop of bright orange/red needle crystals were deposited (0.46 g, 51%). $^1$H (400.13 MHz, 298 K, $C_6D_6$) δ ppm: 1.13 (s br, 6H, Me-TMP), 1.29 (s br, 2H, β-TMP), 1.41 (s br, 8H, THF), 1.42 (s br, 6H, Me-TMP), 1.58 (s br, 2H, β-TMP), 1.62 (s br, 1H, γ-TMP), 1.75 (s br, 9H, *t*Bu), 1.92 (s br, 1H, γ-TMP), 3.48 (m, 8H, THF), 9.19 (s, 1H, *H*-pyrazine). $^{13}$C {$^1$H} (100.62 MHz, 298 K, $C_6D_6$) δ ppm: 19.84 (γ-TMP), 20.81 (q-*t*Bu), 25.42 (THF), 33.52 (Me-TMP), 35.07 (Me-TMP), 35.30 (*t*Bu), 40.18 (β-TMP), 52.89 (q-TMP), 68.14 (THF), 155.35 (C-H pyrazine), 187.13 (C-Zn).

### 8.3.27 Synthesis of 2,5-diiodopyrazine[235]

To a solution of **24** in THF, $I_2$ (7 mL of a 1 M solution in THF, 7 mmol) was added at 0 °C and allowed to stir for 18 hours at room temperature before addition of saturated aq $NH_4Cl$ (10 mL) and saturated aq $Na_2S_2O_3$ until bleaching (5 mL). The product was extracted with DCM (3 X 10 mL) and the combined organic phases dried ($MgSO_4$), filtered and concentrated under reduced pressure. The product was purified by column chromatography on silica gel (eluent DCM:Hexane 1:1) to give 2,5-diiodopyrazine as an off-white crystalline solid (0.21 g, 63%). $^1$H (400.13 MHz, 298 K, $CDCl_3$) δ ppm: 8.63 (s, 2H). $^{13}$C {$^1$H} (100.62 MHz, 298 K, $CDCl_3$) δ ppm: 116.50 (C-I pyrazine), 153.76 (C-H pyrazine) agree with those reported in the literature.

### 8.3.28 Preparation of [(PMDETA)LiZn(*t*Bu)$_3$] (23)

To a solution of *t*Bu$_2$Zn (0.09 g, 0.5 mmol) in hexane (5 mL) *t*BuLi (0.26 mL of a 1.7 M solution, 0.5 mmol) was added to give a colourless solution which was stirred for 1 h. PMDETA (0.11 mL, 0.5 mmol) was added to give a white precipitate. Following 1 h of stirring all volatiles were removed. $^1$H NMR (400.13 MHz, 298 K d$_8$-THF) δ ppm: 0.91 (s, 27H, *t*Bu), 2.24 (s, 12H, PMDETA-(C*H*$_3$)$_2$), 2.33 (s, 3H, PMDETA-C*H*$_3$), 2.41 (t, 4H, PMDETA-C*H*$_2$), 2.51 (t, 4H, PMDETA-C*H*$_2$). $^{13}$C {$^1$H} (100.62

MHz, 298 K, $d_8$-THF) δ ppm: 23.93 (q-*t*Bu), 36.56 (*t*Bu), 43.90 (PMDETA-*C*$H_3$), 45.88 (PMDETA-(*C*$H_3$)$_2$), 55.39 (PMDETA-*C*$H_2$), 58.21 (PMDETA-*C*$H_2$).

### 8.3.29 Synthesis of [(PMDETA)Li{$C_4N_2H_4$(*t*Bu)}Zn(*t*Bu)$_2$] (25)

To a solution of *t*Bu$_2$Zn (0.36 g, 2 mmol) in hexane (10 mL) *t*BuLi (1.17 mL of a 1.7 M solution, 2 mmol) was added to give a colourless solution. PMDETA (0.42 mL, 2 mmol) was added to give a white precipitate. The suspension was allowed to stir at room temperature for 10 minutes before pyrazine (0.16 g, 2 mmol) was added at room temperature, forming a bright yellow oil, and the reaction mixture was placed in the freezer (-28 °C). After 24 hours a crop of bright yellow crystals were deposited (0.76 g 76%). $^1$H (400.13 MHz, 298 K, $C_6D_6$) δ ppm: 1.19 (s, 9H, *t*Bu-pyrazine), 1.59 (s br, 18H, 2x *t*Bu-Zn), 1.71 (s br, 3H, PMDETA-C*H*$_3$), 1.78 (s br, 12H PMDETA-C*H*$_3$), 1.82 (s br, 8H, PMDETA-C*H*$_2$), 4.08 (s br, 1H, C*H* pyrazine *t*Bu), 5.37 (s br, 1H, pyrazine), 5.59 (s br, 1H, pyrazine), 7.16 (s br, 1H, pyrazine). $^{13}$C {$^1$H} (100.62 MHz, 298 K, $C_6D_6$) δ ppm: 22.62 (q-*C* *t*Bu-Zn), 25.35 (*t*Bu-pyrazine ring), 35.55 (Zn-*t*Bu), 40.72 (q-*C*-*t*Bu pyrazine ring), 43.73 (PMDETA-*C*$H_2$), 44.95 (PMDETA-*C*$H_3$), 53.21 (PMDETA-*C*$H_3$), 56.73 (PMDETA-*C*$H_3$), 66.28 (*C*-*t*Bu-pyrazine), 107.29 (*C*H pyrazine), 123.44 (*C*H pyrazine), 145.21 (*C*H pyrazine).

### 8.3.30 Synthesis of 2-*tert*-butyl pyrazine (26)

To a solution of *t*Bu$_2$Zn (0.36 g, 2 mmol) in hexane (10 mL) *t*BuLi (1.17 mL of a 1.7 M solution, 2 mmol) was added to give a colourless solution. PMDETA (0.42 mL, 2 mmol) was added to give a white precipitate. The suspension was allowed to stir at room temperature for 10 minutes before pyrazine (0.16 g, 2 mmol) was added and the reaction mixture stirred at room temperature for 1 hour. The reaction was then quenched with $H_2O$ (5 mL) and the product extracted with DCM (3 x 10 mL). The combined organic phases were dried with $MgSO_4$, filtered and evaporated under reduced pressure. The crude product was then purified by column chromatography on silica gel (eluent : DCM then DCM:EtOAc 4:1) to give the product as an yellow oil (0.22 g, 82%). $^1$H (400.13 MHz, 298 K, $CDCl_3$) δ ppm: 1.40 (s, 9H, *t*Bu), 8.39 (d, 1H, pyrazine), 8.51 (t, 2H, pyrazine), 8.85 (d, 1H, pyrazine). $^{13}$C {$^1$H} (100.62 MHz,

298 K, $CDCl_3$) δ ppm: 29.78 (*C*-*t*Bu), 141.59 (*C*H pyrazine), 141.72 (*C*H pyrazine), 143.29 (*C*H pyrazine), agree with those reported in the literature.

### 8.3.31 Synthesis of [{Zn*t*Bu$_2$}$_3${C$_4$N$_2$H$_4$}$_4$] (27)

To a solution of *t*Bu$_2$Zn (0.36 g, 2 mmol) in hexane (10 mL) pyrazine (0.16 g, 2 mmol) was added to give an orange solution. The solution was placed in the freezer (-28 °C) and a crop of red needles deposited after 24 h (0.18 g, 84% based on pyrazine). $^1$H NMR (400.13 MHz, 298 K $d_8$-THF) δ ppm: 0.96 (s, 54H, *t*Bu), 8.57 (s br, 16H, pyrazine), and also some residual hexane solvent at 1.27, 0.86. $^{13}$C {$^1$H} (100.62 MHz, 298 K, $d_8$-THF) δ ppm: 32.96 (*t*Bu), 145.90 (pyrazine) and 32.41, 23.40 and 14.44 (residual hexane).

### 8.3.32 Synthesis of [(THF)$_2$Li$_2$(O*t*Bu)$_2$Zn(*o*-C$_6$H$_4$-OMe)$_2$] (28)

*Method A (using ZnEt$_2$)*

To a solution of LiO*t*Bu (0.16 g, 2 mmol) in THF (10 mL) $ZnEt_2$ (1 mL of a 1 M solution, 1 mmol) was added and the resulting clear solution stirred for 30 minutes. 2-Iodoanisole (0.26 mL, 2 mmol) was then introduced and the solution stirred for 30 minutes before being concentrated to approximately 3 mL. Heating gave a clear solution that was transferred to the freezer (-28 °C) for 16 h depositing a crop of colourless crystals (0.25 g, 43%).

*Method B (using Zn*t*Bu$_2$)*

To a solution of Zn*t*Bu$_2$ (0.36 g, 2 mmol) in THF (15 mL) LiO*t*Bu (0.32 g, 4 mmol) was added and the resulting clear solution stirred for 30 minutes. 2-Iodoanisole (0.52 mL, 4 mmol) was then introduced and the solution stirred for 30 minutes before being concentrated to approximately 3 mL. Heating gave a clear solution that was transferred to the freezer (-28 °C) for 16 h depositing a crop of colourless crystals (0.60 g, 51%).

$^1$H NMR (400.13 MHz, 298 K, $C_6D_6$) δ 1.11 (9H, s, OC(C*H*$_3$)$_3$), 1.31 (9H, s, OC(C*H*$_3$)$_3$), 1.42 (8H, m, C*H*$_2$, THF), 3.58 (8H, m, OC*H*$_2$, THF), 3.66 (3H, s, OC*H*$_3$, anisole), 6.76 (1H, d, Ar*H*), 7.20-7.29 (2H, m, Ar*H*), 8.28 (1H, d, Ar*H*). $^{13}$C {$^1$H} NMR (100.62 MHz, 298 K, $C_6D_6$) δ 25.71, 33.32, 35.73, 56.83, 67.80, 110.18,

123.01, 126.93, 141.43, 148.68, 164.94. $^{7}$Li NMR (155.50 MHz, 298 K, $C_6D_6$) δ 1.05.

### 8.3.33 General reaction conditions for the synthesis of (2-methoxyphenyl)phenyl-methanol (29)[124]

To a solution of MO*t*Bu in THF $ZnR_2$ was added and the resulting clear solution stirred for 30 minutes. 2-Iodoanisole was then introduced and the solution stirred. Following the reaction time PhCHO was added and the solution stirred for 24 hours at room temperature. The reaction was quenched with $NH_4Cl$ and extracted with $Et_2O$. The combined organic phase was washed with brine, dried over sodium sulfate and concentrated. When further purification was carried out this was performed *via* silica column chromatography (hexane to 20% ethyl acetate in hexane gradient eluent).

Following the **General Procedure**, data are presented as (a) MO*t*Bu species and quantity added, (b) quantity of THF added, (c) $ZnR_2$ species and quantity added, (d) quantity of 2-iodoanisole added, (e) reaction temperature, (f) stir time, (g) quantity of PhCHO added, (h) conversion (SM:Product) and (i) isolated yield.

***Entry 1*** (a) LiO*t*Bu (0.16 g, 2 mmol), (b) 10 mL, (c) $ZnEt_2$ (1 mL of a 1 M solution, 1 mmol), (d) 0.26 mL, 2 mmol, (e) reflux, (f) 2.5 h, (g) 0.56 mL, (h) 1:1.54 and (i) 0.0653 g, 15%.

***Entry 2*** (a) LiO*t*Bu (0.16 g, 2 mmol), (b) 10 mL, (c) $ZnEt_2$ (1 mL of a 1 M solution, 1 mmol), (d) 0.26 mL, 2 mmol, (e) room temperature, (f) 24 h, (g) 0.56 mL, (h) 0:1 and (i) 0.1569 g, 37%.

***Entry 3*** (a) LiO*t*Bu (0.32 g, 4 mmol), (b) 15 mL, (c) $ZnEt_2$ (2 mL of a 1 M solution, 2 mmol), (d) 0.52 mL, 4 mmol, (e) room temperature, (f) 4 h, (g) 1.1 mL, (h) 1:0.05 and (i) -.

***Entry 4*** (a) LiO*t*Bu (0.80 g, 10 mmol), (b) 20 mL, (c) $ZnEt_2$ (5 mL of a 1 M solution, 5 mmol), (d) 1.30 mL, 10 mmol, (e) room temperature, (f) 24 h, (g) 2.8 mL, (h) 0:1 and (i) 0.6790 g, 32%.

***Entry 5*** (a) LiO*t*Bu (0.02 g, 0.2 mmol), (b) 10 mL, (c) $ZnEt_2$ (2 mL of a 1 M solution, 2 mmol), (d) 0.52 mL, 4 mmol, (e) room temperature, (f) 24 h, (g) 1.1 mL, (h) 1:0 and (i) -.

***Entry 6*** (a) Li*O*t*Bu* (0.32 g, 4 mmol), (b) 15 mL, (c) Zn*t*Bu$_2$ (0.36 g, 2 mmol), (d) 0.52 mL, 4 mmol, (e) room temperature, (f) 2.5 h, (g) 1.1 mL, (h) 1:0.75 and (i) -.

***Entry 7*** (a) Li*O*t*Bu* (0.32 g, 4 mmol), (b) 15 mL, (c) Zn*t*Bu$_2$ (0.36 g, 2 mmol), (d) 0.52 mL, 4 mmol, (e) room temperature, (f) 24 h, (g) 1.1 mL, (h) 1:0.65 and (i) -.

***Entry 8*** (a) Na*O*t*Bu* (0.34 g, 4 mmol), (b) 15 mL, (c) $ZnEt_2$ (2 mL of a 1 M solution, 2 mmol), (d) 0.52 mL, 4 mmol, (e) reflux, (f) 2.5 h, (g) 1.1 mL, (h) 1:0.47 and (i) 0.0928 g, 11%.

***Entry 9*** (a) K*O*t*Bu* (0.45 g, 4 mmol), (b) 15 mL, (c) $ZnEt_2$ (2 mL of a 1 M solution, 2 mmol), (d) 0.52 mL, 4 mmol, (e) reflux, (f) 2.5 h, (g) 1.1 mL, (h) 1:0 and (i) -.

$^1$H NMR (400.13 MHz, 298 K, $CDCl_3$) δ (ppm) 3.03 (1H, d, *J* = 5.6 Hz, O*H*), 3.83 (3H, s, OC$H_3$), 6.07 (1H, d, *J* = 5.6 Hz, PhC*H*(OH)(Ar)), 6.90 (1H, d, *J* = 8.4 Hz), 6.96 (1H, dt, *J* = 7.6, 1.2 Hz), 7.24-7.28 (3H, m, ring), 7.32-7.36 (2H, m, ring), 7.40-7.42 (2H, m, ring). $^{13}$C {$^1$H} NMR (100.62 MHz, 298 K, $CDCl_3$) δ (ppm) 55.4, 72.2, 110.8, 120.8, 126.5, 127.1, 127.8, 128.1, 128.7, 131.9, 143.2, 156.7.

### 8.3.34 Synthesis of [(THF)$_2$Li$_2$(O*t*Bu)$_2$Mg(*o*-C$_6$H$_4$-OMe)$_2$] (28-Mg)

To a solution of Li*O*t*Bu* (0.16 g, 2 mmol) in THF (10 mL) *n*Bu$_2$Mg (1 mL of a 1 M solution, 1 mmol) was added and the resulting clear solution stirred for 30 minutes. 2-Bromoanisole (0.25 mL, 2 mmol) was then introduced and the solution stirred for 30 minutes before being concentrated to approximately 3 mL. Transferring to the freezer (-28 °C) for 4 days gave a crop of colourless crystals. $^1$H NMR showed a mixture of products.

### 8.3.35 Synthesis of [{(THF)Li(O*t*Bu)$_2$ZnEt}$_2$] (30)

To a suspension of Li*O*t*Bu* (0.16 g, 2 mmol) in hexane (10 mL) $ZnEt_2$ (1 mL of a 1 M solution, 1 mmol) was added and the resulting suspension stirred for 30 minutes. THF (0.32 mL, 4 mmol) were then introduced and the mixture stirred for 15 minutes. Removal of the Schlenk to the freezer resulted in the formation of clear, colourless crystals after 4 days, 0.04 g, 13%. $^1$H NMR (400.13 MHz, 298 K, $C_6D_6$) δ 0.11 (2H,

q, Zn$CH_2$), 1.14 (3H, t, $ZnCH_2CH_3$), 1.28 (18H, s, $OC(CH_3)_3$), 1.31 (4H, m, $CH_2$, THF), 3.57 (4H, m, $OCH_2$, THF). $^7$Li NMR (155.50 MHz, 298 K, $C_6D_6$) δ 1.00. $^{13}$C {$^1$H} NMR could not be collected due to the relative insolubility of the product.

### 8.3.36 Preparation of IPr (31)[212a]

To a solution of 2,6-diisoproylphenylamine (52.4 mL, 0.28 mol) in propanol (200 mL) were added glyoxal (14.3 mL of a 40% solution in water) in propanol (20 mL) and water (50 mL). After stirring at 70 °C for 1 h, water (200 mL) was added and the resulting precipitate collected and recrystallized from acetone to give the diimine (average yield after two crops 42 g, 80%).

A Schlenk was charged with the diimine (6.89 g, 18.3 mmol) and evacuated three times. THF (40 mL) was charged followed by chloromethylethyl ether (1.8 mL, 18.3 mmol) and 2 drops of water. The mixture was stirred overnight at 40 °C and the colourless imidazolium salt isolated (average yield 3.90 g, 50%).

Imidazolium salt (4.55 g, 10.7 mmol) was dissolved in THF (50 mL) and the suspension stirred for 15 minutes. KO*t*Bu (1.28 g, 11.4 mmol) and the orange solution stirred for 20 minutes after which the solvent was exchanged *in vacuo* for toluene. After filtration through celite and glass wool, all volatiles were removed to give the product as an off-white solid (average yield 4.1 g, 98%).$^1$H NMR (400.13 MHz, 298 K, $C_6D_6$) δ 1.19 (12H, d, $CH(CH_3)_2$), 1.29 (12H, d, $CH(CH_3)_2$), 2.97 (4H, septet, $CH(CH_3)_2$), 6.63 (2H, s, imidazole backbone C*H*), 7.19 (4H, d, *m*-C*H*), 7.29 (2H, t, *p*-C*H*). $^{13}$C {$^1$H} NMR (100.62 MHz, 298 K, $C_6D_6$) δ (ppm) 23.56 ($CH(CH_3)_2$), 24.78 ($CH(CH_3)_2$), 28.74 ($CH(CH_3)_2$), 121.49 (imidazole backbone *C*H), 123.64 (*m*-*C*H), 128.97 (*p*-*C*H), 138.94 (*i*-*C*), 146.23 (*o*-*C*H), 220.52 (*C*:).

### 8.3.37 Preparation of IMes (32)[212a]

To a solution of 2,4,6-trimethylphenylamine (70.3 mL, 0.5 mol) in propanol (300 mL) were added glyoxal (28.6 mL of a 40% solution in water) in propanol (100 mL) and water (50 mL). After stirring overnight for at r.t. then for 4 h at 60 °C, water (200 mL) was added and the resulting yellow precipitate collected and recrystallized from acetone to give the diimine (average yield after two crops 116.5 g, 80%).

A Schlenk was charged with the diimine (9.0 g, 30.8 mmol) and evacuated three times. THF (100 mL) was charged followed by chloromethylethyl ether (3.0 mL, 30.8 mmol) and 2 drops of water. The mixture was stirred overnight at r.t. and the peach imidazolium salt isolated (average yield 7.70 g, 50%).

Imidazolium salt (7.70 g, 15.4 mmol) was dissolved in THF (50 mL) and the suspension stirred for 15 minutes. KO*t*Bu (1.83 g, 16.3 mmol) and the orange solution stirred for 20 minutes after which the solvent was exchanged *in vacuo* for toluene. After filtration through celite and glass wool, all volatiles were removed to give the product as a peach solid (average yield 4.6 g, 98%).$^{1}$H NMR (400.13 MHz, 298 K, $C_6D_6$) δ 2.16 (18H, s, C*H*$_3$), 6.49 (2H, s, imidazole backbone C*H*), 6.81 (4H, s, C*H*). $^{13}$C {$^{1}$H} NMR (100.62 MHz, 298 K, $C_6D_6$) δ (ppm) 17.91 (*o*-*C*H$_3$), 20.87 (*p*-*C*H), 120.38 (imidazole backbone *C*H), 128.97 (*m*-*C*H), 135.29 (*p*-*C*), 137.09 (*o*-*C*), 139.13 (*i*-*C*), 220.01 (C:).

### 8.3.38 Preparation of IBu (33)[212b]

To a solution of paraformaldehyde (0.3 g, 10 mmol) in toluene (10 mL) was added *tert*-butylamine (1.06 mL, 10 mmol) dropwise and the mixture heated to 40 °C for 20 minutes giving a clear solution. After cooling to 0 °C a further aliquot of *tert*-butylamine (1.06 mL, 10 mmol) was added dropwise. 4N HCl (3.33 mL) was added slowly at 0 °C and then the cooling was removed. Glyoxal (1.14 mL of a 40% solution in water) were then added and the mixture stirred overnight at 40 °C. The mixture was quenched with $NaHCO_3$ (10 mL of an aqueous solution) washed with ether (3 x 25 mL) and the product extracted with DCM (average yield 1.4 g, 65%).

The imidazolium salt (1.50 g, 6.9 mmol) was added to a Schlenk and evacuated three times. THF (20 mL) were added and the solution cooled to -78 °C and stirred for 20 minutes. KO*t*Bu (1.01 g, 9.0 mmol) was added and the solution was allowed to warm to r.t. over 30 minutes after which the solvent was exchanged *in vacuo* for toluene. After filtration through celite and glass wool, all volatiles were removed to give the product as brown solid (average yield 1.0 g, 80%).$^{1}$H NMR (400.13 MHz, 298 K, $C_6D_6$) δ 1.50 (18H, s, C*H*$_3$), 6.75 (2H, s, imidazole backbone C*H*). $^{13}$C {$^{1}$H} NMR (100.62 MHz, 298 K, $C_6D_6$) δ (ppm) 32.2 (*C*H$_3$), 56.5 (q-*t*Bu), 115.6 (imidazole backbone *C*H), 213.4 (*C*:).

### 8.3.39 Preparation of [Zn(*t*Bu)$_2$][236]

$ZnCl_2$ (5.45 g, 40 mmol) was suspended in $Et_2O$ (60 mL) and placed in the sonic bath for 15 minutes. After cooling to 0 °C *t*BuLi (47 mL of a 1.7 M solution) was added dropwise and the solution stirred in the dark for 2 h. The solid was filtered through celite and glass wool and concentrated *in vacuo* to approximately 15 mL. The remaining solution was transferred *via* cannula to a sublime for purification. Typical yield 5.70 g, 79%.

### 8.3.40 Synthesis of [IPr·ZnMe$_2$] (34)

A suspension of IPr (0.20 g, 0.5 mmol) in hexane (5 mL) was placed in a sonic bath and $ZnMe_2$ (0.5 mL of a 1 M solution in heptane, 0.5 mmol) was added, giving a peach suspension. Toluene (3 mL) was charged, giving a clear salmon solution which deposited a crop of crystals after storage in the freezer overnight: 0.04 g, 16% (filtrate analysis showed quantitative conversion). $^1$H NMR (400.03 MHz, 298 K, $C_6D_6$) δ (ppm) -0.78 (6H, s, ZnC$H_3$), 1.05 (12H, d, CH(C$H_3$)$_2$), 1.31 (12H, d, CH(C$H_3$)$_2$), 2.76 (4H, septet, C$H$(CH$_3$)$_2$), 6.47 (2H, s, imidazole backbone C$H$), 7.11 (4H, d, *m*-C$H$), 7.24 (2H, t, *p*-C$H$). $^{13}$C {$^1$H} NMR (100.62 MHz, 298 K, $C_6D_6$) δ (ppm) -8.12 (Zn$C$H$_3$)$_2$), 23.50 (CH($C$H$_3$)$_2$), 24.74 (CH($C$H$_3$)$_2$), 28.70 ($C$H(CH$_3$)$_2$), 122.88 (imidazole backbone $C$H), 124.06 (*m*-$C$H), 130.18 (*p*-$C$H), 135.52 (*i*-*C*), 145.43 (*o*-*C*). Carbene C could not be detected.

### 8.3.41 Synthesis of [IPr·Zn*t*Bu$_2$] (35)

To a solution of Zn*t*Bu$_2$ (1.26 g, 7 mmol) in hexane (35 mL) was added IPr (2.73 g, 7 mmol), giving a pale yellow suspension. After stirring for 30 minutes THF (10 mL) was charged, giving a clear yellow solution which deposited a crop of crystals after storage in the freezer overnight: 3.01 g, 76%. Crystals suitable for X-ray determination were crystallised from methylcyclohexane. $^1$H NMR (400.03 MHz, 298 K, $C_6D_6$) δ (ppm) 0.96 (12H, d, CH(C$H_3$)$_2$), 1.10 (18H, s, C(C$H_3$)$_3$), 1.35 (12H, d, CH(C$H_3$)$_2$), 3.06 (4H, septet, C$H$(CH$_3$)$_2$), 6.63 (2H, s, imidazole backbone C$H$), 7.12 (4H, d, *m*-C$H$), 7.19 (2H, t, *p*-C$H$). $^{13}$C {$^1$H} NMR (100.62 MHz, 298 K, $C_6D_6$) δ (ppm) 22.63 ($C$H(CH$_3$)$_2$), 23.71 ($C$(CH$_3$)$_3$), 25.98 (CH($C$H$_3$)$_2$), 28.48 ($C$H(CH$_3$)$_2$),

34.07 (CH($CH_3$)$_2$), 123.30 (imidazole backbone *C*H), 124.63 (*m*-*C*H), 130.09 (*p*--*C*H), 136.26 (*i*-*C*), 144.84 (*o*-*C*). Carbene C could not be detected.

### 8.3.42 Synthesis of [IMes·ZnMe$_2$] (36)

A suspension of IMes (0.15 g, 0.5 mmol) in hexane (5 mL) was placed in a sonic bath and $ZnMe_2$ (0.5 mL of a 1 M solution in heptane, 0.5 mmol) was added, giving a peach suspension. Toluene (5 mL) was charged, giving a clear peach solution which deposited a crop of crystals after storage in the freezer overnight: 0.07 g, 17% (filtrate analysis showed quantitative conversion). $^1$H NMR (400.03 MHz, 298 K, $C_6D_6$) δ (ppm) -0.49 (6H, s, Zn(C$H_3$)$_2$), 2.06 (18H, s, CC$H_3$), 6.12 (2H, s, imidazole backbone C*H*), 6.71 (4H, d, *m*-C*H*). $^{13}$C {$^1$H} NMR (100.62 MHz, 298 K, $C_6D_6$) δ (ppm) -8.54 (Zn*C*H$_3$), 17.45 (*o*-C*C*H$_3$), 20.87 (*p*-C*C*H$_3$), 121.29 (imidazole backbone *C*H), 129.28 (*m*-*C*H), 134.99 (*o*-*C*), 135.52 (*i*-*C*), 138.90 (*p*-*C*). Carbene C could not be detected.

### 8.3.43 Synthesis of [IMes·Zn*t*Bu$_2$] (cocrystallised with 1.5hexane) (37)

To a suspension of IMes (0.60 g, 2 mmol) in hexane (10 mL) a solution of Zn*t*Bu$_2$ (0.36 g, 2 mmol) in hexane (5 mL) was added, giving a tan solution which was transferred to the freezer overnight. A crop of yellow crystals were isolate: 0.67 g, 69%. $^1$H NMR (400.03 MHz, 298 K, $C_6D_6$) δ (ppm) 1.18 (18H, s, C(C$H_3$)$_3$), 2.05 (6H, s, *p*-CC$H_3$), 2.08 (12H, s, *o*-CC$H_3$), 6.17 (2H, s, imidazole backbone C*H*), 6.73 (4H, d, *m*-C*H*). $^{13}$C {$^1$H} NMR (100.62 MHz, 298 K, $C_6D_6$) δ (ppm) 18.32 (*o*-C*C*H$_3$), 20.71 (*p*-C*C*H$_3$), 23.61 (*C*(CH$_3$)$_3$), 34.22 (C(*C*H$_3$)$_3$), 122.07 (imidazole backbone *C*H), 129.75 (*m*-*C*H), 134.25 (*o*-*C*), 135.64 (*i*-*C*), 139.00 (*p*-*C*). Carbene C could not be detected.

### 8.3.44 Synthesis of [IBu·ZnMe$_2$] (38)

To a solution of IBu (0.18 g, 1 mmol) in hexane (10 mL) was added $ZnMe_2$ (1 mL of a 1 M solution in heptane, 1 mmol) giving a pale yellow solution which was transferred to the freezer. A crop of crystals was formed overnight: 0.09 g, 32%. $^1$H NMR (400.03 MHz, 298 K, $d_8$-THF) δ (ppm) -0.94 (6H, s, Zn(C$H_3$)$_2$), 1.61 (18H, s, C(C$H_3$)$_3$), 7.32 (2H, s, imidazole backbone C*H*). $^{13}$C {$^1$H} NMR (100.62 MHz, 298

K, $d_8$-THF) δ (ppm) -9.21 (Zn($CH_3$)$_2$), 30.34 (C$CH_3$), 57.31 ($C$CH$_3$), 117.32 (imidazole backbone $C$H), 186.88 ($C$:).

### 8.3.45 Synthesis of [IBu·Zn*t*Bu$_2$] (39)

A solution of Zn*t*Bu$_2$ (0.36 g, 2 mmol) in hexane (10 mL) was added to IBu (0.36 g, 2 mmol) giving a clear tan solution which was transferred to the freezer. A crop of crystals was formed after overnight: 0.22 g, 31%. $^1$H NMR (400.03 MHz, 298 K, $C_6D_6$) δ (ppm) 1.24 (18H, s, C(C$H_3$)$_3$), 1.50 (18H, s, C(C$H_3$)$_3$), 6.39 (2H, s, imidazole backbone C$H$). $^{13}$C {$^1$H} NMR (100.62 MHz, 298 K, $C_6D_6$) δ (ppm) 20.36 ($C$CH$_3$), 30.11 (C$C$H$_3$), 35.23 (C$C$H$_3$), 56.87 ($C$CH$_3$), 117.88 (imidazole backbone $C$H), 183.02 ($C$:).

### 8.3.46 Preparation of [BuNa][237]

NaO*t*Bu (3.84 g, 40 mmol) was suspended in hexane (90 mL) and stirred for 30 minutes before cooling to 0 °C and *n*BuLi (25 mL of a 1.6 M solution, 40 mmol) added dropwise. The white suspension was stirred overnight and the product isolated by filtration and washed with hexane (40 mL). Typical yield 2.62 g, 82%.

### 8.3.47 Preparation of [(TMEDA)Na(μ-TMP)(μ-*t*Bu)Zn(*t*Bu)] (40)[214]

BuNa (2 g, 25 mmol) was suspended in hexane (20 mL) and TMP(H) (4.3 mL, 25 mmol) added and the solution stirred for 1 h before being transferred *via* cannula to a second Schlenk tube containing a solution of Zn*t*Bu$_2$ (4.5 g, 25 mmol) in hexane (10 mL). To this were added TMEDA (3.8 mL, 25 mmol) and the orange solution was concentrated *in vacuo* to approximately 10 mL giving a cloudy solution. Gentle heat gave a clear solution that deposited a crop of crystals overnight in the freezer (typical yield 9.35 g, 81%). $^1$H NMR (400.13 MHz, 298 K, $C_6D_{12}$) δ 0.95-1.19 (18H, m, broad, C(C$H_3$)$_3$), 1.29 (12H, s, C$H_3$ (TMP)), 1.72 (4H, m, TMP- β and TMP-γ], 2.25 (12H, s, C$H_3$ (TMEDA)), 2.36 (4H, s, C$H_2$ (TMEDA)).

### 8.3.48 Synthesis of [(THF)$_3$Na(IPr*)Zn(*t*Bu)$_2$] (41)

To a solution of [(TMEDA)Na(μ-TMP)(μ-*t*Bu)Zn(*t*Bu)] (2.30 g, 5 mmol) in hexane (30 mL) IPr (1.95 g, 5 mmol) was added and the resulting cream suspension was

stirred for 30 minutes after which all volatiles were removed. THF (10 mL) and gentle heat gave a clear tan solution which was transferred to the freezer (-28 °C), which overnight deposited a crop of colourless crystals (3.46 g, 86%). $^{1}$H NMR (400.03 MHz, 298 K, $d_8$-THF) δ (ppm) 0.73 (18H, s, C(C*H*$_3$)$_3$), 1.12 (6H, d, CH(C*H*$_3$)$_2$), 1.15 (6H, d, CH(C*H*$_3$)$_2$), 1.18 (6H, d, CH(C*H*$_3$)$_2$), 1.23 (6H, d, CH(C*H*$_3$)$_2$), 1.77 (8H, m, C*H*$_2$ (THF)), 2.95 (2H, septet, C*H*(CH$_3$)$_2$), 3.16 (2H, septet, C*H*(CH$_3$)$_2$), 3.62 (8H, m, OC*H*$_2$ (THF)), 6.66 (1H, s, imidazole backbone C*H*), 7.19-7.25 (5H, overlapping m, ArC*H*), 7.32 (1H, t, *p*-C*H*). $^{13}$C {$^{1}$H} NMR (100.62 MHz, 298 K, $d_8$-THF) δ (ppm) 22.49 (*C*CH$_3$), 23.69 (CH(*C*H$_3$)$_2$), 24.67 (CH(*C*H$_3$)$_2$), 25.06 (CH(*C*H$_3$)$_2$), 26.03 (CH(*C*H$_3$)$_2$), 26.38 (*C*H$_2$ (THF)), 28.72 (*C*H(CH$_3$)$_2$), 28.79 (*C*H(CH$_3$)$_2$), 34.50 (C*C*H$_3$), 68.22 (O*C*H$_2$ (THF)), 123.88 (Ar*C*H), 123.92 (Ar*C*H), 127.63 (Ar*C*H), 128.59 (Ar*C*H), 129.91 (imidazole backbone *C*H), 140.74 (Ar*C*), 145.41 (Ar*C*), 146.47 (Ar*C*), 147.46 (Ar*C*), 159.49 (Zn*C*), 201.44 (*C*:).

### 8.3.49 Synthesis of [(THF)$_3$Na(IPr*)Zn(IPr*)(*t*Bu)] (42)

[(TMEDA)Na(μ-TMP)(μ-*t*Bu)Zn(*t*Bu)] (0.23 g, 0.5 mmol) and IPr (0.39 g, 1 mmol) were suspended in hexane (10 mL) and stirred overnight. All the volatiles were then removed and toluene added (5 mL) and the mixture stirred for 3 days after which all the solvent was removed again and THF (2 mL) and hexane (4 mL) gave a brown solution. Storage in the freezer (-28 °C) overnight deposited a crop of colourless crystals (0.25 g, 44%). $^{1}$H NMR (400.03 MHz, 298 K, $d_8$-THF) δ (ppm) 0.29 (9H, s, C(C*H*$_3$)$_3$), 1.07 (36H, overlapping m, CH(C*H*$_3$)$_2$), 1.16 (12H, d, CH(C*H*$_3$)$_2$), 1.78 (12H, m, C*H*$_2$ (THF)), 2.89 (4H, septet, C*H*(CH$_3$)$_2$), 3.09 (4H, septet, C*H*(CH$_3$)$_2$), 3.62 (8H, m, OC*H*$_2$ (THF)), 6.25 (2H, s, imidazole backbone C*H*), 7.08 (6H, s, ArC*H*), 7.16 (4H, d, ArC*H*), 7.25 (2H, d, ArC*H*). $^{13}$C {$^{1}$H} NMR (100.62 MHz, 298 K, $d_8$-THF) δ (ppm) 20.96 (*C*CH$_3$), 23.18 (CH(*C*H$_3$)$_2$), 24.45 (CH(*C*H$_3$)$_2$), 24.92 (CH(*C*H$_3$)$_2$), 25.86 (CH(*C*H$_3$)$_2$), 26.37 (*C*H$_2$ (THF)), 28.71 (*C*H(CH$_3$)$_2$), 28.77 (*C*H(CH$_3$)$_2$), 34.42 (C*C*H$_3$), 68.22 (O*C*H$_2$ (THF)), 123.50 (Ar*C*H), 123.57 (Ar*C*H), 127.24 (Ar*C*H), 128.06 (Ar*C*H), 130.39 (imidazole backbone *C*H), 141.21 (Ar*C*), 145.46 (Ar*C*), 146.61 (Ar*C*), 147.07 (Ar*C*), 156.99 (Zn*C*), 209.57 (*C*:).

### 8.3.50 Preparation of [(PMDETA)K(μ-TMP)(μ-*t*Bu)Zn(*t*Bu)] (43)[222]

$KCH_2SiMe_3$ (0.24 g, 2 mmol) was suspended in hexane (10 mL) and PMDETA (0.42 mL, 2 mmol) was added giving a clear orange solution. TMP(H) (0.34 mL, 2 mmol) was added and the solution transferred *via* cannula to a second Schlenk tube containing Zn*t*Bu$_2$ (0.36 g, 2 mmol) dissolved in hexane (10 mL). The resulting solution was transferred to the freezer overnight giving clear, colourless crystals were isolated (typical yield 0.74 g, 70%). $^1$H NMR (400.13 MHz, 298 K, $C_6D_{12}$) δ 1.02 (18H, s, C(C*H*$_3$)$_3$), 1.11 (12H, s, C*H*$_3$ (TMP)), 1.37 (4H, t, C*H*$_2$ (TMP-β)), 1.74 (2H, m, C*H*$_2$ (TMP-γ)), 2.23 (3H, s, C*H*$_3$ (PMDETA)), 2.25 (12H, s, C*H*$_3$ (PMDETA)), 2.40 (8H, m, C*H*$_2$ (PMDETA)).

### 8.3.51 Synthesis of [(THF)$_3$K(IPr*)Zn(*t*Bu)$_2$] (44)

To a solution of [(PMDETA)K(μ-TMP)(μ-*t*Bu)Zn(*t*Bu)] (0.52 g, 1 mmol) in hexane (10 mL) IPr (0.39 g, 1 mmol) was added and the resulting yellow suspension was stirred for 30 minutes after which THF (4.5 mL) was added and the straw solution was transferred to the freezer (-28 °C), which overnight deposited a crop of colourless crystals (0.29 g, 35%). $^1$H NMR (400.03 MHz, 298 K, d$_8$-THF) δ (ppm) 0.74 (18H, s, C(C*H*$_3$)$_3$), 1.10-1.24 (24H, overlapping m, CH(C*H*$_3$)$_2$), 1.78 (12H, m, C*H*$_2$ (THF)), 3.02 (2H, septet, C*H*(CH$_3$)$_2$), 3.15 (2H, septet, C*H*(CH$_3$)$_2$), 3.62 (8H, m, OC*H*$_2$ (THF)), 6.60 (1H, s, imidazole backbone C*H*), 7.16-7.29 (6H, overlapping m, ArC*H*). $^{13}$C {$^1$H} NMR (100.62 MHz, 298 K, d$_8$-THF) δ (ppm) 22.37 (*C*CH$_3$), 23.47 (CH(*C*H$_3$)$_2$), 24.62 (CH(*C*H$_3$)$_2$), 25.03 (CH(*C*H$_3$)$_2$), 26.11 (CH(*C*H$_3$)$_2$), 26.37 (*C*H$_2$ (THF)), 28.60 (*C*H(CH$_3$)$_2$), 28.71 (*C*H(CH$_3$)$_2$), 35.55 (C*C*H$_3$), 68.22 (O*C*H$_2$ (THF)), 123.58 (Ar*C*H), 123.88 (Ar*C*H), 127.29 (Ar*C*H), 128.09 (Ar*C*H), 128.79 (imidazole backbone *C*H), 146.57 (Ar*C*), 147.32 (Ar*C*), 157.83 (Zn*C*), 209.16 (*C*:).

### 8.3.52 Synthesis of [{TMS-IPr(H)}$^+${(THF)ZnCl$_2$*t*Bu}$^-$] (45)

A solution of [(THF)$_3$K(IPr*)Zn(*t*Bu)$_2$] (0.11 g, 0.125 mmol) in THF (3 mL) was cooled to 0 °C and TMSCl (0.03 mL, 0.25 mmol) added, giving a vibrant yellow solution which paled after a few minutes to a straw colour. The mixture was stirred for 5 days and then hexane (8 mL) added before storage in the freezer overnight gave a crop of crystals (0.04 g, 37%). Analysis by NMR showed mostly product, however,

an impurity was also present that was not removed on washing the crystals. $^{1}$H NMR (400.03 MHz, 298 K, $C_6D_6$) δ (ppm) -0.13 (9H, s, Si(C*H*$_3$)$_2$), 0.12 (2H, s, impurity), 1.07-1.14 (24H, overlapping m, CH(C*H*$_3$)$_2$ plus impurity), 1.29 (6H, d, CH(C*H*$_3$)$_2$), 1.33 (6H, d, CH(C*H*$_3$)$_2$), 1.45 (9H, s, C(C*H*$_3$)$_3$), 2.34-2.57 (4H, overlapping septets, C*H*(CH$_3$)$_2$), 3.58 (4H, m, OC*H*$_2$ (THF)), 7.01 (3H, t, ArC*H*), 7.11 (2H, d, ArC*H*). 7.20 (2H, t, ArC*H*), 7.29 (2H, m, ArC*H*), 10.19 (1H, s, imidazolium *H*).

### 8.3.53 Synthesis of [{Na(THF)$_6$}$^+${(*t*Bu)$_2$Zn(IPr*)Zn(*t*Bu)$_2$}$^-$] (46)

To a solution of Zn*t*Bu$_2$ (0.18 g, 1 mmol) in hexane (10 mL) was added [(THF)$_3$Na(IPr*)Zn(*t*Bu)$_2$] (0.81 g, 1 mmol) and the off-white suspension was stirred for 15 minutes. THF (5 mL) was added and the straw solution was frozen in liquid nitrogen before transferral to the freezer (-28 °C). A crop of colourless crystals was deposited overnight (0.36 g, 30%). $^{1}$H NMR (400.03 MHz, 298 K, d$_8$-THF) δ (ppm) 0.50 (18H, s, C(C*H*$_3$)$_3$), 0.74 (18H, s, C(C*H*$_3$)$_3$), 1.10 (6H, d, CH(C*H*$_3$)$_2$), 1.14 (6H, d, CH(C*H*$_3$)$_2$), 1.23 (6H, d, CH(C*H*$_3$)$_2$), 1.27 (6H, d, CH(C*H*$_3$)$_2$), 1.77 (16H, m, C*H*$_2$ (THF)), 3.23 (2H, septet, C*H*(CH$_3$)$_2$), 3.38 (2H, septet, C*H*(CH$_3$)$_2$), 3.62 (16H, m, OC*H*$_2$ (THF)), 6.88 (1H, s, imidazole backbone C*H*), 7.16-7.26 (6H, overlapping m, ArC*H*). $^{13}$C {$^{1}$H} NMR (100.62 MHz, 298 K, d$_8$-THF) δ (ppm) 22.14 (*C*CH$_3$), 23.05 (CH(*C*H$_3$)$_2$), 23.19 (*C*CH$_3$), 24.26 (CH(*C*H$_3$)$_2$), 26.11 (CH(*C*H$_3$)$_2$), 26.41 (*C*H$_2$ (THF)), 26.84 (CH(*C*H$_3$)$_2$), 28.83 (*C*H(CH$_3$)$_2$), 28.97 (*C*H(CH$_3$)$_2$), 34.93 (C*C*H$_3$), 35.49 (C*C*H$_3$), 68.22 (O*C*H$_2$ (THF)), 124.40 (Ar*C*H), 124.60 (Ar*C*H), 127.61 (Ar*C*H), 128.73 (Ar*C*H), 131.48 (imidazole backbone *C*H), 139.34 (Ar*C*), 143.65 (Ar*C*), 144.94 (Ar*C*), 146.03 (Ar*C*), 160.85 (Zn*C*), 187.88 (*C*:).

### 8.3.54 Synthesis of [ClAu(IPr*)Au(PPh$_3$)] (47)

To a solution of [(THF)$_3$Na(IPr*)Zn(*t*Bu)$_2$] (0.40 g, 0.5 mmol) in THF (20 mL) was added [ClAu(PPh$_3$)] (0.50 g, 1 mmol) and stirred at room temperature for 1 h to yield a colourless solution. This solution was then evaporated to dryness and the solid residue extracted with diethyl ether (20 mL) and filtered. The resultant solution was then concentrated to approximately 2 mL and purified by column chromatography; eluent 1:1 hexane: ethyl acetate (0.33 g, 61%). $^{1}$H NMR (400.03 MHz, 298 K, $CD_2Cl_2$) δ (ppm) 1.17 (d, 6H, CH(C*H*$_3$)$_2$), 1.27 (d, 6H, CH(C*H*$_3$)$_2$), 1.32 (d, 6H,

$CH(CH_3)_2$), 1.37 (d, 6H, $CH(CH_3)_2$), 2.74 (m, 4H, $CH(CH_3)_2$), 6.91 (s, 1H, imidazole backbone C*H*), 7.27-7.64 (m, 21H, ArC*H*). $^{31}P\{^1H\}$ NMR (400.03 MHz, 298 K, $CD_2Cl_2$) δ (ppm) 42.68 (s, Au-$PPh_3$). $^{13}C$ $\{^1H\}$ NMR (100.62 MHz, 298 K, $CD_2Cl_2$) δ (ppm) 23.84 ($CH(CH_3)_2$), 24.41 ($CH(CH_3)_2$), 28.52 ($CH(CH_3)_2$), 123.81 (imidazole backbone *C*H), 126.71-146.09 (m, Ar*C*H, Ar*C*, *C*-Au(backbone)), 172.81 (*C*:).

### 8.3.55 Synthesis of [IPr·LiZn*t*Bu$_3$] (48)

A solution of Zn*t*Bu$_2$ (0.18 g, 1 mmol) in hexane (5 mL) was added to IPr (0.39 g, 1 mmol) and the pale yellow suspension stirred for 90 minutes before *t*BuLi (0.6 mL of a 1.7 M solution in pentane) was added giving a clear solution which was transferred to the freezer. A crop of crystals was formed after 3 days: 0.52 g, 82%. $^1H$ NMR (400.03 MHz, 298 K, $C_6D_6$) δ (ppm) 0.96 (12H, d, $CH(CH_3)_2$), 1.95 (27H, s, $C(CH_3)_3$), 1.26 (12H, d, $CH(CH_3)_2$), 2.64 (4H, br, $CH(CH_3)_2$), 6.47 (2H, s, imidazole backbone C*H*), 7.07 (4H, d, *m*-C*H*). 7.21 (2H, t, *p*-C*H*). $^{13}C$ $\{^1H\}$ NMR (100.62 MHz, 298 K, $C_6D_6$) δ (ppm) 23.15 ($CH(CH_3)_2$), 24.68 ($CH(CH_3)_2$), 28.47 ($CCH_3$), 28.63 ($CH(CH_3)_2$), 34.22 ($CCH_3$), 123.40 (imidazole backbone *C*H), 124.34 (*m*-*C*H), 130.46 (*p*-*C*H), 136.00 (*i*-*C*), 145.29 (*o*-*C*). Carbene C could not be detected. $^7Li$ NMR (155.50 MHz, $C_6D_6$) δ -0.10 (s).

### 8.3.56 Synthesis of [IPr$_2$Na$_2$Mg(CH$_2$SiMe$_3$)$_4$] (49)

To a suspension of $NaCH_2SiMe_3$ (0.055 g, 0.5 mmol) in hexane (10 mL) $Mg(CH_2SiMe_3)_2$ (0.1 g, 0.5 mmol) was added and the suspension stirred for 1 hour. Benzene (15 mL) was then added giving an almost clear solution followed by IPr (0.20 g, 0.5 mmol) giving a straw solution. All the volatiles were removed and hexane (5 mL) was added which gave a clear solution on gentle heating. Storage in the freezer (-28 °C) overnight produced a crop of crystals which was isolated (0.04 g, 13%). $^1H$ NMR (400.13 MHz, 298 K, $C_6D_6$) δ -1.91 (8H, s, $SiCH_2$), 0.20 (36H, s, $Si(CH_3)_3$), 1.02 (24H, d, $CH(CH_3)_2$), 1.26 (24H, d, $CH(CH_3)_2$), 2.58 (8H, septet, $CH(CH_3)_2$), 6.41 (4H, s, imidazole backbone C*H*), 7.10 (8H, d, *m*-C*H*), 7.27 (4H, t, *p*-C*H*). $^{13}C$ $\{^1H\}$ NMR (100.62 MHz, 298 K, $C_6D_6$) δ (ppm) -3.00 ($SiCH_2$), 4.80 ($Si(CH_3)_3$), 24.33 ($CH(CH_3)_2$), 24.52 ($CH(CH_3)_2$), 28.65 ($CH(CH_3)_2$), 122.74

(imidazole backbone *C*H), 124.40 (*m*-*C*H), 130.51 (*p*-*C*H), 136.30 (*i*-*C*), 145.55 (*o*--*C*), 202.95 (*C*:).

### 8.3.57 Synthesis of $[(THF)_3Na(IPr^*)Mg(CH_2SiMe_3)_2(THF)]$ (50)

To a solution of IPr (1.40 g, 3.6 mmol) in hexane (40 mL) was added NaR (0.44 g, 4 mmol) and the solution stirred for 1 hour, after which $MgR_2$ was added (0.79 g, 4 mmol) was added and the suspension stirred overnight. THF was added dropwise (11 mL) and the clear solution transferred to the freezer which overnight deposited a crop of colourless crystals (1.86 g, 58%). $^1$H NMR (400.03 MHz, 298 K, $d_8$-THF) δ (ppm) -2.11 (4H, s, SiC*H*$_2$), 0.23 (18H, s, Si(C*H*$_3$)$_3$), 1.09 (6H, d, CH(C*H*$_3$)$_2$), 1.13 (6H, d, CH(C*H*$_3$)$_2$), 1.16 (6H, d, CH(C*H*$_3$)$_2$), 1.23 (6H, d, CH(C*H*$_3$)$_2$), 1.78 (10H, m, C*H*$_2$ (THF)), 2.95 (2H, septet, C*H*(CH$_3$)$_2$), 3.08 (2H, septet, C*H*(CH$_3$)$_2$), 3.61 (10H, m, OC*H*$_2$ (THF)), 6.55 (1H, s, imidazole backbone C*H*), 7.13-7.22 (6H, overlapping m, ArC*H*), $^{13}$C {$^1$H} NMR (100.62 MHz, 298 K, $d_8$-THF) δ (ppm) -5.90 (Si*C*H$_2$), 5.22 (Si*C*H$_3$)$_3$), 24.14 (CH(*C*H$_3$)$_2$), 24.87 (CH(*C*H$_3$)$_2$), 25.31 (CH(*C*H$_3$)$_2$), 25.73 (CH(*C*H$_3$)$_2$), 26.37 (*C*H$_2$ (THF)), 28.61 (*C*H(CH$_3$)$_2$), 68.22 (O*C*H$_2$ (THF)), 123.49 (Ar*C*H), 123.80 (Ar*C*H), 127.35 (Ar*C*H), 128.36 (Ar*C*H), 131.22 (imidazole backbone *C*H), 141.09 (Ar*C*), 145.74 (Ar*C*), 146.87 (Ar*C*), 147.29 (Ar*C*), 163.90 (Mg*C*), 200.19 (*C*:).

**Bibliography**


[1] A. D. McNaught, A. Wilkinson, *IUPAC Compendium of Chemical Terminology*, 2nd ed., Blackwell Scientific Publications, Oxford, **1997**.

[2] F. A. Cotton, G. Wilkinson, C. A. Murillo, M. Bochmann, *Advanced inorganic chemistry*, 6th ed., John Wiley & Sons, New York, **1999**.

[3] J. A. Wanklyn, *Ann.* **1858**, *108*, 67.

[4] a) J. A. Wanklyn, *Ann.* **1858**, *107*, 125; b) J. A. Wanklyn, *Ann.* **1859**, *111*, 234; cJ. A. Wanklyn, *Ann.* **1866**, *139*, 211.

[5] G. Wittig, F. J. Meyer, G. Lange, *Justus Liebegs, Ann. Chem.* **1951**, *571*, 167.

[6] E. Weiss, *Angew. Chem., Int. Ed.* **1993**, *32*, 1501.

[7] T. Greiser, J. Kopf, D. Thoennes, E. Weiss, *Chem. Ber.* **1981**, *114*, 209.

[8] a) A. Krasovskiy, P. Knochel, *Angew. Chem., Int. Ed.* **2004**, *43*, 3333; b) A. Krasovskiy, V. Krasovskaya, P. Knochel, *Angew. Chem., Int. Ed.* **2006**, *45*, 2958.

[9] T. Furuyama, M. Yonehara, S. Arimoto, M. Kobayashi, Y. Matsumoto, M. Uchiyama, *Chem. Eur. J.* **2008**, *14*, 10348.

[10] R. E. Mulvey, *Acc. Chem. Res.* **2009**, *42*, 743.

[11] P. C. Andrikopoulos, D. R. Armstrong, E. Hevia, A. R. Kennedy, R. E. Mulvey, C. T. O'Hara, *Chem. Commun.* **2005**, 1131.

[12] E. Hevia, R. E. Mulvey, *Angew. Chem. Int. Ed.* **2011**, *50*, 6448.

[13] J. Clayden, *Organolithiums: Selectivity for Synthesis, Vol. 23*, Pergamon, **2002**.

[14] H. Awad, F. Mongin, F. Trecourt, G. Queguiner, F. Marsais, F. Blanco, B. Abarca, R. Ballestros, *Tetrahedron Lett.* **2004**, *45*, 6697.

[15] O. Bayh, H. Awad, F. Mongin, C. Hoarau, F. Trecourt, G. Queguiner, F. Marsais, F. Blanco, B. Abarca, R. Ballestros, *Tetrahedron* **2005**, *61*, 4779.

[16] F. Mongin, A. Bucher, J. P. Bazureau, O. Bayh, H. Awah, F. Trecourt, *Tetrahedron Lett.* **2005**, *46*, 7989.

[17] O. Bayh, H. Awad, F. Mongin, C. Hoarau, L. Bischoff, F. Trecourt, G. Queguiner, F. Marsais, F. Blanco, B. Abarca, R. Ballestros, *J. Org. Chem.* **2005**, *70*, 5190.

[18] G. Bentabed-Ababsa, F. Blanco, A. Derdour, F. Mongin, F. Trecourt, G. Queguiner, R. Ballestros, B. Abarca, *J. Org. Chem.* **2009**, *74*, 163.

[19] A. Seggio, F. Chevallier, M. Vaultier, F. Mongin, *J. Org. Chem.* **2007**, *72*, 6602-6605.

[20] a) A. Seggio, M.-I. Lannou, F. Chevallier, D. Nobuto, M. Uchiyama, S. Golhen, T. Roisnel, F. Mongin, *Chem. Eur. J.* **2007**, *13*, 9982; b) J.-M. L'Helgoual'ch, A. Seggio, F. Chevallier, M. Yonehara, E. Jeanneau, M. Uchiyama, F. Mongin, *J. Org. Chem.* **2008**, *73*, 177.

[21] K. Snegaroff, S. Komagawa, F. Chevallier, P. C. Gros, S. Golhen, T. Roisnel, M. Uchiyama, F. Mongin, *Chem. Eur. J.* **2010**, *16*, 8191.

[22] A. Seggio, F. Chevallier, M. Vaultier, F. Mongin, *J. Org. Chem.* **2007**, *72*, 6602.

[23] J.-M. L'Helgoual'ch, A. Seggio, F. Chevallier, M. Yonehara, E. Jeanneau, M. Uchiyama, F. Mongin, *J. Org. Chem.* **2008**, *73*, 177.

[24] L. Gupta, A. C. Hoepker, K. J. Singh, D. B. Collum, *J. Org. Chem.* **2009**, *74*, 2231.
[25] P. Garcia-Alvarez, R. E. Mulvey, J. A. Parkinson, *Angew. Chem. Int. Ed.* **2011**, *50*, 9668.
[26] Y. Kondo, M. Shilai, M. Uchiyama, T. Sakamoto, *J. Am. Chem. Soc.* **1999**, *121*, 3539.
[27] T. Imahori, M. Uchiyama, T. Sakamoto, Y. Kondo, *Chem. Commun.* **2001**, 2450.
[28] P. C. Andrikopoulos, D. R. Armstrong, D. V. Graham, E. Hevia, A. R. Kennedy, R. E. Mulvey, C. T. O'Hara, C. Talmard, *Angew. Chem., Int. Ed.* **2005**, *44*, 3459.
[29] D. R. Armstrong, A. R. Kennedy, R. E. Mulvey, R. B. Rowlings, *Angew. Chem., Int. Ed.* **1999**, *38*, 131.
[30] E. Hevia, D. J. Gallagher, A. R. Kennedy, R. E. Mulvey, C. T. O'Hara, C. Talmard, *Chem. Commun.* **2004**, 2422.
[31] A. R. Kennedy, J. Klett, R. E. Mulvey, D. S. Wright, *Science* **2009**, *326*, 706.
[32] J. Garcia-Alvarez, A. R. Kennedy, J. Klett, R. E. Mulvey, *Angew. Chem., Int. Ed.* **2007**, *46*, 1105.
[33] a) A. Krasovskiy, B. F. Straub, P. Knochel, *Angew. Chem., Int. Ed.* **2006**, *45*, 159; b) W. Lin, O. Baron, P. Knochel, *Org. Lett.* **2006**, *8*, 5673; c) C. J. Rohbogner, S. H. Wunderlich, G. C. Clososki, P. Knochel, *Eur. J. Org. Chem.* **2009**, 1781; d) A. H. Stoll, P. Mayer, P. Knochel, *Organometallics* **2007**, *26*, 6694; e) G. C. Clososki, C. J. Rohbogner, P. Knochel, *Angew. Chem., Int. Ed.* **2007**, *46*, 7681; f) C. J. Rohbogner, G. C. Clososki, P. Knochel, *Angew. Chem., Int. Ed.* **2008**, *47*, 1503; g) M. Mosrin, P. Knochel, *Org. Lett.* **2008**, *10*, 2497; h) F. M. Piller, P. Knochel, *Org. Lett.* **2009**, *11*, 445; i) L. Melzig, C. B. Rauhut, P. Knochel, *Chem. Commun.* **2009**, 3536; j) M. Mosrin, T. Bresser, P. Knochel, *Org. Lett.* **2009**, *11*, 3406.
[34] S. H. Wunderlich, C. J. Rohbogner, A. Unsinn, P. Knochel, *Org. Proc. Res. Dev.* **2010**, *14*, 339.
[35] J. Garcia-Alvaerz, D. V. Graham, E. Hevia, A. R. Kennedy, J. Klett, R. E. Mulvey, C. T. O'Hara, S. Weatherstone, *Angew. Chem., Int. Ed.* **2008**, *47*, 8079.
[36] D. R. Armstrong, P. Garcia-Alvarez, A. R. Kennedy, R. E. Mulvey, J. A. Parkinson, *Angew. Chem., Int. Ed.* **2010**, *49*, 3185.
[37] D. Li, I. Keresztes, R. Hopson, P. G. Williard, *Acc. Chem. Res.* **2009**, *42*, 270.
[38] a) L. Lochmann, J. Pospisol, D. Lim, *Tetrahedron Lett.* **1966**, 257; b) M. Schlosser, *J. Organomet. Chem.* **1967**, *8*, 9.
[39] a) A. A. Morton, M. E. T. Holden, *J. Am. Chem. Soc.* **1947**, *69*, 1675; b) A. A. Morton, E. E. Magat, R. L. Letsinger, *J. Am. Chem. Soc.* **1947**, *69*, 950.
[40] A. A. Morton, F. D. Marsh, R. D. Coombs, A. L. Lyons, S. E. Penner, H. E. Ramsden, V. B. Baker, E. L. Little, R. L. Letsinger, *J. Am. Chem. Soc.* **1950**, *72*, 3785.
[41] L. Lochmann, *Eur. J. Inorg. Chem.* **2000**, 1115.
[42] M. Schlosser, *Organometallics in Synthesis*, John Wiley & Sons, Ltd, Chichester, England, **2004**.
[43] H. Gilman, R. G. Jones, *J. Am. Chem. Soc.* **1941**, *63*, 1441.
[44] E. J. Corey, D. J. Beames, *J. Am. Chem. Soc.* **1972**, *94*, 7210.

[45] W. Langham, R. Q. Brewster, H. Gilman, *J. Am. Chem. Soc.* **1941**, *63*, 545.
[46] S. Yamada, T. Takahashi, T. Konno, T. Ishihara, *Chem. Commun.* **2007**, 3679.
[47] H. Gilman, R. D. Gorsich, *J. Am. Chem. Soc.* **1956**, *78*, 2217.
[48] a) H. Gilman, A. L. Jacoby, *J. Am. Chem. Soc.* **1938**, *3*, 108; b) H. Gilman, W. Langham, A. L. Jacoby, *J. Am. Chem. Soc.* **1939**, *61*, 106; c) G. Wittig, U. Pockels, H. Droge, *Chem. Ber.* **1938**, *71*, 1903.
[49] D. Seyferth, *Organometallics* **2001**, *20*, 2940.
[50] F. F. Kneisel, M. Dochnahl, P. Knochel, *Angew. Chem., Int. Ed.* **2004**, *43*, 1017.
[51] E. Negishi, *Acc. Chem. Res.* **1982**, *15*, 340.
[52] Y. Kondo, N. Takazawa, C. Yamakazi, T. Sakamoto, *J. Org. Chem.* **1994**, *59*, 4717.
[53] M. Uchiyama, M. Koike, M. Kameda, Y. Kondo, T. Sakamoto, *J. Am. Chem. Soc.* **1996**, *118*, 8733.
[54] K. Kitagawa, A. Inoue, H. Shinokubo, K. Oshima, *Angew. Chem., Int. Ed.* **2000**, *39*, 2481.
[55] S. Dumouchel, F. Mongin, F. Trecourt, G. Queguiner, *Tetrahedron Lett.* **2003**, *44*, 2033.
[56] a) H. Ila, O. Baron, A. J. Wagner, P. Knochel, *Chemistry Letters* **2006**, *35*, 2; b) H. Ila, O. Baron, A. J. Wagner, P. Knochel, *Chem. Commun.* **2006**, 583.
[57] F. Kopp, P. Knochel, *Org. Lett.* **2007**, *9*, 1639.
[58] M. Hatano, T. Matsumura, T. Ishihara, *Org. Lett.* **2005**, *7*, 573.
[59] a) R. A. Kjonaas, R. K. Hoffer, *J. Org. Chem.* **1988**, *53*, 4133; b) R. A. Watson, R. A. Kjonaas, *Tet. Lett.* **1986**, *27*, 1437; c) W. Tuckmantel, K. Oshima, N. Hozaki, *Chem. Ber.* **1986**, *119*, 1581.
[60] a) F. Diedrich, P. J. Stang, *Metal-Catalysed Cross-Coupling Reactions*, Wiley-VCH, Weinheim, **1998**; b) P.-J. Corbet, G. Mignani, *Chem. Rev.* **2006**, *106*, 2651; c) E. A. B. Kantchev, C. J. O'Brien, M. G. Organ, *Angew. Chem. Int. Ed.* **2007**, *46*, 2768.
[61] "The Nobel Prize in Chemistry 2010". Nobelprize.org. http://www.nobelprize.org/nobel_prizes/chemistry/laureates/2010/.
[62] a) E. Negishi, A. King, O. Okukado, *J. Org. Chem.* **1978**, *42*, 1821; b) A. King, E. Negishi, F. J. Villani Jr., A. Silveria Jr., *J. Org. Chem.* **1978**, *43*, 358; c) E. Negishi, S. Gagneur, *Handbook of Organopalladium Chemistry for Organic Synthesis, Vol. 1*, Wiley, New York, **2002**.
[63] E. Hevia, J. Z. Chua, P. Garcia-Alvarez, A. R. Kennedy, M. D. McCall, *Proc. Nat. Acd. Sci. USA* **2010**, *107*, 5294.
[64] a) H. Dietrich, *Acta Crystallogr.* **1963**, *16*, 681; b) H. Dietrich, *J. Organomet. Chem.* **1981**, *205*, 291.
[65] E. Weiss, E. A. C. Lucken, *J. Organomet. Chem.* **1964**, *2*, 197.
[66] E. Weiss, G. Sauermann, G. Thirase, *Chem. Ber.* **1983** *116*, 74.
[67] E. Weiss, S. Corbelin, J. K. Cockcroft, A. N. Fitch, *Angew. Chem., Int. Ed.* **1990**, *29*, 650.
[68] E. Weiss, G. Sauremann, *Angew. Chem., Int. Ed.* **1968**, *7*, 133.
[69] E. Weiss, H. Koster, *Chem. Ber.* **1977**, *110*, 717.
[70] a) H. L. Lewis, T. L. Brown, *J. Am. Chem. Soc.* **1970**, *92*, 4664; b) D. Margerison, J. P. Newport, *Trans. Faraday Soc.* **1963**, *59*, 2058.

[71] A. W. Langer, *Adv. Chem. Ser.* **1974**, 130.
[72] N. D. R. Barnett, R. E. Mulvey, W. Clegg, P. A. O'Neil, *J. Am. Chem. Soc.* **1993**, *115*, 1573.
[73] M. A. Nichols, P. G. Williard, *J. Am. Chem. Soc.* **1993**, *115*, 1568.
[74] M. Geissler, J. Kopf, E. Weiss, *Chem. Ber.* **1989**, *122*, 1395.
[75] M. Granitzka, A.-C. Poppler, E. K. Schwarze, D. Stern, T. Schulz, M. John, R. Herbst-Irmer, S. K. Pandey, D. Stalke, *J. Am. Chem. Soc.* **2012**, *134*, 1344.
[76] D. H. Williams, I. Fleming, *Spectroscopic methods in organic chemistry*, 5th ed., McGraw-Hill Publishing Company, Maidenhead, **1995**.
[77] aE. O. Stejskal, *J. Chem. Phys.* **1965** *43*, 3597; bE. O. Stejskal, J. E. Tanner, *J. Chem. Phys.* **1965**, *42*, 288.
[78] K. F. Morris, C. S. J. Johnson, *J. Am. Chem. Soc.* **1992**, *114*, 3139.
[79] a) G. S. Armstrong, N. M. Loening, J. E. Curtis, A. J. Shaka, V. A. Mandelshtam, *J. Magn. Reson.* **2003**, *163*, 139; b) M. D. Pelta, H. Barjat, J. A. Morris, A. L. Davis, S. J. Hammond, *Magn. Reson. Chem.* **1998**, *36*, 706.
[80] a) M. Lin, M. J. Shapiro, J. R. Wareing, *J. Am. Chem. Soc.* **1997**, *119*, 5249; b) M. Lin, M. J. Shapiro, J. R. Wareing, *J. Org. Chem.* **1997**, *62*, 8930.
[81] I. Keresztes, P. G. Williard, *J. Am. Chem. Soc.* **2000**, *122*, 10228.
[82] D. Li, G. Kagan, R. Hopson, P. G. Williard, *J. Am. Chem. Soc.* **2009**, *131*, 5627.
[83] D. Li, C. Sun, J. Liu, R. Hopson, W. Li, P. G. Williard, *J. Org. Chem.* **2008**, *73*, 2373.
[84] T. Tatic, K. Meindl, J. Henn, S. K. Pandey, D. Stalke, *Chem. Commun.* **2010**, *46*, 4562.
[85] T. Tatic, S. Hermann, M. John, A. Loquet, A. Lange, D. Stalke, *Angew. Chem. Int. Ed.* **2011**, *50*, 6666.
[86] D. Li, R. Hopson, W. Li, J. Liu, P. G. Williard, *Org. Lett.* **2008**, *10*, 909.
[87] W. Li, G. Kagan, H. Yang, C. Cai, R. Hopson, W. Dai, D. A. Sweigart, P. G. Williard, *Organometallics* **2010**, *29*, 1309.
[88] S. Merkel, D. Stern, J. Henn, D. Stalke, *Angew. Chem. Int. Ed.* **2009**, *48*, 6350.
[89] D. B. Collum, *Acc. Chem. Res.* **1993**, *26*, 227.
[90] a) W. Clegg, F. J. Craig, K. W. Henderson, A. R. Kennedy, R. E. Mulvey, P. A. O'Neil, D. Reed, *Inorg. Chem.* **1997**, *36*, 6238; b) M. Westerhausen, *Inorg. Chem.* **1991**, *30*, 96.
[91] R. E. Mulvey, *Chem. Soc. Rev.* **1991**, *20*, 167.
[92] K. W. Henderson, W. J. Kerr, *Chem. Eur. J.* **2001**, *7*, 3430.
[93] a) P. Knochel, A. Gavryushin, K. Brade, *The Chemistry of Organomagnesium Compounds*, John Wiley & Sons, Chichester, **2008**; b) R. E. Mulvey, *Chem. Commun.* **2001**, 1049; c) R. E. Mulvey, *Organometallics* **2006**, *25*, 1060; d) R. E. Mulvey, F. Mongin, M. Uchiyama, Y. Kondo, *Angew. Chem. Int. Ed.* **2007**, *46*, 3802.
[94] a) J. G. Sosnicki, *Tetrahedron Lett.* **2009**, *50*, 178; b) J. G. Sosnicki, *Tetrahedron* **2007**, *63*, 11862; c) J. G. Sosnicki, *Tetrahedron* **2009**, *65*, 1336; d) J. G. Sosnicki, L. Struk, *Synlett* **2009**, 1812.
[95] a) B. Esser, A. Bandyopadhyay, F. Rominger, R. Gleiter, *Chem. Eur. J.* **2009**, *15*, 3368; b) F. Gallou, R. Haenggi, H. Hirt, W. Marterer, F. Schaefer, M. Seeger-Weibel, *Tetrahedron Lett.* **2008**, *49*, 5024; c) S. Y. W. Lau, G.

Hughes, P. D. O'Shea, I. W. Davies, *Org. Lett.* **2007**, *9*, 2239; d) H. Li, J. Balsells, *Tetrahedron Lett.* **2008**, *49*, 2034; e) T. Shoji, S. Ito, K. Toyota, T. Iwamoto, M. Yasunami, N. Morita, *Eur. J. Org. Chem.* **2009**, 4307; f) J. G. Sosnicki, *Synlett* **2009**, 2508; g) M. C. Stefan, A. E. Javier, I. Osaka, R. D. McCullough, *Macromolecules* **2009**, *42*, 30.

[96] H. Hawad, O. Bayh, C. Hoarau, F. Trecourt, G. Queguiner, F. Marsais, *Tetrahedron* **2008**, *64*, 3236.

[97] W. Clegg, K. W. Henderson, A. R. Kennedy, R. E. Mulvey, C. T. O'Hara, R. B. Rowlings, D. M. Tooke, *Angew. Chem. Int. Ed.* **2001**, *40*, 3902.

[98] B. Schubert, E. Weiss, *Chem. Ber.* **1984**, *117*, 366.

[99] D. Stalke, *Angew. Chem. Int. Ed.* **2012**, *51*, 9730.

[100] W. Schlenk, W. J. Shlenk, *Ber. Dtsch. Chem. Ges.* **1929**, *62*, 920.

[101] H. Yorimitsu, K. Oshima, *The Chemistry of Organomagnesium Compounds*, John Wiley & Sons, Ltd, Chichister, **2008**.

[102] a) D. R. Armstrong, C. Dougan, D. V. Graham, E. Hevia, A. R. Kennedy, *Organometallics* **2008**, *27*, 6063; b) N. T. T. Chau, M. Meyer, S. Komagawa, F. Chevallier, Y. Fort, M. Uchiyama, F. Mongin, P. C. Gros, *Chem. Eur. J.* **2010**, *16*, 12425; c) T. A. Mobley, S. Berger, *Angew. Chem., Int. Ed.* **1999**, *38*, 3070.

[103] a) D. R. Armstrong, E. Herd, D. V. Graham, E. Hevia, A. R. Kennedy, W. Clegg, L. Russo, *Dalton Trans.* **2008**, 1323; b) D. R. Armstrong, R. P. Davies, D. J. Linton, R. Snaith, P. Schooler, A. E. H. Wheatley, *J. Chem. Soc., Dalton Trans.* **2001**, 2838; c) M. Niemeyer, P. P. Power, *Organometallics* **1995**, *14*, 5488.

[104] M. Gartner, R. Fischer, J. L. Langer, H. Gorls, D. Walther, M. Westerhausen, *Inorg. Chem.* **2007**, *46*, 5118.

[105] V. L. Blair, A. R. Kennedy, J. Klett, R. E. Mulvey, *Chem. Commun.* **2008**, 5426.

[106] W. Clegg, B. Conway, P. Garcia-Alvaerz, A. R. Kennedy, R. Mulvey, L. Russo, J. Sassmannshausen, T. Tuttle, *Chem. Eur. J.* **2009**, *15*, 10702.

[107] W. Uhl, K.-W. Klinkhammer, M. Layh, W. Massa, *Chem. Ber.* **1991**, *124*, 279.

[108] a) E. Hevia, K. W. Henderson, A. R. Kennedy, R. E. Mulvey, *Organometallics* **2006**, *25*, 1778; b) M.-L. Hsueh, B.-T. Ko, T. Athar, C.-C. Lin, T.-M. Wu, S.-F. Hsu, *Organometallics* **2006**, *25*, 4144; c) S. C. Cole, M. P. Coles, P. B. Hitchcock, *Organometallics* **2004**, *23*, 5159.

[109] S. E. Baillie, W. Clegg, P. Garcia-Alvaerz, E. Hevia, A. R. Kennedy, J. Klett, L. Russo, *Chem. Commun.* **2011**, *47*, 388.

[110] W. Clegg, S. T. Liddle, R. E. Mulvey, A. Robertson, *Chem. Commun.* **2000**, 223.

[111] D. Thoennes, E. Weiss, *Chem. Ber.* **1978**, *111*, 3726.

[112] T. Tatic, H. Ott, D. Stalke, *Eur. J. Inorg. Chem.* **2008**, 3765.

[113] a) A. D. Pajerski, E. P. Squiller, M. Parvex, R. R. Whittle, H. G. Richey Jr, *Organometallics* **2005**, *24*, 809; b) K. W. Henderson, G. W. Honeyman, A. R. Kennedy, R. E. Mulvey, J. A. Parkinson, D. C. Sherrington, *Dalton Trans.* **2003**, 1365; c) E. Hevia, A. R. Kennedy, R. E. Mulvey, S. Weatherstone, *Angew. Chem., Int. Ed.* **2004**, *43*, 1709; d) J. Gromada, J. Mortreux, T. Chenal, J. W. Ziller, F. Leising, J. F. Carpentier, *Chem. Eur. J.* **2002**, *8*, 3773.

[114] C. A. Zechmann, T. J. Boyle, M. A. Rodriguez, R. A. Kemp, *Inorg. Chim. Acta* **2001**, *319*, 137.
[115] a) S. E. Baillie, V. L. Blair, E. Hevia, A. R. Kennedy, *Acta Crystallogr. Sect. C-Cryst. Struct. Commun.* **2011**, *67*, M249; b) A. R. Barron, *Chem. Soc. Rev.* **1993**, 93; c) A. R. Kennedy, R. E. Mulvey, C. L. Rason, B. A. Roberts, R. B. Rowlings, *Chem. Commun.* **1999**, 353; d) G. C. Forbes, A. R. Kennedy, R. E. Mulvey, R. B. Rowlings, W. Clegg, S. T. Liddle, C. C. Wilson, *Chem. Commun.* **2000**, 1759.
[116] a) Y. Sarazin, M. Schormann, M. Bochmann, *Organometallics* **2004**, *23*, 3296; b) B. J. Ireland, C. A. Wheaton, P. G. Hayes, *Organometallics* **2010**, *29*, 1079.
[117] a) A. Macchioni, G. Ciancaleoni, C. Zuccaccia, D. Zuccaccia, *Chem. Soc. Rev.* **2008**, *37*, 479; b) S. E. Baillie, W. Clegg, P. Garcia-Alvaerz, E. Hevia, A. R. Kennedy, J. Klett, L. Russo, *Chem. Commun.* **2011**, *47*, 388.
[118] G. W. Gokel, S. L. De Wall, E. S. Meadows, *Eur. J. Org. Chem.* **2000**, 2967.
[119] a) C. Yu, G. C. Levy, *J. Am. Chem. Soc.* **1984**, *106*, 6533; b) W. Bauer, T. Clark, R. Schleyer, *J. Am. Chem. Soc.* **1987**, *109*, 970.
[120] D. R. Armstrong, P. Garcia-Alvaerz, A. R. Kennedy, R. E. Mulvey, S. D. Robertson, *Chem. Eur. J.* **2011**, *17*, 6725.
[121] L. Yang, D. R. Powell, R. P. Houser, *Dalton Trans.* **2007**, 955.
[122] J. Garcia-Alvaerz, D. V. Graham, E. Hevia, A. R. Kennedy, R. E. Mulvey, *Dalton Trans.* **2008**, 1481.
[123] W. Clegg, B. Conway, A. R. Kennedy, J. Klett, R. E. Mulvey, L. Russo, *Eur. J. Inorg. Chem.* **2011**, 721.
[124] a) H. Viebrock, T. Panther, U. Behrens, E. Weiss, *J. Organomet. Chem.* **1995**, *491*, 19; b) C. Eaborn, W. Clegg, P. B. Hitchcock, M. Hopman, K. Izod, P. N. O'Shaughnessy, J. D. Smith, *Organometallics* **1997**, *16*, 4728.
[125] M. G. Davidson, D. Garcia-Vivo, A. R. Kennedy, R. E. Mulvey, S. D. Robertson, *Chem. Eur. J.* **2011**, *17*, 3364.
[126] A. R. Kennedy, J. Klett, C. T. O'Hara, R. E. Mulvey, G. M. Robertson, *Eur. J. Inorg. Chem.* **2009**, 5029.
[127] B. Conway, D. V. Graham, E. Hevia, A. R. Kennedy, J. Klett, R. E. Mulvey, *Chem. Commun.* **2008**, 2638.
[128] D. R. Armstrong, W. Clegg, A. M. Drummond, S. T. Liddle, R. E. Mulvey, *J. Am. Chem. Soc.* **2000**, *122*, 11117.
[129] M. J. Zawarotko, *Chem. Commun.* **2001**, 1.
[130] a) K. W. Henderson, A. R. Kennedy, A. E. McKeown, D. Strachan, *J. Chem. Soc., Dalton Trans.* **2000**, 4348; b) K. W. Henderson, A. R. Kennedy, L. MacDonald, D. J. MacDougall, *Inorg. Chem.* **2003**, *42*, 2839.
[131] E. Weiss, G. Sauremann, *J. Organomet. Chem.* **1970**, *21*, 1.
[132] P. B. Hitchcock, M. F. Lappert, W. P. Leung, T. Shun, *Chem. Commun.* **1993**, 1386.
[133] M. Niemeyer, P. P. Power, *Organometallics* **1997**, *16*, 3258.
[134] T. Kottke, D. Stalke, *Angew. Chem., Int. Ed.* **1993**, *32*, 580.
[135] B. Tecle, A. F. M. Maqsudur Rahman, J. P. Oliver, *J. Organomet. Chem.* **1986**, *317*, 267.
[136] J. L. Wardell, *Comprehensive Organometallic Chemistry Vol. 1* (Eds.: G. Wilkinson, F. G. A. Stone, E. W. Abel), Pergamon, Oxford, **1982**.

[137] A. E. H. Wheatley, *Chem. Soc. Rev.* **2001**, *30*, 265.
[138] a) N. D. R. Barnett, W. Clegg, A. R. Kennedy, R. E. Mulvey, S. Weatherstone, *Chem. Commun.* **2005**, 375; b) A. R. Kennedy, R. E. Mulvey, C. L. Raston, B. A. Roberts, R. B. Rowlings, *Chem. Commun.* **1999**, 353; c) A. R. Kennedy, J. Klett, R. E. Mulvey, S. Newton, D. S. Wright, *Chem. Commun.* **2008**, 308; d) K. J. Drewette, K. W. Henderson, A. R. Kennedy, R. E. Mulvey, C. T. O'Hara, R. B. Rowlings, *Chem. Commun.* **2002**, 1176.
[139] J. Lewinski, W. Marciniak, J. Lipkowski, I. Justyniak, *J. Am. Chem. Soc.* **2003**, *125*, 12698.
[140] a) D. J. Gallagher, K. W. Henderson, A. R. Kennedy, C. T. O'Hara, R. E. Mulvey, R. B. Rowlings, *Chem. Commun.* **2002**, 376; b) P. C. Andrikopoulos, D. R. Armstrong, A. R. Kennedy, R. E. Mulvey, C. T. O'Hara, R. B. Rowlings, *Eur. J. Inorg. Chem.* **2003**, 3354.
[141] C. Eaborn, P. B. Hitchcock, K. Izod, A. J. Jaggar, J. D. Smith, *Organometallics* **1994**, *13*, 753.
[142] F. Feil, S. Harder, *Organometallics* **2000**, *19*, 5010.
[143] P. B. Hitchcock, A. V. Khvostov, M. F. Lappert, *J. Organomet. Chem.* **2002**, *663*, 263.
[144] A. Wu, G. Guo, F. Zheng, M. Wang, Y. Li, G. Guo, J. Huang, *Inorg. Chem. Commun.* **2005**, *8*, 1078.
[145] J. C. Ma, D. A. Dougherty, *Chem. Rev.* **1997**, *97*, 1303.
[146] a) G. C. Forbes, A. R. Kennedy, R. E. Mulvey, B. A. Roberts, R. B. Rowlings, *Organometallics* **2002**, *21*, 5115; b) N. Wiberg, W. Niedermayer, H. Noth, M. Warchhold, *J. Organomet. Chem.* **2001**, *46*, 628; c) J. L. Atwood, K. D. Crissinger, R. D. Rogers, *J. Organometal. Chem.* **1978**, *155*, 1; d) C. Schade, P. v. R. Schleyer, *Adv. Organomet. Chem.* **1987**, *27*, 169.
[147] a) G. W. Honeyman, A. R. Kennedy, R. E. Mulvey, D. C. Sherrington, *Organometallics* **2004**, *23*, 1197; b) J. A. Morris, B. C. Noll, G. W. Honeyman, C. T. O'Hara, A. R. Kennedy, R. E. Mulvey, K. W. Henderson, *Chem. Eur. J.* **2007**, *13*, 4418.
[148] P. C. Andrikopoulos, D. R. Armstrong, W. Clegg, C. J. Gilfillan, E. Hevia, A. R. Kennedy, R. E. Mulvey, C. T. O'Hara, J. A. Parkinson, D. M. Tooke, *J. Am. Chem. Soc.* **2004**, *126*, 11612.
[149] a) W. Clegg, B. Conway, P. Garcia-Alvaerz, A. R. Kennedy, J. Klett, R. E. Mulvey, L. Russo, *Dalton Trans.* **2010**, *39*, 62; b) A. H. Ilkhechi, M. Bolte, H.-W. Lerner, M. Wagner, *J. Organomet. Chem.* **2005**, *690*, 1971; c) L. Kaufmann, H. Vitze, M. Bolte, H.-W. Lerner, M. Wagner, *Organometallics* **2007**, *26*, 1771; d) S. Scholz, J. C. Green, H.-W. Lerner, M. Bolte, M. Wagner, *Chem. Commun.* **2002**, 36.
[150] C. D. Broaddus, D. L. Muck, *J. Am. Chem. Soc.* **1967**, *89*, 6533.
[151] P. C. Andrews, A. R. Kennedy, R. E. Mulvey, C. L. Raston, B. A. Roberts, R. B. Rowlings, *Angew. Chem. Int. Ed.* **2000**, *39*, 1960.
[152] R. R. Fraser, T. S. Mansour, S. Savard, *Can. J. Chem.* **1985**, *63*, 3505.
[153] V. Snieckus, *Chem. Rev.* **1990**, *90*, 879.
[154] a) I. de Riggi, A. Virgili, M. de Morgas, C. Jaime, *J. Org. Chem.* **1992**, *60*, 27; b) C. Wolf, W. A. Konig, C. Roussel, *Liebigs Ann. Chem.* **1995**, 781.

[155] D. R. Armstrong, V. L. Blair, W. Clegg, S. H. Dale, J. Garcia-Alvaerz, G. W. Honeyman, E. Hevia, R. E. Mulvey, L. Russo, *J. Am. Chem. Soc.* **2010**, *132*, 9480.
[156] Y. Kondo, M. Shilai, M. Uchiyama, T. Sakamoto, *J. Am. Chem. Soc.* **1999**, *121*, 3539.
[157] P. C. Andrikopoulos, D. R. Armstrong, H. R. L. Barley, W. Clegg, S. H. Dale, E. Hevia, G. W. Honeyman, A. R. Kennedy, R. E. Mulvey, *J. Am. Chem. Soc.* **2005**, *127*, 6184.
[158] D. Nobuto, M. Uchiyama, *J. Org. Chem.* **2008**, *73*, 1117.
[159] Y. Kondo, J. V. Morey, J. C. Morgan, H. Naka, D. Nobuto, P. R. Raithby, M. Uchiyama, A. E. H. Wheatley, *J. Am. Chem. Soc.* **2007**, *129*, 12734.
[160] M. Uchiyama, Y. Matsumoto, S. Usui, Y. Hashimoto, K. Morokuma, *Angew. Chem. Int. Ed.* **2007**, *46*, 926.
[161] M. Uchiyama, Y. Matsumoto, D. Nobuto, T. Furuyama, K. Yamaguchi, K. Morokuma, *J. Am. Chem. Soc.* **2006**, *128*, 8748.
[162] D. R. Armstrong, C. Dougan, D. V. Graham, E. Hevia, A. R. Kennedy, *Organometallics* **2008**, *27*, 6063.
[163] W. Clegg, B. Conway, E. Hevia, M. D. McCall, L. Russo, R. E. Mulvey, *J. Am. Chem. Soc.* **2009**, *131*, 2375.
[164] S. H. Wunderlich, P. Knochel, *Angew. Chem. Int. Ed.* **2007**, *46*, 7685.
[165] Y. Ma, A. C. Hoepker, L. Gupta, M. F. Faggin, D. B. Collum, *J. Am. Chem. Soc.* **2010**, *132*, 15610.
[166] A. C. Hoepker, L. Gupta, Y. Ma, M. F. Faggin, D. B. Collum, *J. Am. Chem. Soc.* **2011**, *133*, 7135.
[167] A. R. Katritzky, *Handbook of Heterocyclic Chemistry*, 1st ed., Pergamon, New York, **1985**.
[168] F. Chevallier, F. Mongin, *Chem. Soc. Rev.* **2008**, *37*, 595.
[169] G. Queguiner, F. Marsais, V. Snieckus, J. Epsztajn, *Adv. Heterocycl. Chem.* **1991**, *52*, 187.
[170] N. Ple, A. Turck, K. Couture, G. Queguiner, *J. Org. Chem.* **1995**, *60*, 3781.
[171] Z. Dong, G. C. Clososki, S. H. Wunderlich, A. Unsinn, J. Li, P. Knochel, *Chem. Eur. J.* **2009**, *15*, 457.
[172] D. Nobuto, M. Uchiyama, *J. Org. Chem.* **2008**, *73*, 1117.
[173] M. S. Hill, D. J. MacDougall, M. F. Mahon, *Dalton Trans.* **2010**, *39*, 11129.
[174] a) W. Clegg, L. Dunbar, L. Horsburgh, R. E. Mulvey, *Angew. Chem., Int. Ed.* **1996**, *35*, 753; b) J. Matthieu, P. Gros, Y. Fort, *Chem. Commun.* **2000**, 951.
[175] a) M. Tobisu, I. Hyodo, N. Chatani, *J. Am. Chem. Soc.* **2009**, *131*, 12070; b) I. Hyodo, M. Tobisu, N. Chatani, *Chem. Asian J.* **2012**, *DOI: 10.1002/asia.201100971*.
[176] J. Lewinski, M. Dranka, W. Bury, W. Sliwinski, I. Justyniak, J. Lipkowski, *J. Am. Chem. Soc.* **2007**, *129*, 3096.
[177] Y. Cohen, L. Avram, L. Frish, *Angew. Chem. Int. Ed.* **2005**, *44*, 520.
[178] H. N. Hunter, N. Hadei, V. Blagojecvic, P. Patschinnski, G. T. Achonduh, S. Avola, D. K. Bohme, M. G. Organ, *Chem. Eur. J.* **2011**, *17*, 7845.
[179] a) K. C. Nicolaou, A. E. Koumbis, M. Takayanagi, S. Natarajan, N. F. Jain, T.Bando, H. Li, R. Hughes, *Chem. Eur. J.* **1999**, *5*, 2622; b) K. C. Nicolaou, M. Takayanagi, N. F. Jain, S. Natarajan, A. E. Koumbis, T. Bando, J. M. Ramanjulu, *Angew. Chem., Int. Ed.* **1998**, *37*, 2717.

[180] K. Tamao, K. Sumitani, M. Kumada, *J. Am. Chem. Soc.* **1972**, *94*, 4374.
[181] A. M. DeBerardinis, M. Turlington, L. Pu, *Org. Lett.* **2008**, *10*, 2709.
[182] R. M. Fabicon, M. Parvez, H. G. Richey Jr, *J. Am. Chem. Soc.* **1991**, *113*, 1412.
[183] a) H. R. L. Barley, W. Clegg, S. H. Dale, E. Hevia, G. W. Honeyman, A. R. Kennedy, R. E. Mulvey, *Angew. Chem., Int. Ed.* **2005**, *44*, 6018; b) S. R. Boss, M. P. Coles, R. Haigh, P. B. Hitchcock, R. Snaith, A. E. H. Wheatley, *Angew. Chem., Int. Ed.* **2003**, *42*, 5593.
[184] a) A. D. Bond, D. J. Linton, P. Schooler, A. E. H. Wheatley, *J. Chem. Soc., Dalton Trans.* **2001**, 3173; b) T. J. Boyle, S. D. Bunge, N. L. Andrews, L. E. Matzen, K. Sieg, M. A. Rodriguez, T. J. Headley, *Chem. Mater.* **2004**, *16*, 3279; c) R. P. Davies, D. J. Linton, P. Schooler, R. Snaith, A. E. H. Wheatley, *Chem. Eur. J.* **2001**, *7*, 3696; d) K. Merz, S. Block, R. Schoenen, M. Driess, *Dalton Trans.* **2003**, 3365.
[185] S. C. Moratti, J. Simpson, *Acta Crystallogr., Sect.E: Struct. Rep. Online* **2007**, *63*, m2444.
[186] E. O. Fischer, A. Maasbol, *Angew. Chem. Int. Ed. Engl.* **1964**, *3*, 580.
[187] R. R. Schrock, *J. Am. Chem. Soc.* **1974**, *96*, 6796.
[188] D. Bourissou, O. Guerret, F. P. Gabbai, G. Bertrand, *Chem. Rev.* **2000**, *100*, 39.
[189] A. J. Arduengo III, R. L. Harlow, M. Kline, *J. Am. Chem. Soc.* **1991**, *113*, 361.
[190] C. Valente, S. Calimsiz, K. H. Hoi, D. Mallik, M. Sayah, M. G. Organ, *Angew. Chem. Int. Ed.* **2012**, *51*, 3314.
[191] M. Scholl, S. Ding, C. W. Lee, R. H. Grubbs, *Org. Lett.* **1999**, *1*, 953.
[192] Y. Wang, Y. Xie, P. Wei, R. B. King, H. F. Schaefer III, P. v. R. Schleyer, G. H. Robinson, *Science* **2008**, *321*, 1050.
[193] Y. Wang, Y. Xie, P. Wei, R. B. King, H. F. Schaefer III, P. v. R. Schleyer, G. H. Robinson, *J. Am. Chem. Soc.* **2008**, *130*, 14970.
[194] A. Sidiropoulos, C. Jones, A. Stasch, S. Klein, G. Frenking, *Angew. Chem. Int. Ed.* **2009**, *48*, 9701.
[195] H. Braunschweig, R. D. Dewhurst, K. Hammond, J. Mies, K. Radacki, A. Vargas, *Science* **2012**, *336*, 1420.
[196] O. Jackowski, A. Alexakis, *Angew. Chem. Int. Ed.* **2010**, *49*, 3346.
[197] A. R. Kennedy, S. D. Robertson, R. E. Mulvey, *Dalton Trans.* **2010**, *39*, 9091.
[198] M. Arrowsmith, M. S. Hill, D. J. MacDougall, M. F. Mahon, *Angew. Chem. Int. Ed.* **2009**, *48*, 4013.
[199] A. J. Arduengo III, F. Davidson, H. V. R. Dias, J. R. Goerlich, D. Khasnis, W. J. Marshall, T. K. Prakasha, *J. Am. Chem. Soc.* **1997**, *119*, 12742.
[200] a) C. Samojowicz, M. Bieniek, K. Grela, *Chem. Rev.* **2009**, *109*, 3708; b) S. Monfette, D. E. Fogg, *Chem. Rev.* **2009**, *109*, 3783.
[201] W. A. L. van Otterlo, C. B. de Koning, *Chem. Rev.* **2009**, *109*, 3743.
[202] B. Alcaide, P. Almendros, A. Luna, *Chem. Rev.* **2009**, *109*, 3817.
[203] S. Grundemann, A. Kovacevic, M. Albrecht, J. W. Faller, R. H. Crabtree, *Chem. Commun.* **2001**, 2274.
[204] A. R. Chianese, A. Kovacevic, B. M. Zeglis, J. W. Faller, R. H. Crabtree, *Organometallics* **2004**, *23*, 2461.

[205] E. Aldeco-Perez, A. J. Rosenthal, B. Donnadieu, P. Parameswaran, G. Frenking, G. Bertrand, *Science* **2009**, *326*, 556.
[206] Y. Wang, Y. Xie, M. Y. Abraham, P. Wei, H. F. Schaefer III, P. v. R. Schleyer, G. H. Robinson, *J. Am. Chem. Soc.* **2010**, *132*, 14370.
[207] Y. Wang, M. Y. Abraham, R. J. Gilliard Jr., P. Wei, J. C. Smith, G. H. Robinson, *Organometallics* **2012**, *31*, 791.
[208] A. Jana, R. Azhakar, G. Tavcar, H. W. Roesky, I. Objartel, D. Stalke, *Eur. J. Inorg. Chem.* **2011**, 3686.
[209] D. Mendoza-Espinosa, B. Donnadieu, G. Bertrand, *J. Am. Chem. Soc.* **2010**, *132*, 7264.
[210] P. L. Arnold, S. T. Liddle, *Organometallics* **2006**, *25*, 1485.
[211] M. S. Hill, G. Kociok-Kohn, D. J. MacDougall, *Inorg. Chem.* **2011**, *50*, 5234.
[212] a) A. J. Arduengo III, R. Krafczyk, R. Schmutzler, *Tetrahedron* **1999**, *55*, 14523; b) E. C. Hurst, K. Wilson, I. J. S. Fairlamb, V. Chechik, *New J. Chem.* **2009**, *33*, 1837.
[213] A. J. Arduengo III, H. V. R. Dias, F. Davidson, R. L. Harlow, *J. Organomet. Chem.* **1993**, *462*, 13.
[214] P. C. Andrikopoulos, D. R. Armstrong, H. R. L. Barley, W. Clegg, S. H. Dale, E. Hevia, G. W. Honeyman, A. R. Kennedy, R. E. Mulvey, *J. Am. Chem. Soc.* **2005**, *127*, 6184.
[215] D. R. Armstrong, J. Garcia-Alvarez, D. V. Graham, G. W. Honeyman, E. Hevia, R. E. Mulvey, *Chem. Eur. J.* **2009**, *15*, 3800.
[216] D. R. Armstrong, W. Clegg, S. H. Dale, E. Hevia, L. M. Hogg, G. W.Honeyman, R. E.Mulvey, *Angew. Chem. Int. Ed.* **2006**, *45*, 3775.
[217] W. Clegg, S. H. Dale, E. Hevia, L. M. Hogg, G. W. Honeyman, R. E. Mulvey, C. T. O'Hara, L. Russo, *Angew. Chem. Int. Ed.* **2008**, *47*, 731.
[218] a) W. Clegg, S. H. Dale, R. W. Harrington, E. Hevia, G. W. Honeyman, R. E. Mulvey, *Angew. Chem. Int. Ed.* **2006**, *45*, 2374; b) L. Balloch, A. R. Kennedy, R. E. Mulvey, T. Rantanen, S. D. Robertson, V. Snieckus, *Organometallics* **2011**, *30*, 145.
[219] W. Clegg, S. H. Dale, E. Hevia, L. M. Hogg, G. W. Honeyman, R. E. Mulvey, C. T. O'Hara, *Angew. Chem. Int. Ed.* **2006**, *45*, 6548.
[220] L. Balloch, A. R. Kennedy, J. Klett, R. E. Mulvey, C. T. O'Hara, *Chem. Commun.* **2010**, *46*, 2319.
[221] W. Clegg, S. H. Dale, E. Hevia, G. W. Honeyman, R. E. Mulvey, *Angew. Chem. Int. Ed.* **2006**, *45*, 2370.
[222] B. Conway, *University of Strathclyde, Ph.D. Thesis* **2010**.
[223] K. L. Hull, I. Carmichael, B. C. Noll, K. W. Henderson, *Chem.-Eur. J.* **2008**, *14*, 3939.
[224] a) P. L. Arnold, M. Rodden, C. Wilson, *Chem. Commun.* **2005**, 1743; b) S. P. Downing, A. A. Danopoulos, *Organometallics* **2006**, *25*, 1337.
[225] I. S. MacIntosh, C. N. Sherren, K. N. Robertson, J. D. Masuda, C. C. Pye, J. C. C. Clyburne, *Organometallics* **2010**, *29*, 2063.
[226] Y. Wang, Y. Xie, M. Y. Abraham, P. Wei, H. F. Schaefer III, P. v. R. Schleyer, G. H. Robinson, *Organometallics* **2011**, *30*, 1303.
[227] a) S. P. Nolan, *Acc. Chem. Res.* **2011**, *44*, 91; b) Y.-P. Xiao, X.-Y. Liu, C. C.-M., *Angew. Chem. Int. Ed.* **2011**, *50*, 4937; c) E. Jimenez-Nunez, A. M. Echavarren, *Chem. Rev.* **2008**, *108*, 3326; d) Z. Li, C. Brouwer, C. He, *Chem.*

*Rev.* **2008**, *108*, 3239; e) D. J. Gorin, B. D. Sherry, F. D. Toste, *Chem. Rev.* **2008**, *108*, 3351.
[228] K. M. Hindi, M. J. Panzer, C. A. Tessier, C. L. Cannon, W. J. Youngs, *Chem. Rev.* **2009**, *109*, 3859.
[229] P. De Fremont, N. M. Scott, E. D. Stevens, S. P. Nolan, *Organometallics* **2005**, *24*, 2411.
[230] M.-C. Brandys, M. C. Jennings, R. J. Puddephatt, *J. Chem. Soc., Dalton Trans.* **2000**, 4601.
[231] a) R. A., T. Pape, F. E. Hahn, *Organometallics* **2011**, *30*, 6393; b) W. Wang, J. Yang, F. Wang, M. Shi, *Organometallics* **2011**, *30*, 3859; c) C. Hirtenlehner, C. Krims, J. Holbling, M. List, M. Zabel, M. Fleck, R. J. F. Berger, W. Schoefberger, U. Monkowius, *Dalton Trans.* **2011**, *40*, 9899; d) E. Tkatchouk, N. P. Mankad, D. Benitez, W. A. Goddard III, F. D. Toste, *J. Am. Chem. Soc.* **2011**, *133*, 14293; e) B. W. Gung, L. N. Bailey, D. T. Craft, C. L. Barnes, K. Kirschbaum, *Organometallics* **2010**, *29*, 3450; f) J. I. Bates, P. Kennepohl, D. P. Gates, *Angew. Chem. Int. Ed.* **2009**, *48*, 9844.
[232] G. C. Fortman, A. Poater, J. W. Levell, S. Gaillard, A. M. Z. Slawin, I. D. W. Samuel, L. Cavallo, S. P. Nolan, *Dalton Trans.* **2010**, *39*, 10382.
[233] A. R. Kennedy, J. Klett, R. E. Mulvey, S. D. Robertson, *Eur. J. Inorg. Chem.* **2011**, 4675.
[234] G. M. Sheldrick, *Acta Crystallogr. Sect. A* **2008**, *64*, 112.
[235] J.-M. L'Helgoual'ch, G. Bentabed-Ababsa, F. Chevallier, M. Yonehara, M. Uchiyama, A. Derdour, F. Mongin, *Chem. Commun.* **2008**, 5375.
[236] H. Lehmkuhl, O. Olbrychs, *Liebigs Ann. Chem.* **1975**, 1162.
[237] L. Lochmann, J. Pospisol, D. Lim, *Tetrahedron Lett.* **1966**, *7*, 257.